

学位論文

Aspects of Supersymmetry after LHC Run I (LHC Run Iを踏まえた超対称性理論の諸問題)

平成 25年 12月 博士 (理学)
申請

東京大学大学院理学系研究科
物理学専攻

飛岡 幸作

Aspects of Supersymmetry after LHC Run I

*A dissertation submitted in partial satisfaction of
the requirement for the degree of*

Doctor of Philosophy

in

Physics

by

Kohsaku Tobioka

Kavli Institute for the Physics and Mathematics of the Universe
Department of Physics, Graduate School of Science
University of Tokyo



December 2013

Abstract

Supersymmetry (SUSY) is a prime candidate for physics beyond the Standard Model, and we investigate aspects of supersymmetry in light of Large Hadron Collider (LHC) results. The main accomplishment of LHC Run I is discovery of Higgs boson, and it is a momentous step towards understanding electroweak symmetry breaking. The Standard Model Higgs sector, however, is not theoretically satisfactory. Since the Higgs mass scale is not protected by any symmetry, the electroweak scale is unstable to be at observed scale and hence unacceptable fine-tuning is required. Unlike the Standard Model, low-energy supersymmetry stabilizes the Higgs mass avoiding fine-tuning and leads to natural electroweak symmetry breaking. The natural scale of supersymmetric particles (sparticles) is below \approx TeV. The minimal supersymmetric Standard Model (MSSM) has been studied, and it was found the lightest supersymmetric particle (LSP) is a good dark matter candidate.

However, there are tensions between low-energy supersymmetry and the LHC results. Firstly, searches at the LHC for sparticles have not found any signal and give strong limits on mass of gluino and squark up to \approx 1.8 TeV for a conventional model, constrained minimal supersymmetric Standard Model (CMSSM). Next, the observed Higgs mass of 125 GeV is not easily accommodated in the MSSM, where one has to rely on the radiative corrections to boost the Higgs mass beyond the tree-level upper bound of $m_Z \simeq$ 91 GeV. This requirement push sparticles scale well beyond the TeV within CMSSM, leading to fine-tuning. In this thesis we particularly study two scenarios of supersymmetry originating the tensions.

A nearly degenerate (compressed) spectrum ameliorates the bounds from the current searches at the LHC whereas the CMSSM typically generates a widely spread spectrum. For the lack of SUSY signal, the scenario with a compressed spectrum recently has more attentions, but motivations and explicit models for the scenario have not been discussed. Therefore we study this direction in detail.

Supersymmetry broken geometrically in extra dimensions, by the Scherk-Schwartz mechanism, naturally leads to a compressed spectrum. We present a minimal such model with a single extra dimension, which we call “Compact Supersymmetry,” and show that it leads to viable phenomenology despite the fact that it essentially has two less free parameters than the CMSSM. The theory does not suffer from the supersymmetric flavor or CP problem because of universality of geometric breaking, and automatically yields near-maximal mixing in the scalar top sector with $|A_t| \approx 2m_{\tilde{t}}$ to boost the Higgs boson mass. Despite the rather constrained structure, the theory is less fine-tuned than many supersymmetric models. The LSP is Higgsino-like and can be a component of dark matter. We find direct detection experiments will cover a large portion of parameter space. The collider constraint on the Compact Supersymmetry is certainly weaker than that on the CMSSM as gluino and squark mass bound is relaxed down to \approx 1 TeV. In order to increase sensitivity to models with a compressed spectrum, we suggest a kinematic variable, M_{T2} , can be useful since the Standard Model background is systematically removed by requiring $M_{T2} > m_{\text{top}}$.

Naturalness implies new dynamics beyond the minimal theory. There have been many attempts to extend the MSSM to accommodate the Higgs mass. In such extensions, new states interact with the Higgs, raising its mass by increasing the strength of the quartic

interaction of the scalar potential. One possibility is a non-decoupling F -term, as in the NMSSM (MSSM plus a singlet S). If the new states are integrated out supersymmetrically, their effects decouple and the Higgs mass is not increased. On the other hand, SUSY breaking can lead to non-decoupling effects that increase the Higgs mass. However, in general, these extensions require new states at the few hundred GeV scale, so that the new sources of SUSY breaking do not spoil naturalness.

In this thesis, we have identified a new model where the Higgs couples to two singlet fields with a Dirac mass, which we call Dirac NMSSM,

$$W \supset \lambda S H_u H_d + M S \bar{S}.$$

The non-decoupling F -term increases the Higgs mass while maintaining naturalness even in the presence of large SUSY breaking in the singlet sector as $m_{\bar{S}} \gtrsim 10$ TeV. The key feature in the Dirac NMSSM is that \bar{S} couples to the MSSM only through the dimensionful Dirac mass, M . We note that interactions between \bar{S} and other new states are not constrained by naturalness, even if these states experience SUSY breaking. Therefore, the Dirac NMSSM represents a new type of portal, whereby our sector can interact with new sectors, with large SUSY breaking, without spoiling naturalness in our sector.

Collider signatures of the Dirac NMSSM are discussed. The low-energy phenomenology is that of a two Higgs doublet model. We obtain constraints from direct searches for heavier Higgs boson and coupling measurements for the lightest Higgs boson at the LHC. We also study the future reach based on prospects of high-luminosity LHC and future international linear collider, and show large parameter space can be probed.

Contents

1	Invitation	1
1.1	Last Piece of the Standard Model	1
1.2	Beyond the Standard Model	3
1.3	Supersymmetry	5
1.3.1	Motivation	5
1.3.2	Algebra	6
1.3.3	The Minimal Supersymmetric Standard Model	8
1.3.4	Naturalness in a nutshell	11
1.4	LHC Run I: Higgs Boson	12
1.5	LHC Run I: Supersymmetric Particles	14
1.6	Directions for low-energy Supersymmetry	17
1.6.1	Tensions by LHC Run I	17
1.6.2	Organization of this thesis	19
I	Supersymmetry, Extra Dimension and Compressed Spectrum	21
2	Compact Supersymmetry	23
2.1	Introduction	23
2.2	5D Supersymmetric Lagrangian	24
2.2.1	Non-Abelian gauge field	25
2.2.2	Hypermultiplet	27
2.3	Supersymmetry Breaking by Boundary Conditions	28
2.3.1	Scherk-Schwarz mechanism	28
2.3.2	Soft masses of scalar and gaugino	30
2.3.3	Soft terms on brane	32
2.4	Radion Mediation	34
2.4.1	Lagrangian	34
2.4.2	Radion mediation	35
2.4.3	Soft terms on brane	38
2.5	Model Setup	39
2.5.1	Bulk gauge and matter fields	39
2.5.2	Higgs fields and Yukawa interactions	39
2.5.3	Lagrangian on brane with Yukawa coupling	40
2.5.4	Lagrangian on brane with gauge coupling	45
2.6	Radiative Corrections	47

2.6.1	Dimensional analysis for radiative corrections	47
2.6.2	Finite threshold corrections	48
2.7	Brane Kinetic Terms at Tree-Level	53
3	Phenomenology of Compact Supersymmetry	55
3.1	Higgs Sector	55
3.1.1	Electroweak symmetry breaking	55
3.1.2	Higgs mass and naturalness	56
3.2	Sparticle Spectrum	57
3.3	Experimental Limits	58
3.3.1	LHC Run I	58
3.3.2	Other measurements	61
3.3.3	Comment on brane kinetic terms	61
3.4	Dark Matter	62
3.5	Summary and Discussion	63
II	Natural Higgs Mass in Supersymmetry with Two Singlets	65
4	Dirac NMSSM	67
4.1	Introduction	67
4.1.1	Beyond the MSSM	68
4.2	Model Setup	69
4.2.1	Spurion analysis	69
4.2.2	Dirac NMSSM	70
4.2.3	NMSSM	71
4.3	Raising the Higgs Mass without Fine-tuning	71
4.3.1	Non-decoupling effects	71
4.3.2	Renormalization group equations	73
4.3.3	Threshold corrections	73
4.3.4	Semi-soft SUSY breaking	74
4.4	Higgs Mass at Tree-Level	75
4.4.1	CP-even neutral scalars	75
4.5	Radiative Corrections	76
4.5.1	One-loop corrections	76
4.5.2	RG-improved calculation	78
4.6	Benchmark Parameters and Stop Mass	79
4.7	Raising Higgs Mass for Explicit μ in the NMSSM	81
4.8	Naturalness	81
5	Phenomenology of Dirac NMSSM	85
5.1	Current Constraints	85
5.1.1	SM-like Higgs	85
5.1.2	Heavier doublet-like Higgs	87
5.2	Future Reach	87

5.3	Summary and Discussion	90
6	Overall Summary	91
	Acknowledgments	93
A	Structure of 5D Supersymmetry	95
A.1	Gauge Invariance of 5D Supersymmetry Action	95
A.2	$SU(2)_R$ invariance	97
B	Kaluza-Klein Expansion	99
B.1	KK Expansion in S^1/\mathbb{Z}_2	100
B.2	Mass Matrix and Propagator	100
B.2.1	Squarks and sleptons	100
B.2.2	Quarks and leptons	102
B.2.3	Gauginos	103
B.2.4	Gauge fields	104
B.2.5	Adjoint real scalars	105
B.3	Formulae	105
B.3.1	Formulae for KK Expansion	105
B.4	Interactions	106
C	Formulae for Summation and Integral	107
C.1	Infinite Sum to Analytic Function	107
C.1.1	Formulae	109
C.1.2	Loop integral of infinite sum	109
C.2	Example: $m_{H_u}^2$ from all KK particles with top-Yukawa coupling	111
D	Search for New Physics with Compressed Spectrum by M_{T2}	113
D.1	Introduction	113
D.2	MUED	114
D.2.1	Mass spectrum	115
D.2.2	Production and decay at the LHC	116
D.3	Definition of M_{T2}	116
D.4	Use of M_{T2} as event selection	118
D.4.1	Properties	118
D.4.2	Comparison in realistic situation	119
D.5	Application for the MUED	121
D.5.1	Simulation	122
D.5.2	Event selection	123
D.5.3	Discovery potential	123
D.6	Summary and Discussion	126
	Bibliography	129

1

Invitation

1.1 Last Piece of the Standard Model

One of the greatest accompaniments of physics in the past few decades is discovery of a Higgs-like boson. It was reported on July 3, 2012 by the ATLAS and CMS collaborations of the Large Hadron Collider (LHC), CERN [1]. It has been about 50 years since its theoretical prediction. Eventually, the mass is confirmed to be about 125 GeV, and the properties of spin and coupling are compatible with ones predicted by the Standard Model of particle physics (SM). To begin with, let us briefly explain the importance of Higgs boson and its discovery.

The Higgs boson is the only scalar among the SM particles, and does the most important role that triggers the electroweak symmetry breaking (EWSB). In the SM, electroweak symmetry of $SU(2)_L \times U(1)_Y$ is broken down to the electromagnetic symmetry of $U(1)_{EM}$. The Higgs boson with $SU(2)_L \times U(1)_Y$ charge forms wine-bottle (or mexican-hat) type potential,

$$V = \mu_H^2 |H|^2 + \frac{\lambda_H}{4} |H|^4 \quad (1.1)$$

where curvature at origin is negative, $\mu_H^2 < 0$. Since the origin of potential is unstable, the vacuum shifts a stable vacuum with a finite vacuum expectation value (VEV),

$$\langle H \rangle = \sqrt{\frac{-2\mu_H^2}{\lambda_H}} \equiv v . \quad (1.2)$$

Thus the symmetry is *spontaneously broken* because the new vacuum respects only $U(1)_{EM}$ symmetry but the original $SU(2)_L \times U(1)_Y$ symmetry. The Higgs field is re-parametrized as

$$H = v + \frac{h + i\pi}{\sqrt{2}} . \quad (1.3)$$

In the case of global symmetries, Nambu-Goldstone (NG) boson corresponding to a broken symmetry is generated, while in the case of gauge symmetry the NG boson π is absorbed to a

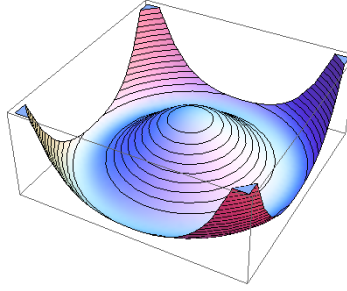


Figure 1.1: Schematic view of Higgs potential

gauge boson making it massive. The radial mode of the potential, h , still remains as physical particle that is what is currently observed at the LHC experiment. The Higgs potential has only two parameters. The VEV, v , is well measured by electroweak precision studies, and the measurement of Higgs mass,

$$m_H^2 = -2\mu_H^2 = \lambda_H v^2 \approx 125 \text{ GeV}, \quad (1.4)$$

determines the last remained parameter. This spontaneous breaking of gauge symmetry is called by Higgs mechanism, which is developed by R. Brout, F. Englert, P. Higgs, G. Guralnik, C.R. Hagen, and T. Kibble [2].¹

The Higgs boson in the SM also gives masses to quarks and leptons through Yukawa interactions. Yukawa interactions are bilinear of fermions plus Higgs field, and once Higgs field obtains a finite VEV, the interactions turn out to be the masses of quarks and leptons. The size of mass is proportional to the strength of each Yukawa interaction. The Higgs field couples to most of elementary particles, Z, W , quarks, and leptons, giving their masses, so the Higgs is ubiquitous in our Universe.

The Higgs boson discovery is triumphs of theoretical prediction based on Quantum Field Theory and of experiments with frontier technologies and international collaborations. The mass of Higgs boson seems arbitrary and might be very heavy, but it is suggested physics without Higgs boson does not guarantee the perturbative unitarity. Massive gauge boson's scattering amplitude grows with $(\text{energy})^2$ due to their longitudinal modes and breaks perturbative unitarity at energy about TeV unless the Higgs boson appears. This is a motivation to construct the collider which focuses on the TeV range. In addition, precise measurements of the electroweak sector favor Higgs mass $\lesssim 150 \text{ GeV}$ as in Fig. 1.2.

The experimental efforts are tremendous. It is basically necessary to design the highest energy machine for search for undiscovered particles. The center of mass energy of LHC was $\sqrt{s} = 7 \text{ TeV}$ and 8 TeV for physics run I and the energy will be upgraded to 14 TeV in run II. Between 2010 and 2012, integrated luminosity is $\sim 30 \text{ fb}^{-1}$,² and in the high-luminosity upgrade the integrated luminosity will be 300 fb^{-1} or more. In contrast, the previous strongest collider, Tevatron at Fermilab, had the maximum energy of $\sqrt{s} = 1.96 \text{ TeV}$ and total integrated luminosity of $\sim 10 \text{ fb}^{-1}$. Developments occurred in the analysis level as well. For instance, since the backgrounds is well understood even in the proton-proton

¹P. Higgs and F. Englert received the Nobel Prize in physics in 2013 for the theoretical discovery of Higgs mechanism.

²b (barn) is an unit of interacting cross section. $\text{b} = 10^{-28} \text{ m}^2 = 100 \text{ fm}^2$.

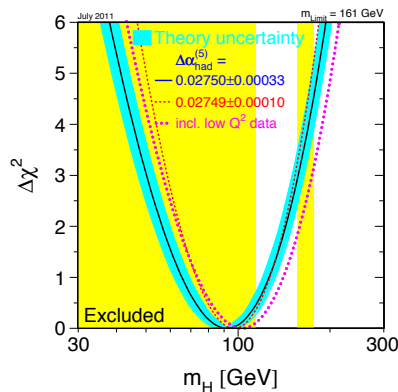


Figure 1.2: $\Delta\chi^2$ for Higgs boson mass based on the electroweak precision measurements before its discovery from Ref. [3]. With 1σ level, $m_H \lesssim 150$ GeV was favored.

collisions where huge and various background usually exists, $h \rightarrow \gamma\gamma$ channel significantly contributed to the Higgs boson discovery even if the Higgs signal is very weak compared to the background in this channel.

Now we understand the electroweak symmetry breaking better; the Higgs potential actually exists. However, the potential in particular its mass term is unsatisfactory because no symmetry protects the mass scale of Higgs, and hence the electroweak scale is unstable against the radiative correction. Supersymmetry (SUSY)[4] is the leading theory beyond the SM (BSM) to deal with this issue. In this article we study aspects of supersymmetry in light of LHC run I results.

1.2 Beyond the Standard Model

Observations at the ATLAS and CMS for a new boson is well consistent with the Higgs boson predicted by the SM. Then a question arises: Is particle physics at the end? The answer is clearly no since there are experimental results that cannot be explained within the SM,

- Dark matter in the Universe
- Dark energy in the Universe
- Matter asymmetry in the Universe
- Neutrino masses
- Acausal correlation in the Universe

and also strong CP problem could be categorized together with subjects above. The best example is seen in the pie chart of the Universe's energy content (Fig. 1.3) which is measured by the WMAP satellite and recently updated by the Planck satellite.

The dark energy, dominant composition, is unknown energy source which accelerate expansion of the Universe, and the dark matter is unknown relic abundance created in the early

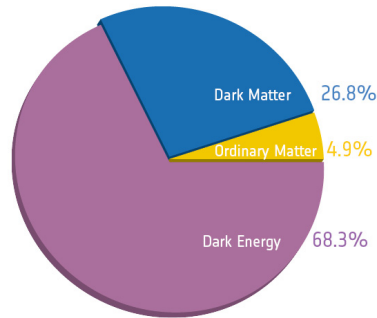


Figure 1.3: Cosmic pie chart of the Universe’s content by Planck satellite. [Credit: ESA/Planck Collaboration [5]]

Universe. It is expected that the dark matter can be explained by a new elementary particle. A typical scenario is that the dark matter is a weakly interacting massive particle (WIMP), and many BSM models provide WIMP candidates. In WIMP scenario, experiments for direct and indirect detection of dark matter particle have discovery potential. Since the typical mass scale of WIMPs is order of TeV, there is a good chance to discover the dark matter at the LHC. On the other hand, the dark energy is still very mysterious.

We do not understand an origin of ordinary matter (particle) of 4.9% in the pie chart. This is because particles and antiparticles have almost the same nature, and in the early Universe they equally existed and are supposed to annihilate each other. However, the current Universe has only matters. This occurs for the CP-violation, asymmetry between particle and antiparticle, but the size of CP-violation in the SM is not sufficient to explain the current abundance of matter.

Neutrino masses are confirmed by observations of neutrino oscillation. The mass difference and mixing are measured by various experiments, and one neutrino at least has mass of $\gtrsim 50$ meV. On the other hand, the SM predicts that all the neutrinos are massless. This clearly shows new physics must exist.

In our observable sky, there are correlation between points crossing the causal horizon. It is understood by inflation theory, an essential idea in the modern cosmology. Inflation leads to exponential expansion in a very early stage of the Universe stretching small fluctuations to a large scale. A new scalar field that makes inflation dynamics is needed unless Higgs field, a unique scalar in the SM, plays such a role of inflaton. This does not directly suggests that new physics in the electroweak sector but imply some new physics.

Each of experimental results above requires some new physics beyond the Standard model. Another motivation to extend the SM is actually from the Higgs boson. Although the Higgs boson or mechanism plays a crucial role leading to the electroweak scale, the mass scale is not protected by any symmetry. Note that this is not theoretical contradiction, but thinking of the high-scale physics such as Grand Unification, quantum gravity or String Theory, the scale mass unlike the electron (fermion) mass is too sensitive to stabilize their scale. This is so-called the “naturalness problem” and quantified by “fine-tuning.” The leading candidate to solve the issue is supersymmetry. Supersymmetry embeds a scalar in a multiplet with a fermion, and, roughly speaking, the multiplet is protected by sort of “chiral symmetry” thanks

to the fermion. We will discuss the point in the next section.

Another approach to the problem is to consider the Higgs boson as a pseudo-NG boson of some global symmetry like a pion. The global symmetry which is broken and generates pseudo-NG bosons guarantees technical naturalness of Higgs boson mass.

1.3 Supersymmetry

1.3.1 Motivation

There is a question why electroweak scale, or vacuum expectation value, is at a scale we observe. Low-energy supersymmetry was introduced to answer such a question. We know at least there must be a new scale, planck scale (M_{pl}) at which quantum gravity appears,³ and the electroweak scale can receive radiative corrections of the order of M_{pl} . In other words, this is because no symmetry forbids emergence of quadratic divergence to Higgs boson mass. Supersymmetry saves this issue leading the divergence to logarithmic one. Before going to the detail, let us give an example where this way of thinking such as naturalness worked. This analogy is given by H. Murayama [6].

Back to 19th century, the electrodynamics had a similar problem that self-energy of the electron is linearly divergent. In the nonrelativistic electrodynamics, the Coulomb part of the self-energy is just the expectation value of $\frac{e^2}{2} \frac{1}{4\pi|\mathbf{x}-\mathbf{x}'|}$ as \mathbf{x}' approaches \mathbf{x} ,

$$\begin{aligned} E_{self} &= \frac{e^2}{2} \int d^3x \psi_{NR}(\mathbf{x}) \left(\int \frac{d^3x'}{4\pi|\mathbf{x}-\mathbf{x}'|} \delta^3(\mathbf{x}-\mathbf{x}') \right) \psi_{NR}^*(\mathbf{x}') \\ &= \frac{e^2}{2} \int d^3x \psi_{NR}(\mathbf{x}) \left(\int d^3p \int \frac{d^3x'}{(2\pi)^3} \frac{e^{i\mathbf{p}(\mathbf{x}-\mathbf{x}')}}{4\pi|\mathbf{x}-\mathbf{x}'|} \right) \psi_{NR}^*(\mathbf{x}) \\ &= \frac{e^2}{2(2\pi)^3} \int \frac{d^3p}{\mathbf{p}^2} = \frac{\alpha}{\pi} \int^\Lambda d|\mathbf{p}|, \end{aligned} \quad (1.5)$$

where Λ is a cutoff scale of the theory. Then the correction above leads to the relation between bare mass and observed mass of electron,

$$m_{e,\text{obs}} = m_{e,0} + E_{self}, \quad (1.6)$$

where $m_{e,0}$ is a bare electron mass. If we substitute $\Lambda = 10^3 \times 200$ MeV corresponding to observed electron size 10^{-3} fm, the bare mass must be highly-tuned with three orders of magnitude to give the observed electron mass of 0.51 MeV. Furthermore, the perturbation theory does not work anymore below $r \approx \frac{\alpha}{\pi}/m_e \simeq 1$ fm.

The unnaturalness is cured by the discovery of positron. The relativistic theory of electrodynamics requires the existence of positron, and in the short distance, quantum fluctuation allows electron-positron pair creation and annihilation. It leads to a new correction of electron self-energy, and as a result cutoff dependence of the self-energy in the short-distance

³There are scenarios that the planck scale itself is actually close to the weak scale. This happens when multiple extra dimensions or warped extra dimension exist where only gravity can propagate that is why the gravity force seems much weaker.

becomes logarithmic rather than linear,

$$E_{self} = \frac{3}{2\pi} \frac{e^2}{4\pi} m_e \log \frac{\Lambda}{m_e}. \quad (1.7)$$

The result is first calculated by V.F. Weisskopf in 1939 [8].⁴ In the modern understanding by Quantum Field Theory, the cancelation is a consequence of chiral symmetry. The chiral symmetry is actually broken but only *softly* by the electron mass. In the exact limit of chiral symmetry, the mass of electron mass is not generated perturbatively, and therefore the radiative corrections to the electron mass must be proportional to the breaking parameter, the electron mass itself. The chiral symmetry controls the radiative correction better.

The motivation for supersymmetry is very similar to the self-energy of electron; simply replacing the electron self-energy in the electrodynamics and chiral symmetry with the Higgs mass in the Standard Model and supersymmetry, respectively. In the SM, the radiative correction from some high scale is expected to be

$$\mu_H^2 = \mu_{H,0}^2 + \frac{g^2}{16\pi^2} \Lambda^2. \quad (1.8)$$

where $\mu_{H,0}^2$ is a bare Higgs mass, and g is $\mathcal{O}(1)$ coupling. The scalar mass term $|H|^2$ is singlet under any symmetry, and the coefficient cannot be a soft breaking parameter of some symmetry. Supersymmetry cures this problem in a way that chiral symmetry is promoted for bosons because fermion and boson are transformed each other by supersymmetry. However, since we have not observed supersymmetric particles in the low-energy, it must be broken *softly* by a breaking scale of M_{SUSY} . The self-energy of the Higgs boson is roughly

$$\mu_H^2 = \mu_{H,0}^2 + \frac{g^2}{16\pi^2} M_{SUSY}^2 \log \frac{\Lambda^2}{m_{weak}^2}. \quad (1.9)$$

The structure is same as the self-energy of electron: the correction must be proportional to the breaking parameter of M_{SUSY} and the cutoff sensitivity is only logarithmic. Since the Higgs mass parameter is at weak scale, we expect the SUSY breaking scale is also in the same scale. In the most natural case,

$$m_{SUSY} \sim m_{weak}. \quad (1.10)$$

However the naïve expectation of Eq. (1.10) is challenged by the observed Higgs mass and the direct search for supersymmetric particles at the LHC. We discuss these tensions in Sec. 1.6. In this article, we study possible scenarios of low-energy supersymmetry in light of these results.

1.3.2 Algebra

Supersymmetry is a continuous symmetry which transforms boson to fermion and vice versa. The supersymmet charge Q is grassmanian, and its conjugate is denoted by Q^\dagger ,

$$\{Q, Q\} = \{Q^\dagger, Q^\dagger\} = 0, \quad (1.11)$$

⁴For more discussion and calculation, see for example Sec. 2-8, 4-7 of “Advanced Quantum Mechanics” by J.J. Sakurai [7].

and Q acts on a state such that

$$Q|\text{Boson}\rangle = |\text{Fermion}\rangle, \quad (1.12)$$

and vice versa. Supersymmetry is non-trivial extension of Poincaré symmetry, and then it relates to the special transformation operator, P_μ ,

$$\{Q, Q^\dagger\} \sim P_\mu, \quad (1.13)$$

$$[Q, P_\mu] = [Q^\dagger, P_\mu] = 0. \quad (1.14)$$

The first line tells supersymmetric vacuum should be zero energy vacuum since $H = P_0 \sim QQ^\dagger$. In other words, the supersymmetry breaking vacuum $Q|0\rangle \neq 0$ has non-zero energy,

$$\langle 0|H|0\rangle \sim \langle 0|QQ^\dagger|0\rangle \neq 0. \quad (1.15)$$

The second line holds energies (masses) of boson and fermion same,

$$E_F|\text{Fermion}\rangle = H|\text{Fermion}\rangle = HQ|\text{Boson}\rangle = E_BQ|\text{Boson}\rangle. \quad (1.16)$$

Let us briefly comment on construction of massless multiplet. For the minimal supersymmetric case in 4D, referred to as $\mathcal{N} = 1, D = 4$, have two kinds of multiplet for renormalizable theories. If we start with a state with zero helicity using $(Q^\dagger)^2 = 0$,

$$|h = 0\rangle, \quad Q^\dagger|h = 0\rangle \sim |h = \frac{1}{2}\rangle, \quad (1.17)$$

and their the CPT conjugate states form a supersymmetric multiplet, called chiral supermultiplet,⁵ consisting of a Weyl fermion (quark and lepton) and a complex scalar. Starting with a state with helicity $\frac{1}{2}$,

$$|h = \frac{1}{2}\rangle, \quad Q^\dagger|h = \frac{1}{2}\rangle \sim |h = 1\rangle, \quad (1.18)$$

and their CPT conjugate states form another supermultiplet consisting of a Weyl fermion and a vector. We call this multiplet vector supermultiplet.

In the extended supersymmetry, the multiplets become bigger because there are multiple supersymmetry charges. For example in $\mathcal{N}=2$ case, two kinds of charge Q_1 and Q_2 have properties,

$$Q_1^\dagger Q_2^\dagger \neq 0, \quad (Q_1^\dagger)^2 = (Q_2^\dagger)^2 = 0. \quad (1.19)$$

From a state with helicity $-\frac{1}{2}$,

$$\begin{aligned} &|h = -\frac{1}{2}\rangle, \\ &Q_1^\dagger|h = -\frac{1}{2}\rangle, \quad Q_2^\dagger|h = -\frac{1}{2}\rangle, \\ &Q_1^\dagger Q_2^\dagger|h = -\frac{1}{2}\rangle, \end{aligned} \quad (1.20)$$

⁵Strictly speaking, the condition for chiral multiplet is given by $\bar{D}\Phi = 0$ where Φ is a superfield and \bar{D} is super-covariant derivative.

and their CPT conjugate states form a multiplet, called hypermultiplet, of two complex scalars and two Weyl fermions. A hypermultiplet corresponds to two chiral supermultiplets. On the other hand, a new vector supermultiplet is obtained by,

$$\begin{aligned} & |h = 0\rangle, \\ & Q_1^\dagger |h = 0\rangle, Q_2^\dagger |h = 0\rangle, \\ & Q_1^\dagger Q_2^\dagger |h = 0\rangle. \end{aligned} \tag{1.21}$$

Hence there are a complex scalar, a vector and two Weyl fermions. This multiplet corresponds to a chiral supermultiplet and a vector supermultiplet of $\mathcal{N}=1$. Note that there is a rotation symmetry which exchanges Q_1 and Q_2 , called $SU(2)_R$ symmetry. Scalars of hypermultiplet and fermions of vector supermultiplet (gauginos) are doublets of $SU(2)_R$, and the others are singlet. When one considers 5D theory, minimal supersymmetry corresponds to $\mathcal{N} = 2, D = 4$ since Weyl fermions cannot exist because γ_5 is not 5D Lorentz invariant.

1.3.3 The Minimal Supersymmetric Standard Model

In order to build models, we use superfield and superspace for explicit supersymmetric invariance. Here we use the consequences, for more detail see Refs. [4, 9]. We describe the Minimal Supersymmetric Standard Model (MSSM) in the following.

Higgs, quark and lepton fields are contained in a chiral superfield (a superfield of chiral supermultiplet). Multiplication of chiral superfields is also a chiral superfield. Terms written in superpotential, $W(\Phi)$, are explicitly supersymmetric where Φ is a chiral superfield and superpotential is a holomorphic function. Yukawa-type interactions are in the superpotential,

$$W = y_U^{ij} H_u Q_i U_j + y_D^{ij} H_d Q_i D_j + y_E^{ij} H_d L_i E_j + \mu H_u H_d. \tag{1.22}$$

Note that there are two chiral superfields for Higgs, H_u and H_d for two reasons. Firstly, a fermionic partner of Higgs boson, Higgsino, gives a new anomaly of gauge symmetry, and then we need an additional Higgs field with opposite charge. Secondly, since the superpotential is holomorphic function, two Higgs bosons are necessary to give masses of up-type and down-type quarks. Scalar components of quark and lepton chiral superfield are called squark and slepton.

Here, we have introduced an assumption, R -parity,

$$R = (-1)^{3(B-L)+F}, \tag{1.23}$$

where B and L are baryon and lepton number, respectively, and $F = 1(0)$ for fermions (bosons). As a superfield, Q, U, D, L , and E are -1 while H_u and H_d are $+1$. This symmetry forbids B and L violating terms, UDD and DQL , which induces proton decay. As long as coupling constants of these terms are sufficiently small to be consistent with lower bound of proton lifetime, R -parity can be broken, and this small breaking is relevant to collider phenomenology.

The gauge interactions and kinetic terms of chiral superfields appear in Kähler potential $K(\Phi, e^{gT^a V^a} \Phi^\dagger)$ where K is a real function and V^a is a vector superfield, a superfield of vector supermultiplet. Pure supersymmetric Yang-Mills theory is also given in Kähler potential. A

fermionic part of V is called gaugino. There are three kinds of gaugino in the MSSM, gluino, Wino, and Bino, corresponding to $SU(3)_C$, $SU(2)_L$, and $U(1)_Y$ gauge symmetry, respectively. The gauginos are R -parity -1 while gauge bosons are $+1$.

The new particles beyond the SM (and additional Higgs boson), Higgsinos, squarks, sleptons, and gauginos are all R -parity -1 , and denoted as \tilde{X} . More detail is given in Table 1.1.

	(Fermion, Boson)	$SU(3)_C$	$SU(2)_L$	$U(1)_Y$	R -parity
H_u	(\tilde{H}_u, H_u)	1	2	1/2	$(-, +)$
H_d	(\tilde{H}_d, H_d)	1	2	-1/2	$(-, +)$
Q	(Q_i, \tilde{Q}_i)	3	2	1/6	$(+, -)$
U	$(u_{Ri}^c, \tilde{u}_{Ri}^c)$	$\bar{\mathbf{3}}$	2	-2/3	$(+, -)$
D	$(d_{Ri}^c, \tilde{d}_{Ri}^c)$	$\bar{\mathbf{3}}$	1	1/3	$(+, -)$
L	(L_i, \tilde{L}_i)	1	2	-1/2	$(+, -)$
E	$(e_{Ri}^c, \tilde{e}_{Ri}^c)$	1	1	1	$(+, -)$
V_C	(\tilde{g}, G_μ)	8	1	1	$(-, +)$
V_L	(\tilde{W}, W_μ)	1	2	1	$(-, +)$
V_Y	(\tilde{B}, B_μ)	1	1	1	$(-, +)$

Table 1.1: MSSM particle contents.

Components of $SU(2)_L$ doublet are labeled by the electromagnetic charge Q given by $Q = T_L^3 + Y$ where $T_L^3(Y)$ is a generator of $SU(2)_L$ ($U(1)_Y$), and then,

$$\begin{aligned} H_u &= (H_u^+, H_u^0), & H_d &= (H_d^0, H_d^-), \\ Q_i &= (u_L, d_L)_i, & L_i &= (\nu, e_L)_i. \end{aligned}$$

The index i represents generation of particles,

$$\begin{aligned} u_i &= (u, c, t), & d_i &= (d, s, b), \\ e_i &= (e, \mu, \tau), & \nu_i &= (\nu_e, \nu_\mu, \nu_\tau). \end{aligned}$$

The lightest sparticle (LSP) is stable for the R -parity conservation. If the LSP is neutralino, that is a mixture of \tilde{B} , \tilde{W}^0 , \tilde{H}_u^0 , and \tilde{H}_d^0 , two important phenomenological consequences are led. First, the LSP is a good dark matter candidate as WIMP, and the weak to TeV scale LSP gives a thermal relic abundance which is the same order of observed relic abundance of the dark matter. Next, the LSP cannot be detected at collider experiments, which leads to a distinct signal with \cancel{E}_T .

There are soft supersymmetry breaking terms,

$$\begin{aligned} \mathcal{L}_{\text{soft}} &= -m_{H_u}^2 |H_u|^2 - m_{H_d}^2 |H_d|^2 - (bH_u H_d + \text{h.c.}) \\ &\quad - m_{Qij}^2 \tilde{Q}_i^\dagger \tilde{Q}_j - m_{u_{ij}}^2 \tilde{u}_{Ri}^{c\dagger} \tilde{u}_{Rj}^c - m_{d_{ij}}^2 \tilde{d}_{Ri}^{c\dagger} \tilde{d}_{Rj}^c - m_{Lij}^2 \tilde{L}_i^\dagger \tilde{L}_j - m_{e_{ij}}^2 \tilde{e}_{Ri}^{c\dagger} \tilde{e}_{Rj}^c \\ &\quad - a_U^{ij} H_u \tilde{Q}_i \tilde{u}_{Rj}^c - a_D^{ij} H_d \tilde{Q}_i \tilde{d}_{Rj}^c - a_E^{ij} H_d \tilde{L}_i \tilde{e}_{Rj}^c + \text{h.c.} \\ &\quad + \frac{M_1}{2} \tilde{B}\tilde{B} + \frac{M_2}{2} \tilde{W}\tilde{W} + \frac{M_3}{2} \tilde{g}\tilde{g} + \text{h.c.} \end{aligned} \tag{1.24}$$

where b is sometimes written as $B\mu$ in the literature. The trilinear terms are often parametrized with an explicit factor of Yukawa coupling as $(a_U)_{ij} = (y_U A_U)_{ij}$. The MSSM

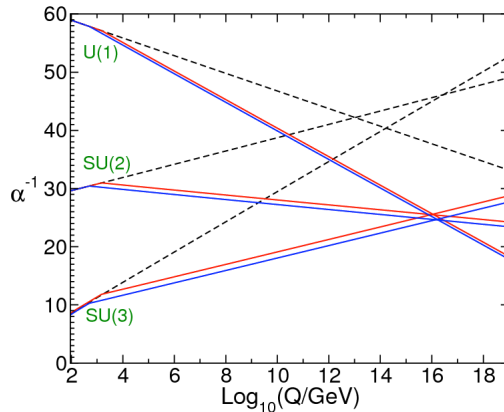


Figure 1.4: Two-loop renormalization group evolution of the inverse gauge couplings $\alpha^{-1}(Q)$ in the Standard Model (dashed lines) and the MSSM (solid lines) from Ref. [4]

has many parameters in these soft breaking terms. And potentially there are a lot of dangerous terms leading to flavor-violation and/or CP-violation which are strongly constrained by the low-energy experiments. A simple solution to this is that the soft-terms have a structure of Minimal Flavor Violation (MFV) where the flavor violation and CP-violation only come from the SM Yukawa couplings. This occurs, for instance, if the supersymmetry breaking is transferred to the MSSM sector through gauge couplings or geometry because either of them does not discriminate flavors. In constructing supersymmetry breaking models, we must address this issue.

A nice feature of the MSSM is that quartic terms of Higgs potential are not free parameters but determined by the gauge couplings,

$$V(H_u^0, H_d^0) = (\mu^2 + m_{H_u}^2)|H_u^0|^2 + (\mu^2 + m_{H_d}^2)|H_d^0|^2 - (bH_u^0 H_d^0 + \text{h.c.}) + \frac{g_1^2 + g_2^2}{8} (|H_u^0|^2 - |H_d^0|^2)^2. \quad (1.25)$$

where g_1 and g_2 are $U(1)_Y$ and $SU(2)_L$ gauge coupling, respectively. H_u^0 and H_d^0 get VEVs,

$$\langle H_u^0 \rangle = v_u = v \sin \beta, \quad \langle H_d^0 \rangle = v_d = v \cos \beta, \quad v \approx 174 \text{ GeV}. \quad (1.26)$$

As in the SM, the lightest Higgs mass at tree-level is determined by the size of quartic coupling,

$$m_h^2 \lesssim m_Z^2 \cos^2(2\beta) \leq (91.2 \text{ GeV})^2, \quad (1.27)$$

where $m_Z^2 = (g_1^2 + g_2^2)v^2/8$. This upper bound is applied for the MSSM, and the Higgs mass can be larger if there are other matters which couple to the Higgs sector, for example, in an extension with a gauge singlet S , a new interaction $W \supset \lambda S H_u H_d$ gives an additional quartic interaction at tree-level. In the MSSM, radiative corrections boost the lightest Higgs mass, and an approximate formula at one-loop level is given by [10]

$$m_{h,\text{MSSM}}^2 \simeq m_Z^2 \cos 2\beta + \frac{3m_t^4}{4\pi^2 v^2} \left(\log \frac{m_t^2}{m_t^2} + X_t^2 \left(1 - \frac{X_t^2}{12m_t^2} \right) \right), \quad (1.28)$$

where we use the common mass for stops, $m_{\tilde{t}} \equiv m_{\tilde{Q}_3} = m_{\tilde{u}_3}$, and $X_t = A_t - \mu \cot \beta$ is left-right mixing. The correction from X_t is maximized at $X_t = \sqrt{6}m_{\tilde{t}}$. The corrections are interpreted as effective Higgs quartic couplings generated at one-loop level. The large stop mass and/or large mixing are needed to accommodate $m_h = 125$ GeV, but they lead to a tension that the naturalness may be suffered from the large supersymmetry breaking in the MSSM. These are discussed in Sec. 1.6.

Supersymmetry, in particular conventional MSSM, is also motivated by the Grand Unification of gauge couplings. In presence of new sparticles, the beta functions of gauge couplings are changed and their couplings seem to unify for introducing supersymmetry in Fig. 1.4. The unification scale is about 10^{16} GeV.

1.3.4 Naturalness in a nutshell

Here we review a basic argument of naturalness and fine-tuning. The original discussion is given in Ref. [11] and others are found in Refs. [12, 13, 14].

In some BSM models, there are various contributions to the quadratic terms of the Higgs potential, and their scale should be of order of weak scale $\mathcal{O}(200$ GeV) or less for the natural EWSB. Since the relevant terms are particularly those in the direction of Higgs VEV, the discussion can be reduced to the one-dimensional potential problem as in the SM. Once again, the Higgs potential and the physical Higgs mass after the EWSB are

$$V = \mu_H^2 |H|^2 + \frac{\lambda_H}{4} |H|^4, \quad (1.29)$$

$$m_H^2 = -2\mu_H^2. \quad (1.30)$$

The quadratic term μ_H^2 is in general a linear combination of various terms of scalar fields. Each contribution δm_H^2 to the Higgs mass should not be much greater than m_H^2 , otherwise different parameters need to be tuned so that m_H^2 is at weak scale. Therefore, a ratio $\delta m_H^2/m_H^2$ should not be large. By using $\delta m_H^2 = -2\delta\mu_H^2$,

$$\Delta \equiv \left| \frac{2\delta\mu_H^2}{m_H^2} \right| \quad (1.31)$$

can be used as a fine-tuning measure. Before knowing the Higgs mass, m_H is replaced with m_Z . Following the same philosophy, the commonly used measure to consider effects from dimensionless parameters [11] is

$$\Delta = \max_x \left| \frac{\partial \log m_{Z(h)}}{\partial \log x} \right|, \quad (1.32)$$

where x is a parameter of the given theory.

Let us give some exercises. Suppose the SM Higgs sector couples to a particle of M_{pl} mass with $\mathcal{O}(1)$ coupling, and we estimate a radiative correction,

$$\delta\mu_H^2 \sim \frac{1}{16\pi^2} M_{pl}^2 \sim 10^{34} \text{ GeV}^2 \quad (1.33)$$

which leads to an extreme fine-tuning,

$$\Delta \sim \frac{2 \times 10^{34} \text{ GeV}^2}{125^2 \text{ GeV}^2} \sim 10^{30}. \quad (1.34)$$

This tuning-level is extremely high, and thus our EWSB is unlikely to happen. Next, let us consider a MSSM scenario where SUSY breaking effects are mediated at a scale of Λ_{mess} . The important contribution is from top-stop sector for y_t coupling. Renormalization group equation gives a large correction to the soft-mass of H_u ,

$$\delta m_{H_u}^2 = -\frac{3y_t^2}{8\pi^2}(m_{Q_3}^2 + m_{u_3}^2 + |A_t|^2) \log \frac{\Lambda_{\text{mess}}}{m_{\text{weak}}}, \quad (1.35)$$

up to one-loop leading-log. For the low-scale mediation, we have

$$\Delta \sim 10 \left(\frac{m_0}{600 \text{ GeV}} \right)^2 \left(\frac{\log \frac{\Lambda_{\text{mess}}}{m_{\text{weak}}}}{6} \right), \quad (1.36)$$

where we choose $m_0^2 = m_{Q_3}^2 = m_{u_3}^2 = |A_t|^2$ for simplicity. We believe $\Delta \sim 10$ tuning is acceptable.

1.4 LHC Run I: Higgs Boson

Production and decay

At the LHC, the Higgs boson is produced in several processes, and their cross sections including corrections of higher order QCD and electroweak interactions are given in Ref. [15]. The result for $\sqrt{s} = 8 \text{ TeV}$ is seen in Fig. 1.5 left.

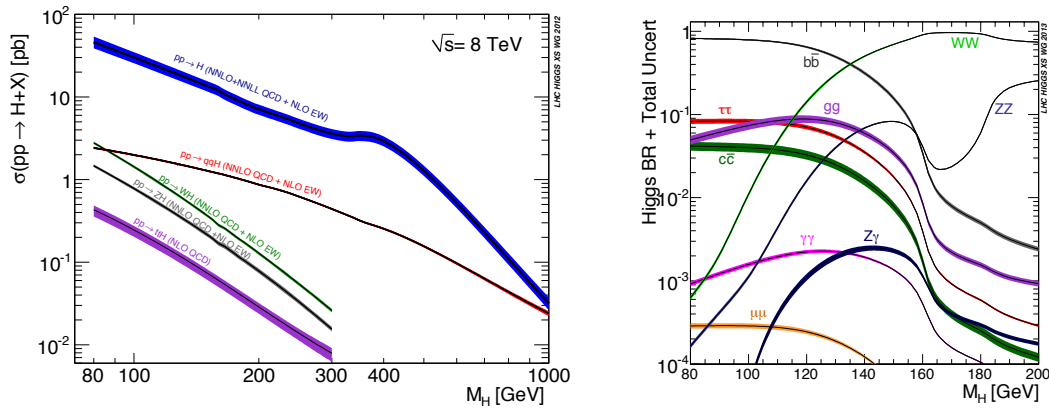


Figure 1.5: *Left*: cross section of Higgs boson as a function of its mass [15]. *Right*: branching Ratio of Higgs boson as a function of its mass [16]. The band shows uncertainties.

The dominant production is a loop-induced channel, gluon-fusion (ggF), that is, two gluons go to Higgs boson via top quark. The cross section is about 19 pb with $+7.2\%$ scale uncertainty⁶ and -6.9% PDF uncertainty at $m_H = 125 \text{ GeV}$ at $\sqrt{s} = 8 \text{ TeV}$. Another production process with top-Yukawa coupling is that a gluon splits into two top quarks and two top quarks from different gluons are fused into a Higgs boson. The final state has a Higgs boson and two top quarks, and this production is denoted by ttH. The cross section is small,

⁶Scale uncertainty is due to choices of factorization scale and renormalization scale.

but this is important because it is a direct information of the Higgs coupling to top quark. Scale and PDF uncertainties of ttH are similar to those of ggF.

Next, there are production processes by electroweak gauge interactions. Two weak gauge bosons (W/Z) which are radiated by initial quarks are fused into a Higgs boson, called Vector Boson Fusion (VBF). To tag this process in the experiments, the Higgs boson should be produced with two forward jets. Another important process is associate production. A virtual W/Z boson emits a Higgs boson, and the final state simply has a W/Z boson and a Higgs boson, and they are denoted by WH and ZH, respectively (VH is referred to both WH and ZH). Scale and PDF uncertainties of VBF and WH are about 0.2 % and 2 %, respectively, while those of ZH are about 2 % and 3 % at $\sqrt{s} = 8$ TeV.

The Higgs boson at mass of 125 GeV has many decay modes as shown in Fig. 1.5 right. The ATLAS and CMS detectors are designed to have good resolutions for $H \rightarrow \gamma\gamma$, and this diphoton decay occurs via top quark and W boson loops. Two contributions are deconstructive and W contribution is larger. A typical process of Higgs production to decay at the LHC is $gg \rightarrow H \rightarrow \gamma\gamma$. Decays into ZZ^* and WW^* are also important, and in particular there are less backgrounds in final states with more electrons and muons by $Z \rightarrow ee, \mu\mu$, and $W \rightarrow e\nu, \mu\nu$. The golden channel is $H \rightarrow ZZ^* \rightarrow 4l$ ($l = e, \mu$). Although large portion of decay is in final states of $b\bar{b}$ and gg , they are not easily discriminated from QCD background. However, a process from VH production to $H \rightarrow b\bar{b}$ decay is be used in the current analysis requiring b -jets and charged leptons.

Higgs mass

Mass of Higgs boson has been measured in $H \rightarrow \gamma\gamma$ and $H \rightarrow ZZ^* \rightarrow 4l$ channels at both ATLAS and CMS. The combined results of each experiment are

$$m_H = 125.5 \pm 0.2 \text{ (stat)}^{+0.5}_{-0.6} \text{ (sys) GeV (ATLAS [17])}, \quad (1.37)$$

$$m_H = 125.7 \pm 0.3 \text{ (stat)} \pm 0.3 \text{ (sys) GeV (CMS [18])}. \quad (1.38)$$

The uncertainty is already within 1 GeV level. Note that there is a difference of measured mass in the two different channels at the ATLAS with $\approx 2.5\sigma$ level. A mass of $m_H = 126.8 \pm 0.2 \text{ (stat)} \pm 0.7 \text{ (sys) GeV}$ is found in the $H \rightarrow \gamma\gamma$ channel and a mass of $m_H = 124.3^{+0.6}_{-0.6} \text{ (stat)}^{+0.5}_{-0.63} \text{ (sys) GeV}$ is found in the $H \rightarrow ZZ^* \rightarrow 4l$ channel. However, for simplicity, we neglect this deviation so far and take the observed mass to be 125 GeV.

Spin and parity

We have treated the observed particle as the Higgs *boson* which has spin 0 and parity even. Here, we briefly discuss other possibilities of spin and parity. The spin measurements are performed in $H \rightarrow \gamma\gamma$, $H \rightarrow ZZ^* \rightarrow 4l$, and $H \rightarrow WW^* \rightarrow l\nu l\nu$ channels [19]. First of all, in $H \rightarrow \gamma\gamma$ channel, Landau-Yang theorem excludes spin 1 hypothesis and it is possible to test $J^P = 0^+, 2^+$ where J is spin and P is parity. The $H \rightarrow ZZ^* \rightarrow 4l$ channel has good sensitivities to $J^P = 0^+, 0^-, 1^+, 1^-, 2^+$. For the spin and parity test, one can examine one hypothesis against another hypothesis using ratio of likelihood. The results of ATLAS and CMS disfavor $J^P = 0^-, 1^+, 1^-, 2^+$ in comparison with $J^P = 0^+$ with $\gtrsim 98$ %C.L. Therefore we conclude the observed particle is certainly Higgs boson like-particle of $J^P = 0^+$.

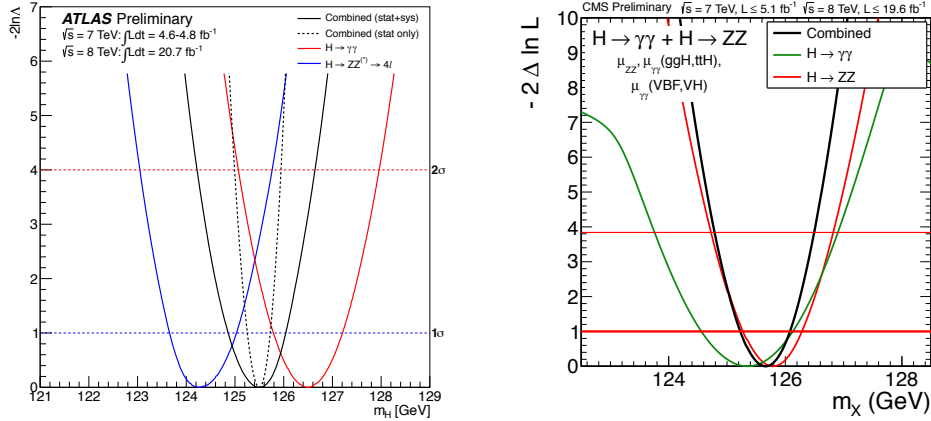


Figure 1.6: 1D likelihood for measured Higgs mass. *Left*: ATLAS result [17], and *right*: CMS result [18]

Signal Strength

Signal strength is studied in various channels. The signal strength is roughly given by

$$n_{\text{signal},i \rightarrow f}^{\text{obs}} = \mu_f B_{SM,f} \times \mu_i \sigma_{SM,i} \times (\text{Integrated Luminosity}), \quad (1.39)$$

where $\sigma_{SM,i}$ is SM production cross section of process i , $B_{SM,f}$ is SM Higgs boson production cross section of process i , the branching ratios $B_{SM,f}$ of the SM Higgs boson decays of f final state, and μ_i and μ_f are relative strengths of production and decay, respectively. The number of signal events expected from each combination of production and decay modes is scaled by the corresponding product $\mu_i \mu_f$.

Results from the ATLAS and CMS are basically consistent with SM prediction. Although the errors of each channel is still large, it is possible to constraint BSM models which predicts large deviation of signal strength. The $H \rightarrow \gamma\gamma$ channel at the ATLAS is slightly larger, but this is not conclusive.

1.5 LHC Run I: Supersymmetric Particles

Searches for supersymmetric particles (sparticles), heavy Z/W -bosons, fourth generation quarks, and many other phenomena predicted by BSM models have been carried out at the LHC. Here we present results of sparticle searches assuming R -parity conservation.

A typical (expected) scenario is that the colored sparticles are produced in pair and they decay into the neutral LSP emitting many jets and/or leptons⁷ (cascade decay). The mass gap between those colored particles and the LSP are expected to be large such as $\gtrsim 500$ GeV, which is certainly true for “Minimal Supergravity” or Constrained Minimal Supersymmetric Standard Model (CMSSM) scenarios [23], and then the LSP carries large momentum reflecting the mass gap. While the neutral LSPs themselves are not detected

⁷Leptons in the sense of collider physics mean electrons and muons, not tau leptons. Since tau leptons decay before reach to the detector, they behave like collimated QCD jets.

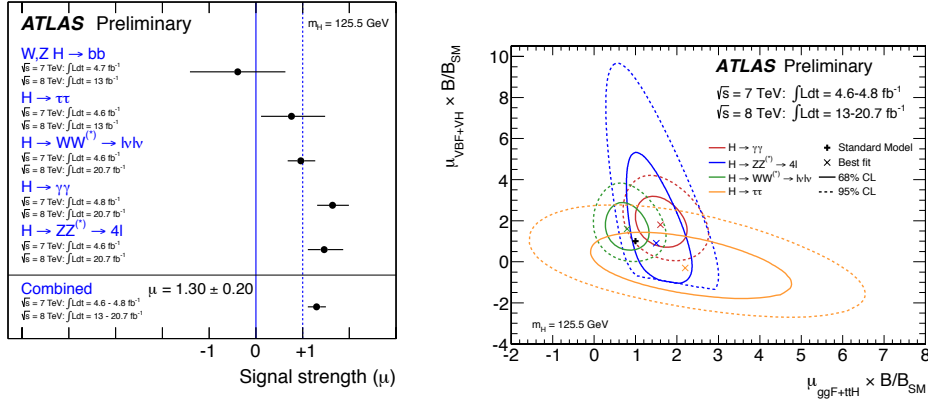


Figure 1.7: *Left*: 1D signal strengths in each decay mode measured by the ATLAS. *Right*: 2D signal strengths depending on production channels. Both plots from Ref. [20].

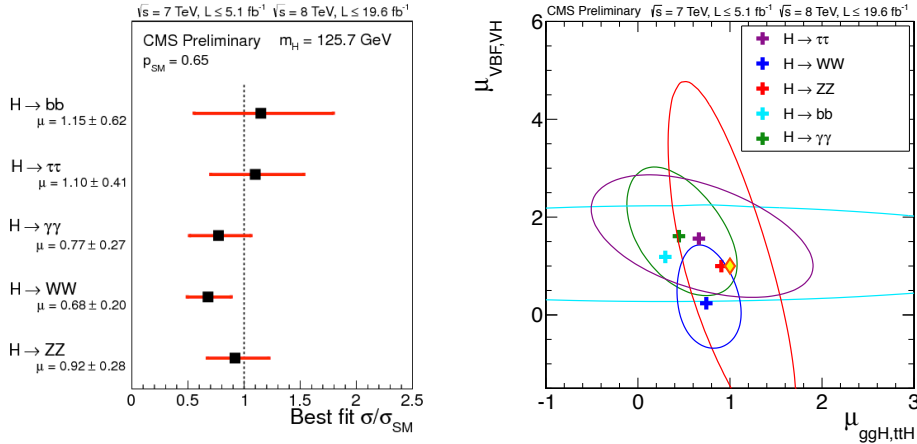


Figure 1.8: *Left*: 1D signal strengths in each decay mode measured by the CMS. *Right*: 2D signal strengths depending on production channels. Both plots are from Ref. [18]

because they are stable for the R -parity, we can know their total transverse momentum thanks to momentum conservation. The size of missing momentum (\cancel{P}_T) is usually referred to \cancel{E}_T . In the SM, neutrinos do the same role of LSP, and therefore high-energy SM processes emitting neutrinos such as $t\bar{t}$ +jets and W +jets are background in the sparticle searches with \cancel{E}_T .

Particles emitted during cascade decays are highly model-dependent, but, in R -parity conserving case, we can expect at least a few jets as well as \cancel{E}_T because the produced parents are colored while the LSP are neutral. If bottom quarks which form b -jets or energetic charged leptons are emitted, the signal becomes more distinct from SM background.

The dominant production of sparticles are $\tilde{g}\tilde{g}, \tilde{g}\tilde{q}$ and $\tilde{q}\tilde{q}$ pair productions where \tilde{q} represents squarks of the first and second generations. Multijet+ \cancel{E}_T searches constrain many simple models of supersymmetry. For example, the CMSSM is excluded up to $m_{\tilde{q}} \approx 1.6 \text{ TeV}$ (gluino decoupling), $m_{\tilde{g}} \approx 1.2 \text{ TeV}$ (squark decoupling) as shown in Fig. 1.9. Right panel of Fig. 1.9 shows multijet+ \cancel{E}_T searches constraint a simplified model of gluino, squarks, and

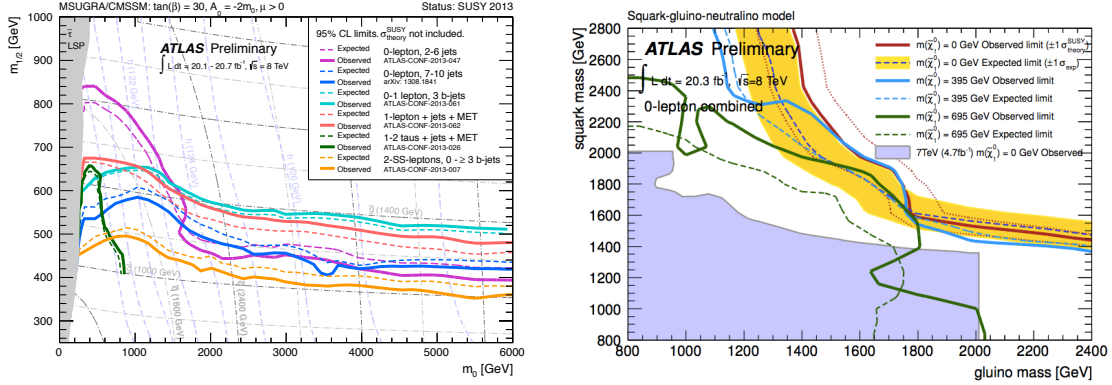


Figure 1.9: *Left*: constraints on CMSSM with large A_t and large $\tan\beta$ by multiple analyses [21, 22]. *Right*: constraint on a simplified model of gluino, squarks, and neutralino in the right [21].

neutralino where gluino and squark masses are varied independently with desecrate choices of neutralino mass. The limit on this model is $m_{\tilde{g}}, m_{\tilde{q}} \gtrsim 1.4$ TeV with massless LSP. When $m_{\tilde{g}} \simeq m_{\tilde{q}}$, the limit for simplified Model and CMSSM is extended up to about 1.7 TeV.

Let us remind that $m_{SUSY} \gg m_{weak}$ gives rise to fine-tuning for the EWSB. The above results seem to disfavor low-scale supersymmetry. However, very different consequences are led if the spectrum is nearly degenerate (compressed), *i.e.* the mass gap between the LSP and produced parent particles are relatively small, say $\lesssim 500$ GeV (not necessarily as small as $\lesssim 50$ GeV). This result shows much weaker constraints because the smaller mass gap lowers \cancel{E}_T . For instance, for the previous simplified model with $m_{\tilde{g}} \approx m_{\tilde{q}}$, the gluino and squark masses are excluded up to 1.7 TeV with massless LSP, while the bound is relaxed down to 900 GeV with 200 GeV mass gap as seen Fig. 1.10. Therefore low-energy is still possible if the spectrum is compressed. In searches for this scenario, initial state radiation (ISR) will be important. An energy scale of ISR reflects the mass scale of parent colored particles, and thus we can expect energetic ISRs for the heavy particle productions. \cancel{E}_T also gets larger because LSPs are also recoiled by ISRs.

Constraints on the first and second generation squarks are indirect information for the naturalness. The third generation squarks, in particular stop, are more relevant to the naturalness. Of course, if one defines an explicit model, the first and second generation squarks bounds are relate to the stop mass bound. Stops are produced from gluons initial state, and there are basically four decay patterns of the light stop: one via chargino, $\tilde{t}_1 \rightarrow b\tilde{\chi}_1^\pm \rightarrow bW^{(*)}\tilde{\chi}_1^0$, and the others directly to the LSP, $\tilde{t}_1 \rightarrow t\tilde{\chi}_1^0$, $\tilde{t}_1 \rightarrow Wb\tilde{\chi}_1^0$, and $\tilde{t}_1 \rightarrow c\tilde{\chi}_1^0$. The former is studied with various assumptions of chargino mass, and the results are shown in left of Fig. 1.11. The strongest limit is $m_{\tilde{t}_1} \gtrsim 600$ GeV. For the latter decays shown in right of Fig. 1.11, the stop mass is excluded up to 700 GeV with massless LSP. However, these limits are also relaxed down to $m_{\tilde{t}_1} \sim 200$ GeV when the mass gap is small. Note that production of stops is not only from direct stop production but also from gluino decays, and in this case limits becomes more stringent. Hence, the constraints are model-dependent.

Finally let us briefly comment on other searches. Direct searches for EW-inos give bounds,

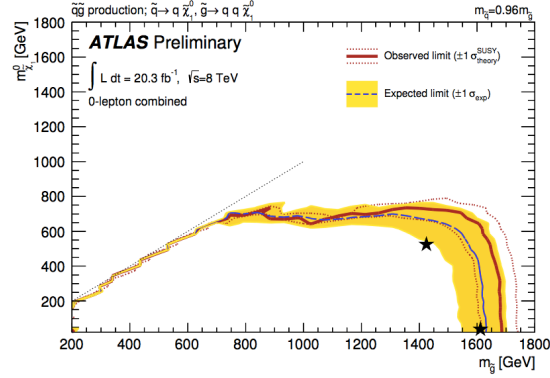


Figure 1.10: Squark-gluino-neutralino simplified model fixing squark mass as $m_{\tilde{q}} = 0.96m_{\tilde{g}}$ [21].

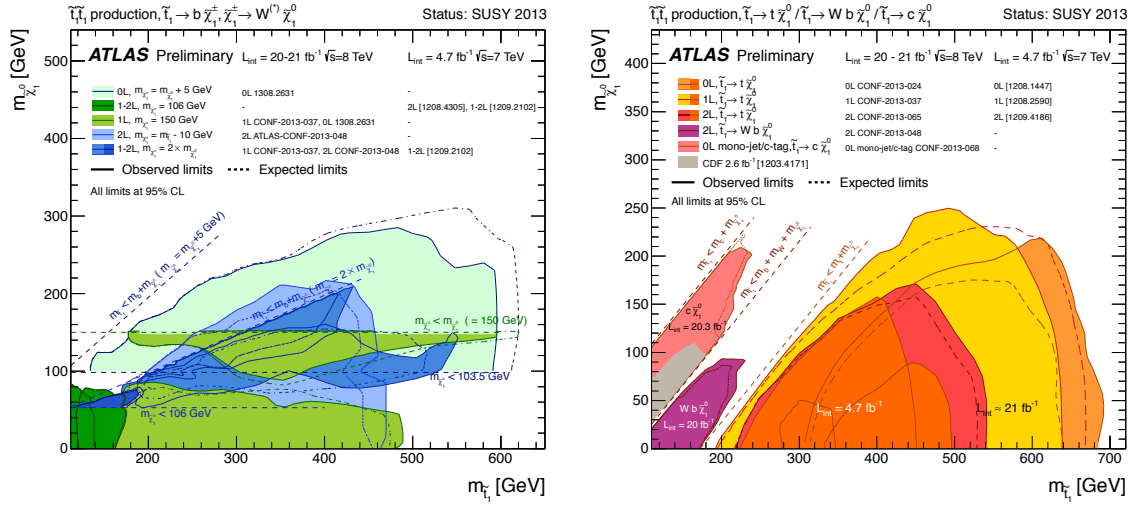


Figure 1.11: Direct stop searches for $\tilde{t}_1 \rightarrow b\tilde{\chi}_1^\pm \rightarrow bW^{(*)}\tilde{\chi}_1^0$ in the left panel and for $\tilde{t}_1 \rightarrow t\tilde{\chi}_1^0$, $\tilde{t}_1 \rightarrow Wb\tilde{\chi}_1^0$, and $\tilde{t}_1 \rightarrow c\tilde{\chi}_1^0$ in the right panel [22]

sometimes up to 600 GeV, but the bound again depends on spectrum and decay patterns [22]. Scenarios with R -parity violation (RPV) are studied. Although baryonic RPV leads to no \cancel{E}_T events, gluino mass is excluded up to about 900 GeV [24].

1.6 Directions for low-energy Supersymmetry

1.6.1 Tensions by LHC Run I

Here is a short summary of the LHC run I results relevant to supersymmetry,

- New discovered particle is compatible with SM Higgs boson
- Observed mass of the new particle is 125 GeV, whereas the MSSM predicts the lightest Higgs mass is $m_h \leq 91.2$ GeV at tree-level

- The CMSSM and simplified model with massless LSP are excluded up to $m_{\tilde{q}} \simeq m_{\tilde{g}} \simeq 1.7$ TeV, while sub-TeV scenario is still possible when the spectrum is compressed
- Constraints on stop mass are model-dependent, and $m_{\tilde{t}_1} \sim 200$ GeV is still allowed.

Searches for particles based on \cancel{E}_T constraint a lot of natural region of many supersymmetric models. As discussed above, if the spectrum is compressed, limits from LHC are much more relaxed. However, a motivation and an explicit model for low-energy supersymmetry with a compressed spectrum have not been discussed while collider studies are carried out by using simplified models. Also, after the Higgs discovery, it is necessary to discuss such a model with a compressed spectrum in the context of Higgs mass and fine-tuning. We give explicit such a model and study its phenomenology.

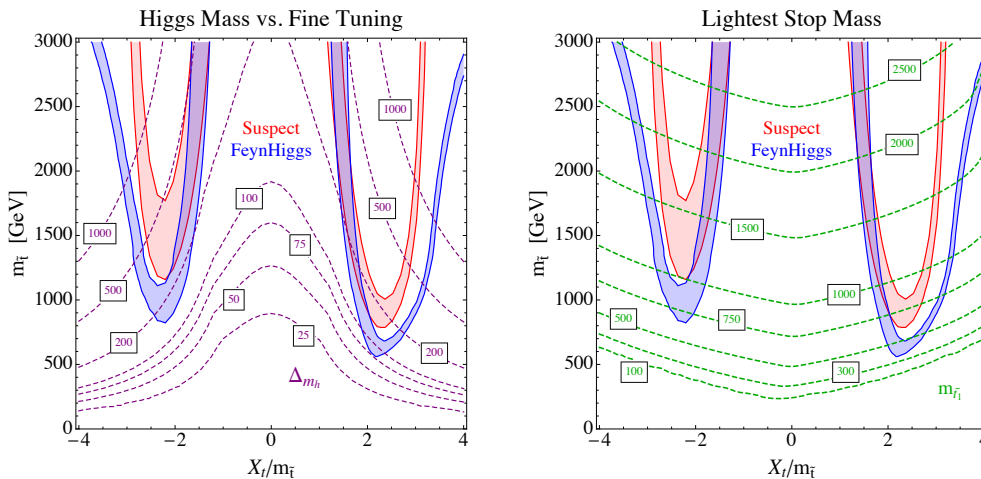


Figure 1.12: Plots for fine-tuning (*left*) and the lightest stop mass (*right*) as function of stop soft mass $m_{\tilde{t}}$ and mixing X_t in Ref. [14]. The SM-like Higgs mass is fixed to be 125 GeV calculated by two different softwares at two-loop level, **FeynHiggs** and **Suspect**. The tuning measure is $\Delta = |\partial \log m_h^2 / \partial \log x|$ with low mediation scale $\Lambda = 10$ TeV.

The collider limits are model-dependent and can be relaxed by a compressed spectrum or R -parity violation, or when particles unnecessary for naturalness are taken to be heavy. Even if particles evade detection for we must address the heavy Higgs mass.

In the MSSM, large radiative corrections by large stop mass and/or large mixing as in Eq. (1.28) to the SM-like Higgs mass are required to accommodate $m_h = 125$ GeV. However, the large stop mass and X_t feed in $m_{H_u}^2$, and therefore the fine-tuning is caused. This tension is seen in Fig. 1.12. Assuming low mediation scale $\Lambda = 10$ TeV it tells $\Delta \gtrsim 100$ ($\Delta^{-1} \lesssim 1\%$) is needed and the large mixing nearly $X_t \sim \sqrt{6}m_{\tilde{t}}$ is favored. The lightest stop mass should be $m_{\tilde{t}_1} \gtrsim 500$ GeV. For the CMSSM scenarios, the tension is worse [25], *i.e.* the fine-tuning is at best $\Delta \gtrsim 10^3$.

Since we know the MSSM requires about 1% tuning at least, possibilities beyond the minimal theory should be taken into account. For example, a singlet extension called Next-to-Minimal Supersymmetric Standard Model (NMSSM) has a new source of the lightest Higgs

mass at tree-level, and therefore the tuning tend to be relaxed. Therefore, we also study an extended Higgs sector focusing on the tension of the Higgs mass and natural EWSB.

1.6.2 Organization of this thesis

In this thesis we discuss low-energy supersymmetry in light of the LHC run I results, with particular concerns as follows.

- Compressed spectrum
- Natural Higgs sector beyond the MSSM

At first, we present an explicit model with a compressed spectrum in Ch. 2. We call it Compact Supersymmetry. The universality of gaugino, squark, and slepton masses is led by SUSY breaking from compactified extra dimensions, called Scherk-Schwarz mechanism. The model is explicitly testable since it has only three parameters, a size of extra dimension, SUSY breaking scale, and supersymmetric Higgs mass. In Ch. 3 we study Higgs mass, fine-tuning, dark matter nature, and collider constraint. The Higgs mass is generally large because large A -term is predicted. Chs. 2, 3 are based on work of Ref. [26]. For future prospect, we discuss that a kinematic variable M_{T2} is useful to search for BSM particles with a compressed spectrum in Appendix D based on work of Ref. [27].

Next, we focus on the Higgs sector in particular the tension between Higgs mass and fine-tuning. We show that an extended Higgs sector with two gauge singlets has a new window of natural theory of EWSB in Ch.4. Unlike the MSSM and NMSSM favor lower mass scale of sparticles, in the new framework a singlet scalar is favored to be extremely heavy. This gives a non-decoupling effect without upsetting naturalness. In Ch. 5 we study constraints and future prospect of the model at the LHC and future e^+e^- linear collider. They are based on work of Ref. [28]. We finish with an overall summary in Ch. 6.

Part I

Supersymmetry, Extra Dimension and Compressed Spectrum

2

Compact Supersymmetry

2.1 Introduction

Supersymmetry has widely been regarded as the prime candidate for physics beyond the standard model [4]. It can explain the dynamical origin of electroweak symmetry breaking through renormalization group effects and provide a natural candidate for the cosmological dark matter in its simplest incarnations. In particular, it stabilizes the large hierarchy between the electroweak scale \approx TeV and the quantum gravity scale $\approx 10^{15}$ TeV against radiative corrections to the Higgs mass parameter. Barring a fine-tuning among parameters of the theory, this consideration strongly suggests the existence of sparticles below \approx TeV. The mass spectrum of sparticles has been mostly discussed within the CMSSM framework [23], which typically generates a widely spread spectrum leading to experimentally identifiable large visible and missing energies.

However, no experimental hints have been seen so far at the Large Hadron Collider (LHC), which has led to substantial anxiety in the community. Moreover, the suggested mass of 125 GeV for the Higgs boson by the LHC data [1, 29] is not easily accommodated in the MSSM, where one has to rely on radiative corrections to push the Higgs boson mass beyond the tree-level upper bound of $m_Z \simeq 91$ GeV. These requirements push the scalar quark masses well beyond the TeV within the CMSSM.

There are three main suggestions to allow for supersymmetry without the signal so far, within the context of R -parity conserving supersymmetry. One is to simply accept a fine-tuning to maintain the hierarchy against radiative corrections, at a level significantly worse than a percent. Quite often, the anthropic principle is brought in to justify this level of fine-tuning [30]. The second is to keep sparticles relevant to the Higgs mass parameter below TeV while to assume all other sparticles well beyond TeV [31]. The third is to assume that all sparticles are compressed (nearly degenerate) making them somewhat hidden from experimental searches due to low Q -values in visible and missing energies. The last option,

however, has been discussed only phenomenologically [32], lacking theoretical justifications based on simple and explicit models of supersymmetry breaking.

In this chapter, we point out that the third possibility of a compressed sparticle spectrum is quite automatic when supersymmetry is broken by boundary conditions in compact extra dimensions, the so-called Scherk–Schwarz mechanism [33, 34]. With the simplest extra dimension—the S^1/\mathbb{Z}_2 orbifold—the mechanism has a rather simple structure [35]. In particular, locating matter and Higgs fields in the bulk and on a brane, respectively, and forbidding local-parity violating bulk mass parameters for the matter fields, the theory has only four parameters relevant for the spectrum of sparticles: the compactification scale $1/R$, the 5D cutoff scale Λ ($> 1/R$), the supersymmetry breaking twist parameter α ($\in [0, \frac{1}{2}]$), and the supersymmetric Higgs mass μ .

Using the common notation in the MSSM, the spectrum of sparticles is given at the compactification scale $\approx 1/R$ as

$$\begin{aligned} M_{1/2} &= \frac{\alpha}{R}, & m_{\tilde{Q}, \tilde{U}, \tilde{D}, \tilde{L}, \tilde{E}}^2 &= \left(\frac{\alpha}{R}\right)^2, & m_{H_u, H_d}^2 &= 0, \\ A_0 &= -\frac{2\alpha}{R}, & \mu &\neq 0, & B &= 0, \end{aligned} \tag{2.1}$$

at tree-level. While these masses receive radiative corrections from physics at and above $1/R$, they are under control because of the symmetries in higher-dimensional spacetime, and thus can naturally be small. Therefore, in this limit, the theory essentially has only three free parameters:

$$\frac{1}{R}, \quad \frac{\alpha}{R}, \quad \mu. \tag{2.2}$$

This rather compact set of parameters gives all the sparticle as well as the Higgs boson masses.

Even though Eq. (2.2) gives two less parameters than in the traditional CMSSM framework, we show that it still leads to viable phenomenology. In addition, it solves the flavor problem that often plagues models of supersymmetry breaking, because the geometry is universal to all scalar particles and hence respect a large flavor symmetry. The problem of accommodating a large enough Higgs boson mass is ameliorated by the near-degeneracy between \tilde{t}_L and \tilde{t}_R , and $|A_t| \approx 2m_{\tilde{t}}$. And the compressed spectrum at tree-level automatically achieves a compact spectrum that allows sparticles to be hidden from the current searches even when they are below TeV.

This chapter is organized as follows. We first review 5D supersymmetric gauge theory. Then we investigate supersymmetry breaking by boundary conditions in the S^1/\mathbb{Z}_2 orbifold, and present the simplest model we study. In Ch. 3 we present the low-energy structure of the model and discuss its phenomenology.

2.2 5D Supersymmetric Lagrangian

To begin with, we need to prepare 5D Lagrangian with a minimal supersymmetry. Constructing this Lagrangian is not trivial and actually quite complicated, but there is a way to write down supersymmetric theories in higher dimensions within the familiar $\mathcal{N}=1$, $D=4$ superspace [36]. However, higher dimensional part of Lorentz symmetry is not clear within

superspace. Lorentz symmetry is manifest after integrating out (or field redefinition of) auxiliary fields.

The minimal supersymmetry of 5D corresponds to $\mathcal{N} = 2$, $D = 4$, and therefore $SU(2)_R$ global symmetry exists. We start the theory in the superspace and derive component Lagrangian with explicit full Lorentz symmetry and $SU(2)_R$ global symmetry. Note that the superspace formalism is useful to interpret the Scherk-Schwarz supersymmetry breaking as Radion Mediation as we will see later in Sec. 2.4.

We basically follow notations of ‘‘Supersymmetry and Supergravity’’ by J. Wess and J. Bagger [9] for spinor formulae and so on. The only difference is that we adopt a metric of $g^{MN} = \text{diag}(+, -, -, -, -)$ instead of one used in the book, $g^{MN} = \text{diag}(-, +, +, +, +)$, where $M = \mu, 5$ and $\mu = 0, 1, 2, 3$. To go to the metric of $g^{MN} = \text{diag}(-, +, +, +, +)$, simply multiply each contraction of Lorentz indices by (-1) , for example, $\partial^2 \rightarrow -\partial^2$ and $F^{MN}F_{MN} \rightarrow (-1)^2 F^{MN}F_{MN}$. The spinor contractions and formulae are found in the Appendices A, B of the book.

The gamma matrices are given by

$$\Gamma^\mu = \gamma^\mu = \begin{pmatrix} 0 & \sigma^\mu \\ \bar{\sigma}^\mu & 0 \end{pmatrix}, \quad \Gamma^5 = i\gamma^5 = \begin{pmatrix} -i & 0 \\ 0 & i \end{pmatrix},$$

and we see $\{\Gamma^M, \Gamma^N\} = 2g^{MN}$. Since γ_5 is incorporated in generators of 5D Lorentz symmetry, the 5D theory cannot have chiral fermions which are essential for the SM.

2.2.1 Non-Abelian gauge field

Supersymmetric Yang-Mills theory in the 5D is given by

$$\begin{aligned} \mathcal{L}_5^{\text{YM}} &= \frac{1}{16kg^2} \text{Tr} \left[\int d^2\theta \mathcal{W}^\alpha \mathcal{W}_\alpha + \text{h.c.} \right] \\ &+ \frac{1}{4kg^2} \int d^4\theta \text{Tr} \left[(\sqrt{2}\partial_5 + 2g\chi^\dagger) e^{-2gV} (-\sqrt{2}\partial_5 + 2g\chi) e^{2gV} \right. \\ &\quad \left. + \partial_5 e^{-2gV} \partial_5 e^{2gV} + 2g^2(\chi\chi + \chi^\dagger\chi^\dagger) \right], \end{aligned} \quad (2.3)$$

where

$$\mathcal{W}_\alpha = \frac{1}{4} \bar{D}\bar{D}e^{2gV} D_\alpha e^{-2gV} \quad \text{and} \quad \text{Tr}[T^a T^b] = k\delta^{ab}. \quad (2.4)$$

$V = V(x, y)$ and $\chi = \chi(x, y)$ are adjoint vector and chiral superfields. The superfields are expanded as follows (with V in the Wess-Zumino gauge, and χ in the y -basis),

$$V = V^a T^a = -\theta\sigma^\mu\bar{\theta}A_\mu + i\theta^2\bar{\theta}\bar{\lambda}_1 - i\bar{\theta}^2\theta\hat{\lambda}_1 + \frac{1}{2}\theta^2\bar{\theta}^2 D \quad (2.5)$$

$$\equiv -\theta\sigma^\mu\bar{\theta}A_\mu - \theta^2\bar{\theta}\bar{\lambda}_1 - \bar{\theta}^2\theta\lambda_1 + \frac{1}{2}\theta^2\bar{\theta}^2 D, \quad (2.6)$$

$$\chi = \chi^a T^a = \frac{\Sigma + iA_5}{\sqrt{2}} + \sqrt{2}\theta\lambda_2 + \theta^2 F_\chi, \quad (2.7)$$

where $\lambda \equiv i\hat{\lambda}$. In 5D, Σ^a is a real scalar in adjoint representation of gauge group, and, in 6D, it behaves as the sixth component of gauge field, $\Sigma \rightarrow A_6$. The last two lines of Eq. (2.3)

are unconventional and describe terms of fifth component of gauge field, such as $F_{\mu 5}$, and all the terms involving λ_2 and Σ including the term combining two Weyl spinors through fifth dimensional derivative, $\lambda_1 \mathcal{D}_5 \lambda_2$. It certainly tells that gaugino in this formalism forms a Dirac fermion. Note that the last term $\chi\chi + \chi^\dagger\chi^\dagger$ in eq.(2.3) vanishes under $\int d^4\theta$ integral, but this remains in the presence of a supersymmetry breaking term and is necessary for the gauge invariance (Appendix A.1).

The conventional part of the Lagrangian is

$$\frac{1}{16kg^2} \text{Tr} \left[\int d^2\theta \mathcal{W}^\alpha \mathcal{W}_\alpha + \text{h.c.} \right] = -\frac{1}{4} F^{a\mu\nu} F_{\mu\nu}^a + i\bar{\lambda}_1^a \bar{\sigma}^\mu \mathcal{D}_\mu \lambda_1^a + \frac{1}{2} D^a D^a, \quad (2.8)$$

where

$$\mathcal{D}_M \lambda_i^a = \partial_M \lambda_i^a + g f^{abc} A_M^b \lambda_i^c, \quad (2.9)$$

$$F_{MN}^a = \partial_M A_N^a - \partial_N A_M^a + g f^{abc} A_M^b A_N^c. \quad (2.10)$$

And the rest part contains extra components of gauge field strength, all the kinetic terms involving Σ and λ_2 , and it shows particularly mixing between λ_1 and λ_2 through 5D derivative. The second and third lines of Eq. (2.3) are decomposed by using $V^3 = 0$ in the Wess-Zumino gauge,

$$\int d^4\theta \frac{1}{4kg^2} \text{Tr} \left[(\sqrt{2}\partial_5 + 2g\chi^\dagger) e^{-2gV} (-\sqrt{2}\partial_5 + 2g\chi) e^{2gV} + \partial_5 e^{-2gV} \partial_5 e^{2gV} + 2g^2 (\chi\chi + \chi^\dagger\chi^\dagger) \right] \quad (2.11)$$

$$= \int d^4\theta \frac{1}{k} \text{Tr} \left[\left\{ (\partial_5 V)^2 + \chi\chi^\dagger - \sqrt{2}(\chi + \chi^\dagger)\partial_5 V + \frac{\chi\chi + \chi^\dagger\chi^\dagger}{2} \right\} + g \left\{ \sqrt{2}(\chi - \chi^\dagger)[(\partial_5 V)V - V(\partial_5 V)] + 2(\chi^\dagger\chi - \chi\chi^\dagger)V \right\} + g^2 \left\{ -4\chi^\dagger V \chi V + 2(\chi^\dagger\chi + \chi\chi^\dagger)V^2 \right\} \right]. \quad (2.12)$$

$$= -\frac{1}{4} (2F^{a\mu 5} F_{\mu 5}^a) - i\lambda_2^a \sigma^\mu \mathcal{D}_\mu \bar{\lambda}_2^a - \lambda_2^a \mathcal{D}_5 \lambda_1^a + \bar{\lambda}_1^a \mathcal{D}_5 \bar{\lambda}_2^a + \frac{1}{2k} \text{Tr} \left[\mathcal{D}_\mu \Sigma \mathcal{D}^\mu \Sigma \right] + ig f^{abc} (\lambda_2^a \Sigma^b \lambda_1^c + \bar{\lambda}_1^a \Sigma^b \bar{\lambda}_2^c) + \frac{1}{2k} \text{Tr} \left[2(\mathcal{D}_5 \Sigma) D \right] + |F_\chi^a|^2, \quad (2.13)$$

where $\mathcal{D}_M (\Sigma^a T^a) = \mathcal{D}_M \Sigma = \partial_M \Sigma - ig[A_M, \Sigma]$. We combine Eq.(2.8) and Eq.(2.13),

$$\begin{aligned} \mathcal{L}_5^{\text{YM}} = & -\frac{1}{4} F^{aMN} F_{MN}^a + i \left[\bar{\lambda}_1^a \bar{\sigma}^\mu \mathcal{D}_\mu \lambda_1^a + \lambda_2^a \sigma^\mu \mathcal{D}_\mu \bar{\lambda}_2^a + i\lambda_2^a \mathcal{D}_5 \lambda_1^a - i\bar{\lambda}_1^a \mathcal{D}_5 \bar{\lambda}_2^a \right] \\ & + \frac{1}{2} \mathcal{D}_\mu \Sigma^a \mathcal{D}^\mu \Sigma^a + \frac{g}{2} f^{abc} \Sigma^a (i\lambda_1^b \lambda_2^c - i\lambda_2^b \lambda_1^c - i\bar{\lambda}_1^b \bar{\lambda}_2^c + i\bar{\lambda}_2^b \bar{\lambda}_1^c) \\ & + \frac{1}{2} D^a D^a + (\mathcal{D}_5 \Sigma^a) D^a + |F_\chi^a|^2 \end{aligned} \quad (2.14)$$

$$= -\frac{1}{4} F^{aMN} F_{MN}^a + \frac{1}{2} \left[i\bar{\lambda}_i^a \bar{\sigma}^\mu \mathcal{D}_\mu \lambda_i^a + \lambda_i^a \varepsilon_{ij} \mathcal{D}_5 \lambda_j^a + \text{h.c.} \right] + \frac{1}{2} \mathcal{D}_M \Sigma^a \mathcal{D}^M \Sigma^a + \frac{g}{2} f^{abc} \Sigma^a (i\lambda_i^b \varepsilon_{ij} \lambda_j^c + \text{h.c.}) + \frac{1}{2} (D^a)^2 + |F_\chi^a|^2, \quad (2.15)$$

where $D'^a \equiv D^a + \mathcal{D}_5 \Sigma^a$ and $\varepsilon_{ij} = (i\sigma_2)_{ij}$. Terms of gauginos are written in $SU(2)_R$ invariant way. If we use Dirac fermions, $\lambda \equiv (\lambda_{1\alpha}, \bar{\lambda}_2^{\dot{\alpha}})^T$ and $\bar{\lambda} \equiv (\lambda_2^\alpha, \bar{\lambda}_{1\dot{\alpha}})$, the Lagrangian becomes explicitly Lorentz invariant,

$$\begin{aligned} \mathcal{L}_5^{\text{YM}} &= -\frac{1}{4} F^{aMN} F_{MN}^a + i\bar{\lambda}^a \Gamma^M \mathcal{D}_M \lambda^a + \frac{1}{2} \mathcal{D}_M \Sigma^a \mathcal{D}^M \Sigma^a + igf^{abc} \Sigma^a \bar{\lambda}^b \lambda^c \\ &\quad + \frac{1}{2} (D'^a)^2 + |F_\chi^a|^2. \end{aligned} \quad (2.16)$$

For simultaneous $SU(2)_R$ invariance and Lorentz invariance, we must use a symplectic Majorana fermion that has four spinors,

$$\lambda_{sm} \equiv \begin{pmatrix} \lambda_{sm,1} \\ \lambda_{sm,2} \end{pmatrix}, \quad \lambda_{sm,1} = \begin{pmatrix} \lambda_1 \\ \bar{\lambda}_2 \end{pmatrix}, \quad \lambda_{sm,2} = \begin{pmatrix} -\lambda_2 \\ \bar{\lambda}_1 \end{pmatrix}. \quad (2.17)$$

Two Dirac fermions $(\lambda_{sm,1}, \lambda_{sm,2})$ transform as $SU(2)_R$ doublet. The kinetic term of gauginos become both Lorentz and $SU(2)_R$ invariant,

$$i\bar{\lambda}^a \Gamma^M \mathcal{D}_M \lambda^a = \frac{i}{2} \bar{\lambda}_{sm}^a \Gamma^M \mathcal{D}_M \lambda_{sm}^a. \quad (2.18)$$

2.2.2 Hypermultiplet

Now we consider the matter sector. Matters are in Hypermultiplet which consists of two chiral supermultiplets in $\mathcal{N} = 1, D = 4$ language. The Lagrangian in superspace is given by

$$\begin{aligned} \mathcal{L}_5^{\text{Hyper}} &= \int d^4\theta \left\{ H_2 e^{2gV} H_2^\dagger + H_1^\dagger e^{-2gV} H_1 \right\} \\ &\quad + \int d^2\theta H_2 (\partial_5 - \sqrt{2}g\chi) H_1 + \text{h.c.}, \end{aligned} \quad (2.19)$$

where $H_{1,2} = H_{1,2}(x, y)$ and $V = V^a T_R^a$, $\chi = \chi^a T_R^a$. $H_1(H_2)$ belongs to a representation $R(\bar{R})$ of the gauge group. The chiral superfields are defined as (in the y -basis)

$$H_1 = \phi_1 + \sqrt{2}\theta\psi_1 + \theta^2 F_1, \quad (2.20)$$

$$H_2 = \phi_2 + \sqrt{2}\theta\psi_2 + \theta^2 F_2. \quad (2.21)$$

The second line of Eq. (2.19) leads to terms of fifth dimensional covariant derivative, such as $F_2 \mathcal{D}_5 \phi_1$ and $\psi_2 \mathcal{D}_5 \psi_1$, and Σ interactions with $\psi_{1,2}$ and $\phi_{1,2}$. When the Lagrangian is written down in component, many terms appear,

$$\begin{aligned} \mathcal{L}_5^{\text{Hyper}} &= (\mathcal{D}^\mu \phi_1)^\dagger \mathcal{D}_\mu \phi_1 + (\mathcal{D}^\mu \phi_2^*)^\dagger \mathcal{D}_\mu \phi_2^* + i\bar{\psi}_1 \bar{\sigma}^\mu \mathcal{D}_\mu \psi_1 + i\psi_2 \sigma^\mu \mathcal{D}_\mu \bar{\psi}_2 \\ &\quad - i\sqrt{2}g(\phi_1^\dagger T^a \psi_1 \hat{\lambda}_1^a - \bar{\lambda}_1^a \bar{\psi}_1 T^a \phi_1) + i\sqrt{2}g(\hat{\lambda}_1^a \psi_2 T^a \phi_2^* - \phi_2 T^a \bar{\psi}_2 \bar{\lambda}_1^a) \\ &\quad - gD^a(\phi_1^\dagger T^a \phi_1) + gD^a(\phi_2 T^a \phi_2^*) \\ &\quad + |F_1|^2 + |F_2|^2 \\ &\quad + F_2 [\partial_5 - g(\Sigma^a + iA_5^a)T^a] \phi_1 + \phi_2 [\partial_5 - g(\Sigma^a + iA_5^a)T^a] F_1 + \text{h.c.} \\ &\quad + \phi_2 [-\sqrt{2}gF_\chi^a T^a] \phi_1 + \text{h.c.} \\ &\quad - \psi_2 [\partial_5 - g(\Sigma^a + iA_5^a)T^a] \psi_1 + \text{h.c.} \\ &\quad + \sqrt{2}g(\psi_2 \lambda_2^a T^a \phi_1 + \phi_2 T^a \lambda_2^a \psi_1) + \text{h.c.} \end{aligned} \quad (2.22)$$

where the covariant derivatives are

$$\mathcal{D}_M X = (\partial_5 - igA_M^a T^a)X, \quad X = \phi_1, \phi_2^*, \psi_1 \text{ and } \bar{\psi}_2. \quad (2.23)$$

It is hard to see especially because ∂_μ and ∂_5 are placed in different terms. We organize Lagrangian in an explicit 5D Lorentz invariant form by redefining auxiliary fields of F and D^a ,

$$F'_1 \equiv F_1 + [-\partial_5 - g(\Sigma^a - iA_5^a)T^a]\phi_2^*, \quad (2.24)$$

$$F_2'^* \equiv F_2^* + [\partial_5 - g(\Sigma^a + iA_5^a)T^a]\phi_1, \quad (2.25)$$

$$D'^a \equiv D^a + \mathcal{D}_5 \Sigma^a, \quad (2.26)$$

and use $\lambda_1 = i\hat{\lambda}_1$. The Lagrangian becomes,

$$\begin{aligned} \mathcal{L}_5^{\text{Hyper}} &= |F'_1|^2 + |F_2'^*|^2 + (\mathcal{D}^M \phi_1)^\dagger \mathcal{D}_M \phi_1 + (\mathcal{D}^M \phi_2^*)^\dagger \mathcal{D}_M \phi_2^* \\ &\quad - g^2 (\Sigma^a T^a \phi_1)^\dagger (\Sigma^a T^a \phi_1) - g^2 (\Sigma^a T^a \phi_2^*)^\dagger (\Sigma^a T^a \phi_2^*) \\ &\quad + i(\psi_2^\alpha, \bar{\psi}_{1\dot{\alpha}}) \Gamma^M \mathcal{D}_M \begin{pmatrix} \psi_{1\alpha} \\ \bar{\psi}_2^{\dot{\alpha}} \end{pmatrix} \\ &\quad + g \Sigma^a (\psi_2 T^a \psi_1 + \bar{\psi}_1 T^a \bar{\psi}_2) \\ &\quad + \sqrt{2} g (\phi_1^*, \phi_2) T^a \left\{ \psi_1 \begin{pmatrix} -\lambda_1^a \\ \lambda_2^a \end{pmatrix} + \bar{\psi}_2 \begin{pmatrix} \bar{\lambda}_2^a \\ \bar{\lambda}_1^a \end{pmatrix} \right\} + \text{h.c.} \\ &\quad - g D'^a (\phi_1^* T^a \phi_1) + g D'^a (\phi_2 T^a \phi_2^*) \\ &\quad + \phi_2 [-\sqrt{2} g F_\chi^a T^a] \phi_1 + \text{h.c.} \end{aligned} \quad (2.27)$$

Furthermore, we lead this to

$$\begin{aligned} \mathcal{L}_5^{\text{Hyper}} &= |F'_i|^2 + (\mathcal{D}^M \Phi_i)^\dagger \mathcal{D}_M \Phi_i - g^2 (\Sigma^a T^a \Phi)^\dagger (\Sigma^a T^a \Phi) \\ &\quad + i \bar{\Psi} \Gamma^M \mathcal{D}_M \Psi + g \Sigma^a (\bar{\Psi} T^a \Psi) \\ &\quad - \sqrt{2} g \Phi_i^\dagger \varepsilon_{ij} T^a \Psi \bar{\lambda}_{sm,j}^a + \text{h.c.} \\ &\quad - g D'^a (\Phi_1^* T^a \Phi_1) + g D'^a (\Phi_2^* T^a \Phi_2) \\ &\quad + \Phi_2^* [-\sqrt{2} g F_\chi^a T^a] \Phi_1 + \text{h.c.}, \end{aligned} \quad (2.28)$$

where

$$\Phi = \begin{pmatrix} \Phi_1 \\ \Phi_2 \end{pmatrix} \equiv \begin{pmatrix} \phi_1 \\ \phi_2^* \end{pmatrix}, \quad \Psi \equiv \begin{pmatrix} \psi_1 \\ \bar{\psi}_2 \end{pmatrix}. \quad (2.29)$$

Here, i, j are indices of $SU(2)_R$ doublet, and $\lambda_{sum,i}$ is given in Eq.(2.17). $SU(2)_R$ symmetry becomes clear except for terms involving gauge auxiliary fields D' and F_χ shown in the last two lines of Eq. (2.28). However, once these are combined with $\mathcal{L}_5^{\text{YM}}$, $SU(2)_R$ is actually realized. For detail see Appendix A.2.

2.3 Supersymmetry Breaking by Boundary Conditions

2.3.1 Scherk-Schwarz mechanism

We consider a single compact extra dimension with the coordinate y identified under $\mathcal{T} : y \rightarrow y + 2\pi R$ and $\mathcal{P} : y \rightarrow -y$. Let ϕ be a column vector representing all fields of the

theory. We require the 5D action is invariant under both operations, which is called orbifold compactification. Invariance of \mathcal{P} is needed so that the low-energy theory has chiral fermions as in the SM and the MSSM. The action of these transformations on the fields can be written as

$$\mathcal{T} : \phi(y) \rightarrow T^{-1}\phi(y + 2\pi R) = \phi(y) , \quad (2.30)$$

$$\mathcal{P} : \phi(y) \rightarrow P\phi(-y) = \phi(y) . \quad (2.31)$$

For the simultaneous imposition of \mathcal{T} and \mathcal{P} , there is a consistency condition that the space-time motion induced by \mathcal{PT} is identical to that induced by $\mathcal{T}^{-1}\mathcal{P}$. Then the two operations satisfy the algebra

$$PTP = T^{-1} , \quad (2.32)$$

$$P^2 = 1 , \quad (2.33)$$

and the resulting extra dimension is an interval $y \in [0, \pi R]$: the S^1/\mathbb{Z}_2 orbifold.¹ For a simple example, let us consider 5D quark where T and P commute. We obtain $T = \pm 1$ and $P = \pm\gamma_5$, and ignore $T = -1$ solutions which do not have massless modes. The Kaluza-Klein (KK) expansion for quark with $T = 1$ and $P = \gamma_5$ is given by

$$\Psi(x, y) = \frac{P_R}{\sqrt{2\pi R}}\Psi_0(x) + \sum_{n=1}^{\infty} \frac{P_R}{\sqrt{\pi R}}\Psi_n(x) \cos \frac{ny}{R} + \sum_{n=1}^{\infty} \frac{P_L}{\sqrt{\pi R}}\Psi_n(x) \sin \frac{ny}{R} \quad (2.34)$$

where $P_R = (1 + \gamma_5)/2$ and $P_L = (1 - \gamma_5)/2$. A massless chiral fermion is certainly obtained as zero mode while non-zero modes have both left- and right-handed components which form a Dirac mass of n/R .

In presence of supersymmetry, T and P are not necessarily commute but we can think of other boundary conditions using $SU(2)_R$ space. The boundary conditions for two dimensional representation such as $SU(2)_R$ doublets can be

$$P = \begin{pmatrix} 1 & 0 \\ 0 & -1 \end{pmatrix} (\otimes \gamma_5 \text{ for fermion}),$$

$$T = \begin{pmatrix} \cos(2\pi\alpha) & \sin(2\pi\alpha) \\ -\sin(2\pi\alpha) & \cos(2\pi\alpha) \end{pmatrix} = e^{i\sigma_2(2\pi\alpha)}, \quad (2.35)$$

under \mathcal{P} and \mathcal{T} (see Ref. [35] for details). The twist parameter of α is real. For one dimensional representation such as $SU(2)_R$ singlets, the condition is $T^2 = 1$ because P and T commute. In this thesis we consider the case $\alpha \ll 1$. As explained later, the twist parameter α in the boundary conditions is equivalent to an F -term vacuum expectation value of the radion superfield [37], which can be generated dynamically through a radion stabilization mechanism and hence can be naturally small. The non-zero α leads to mass-splitting of KK modes between $SU(2)_R$ singlets and doublets, and therefore supersymmetry is broken. This supersymmetry breaking through the non-trivial boundary condition is generally called Scherk-Schwarz mechanism [33]. In other words, for the orbifold boundary condition

¹For practical calculations, we use a larger interval $y \in [0, 2\pi R]$ for convenience.

$SU(2)_R$ is broken down to $U(1)_R$ and thus $\mathcal{N} = 1$ supersymmetry remains. Furthermore the remaining supersymmetry is broken by Scherk-Schwarz mechanism with non-zero α .

The boundary conditions of Eq. (2.35) leave only the MSSM gauge and matter fields below the compactification scale $1/R$. Specifically, the matter supermultiplets yield three generations of quarks and leptons as the zero modes, while their super partners obtain the common soft mass of α/R . (Here, we have assumed that there are no 5D bulk mass terms for the matter multiplets.²) The gauge supermultiplets give massless standard model gauge fields and gauginos of mass α/R . We therefore obtain the first two expressions in Eq. (2.1). (The Kaluza–Klein excitations form $\mathcal{N} = 2$ supermultiplets and have masses $\approx n/R$ ($n = 1, 2, \dots$), with supersymmetry-breaking mass splitting of order α/R .) We see these results explicitly in Sec. 2.3.2.

2.3.2 Soft masses of scalar and gaugino

Now let us investigate how the Scherk-Schwarz mechanism works. It can be seen that the supersymmetry breaking effect, particularly soft term, appears through extra dimensional derivative ∂_5 . The matter scalars, ϕ_1 and ϕ_2^* , given in Eqs.(2.20,2.21) form a $SU(2)_R$ doublet and transform under \mathcal{P} and \mathcal{T} ,

$$\begin{pmatrix} \phi_1(-y) \\ \phi_2^*(-y) \end{pmatrix} = \begin{pmatrix} \phi_1(y) \\ -\phi_2^*(y) \end{pmatrix}, \quad (2.36)$$

$$\begin{pmatrix} \phi_1(y + 2\pi R) \\ \phi_2^*(y + 2\pi R) \end{pmatrix} = e^{i\sigma_2(2\pi\alpha)} \begin{pmatrix} \phi_1(y) \\ \phi_2^*(y) \end{pmatrix}. \quad (2.37)$$

These conditions are satisfied by extracting an exponential factor of twist,

$$\begin{pmatrix} \phi_1(y) \\ \phi_2^*(y) \end{pmatrix} \rightarrow e^{i\sigma_2\alpha y/R} \begin{pmatrix} \phi_1(y) \\ \phi_2^*(y) \end{pmatrix}. \quad (2.38)$$

Here the scalars $\phi_{1,2}$ on the right-hand side have simple boundary conditions,

$$\begin{aligned} \phi_1(y + 2\pi R) &= \phi_1(y), & \phi_1(-y) &= \phi_1(y), \\ \phi_2(y + 2\pi R) &= \phi_2(y), & \phi_2(-y) &= -\phi_2(y), \end{aligned} \quad (2.39)$$

and their KK expansions are given by,

$$\phi_1 = \frac{\phi_{1,0}}{\sqrt{2\pi R}} + \sum_{n=1}^{\infty} \frac{\phi_{1,n}}{\sqrt{\pi R}} \cos \frac{ny}{R}, \quad \phi_2 = \sum_{n=1}^{\infty} \frac{\phi_{2,n}}{\sqrt{\pi R}} \sin \frac{ny}{R}. \quad (2.40)$$

When the Lagrangian is written in terms of fields with simple boundary conditions of Eq. (2.39), the zero mode has wave function in the extra dimension for the exponential factor with non-zero α . Having wave function in the extra dimension means that the mode has momentum in the extra dimensional direction which is seen as “mass” in the 4D picture. On the other hand, $SU(2)_R$ singlets cannot have such a wave function, and the zero mode

²This assumption can be justified by a local parity in the bulk; see, e.g., [39].

of $SU(2)_R$ singlet is kept massless. One may worry that breaking supersymmetry with non-trivial boundary conditions is hard breaking, but the effect of breaking appears only through derivative of fifth dimension ∂_5 , and thus this is always soft breaking.

The derivative ∂_5 interacts with the exponential factor, and extra terms (soft terms) are generated,

$$\begin{aligned}
\mathcal{L}_5^{\text{Hyper}} &\supset -(\mathcal{D}_5\phi_1)^\dagger(\mathcal{D}_5\phi_1) - (\mathcal{D}_5\phi_2^*)^\dagger(\mathcal{D}_5\phi_2^*) = -(\mathcal{D}_5\Phi_i)^\dagger(\mathcal{D}_5\Phi_i) & (2.41) \\
&\rightarrow -\left(\mathcal{D}_5(e^{i\sigma_2\alpha y/R})_{ij}\Phi_j\right)^\dagger\left(\mathcal{D}_5(e^{i\sigma_2\alpha y/R})_{ij}\Phi_j\right) \\
&= -\left((e^{i\sigma_2\alpha y/R})_{ij}\mathcal{D}_5\Phi_j + (e^{i\sigma_2\alpha y/R}i\sigma_2)_{ij}\frac{\alpha}{R}\Phi_j\right)^\dagger \\
&\quad \times \left((e^{i\sigma_2\alpha y/R})_{il}\mathcal{D}_5\Phi_l + (e^{i\sigma_2\alpha y/R}i\sigma_2)_{ik}\frac{\alpha}{R}\Phi_k\right) \\
&= -(\mathcal{D}_5\Phi_i)^\dagger(\mathcal{D}_5\Phi_i) - \left(\frac{\alpha}{R}\right)^2\Phi_i^\dagger\Phi_i \\
&\quad -(\mathcal{D}_5\Phi_i)^\dagger\frac{\alpha}{R}(i\sigma_2\Phi)_i + \Phi_i^\dagger\frac{\alpha}{R}(i\sigma_2\mathcal{D}_5\Phi)_i \\
&= -(\mathcal{D}_5\phi_1)^\dagger(\mathcal{D}_5\phi_1) - (\mathcal{D}_5\phi_2^*)^\dagger(\mathcal{D}_5\phi_2^*) - \left(\frac{\alpha}{R}\right)^2|\phi_1|^2 - \left(\frac{\alpha}{R}\right)^2|\phi_2^*|^2 \\
&\quad + \frac{\alpha}{R}\left(\phi_1^\dagger\mathcal{D}_5\phi_2^* - (\phi_2^*)^\dagger\mathcal{D}_5\phi_1 - (\mathcal{D}_5\phi_1)^\dagger\phi_2^* + (\mathcal{D}_5\phi_2^*)^\dagger\phi_1\right) & (2.42)
\end{aligned}$$

where “ \rightarrow ” means extracting the exponential factor of Eq. (2.37). These terms form a mass matrix of scalars after the KK expansion,

$$\int dy (\phi_1^*(y), \phi_2(y)) \begin{pmatrix} \partial_5^2 - (\alpha/R)^2 & 2(\alpha/R)\partial_5 \\ -2(\alpha/R)\partial_5 & \partial_5^2 - (\alpha/R)^2 \end{pmatrix} \begin{pmatrix} \phi_1(y) \\ \phi_2^*(y) \end{pmatrix} \quad (2.43)$$

$$= -\frac{\alpha^2}{R^2}|\phi_{1,0}|^2 - \frac{1}{R^2}\sum_{n=1}^{\infty}(\phi_{1,n}^*, \phi_{2,n}) \begin{pmatrix} n^2 + \alpha^2 & -2\alpha n \\ -2\alpha n & n^2 + \alpha^2 \end{pmatrix} \begin{pmatrix} \phi_{1,n} \\ \phi_{2,n}^* \end{pmatrix}. \quad (2.44)$$

The zero mode has soft mass of α/R , and the non-zero mode have mass of $(\alpha \pm n)/R$ ($n=1,2,\dots$). Using the mass eigenstates, the KK expansion is written in a more convenient way,

$$\phi_1(y) = \sum_{n=-\infty}^{\infty} \frac{\phi_n}{\sqrt{2\pi R}} \cos \frac{ny}{R}, \quad (2.45)$$

$$\phi_2^*(y) = -\sum_{n=-\infty}^{\infty} \frac{\phi_n}{\sqrt{2\pi R}} \sin \frac{ny}{R}. \quad (2.46)$$

where the mass of ϕ_n is $(\alpha + n)/R$. The detail is given in Appendix. B.2.1.

Conditions for gauginos are similar to those for the scalars. We simply replace ϕ_1, ϕ_2^* with $\lambda_1, -\lambda_2$, respectively. Note that under \mathcal{P} supermultiplets for gauge field transform as,

$$V(x, -y) = V(x, y), \quad \chi(x, -y) = -\chi(x, y), \quad (2.47)$$

because V contains A_μ while χ contains A_5 . The gaugino $SU(2)_R$ doublet must satisfy the boundary conditions for the matter scalars of Eqs. (2.36, 2.37) since $SU(2)_R$ is a common

global symmetry. Thus the gaugino multiplet has also the exponential factor of twist,

$$\begin{pmatrix} \lambda_1(y) \\ -\lambda_2(y) \end{pmatrix} \rightarrow e^{i\sigma_2\alpha y/R} \begin{pmatrix} \lambda_1(y) \\ -\lambda_2(y) \end{pmatrix} \quad (2.48)$$

Fields on the right-hand side are similar to those in Eq.(2.39). As in the case of scalars, there will be extra terms through ∂_5 and we expect the same mass spectrum is generated. The kinetic term of gauginos is

$$\begin{aligned} \mathcal{L}_5^{\text{YM}} &\supset \frac{1}{2} \lambda_i^a (i\sigma_2)_{ij} \mathcal{D}_5 \lambda_j \\ &\rightarrow \frac{1}{2} (e^{-i\sigma_2\alpha y/R})_{ij} \lambda_j^a (i\sigma_2)_{ik} \mathcal{D}_5 (e^{-i\sigma_2\alpha y/R} \lambda^a)_k \\ &= \frac{1}{2} \lambda_i^a (e^{i\sigma_2\alpha y/R} i\sigma_2)_{ij} \left((e^{-i\sigma_2\alpha y/R})_{jk} \mathcal{D}_5 \lambda_k^a + (-e^{-i\sigma_2\alpha y/R} i\sigma_2)_{jk} \frac{\alpha}{R} \lambda_k^a \right) \\ &= \frac{1}{2} \lambda_i^a (i\sigma_2)_{ij} \mathcal{D}_5 \lambda_j + \frac{\alpha}{2R} \lambda_i^a \lambda_i^a \end{aligned} \quad (2.49)$$

These terms form a mass matrix after the KK expansion as follows,

$$\begin{aligned} &\int_0^{2\pi R} dy \frac{1}{2} (\lambda_1^a(y), \lambda_2^a(y)) \begin{pmatrix} \alpha/R & -\partial_5 \\ \partial_5 & \alpha/R \end{pmatrix} \begin{pmatrix} \lambda_1^a(y) \\ \lambda_2^a(y) \end{pmatrix} \\ &= \frac{\alpha}{2R} \lambda_{1,0}^a \lambda_{1,0}^a + \sum_{n=1}^{\infty} (\lambda_{1,n}^a, \lambda_{2,n}^a) \begin{pmatrix} \alpha/R & n/R \\ n/R & \alpha/R \end{pmatrix} \begin{pmatrix} \lambda_{1,n}^a \\ \lambda_{2,n}^a \end{pmatrix}, \end{aligned} \quad (2.50)$$

In fact, these gauginos have the same mass spectrum of the scalars such that $m_{\text{gaugino}} = \alpha/R, (\alpha \pm 1)/R, (\alpha \pm 2)/R, \dots$. Similarly it is understood that KK modes of gravitinos, another $SU(2)_R$ doublet, should have the same mass spectrum.

Let us summarize the generated soft breaking terms in the bulk,

$$\begin{aligned} \mathcal{L}_{5,\text{soft}} &= -\left(\frac{\alpha}{R}\right)^2 |\phi_1|^2 - \left(\frac{\alpha}{R}\right)^2 |\phi_2^*|^2 \\ &\quad + \frac{\alpha}{R} \left(\phi_1^\dagger \mathcal{D}_5 \phi_2^* - (\phi_2^*)^\dagger \mathcal{D}_5 \phi_1 - (\mathcal{D}_5 \phi_1)^\dagger \phi_2^* + (\mathcal{D}_5 \phi_2^*)^\dagger \phi_1 \right) \\ &\quad + \frac{1}{2} \frac{\alpha}{R} \lambda_1^a \lambda_1^a + \frac{1}{2} \frac{\alpha}{R} \lambda_2^a \lambda_2^a + \text{h.c.} \end{aligned} \quad (2.51)$$

2.3.3 Soft terms on brane

For a theory with only bulk fields, soft breaking terms are only terms of Eq. (2.51), but once we consider Yukawa interactions on branes which only respects $\mathcal{N} = 1, D = 4$ supersymmetry, additional soft breaking terms appear. Suppose a bulk field $H_1(x, y)$ interacts with chiral superfields $S_{1,2}(x)$ on $y = 0$ brane,

$$W_{\text{brane1}} = \delta(y) \lambda_1 S_1(x) S_2(x) H_1(x, y). \quad (2.52)$$

where $S_{1,2} = \phi_{S_{1,2}} + \psi_{S_{1,2}} \theta + F_{S_{1,2}} \theta^2$. If some field of brane interactions lives in the bulk and hence receives SUSY breaking by the Scherk-Schwarz mechanism, soft term terms corresponding to superpotential appear through ∂_5 . It can be seen after θ integral and field

redefinition of F -term of bulk field, H_1 , as in Eq.(2.24),

$$\begin{aligned} \int d^2\theta W_{\text{brane1}} &\supset \delta(y)\lambda_1\phi_{S_1}(x)\phi_{S_2}(x)F_1(x,y) \\ &= \delta(y)\lambda_1\phi_{S_1}(x)\phi_{S_2}(x) \left(F_1'(x,y) + [\partial_5 + g(\Sigma^a(x,y) - iA_5^a(x,y))T^a] \phi_2^*(x,y) \right) \end{aligned} \quad (2.53)$$

Several terms vanishes because \mathcal{P} odd field does not have wave function at $y = 0$ such as $A_5, \Sigma \propto \sin(ny/R)$. We rewrite Eq. (3.9) by extracting α dependent factor from $\phi_{1,2}$ as Eq. (2.38),

$$\begin{aligned} &\delta(y)\lambda_1\phi_{S_1}(x)\phi_{S_2}(x) \left(F_1'(x,y) \right. \\ &\quad \left. + [\partial_5 + g(\Sigma^a(x,y) - iA_5^a(x,y))T^a] \left[\cos \frac{\alpha y}{R} \phi_2^*(x,y) - \sin \frac{\alpha y}{R} \phi_1(x,y) \right] \right) \end{aligned} \quad (2.54)$$

$$\begin{aligned} = &\delta(y)\lambda_1\phi_{S_1}(x)\phi_{S_2}(x) \left(F_1'(x,y) - \frac{\alpha}{R} \sin \frac{\alpha y}{R} \phi_2^*(x,y) + \cos \frac{\alpha y}{R} \partial_5 \phi_2^*(x,y) \right. \\ &\quad \left. - \frac{\alpha}{R} \cos \frac{\alpha y}{R} \phi_1(x,y) - \sin \frac{\alpha y}{R} \partial_5 \phi_1(x,y) \right) \end{aligned} \quad (2.55)$$

$$= \delta(y)\lambda_1\phi_{S_1}(x)\phi_{S_2}(x) \left(F_1'(x,y) + \partial_5 \phi_2^*(x,y) - \frac{\alpha}{R} \phi_1(x,y) \right) \quad (2.56)$$

The last term is soft SUSY breaking A -term. The size of soft terms on the brane is uniquely determined by configuration of interaction. Let us consider other types of interaction,

$$W_{\text{brane2}} = \delta(y) \frac{\lambda_2}{2} S_1(x) H_1^2(x,y), \quad W_{\text{brane3}} = \delta(y) \frac{\lambda_3}{3} H_1^3(x,y). \quad (2.57)$$

As the previous procedure, we perform θ integral and redefine F -term of H_1 , and extract α dependent factor,

$$\begin{aligned} \int d^2\theta W_{\text{brane2}} &\supset \delta(y) \frac{\lambda_2}{2} \phi_{S_1}(x) (2\phi_1(x,y)F_1(x,y)) \\ &= \delta(y) \frac{\lambda_2}{2} 2\phi_{S_1}(x)\phi_1(x,y) (F_1'(x,y) + \partial_5 \phi_2^*(x,y)) \end{aligned} \quad (2.58)$$

$$\begin{aligned} \rightarrow &\delta(y) \frac{\lambda_2}{2} 2\phi_{S_1}(x) \left[\cos \frac{\alpha y}{R} \phi_1(x,y) + \sin \frac{\alpha y}{R} \phi_2^*(x,y) \right] \\ &\quad \times \left(F_1'(x,y) + \partial_5 \left[\cos \frac{\alpha y}{R} \phi_2^*(x,y) - \sin \frac{\alpha y}{R} \phi_1(x,y) \right] \right) \end{aligned} \quad (2.59)$$

$$= \delta(y) \frac{\lambda_2}{2} 2\phi_{S_1}(x)\phi_1(x,y) \left(F_1'(x,y) + \partial_5 \phi_2^*(x,y) - \frac{\alpha}{R} \phi_1(x,y) \right) \quad (2.60)$$

$$\begin{aligned} \int d^2\theta W_{\text{brane3}} &\supset \delta(y) \frac{\lambda_3}{3} (3\phi_1^2(x,y)F_1(x,y)) \\ &= \delta(y) \frac{\lambda_3}{3} 3\phi_1^2(x,y) (F_1'(x,y) + \partial_5 \phi_2^*(x,y)) \end{aligned} \quad (2.61)$$

$$\begin{aligned} \rightarrow &\delta(y) \frac{\lambda_3}{3} 3 \left[\cos \frac{\alpha y}{R} \phi_1(x,y) + \sin \frac{\alpha y}{R} \phi_2^*(x,y) \right]^2 \\ &\quad \times \left(F_1'(x,y) + \partial_5 \left[\cos \frac{\alpha y}{R} \phi_2^*(x,y) - \sin \frac{\alpha y}{R} \phi_1(x,y) \right] \right) \end{aligned} \quad (2.62)$$

$$= \delta(y) \frac{\lambda_3}{3} 3\phi_1^2(x,y) \left(F_1'(x,y) + \partial_5 \phi_2^*(x,y) - \frac{\alpha}{R} \phi_1(x,y) \right) \quad (2.63)$$

Increasing number of bulk field on the brane Yukawa interactions, the size of A -term becomes larger. For a superpotential on brane

$$W_{\text{brane}} = \delta(y) \left\{ \lambda_1 S_1(x) S_2(x) H_1(x, y) + \frac{\lambda_2}{2} S_1(x) H_1^2(x, y) + \frac{\lambda_3}{3} H_1^3(x, y) \right\}, \quad (2.64)$$

soft terms are generated through the Scherk-Schwarz mechanism as follows,

$$\mathcal{L}_{\text{brane,soft}} = \delta(y) \left\{ \lambda_1 \frac{-\alpha}{R} \phi_{S1} \phi_{S2} \phi_1 + \frac{\lambda_2}{2} \frac{-2\alpha}{R} \phi_{S1} \phi_1^2 + \frac{\lambda_3}{3} \frac{-3\alpha}{R} \phi_1^3 \right\}. \quad (2.65)$$

In the realistic situation, we will consider brane interactions which have bilinear of bulk fields. For example, Q and U are bulk chiral superfields that are \mathcal{P} even part of hypermultiplets while H_u is brane-localized chiral superfield, and their Yukawa interaction is localized on the brane,

$$W_{\text{brane}}^{yU} = \delta(y) y_{U5} H_u(x) Q(x, y) U(x, y). \quad (2.66)$$

As before F -terms of Q and U are redefined and squarks have same α dependent wave function for the Scherk-Schwarz mechanism. Therefore, the soft term is generated from the Yukawa interaction,

$$\mathcal{L}_{\text{brane,soft}}^{yU} = \delta(y) y_{U5} \left(\frac{-2\alpha}{R} \right) \phi_{H_u}(x) \phi_Q(x, y) \phi_U(x, y). \quad (2.67)$$

In this configuration, the large trilinear term, $A_t = -2\alpha/R$, is naturally realized and it is close to ‘‘maximal mixing’’ ($|A_t| = \sqrt{6}\alpha/R$). The lightest Higgs mass is boosted by this correction without very heavy sparticles.

2.4 Radion Mediation

2.4.1 Lagrangian

In this section, we discuss the Radion mediation in the superfield formalism, and see that it actually corresponds to the Scherk-Schwarz mechanism [37]. We see the dependence of the Radion at first, and then naively construct the Lagrangian by promoting the radion field to a superfield.

In order to extract an explicit radius dependence of Eqs. (2.3,2.19), the coordinate of the fifth dimension is parametrized by $y = R\varphi$ where R is radius and $0 \leq \varphi < 2\pi$, and we count powers of R . The adjoint chiral field is redefined as $\chi \rightarrow \chi/R$ for convenience. The 4D

Lagrangian is given by,

$$\begin{aligned}
\mathcal{L}_4 = \int d\varphi \left\{ \right. & \frac{1}{16kg^2} \text{Tr} \left[\int d^2\theta R \mathcal{W}^\alpha \mathcal{W}_\alpha + \text{h.c.} \right] \\
& + \frac{1}{4kg^2} \int d^4\theta \frac{1}{R} \text{Tr} \left[(\sqrt{2}\partial_\varphi + 2g\chi^\dagger) e^{-2gV} (-\sqrt{2}\partial_\varphi + 2g\chi) e^{2gV} \right. \\
& \quad \left. + \partial_\varphi e^{-2gV} \partial_\varphi e^{2gV} + 2g^2(\chi\chi + \chi^\dagger\chi^\dagger) \right] \\
& + \int d^4\theta R \left(H_2 e^{2gV} H_2^\dagger + H_1^\dagger e^{-2gV} H_1 \right) \\
& \left. + \int d^2\theta H_2 (\partial_\varphi - \sqrt{2}g\chi) H_1 + \text{h.c.} \right\}. \tag{2.68}
\end{aligned}$$

We incorporate R into a chiral superfield,

$$T = R + iB_5 + \theta\Psi_R^5 + \theta^2 F_T. \tag{2.69}$$

The mass dimension of T in this normalization is -1 , and hence F_T is dimensionless. Using this radion chiral superfield, we promote the radius R to the superfield T in such a way that

$$\begin{aligned}
\int d^2\theta R^n & \rightarrow \int d^2\theta T^n, \\
\int d^4\theta R^n & \rightarrow \int d^4\theta \left(\frac{T + T^\dagger}{2} \right)^n. \tag{2.70}
\end{aligned}$$

Then the Lagrangian becomes

$$\begin{aligned}
\mathcal{L}_4 = \int d\varphi \left\{ \right. & \frac{1}{16kg^2} \text{Tr} \left[\int d^2\theta T \mathcal{W}^\alpha \mathcal{W}_\alpha + \text{h.c.} \right] \\
& + \frac{1}{4kg^2} \int d^4\theta \frac{2}{T + T^\dagger} \text{Tr} \left[(\sqrt{2}\partial_\varphi + 2g\chi^\dagger) e^{-2gV} (-\sqrt{2}\partial_\varphi + 2g\chi) e^{2gV} \right. \\
& \quad \left. + \partial_\varphi e^{-2gV} \partial_\varphi e^{2gV} + 2g^2(\chi\chi + \chi^\dagger\chi^\dagger) \right] \\
& + \int d^4\theta \frac{T + T^\dagger}{2} \left(H_2 e^{2gV} H_2^\dagger + H_1^\dagger e^{-2gV} H_1 \right) \\
& \left. + \int d^2\theta H_2 (\partial_\varphi - \sqrt{2}g\chi) H_1 + \text{h.c.} \right\}. \tag{2.71}
\end{aligned}$$

2.4.2 Radion mediation

Now let us assume the Radion has a VEV of its F -term breaking supersymmetry when it stabilizes the radius, such that $\langle T \rangle = R + \theta^2 F_T$. This is called Radion mediation, and we will see it is equivalent to the previous supersymmetry breaking by the Scherk-Schwarz mechanism. To be more explicit, we will show $F_T/2 = \alpha$. Again we rescale the adjoint chiral superfield as $\chi \rightarrow \chi R$, and then terms relevant to the supersymmetry breaking from the

radion superfield are given by

$$\begin{aligned} \mathcal{L}_4 \supset \int Rd\varphi \left\{ \frac{1}{16kg^2} \text{Tr} \left[\int d^2\theta \frac{T}{R} \mathcal{W}^\alpha \mathcal{W}_\alpha + \text{h.c.} \right] \right. \\ + \frac{1}{k} \int d^4\theta \frac{2R}{T+T^\dagger} \text{Tr} \left[\chi \chi^\dagger + \frac{\chi \chi + \chi^\dagger \chi^\dagger}{2} \right] \\ + \int d^4\theta \frac{T+T^\dagger}{2R} \left\{ H_2 H_2^\dagger + H_1^\dagger H_1 \right\} \\ \left. + \int d^2\theta H_2 (R^{-1} \partial_\varphi - \sqrt{2} g \chi) H_1 + \text{h.c.} \right\}. \end{aligned} \quad (2.72)$$

One gaugino mass is generated from the first term,

$$\begin{aligned} \frac{1}{16kg^2} \text{Tr} \left[\int d^2\theta (1 + 2f\theta^2) \mathcal{W}^\alpha \mathcal{W}_\alpha + \text{h.c.} \right] \\ \rightarrow \frac{1}{16kg^2} \text{Tr} \left[\int d^2\theta \mathcal{W}^\alpha \mathcal{W}_\alpha + \text{h.c.} \right] + \frac{f}{2} \lambda_1^a \lambda_1^a + \frac{f^*}{2} \bar{\lambda}_1^a \bar{\lambda}_1^a. \end{aligned} \quad (2.73)$$

where $f \equiv F_T/(2R)$. For T in the denominator, we can expand in θ and $\bar{\theta}$,

$$\begin{aligned} \frac{2R}{T+T^\dagger} &= 1 - \left(\frac{\theta^2 F_T + \bar{\theta}^2 F_T^*}{2R} \right) + \left(\frac{\theta^2 F_T + \bar{\theta}^2 F_T^*}{2R} \right)^2 \\ &= 1 - \theta^2 \frac{F_T}{2R} - \bar{\theta}^2 \frac{F_T^*}{2R} + \theta^4 \frac{|F_T|^2}{2R} \end{aligned} \quad (2.74)$$

$$\equiv 1 - \theta^2 f - \bar{\theta}^2 f^* + 2|f|^2 \theta^4. \quad (2.75)$$

Then χ is not canonically normalized. We redefine the adjoint chiral superfield,

$$\chi \rightarrow (1 + f\theta^2) \chi. \quad (2.76)$$

Hence the first term in the second line of Eq. (2.72) changes with this field redefinition,

$$\begin{aligned} \frac{1}{k} \int d^4\theta \frac{2R}{T+T^\dagger} \text{Tr} \left[\chi \chi^\dagger \right] \\ \rightarrow \frac{1}{k} \int d^4\theta \text{Tr} \left[(1 - f\theta^2 - f^* \bar{\theta}^2 + 2|f|^2 \theta^4) (1 + f\theta^2) (1 + f^* \bar{\theta}^2) \chi \chi^\dagger \right] \\ = \frac{1}{k} \int d^4\theta \text{Tr} \left[\chi \chi^\dagger \right] + |f|^2 |\phi_\chi^a|^2, \end{aligned} \quad (2.77)$$

and the second term changes as,

$$\begin{aligned} \frac{1}{k} \int d^4\theta \frac{2R}{T+T^\dagger} \text{Tr} \left[\frac{\chi \chi + \chi^\dagger \chi^\dagger}{2} \right] \\ \rightarrow \frac{1}{k} \int d^4\theta (1 - f\theta^2 - f^* \bar{\theta}^2 + 2|f|^2 \theta^4) \text{Tr} \left[(1 + 2f\theta^2) \frac{\chi \chi}{2} + \text{h.c.} \right] \\ = -\frac{1}{k} \int d^4\theta \text{Tr} \left[(f^* \bar{\theta}^2) \frac{\chi \chi}{2} + \text{h.c.} \right] \\ = -f^* F_\chi^a \phi_\chi^a + \frac{f^*}{2} \lambda_2^a \lambda_2^a + \text{h.c.}, \end{aligned} \quad (2.78)$$

where we use a complex scalar in the adjoint representation,

$$\phi_\chi^a \equiv \frac{\Sigma^a + iA_5^a}{\sqrt{2}}. \quad (2.79)$$

The term of $|f|^2|\phi_\chi^a|^2$ will vanish after integration out of the auxiliary field F_χ .

For hypermultiplet, similarly we redefine the chiral superfields for canonical normalization,

$$H_1 \rightarrow (1 - f\theta^2)H_1, \quad H_2 \rightarrow (1 - f\theta^2)H_2. \quad (2.80)$$

The third and fourth lines of Eq. (2.72) are,

$$\int d^4\theta \frac{T + T^\dagger}{2R} \{H_2 H_2^\dagger + H_1^\dagger H_1\} \quad (2.81)$$

$$\begin{aligned} &\rightarrow \int d^4\theta (1 + f\theta^2 + f^*\bar{\theta}^2)(1 - f\theta^2)(1 - f^*\bar{\theta}^2) \{H_2 H_2^\dagger + H_1^\dagger H_1\} \\ &= \int d^4\theta (1 - |f|^2\theta^4) \{H_2 H_2^\dagger + H_1^\dagger H_1\} \\ &= \int d^4\theta \{H_2 H_2^\dagger + H_1^\dagger H_1\} - |f|^2 (|\phi_1|^2 + |\phi_2|^2), \end{aligned} \quad (2.82)$$

and,

$$\begin{aligned} &\int d^2\theta H_2 (R^{-1}\partial_\varphi - \sqrt{2}g\chi)H_1 \\ &\rightarrow \int d^2\theta (1 - f\theta^2) H_2 (\partial_5 - \sqrt{2}g(1 + f\theta^2)\chi) (1 - f\theta^2)H_1 \\ &= \int d^2\theta (1 - 2f\theta^2) H_2 (\partial_5 - \sqrt{2}g\chi)H_1 - \theta^2 (\sqrt{2}gfH_2\chi H_1) \\ &= \int d^2\theta \{H_2 (\partial_5 - \sqrt{2}g\chi)H_1 + \theta^2 fH_2 (-2\partial_5 + \sqrt{2}g\chi)H_1\} \\ &= \int d^2\theta H_2 (\partial_5 - \sqrt{2}g\chi)H_1 + f\phi_2 (-2\partial_5 + \sqrt{2}g\phi_\chi^a T^a)\phi_1. \end{aligned} \quad (2.83)$$

So far, the extra terms generated by the Radion VEV of $F_T(f)$ are

$$\begin{aligned} &\left(\frac{f}{2}\lambda_1^a\lambda_1^a + \frac{f^*}{2}\lambda_2^a\lambda_2^a + \text{h.c.} \right) - |f|^2 (|\phi_1|^2 + |\phi_2|^2) \\ &+ |f|^2 |\phi_\chi^a|^2 + \left\{ f\phi_2 (-2\partial_5 + \sqrt{2}g\phi_\chi^a T^a)\phi_1 + \text{h.c.} \right\} \\ &\quad - f^* F_\chi^a \phi_\chi^a - f F_\chi^{a*} \phi_\chi^{a*}. \end{aligned} \quad (2.84)$$

By integrating out F_χ , the second and third lines of Eq. (2.84) are changed into a different form which we can compare to the Scherk-Schwarz mechanism. Terms involving F_χ in Eqs. (2.15, 2.22, 2.84) are,

$$|F_\chi|^2 - \sqrt{2}gF_\chi^a(\phi_2 T^a \phi_1) - \sqrt{2}gF_\chi^{a*}(\phi_1^* T^a \phi_2^*) - f^* F_\chi^a \phi_\chi^a - f F_\chi^{a*} \phi_\chi^{a*}, \quad (2.85)$$

and after integrating out F_χ we have

$$\begin{aligned} &-2g^2(\phi_2 T^a \phi_1)(\phi_1^* T^a \phi_2^*) \\ &-|f|^2 |\phi_\chi^a|^2 - \sqrt{2}gf\phi_\chi^{a*}(\phi_2 T^a \phi_1) - \sqrt{2}gf^*\phi_\chi^a(\phi_1^* T^a \phi_2^*). \end{aligned} \quad (2.86)$$

We combine the above soft terms with terms not involving F_χ from Eq.(2.84). The $|f|^2|\phi_\chi^a|^2$ terms is cancelled and the rest terms are

$$\begin{aligned}
\mathcal{L}_{5,\text{soft}} &= \left(\frac{f}{2} \lambda_1^a \lambda_1^a + \frac{f^*}{2} \lambda_2^a \lambda_2^a + \text{h.c.} \right) - |f|^2 (|\phi_1|^2 + |\phi_2|^2) \\
&\quad - 2 \left\{ f \phi_2 \left(\partial_5 - \sqrt{2}g \frac{\phi_\chi^a - \phi_\chi^{a*}}{2} T^a \right) \phi_1 + \text{h.c.} \right\} \\
&= \left(\frac{f}{2} \lambda_1^a \lambda_1^a + \frac{f^*}{2} \lambda_2^a \lambda_2^a + \text{h.c.} \right) - |f|^2 (|\phi_1|^2 + |\phi_2|^2) \\
&\quad - 2 \{ f \phi_2 (\partial_5 - ig A_5^a T^a) \phi_1 + \text{h.c.} \} \\
&= \left(\frac{f}{2} \lambda_1^a \lambda_1^a + \frac{f^*}{2} \lambda_2^a \lambda_2^a + \text{h.c.} \right) - |f|^2 (|\phi_1|^2 + |\phi_2|^2) \\
&\quad + f^* \phi_1^* (\mathcal{D}_5 \phi_2^*) - f \phi_2 (\mathcal{D}_5 \phi_1) - f^* (\mathcal{D}_5 \phi_1)^\dagger \phi_2^* + f (\mathcal{D}_5 \phi_2^*)^\dagger \phi_1 . \quad (2.87)
\end{aligned}$$

Since the phase of f can be removed by $SU(2)_R$ rotation, it always becomes real. Therefore, soft terms in Eq. (2.51) and those generated by the Scherk-Schwarz mechanism in Eq. (2.87) are same by a relation of

$$f = \frac{F_T}{2R} = \frac{\alpha}{R} \quad (2.88)$$

We can view this type of supersymmetry breaking in two different ways. The Scherk-Schwarz mechanism tells us that this is non-local supersymmetry breaking in the 5D theory. This leads to an important consequence of radiative corrections that the radiative corrections which appear due to the SUSY breaking are UV finite because the UV behavior (divergence) is local effect while the SUSY breaking of this kind is not local (for more detail, see Ref.[35, 42]). We see this in Sec. 2.6.2. The Radion mediation is formulated with $\mathcal{N} = 1$ superfields yielding SUSY breaking in the wave function of hypermultiplet.

2.4.3 Soft terms on brane

The Radion mediation requires the field redefinition, which generates soft terms once we consider interactions on branes. As in Sec.2.3.3, let us consider brane interactions,

$$W_{\text{brane}} = \delta(y) \left\{ \lambda_1 S_1(x) S_2(x) H_1(x, y) + \frac{\lambda_2}{2} S_1(x) H_1^2(x, y) + \frac{\lambda_3}{3} H_1^3(x, y) \right\}.$$

The bulk field H_1 are canonically normalized as Eq. (2.80), which results in soft terms on the brane,

$$\begin{aligned}
\int d^2\theta W_{\text{brane}} &\rightarrow \int d^2\theta \delta(y) \left\{ \lambda_1 S_1(x) S_2(x) (1 - f\theta^2) H_1(x, y) \right. \\
&\quad \left. + \frac{\lambda_2}{2} S_1(x) (1 - f\theta^2)^2 H_1^2(x, y) + \frac{\lambda_3}{3} (1 - f\theta^2)^3 H_1^3(x, y) \right\} \quad (2.89)
\end{aligned}$$

$$\begin{aligned}
&= \int d^2\theta \delta(y) \left\{ \lambda_1 S_1(x) S_2(x) (1 - f\theta^2) H_1(x, y) \right. \\
&\quad \left. + \frac{\lambda_2}{2} S_1(x) (1 - 2f\theta^2) H_1^2(x, y) + \frac{\lambda_3}{3} (1 - 3f\theta^2) H_1^3(x, y) \right\}, \quad (2.90)
\end{aligned}$$

and then,

$$\mathcal{L}_{\text{brane,soft}} = \delta(y) \left\{ \lambda_1(-f)\phi_{S1}\phi_{S2}\phi_1 + \frac{\lambda_2}{2}(-2f)\phi_{S1}\phi_1^2 + \frac{\lambda_3}{3}(-3f)\phi_1^3 \right\}. \quad (2.91)$$

With $f = \alpha/R$, these soft terms are same as those derived by the Scherk-Schwarz mechanism, Eq. (2.65). From this point, we confirm the equivalence between Scherk-Schwarz mechanism and Radion mediation.

2.5 Model Setup

Here a model setup of Compact Supersymmetry is described.

2.5.1 Bulk gauge and matter fields

We consider a supersymmetric $SU(3)_C \times SU(2)_L \times U(1)_Y$ gauge theory in this spacetime, with the gauge and three generations of matter supermultiplets propagating in the bulk where fields must form $\mathcal{N} = 2, D = 4$ multiplet. Then, for instance, $SU(3)_C$ gauge supermultiplet is composed of a vector superfield V_C (in $\mathcal{N} = 1$) and a chiral superfield χ_C , and similarly $SU(2)_L$ and $U(1)_Y$ gauge supermultiplets are given by (V_L, χ_L) and (V_Y, χ_Y) , respectively.

A matter field form a hypermultiplet which requires a chiral superfield with the SM charge and another one with the opposite charge. For example $SU(2)_L$ doublet quark is a hypermultiplet of (Q, Q^c) , whose superscript c means the opposite charge. The other fields are $(U, U^c), (D, D^c), (L, L^c), (E, E^c)$. The bulk Lagrangian of matters is given by Eq. (2.19) replacing,

$$(H_1, H_2) \rightarrow (Q, Q^c), (U, U^c), (D, D^c), (L, L^c), (E, E^c). \quad (2.92)$$

Under $\mathcal{P} : y \rightarrow -y$, fields with superscript c is odd, and thus their zero modes are projected out. The soft masses of squark, slepton, and gaugino are therefore

$$M_{1/2} = \frac{\alpha}{R}, \quad m_{\tilde{Q}, \tilde{U}, \tilde{D}, \tilde{L}, \tilde{E}}^2 = \left(\frac{\alpha}{R}\right)^2. \quad (2.93)$$

in the language of MSSM.

2.5.2 Higgs fields and Yukawa interactions

The Higgs chiral superfields H_u and H_d are located on one of the branes at $y = 0$. The Yukawa couplings, μ term, and kinetic terms can then be written on that brane:

$$\begin{aligned} \mathcal{L}_{\text{brane}} = & \delta(y) \int d^2\theta \{ y_{U5}^{ij} H_u Q_i U_j + y_{D5}^{ij} H_d Q_i D_j + y_{E5}^{ij} H_d L_i E_j + \mu H_u H_d \} \\ & + \delta(y) \int d^4\theta \{ H_u^\dagger e^{-2gV} H_u + H_d^\dagger e^{-2gV} H_d \}, \end{aligned} \quad (2.94)$$

where Yukawa couplings are proportional to those of the SM, and i and j are flavor indices. The \mathcal{P} odd fields (Q^c, U^c, \dots) cannot have these Yukawa interactions since their wave functions are zero at $y = 0$. (Here, we have simply assumed the existence of the μ term on the brane.

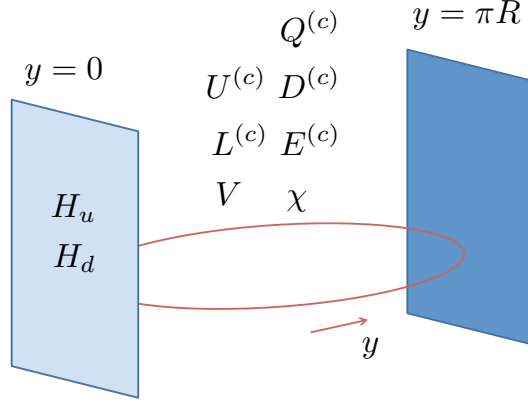


Figure 2.1: Field configuration of Compact Supersymmetry Model

We leave discussions of its origin to future work.) In the Radion mediation, the fields living in the bulk have field redefinition in Eq. (2.80) for the canonical normalization such that

$$\{Q, U, D, L, E\} \rightarrow \left(1 - \frac{\alpha}{R}\theta^2\right) \{Q, U, D, L, E\}. \quad (2.95)$$

In general, $(1 - F\theta^2)^n$ becomes $(1 - nF\theta^2)$, and thus,

$$\begin{aligned} \mathcal{L}_{\text{brane,soft}} = & \delta(y) \left\{ y_{U5}^{ij} \left(\frac{-2\alpha}{R} \right) \phi_{H_u} \phi_{Q_i} \phi_{U_j} + y_{D5}^{ij} \left(\frac{-2\alpha}{R} \right) \phi_{H_d} \phi_{Q_i} \phi_{D_j} \right. \\ & \left. + y_{E5}^{ij} \left(\frac{-2\alpha}{R} \right) \phi_{H_d} \phi_{L_i} \phi_{E_j} \right\} + \text{h.c.} \end{aligned} \quad (2.96)$$

There are no soft masses of Higgs fields. Together with Eq. (2.93), this leads to the expressions of (MSSM) soft terms we gave in Eq. (2.1) in the introduction,

$$\begin{aligned} M_{1/2} = \frac{\alpha}{R}, \quad m_{\tilde{Q}, \tilde{U}, \tilde{D}, \tilde{L}, \tilde{E}}^2 = \left(\frac{\alpha}{R}\right)^2, \quad m_{H_u, H_d}^2 = 0, \\ A_0 = -\frac{2\alpha}{R}, \quad B = 0, \end{aligned} \quad (2.97)$$

at tree-level. Note that the degeneracy among the three generations of scalars and gauginos is automatic because of the geometric nature of the SUSY breaking. In addition, since α and μ can always be taken real by phase redefinitions of fields associated with R and Peccei-Quinn rotations, there is no physical phase in $M_{1/2}$, A_0 , μ , or B . Therefore, the flavor problem as well as the CP problem are automatically solved in this model.

2.5.3 Lagrangian on brane with Yukawa coupling

Let us investigate brane interactions involving up-type quark in KK modes. We use them in the later calculation of radiative corrections through top-Yukawa coupling in Sec. 2.6.2. We

		$SU(3)_C$	$SU(2)_L$	$U(1)_Y$	$SU(2)_R$	$\mathcal{P} : y \rightarrow -y$
$V_C \chi_C$	G_μ	8	1	0	1	+
	(G_5, Σ_G)	8	1	0	1	-
	$(\lambda_{G1}, -\lambda_{G2})$	8	1	0	2	(+, -)
$V_L \chi_L$	W_μ	1	3	0	1	+
	(W_5, Σ_W)	1	3	0	1	-
	$(\lambda_{W1}, -\lambda_{W2})$	1	3	0	2	(+, -)
$V_Y \chi_Y$	B_μ	1	1	0	1	+
	(B_5, Σ_B)	1	1	0	1	-
	$(\lambda_{B1}, -\lambda_{B2})$	1	1	0	2	(+, -)

Table 2.1: Representation of fields in gauge supermultiplet.

		$SU(3)_C$	$SU(2)_L$	$U(1)_Y$	$SU(2)_R$	$\mathcal{P} : y \rightarrow -y$
$Q Q^{c\dagger}$	$(\phi_Q, \phi_{Q^c}^*)$	3	2	1/6	2	(+, -)
	$(\psi_Q, \psi_{Q^c}^*)$	3	2	1/6	1	(+, -)
$U U^{c\dagger}$	$(\phi_U, \phi_{U^c}^*)$	$\bar{\mathbf{3}}$	1	-2/3	2	(+, -)
	$(\psi_U, \psi_{U^c}^*)$	$\bar{\mathbf{3}}$	1	-2/3	1	(+, -)
$D D^{c\dagger}$	$(\phi_D, \phi_{D^c}^*)$	$\bar{\mathbf{3}}$	1	1/3	2	(+, -)
	$(\psi_D, \psi_{D^c}^*)$	$\bar{\mathbf{3}}$	1	1/3	1	(+, -)
$L L^{c\dagger}$	$(\phi_L, \phi_{L^c}^*)$	1	2	-1/2	2	(+, -)
	$(\psi_L, \psi_{L^c}^*)$	1	2	-1/2	1	(+, -)
$E E^{c\dagger}$	$(\phi_E, \phi_{E^c}^*)$	1	1	1	2	(+, -)
	$(\psi_E, \psi_{E^c}^*)$	1	1	1	1	(+, -)
H_u	ϕ_{H_u}	1	2	1/2	1	+
	ψ_{H_u}	1	2	1/2	1	+
H_d	ϕ_{H_d}	1	2	-1/2	1	+
	ψ_{H_d}	1	2	-1/2	1	+

Table 2.2: Representation of fields in hypermultiplet and Higgs chiral supermultiplet.

omit flavor indices for simplicity. Component interactions from Eq. (2.94) are

$$\begin{aligned} \mathcal{L}_{y_{U5},\phi} &= \delta(y) \left[y_{U5} \{ F_{H_u} \phi_Q(y) \phi_U(y) + \phi_{H_u} F_Q(y) \phi_U(y) + \phi_{H_u} \phi_Q(y) F_U(y) \} \right. \\ &\quad \left. + \mu \{ F_{H_u} \phi_{H_d} + \phi_{H_u} F_{H_d} \} + y_{U5} \left(\frac{-2\alpha}{R} \right) \phi_{H_u} \phi_{Q_i} \phi_{U_j} \right] + \text{h.c.} \\ &\quad + \delta(y) \{ |F_{H_u}|^2 + |F_{H_d}|^2 \} + |F'_Q(y)|^2 + |F'_U(y)|^2 \end{aligned} \quad (2.98)$$

$$\begin{aligned} &= \delta(y) \left[y_{U5} \left\{ F_{H_u} \phi_Q(y) \phi_U(y) + \phi_{H_u} [F'_Q(y) + \partial_5 \phi_{Q^c}^*(y)] \phi_U(y) \right. \right. \\ &\quad \left. \left. + \phi_{H_u} \phi_Q(y) [F'_U(y) + \partial_5 \phi_{U^c}^*(y)] \right\} \right. \\ &\quad \left. + \mu \{ F_{H_u} \phi_{H_d} + \phi_{H_u} F_{H_d} \} + y_{U5} \left(\frac{-2\alpha}{R} \right) \phi_{H_u} \phi_{Q_i} \phi_{U_j} \right] + \text{h.c.} \\ &\quad + \delta(y) \{ |F_{H_u}|^2 + |F_{H_d}|^2 \} + |F'_Q(y)|^2 + |F'_U(y)|^2, \end{aligned} \quad (2.99)$$

where F -terms in the bulk are already redefined as

$$F'_Q = F_Q + [-\partial_5 - g(\Sigma - iA_5)]\phi_{Q^c}^*, \quad (2.100)$$

$$F'_U = F_U + [-\partial_5 - g(\Sigma - iA_5)]\phi_{U^c}^*, \quad (2.101)$$

and Σ and A_5 vanish since their wave functions are zero at $y = 0$ brane. If we integrate out F' -term as 5D field, double delta function $\delta(y)\delta(y) \sim \delta(y) \sum_{n=-\infty}^{\infty} (2\pi R)^{-1}$ is led, and then the result seems meaningless. We perform the KK expansion first and integrate out the KK modes of F' -terms so that we understand the meaning. We have the following KK expansions,

$$F'_{Q(U)}(y) = \sum_{n=-\infty}^{\infty} \frac{1}{\sqrt{2\pi R}} F'_{Q(U),n} \cos \frac{ny}{R}, \quad (2.102)$$

$$\phi_{Q(U)}(y) = \sum_{n=-\infty}^{\infty} \frac{1}{\sqrt{2\pi R}} \phi_{Q(U),n} \cos \frac{ny}{R}, \quad (2.103)$$

$$\phi_{Q^c(U^c)}^*(y) = \sum_{n=-\infty}^{\infty} \frac{-1}{\sqrt{2\pi R}} \phi_{Q(U),n} \sin \frac{ny}{R}, \quad (2.104)$$

where $\phi_{Q(U)n}$ is a mass eigenstate with mass of $(\alpha + n)/R$. Perform y integral,

$$\begin{aligned}
\int_0^{2\pi R} dy \mathcal{L}_{yU5,\phi} = & yU5 \left\{ F_{H_u} \sum_{n=-\infty}^{\infty} \frac{\phi_{Qn}}{\sqrt{2\pi R}} \sum_{m=-\infty}^{\infty} \frac{\phi_{Um}}{\sqrt{2\pi R}} \right. \\
& + \phi_{H_u} \sum_{n=-\infty}^{\infty} \frac{F'_{Qn} - \frac{n}{R}\phi_{Qn}}{\sqrt{2\pi R}} \sum_{m=-\infty}^{\infty} \frac{\phi_{Um}}{\sqrt{2\pi R}} \\
& \left. + \phi_{H_u} \sum_{n=-\infty}^{\infty} \frac{\phi_{Qn}}{\sqrt{2\pi R}} \sum_{m=-\infty}^{\infty} \frac{F'_{Um} - \frac{m}{R}\phi_{Um}}{\sqrt{2\pi R}} \right\} + \text{h.c.} \\
& + \mu \{ F_{H_u} \phi_{H_d} + \phi_{H_u} F_{H_d} \} + \text{h.c.} \\
& + yU5 \left(\frac{-2\alpha}{R} \right) \phi_{H_u} \sum_{n=-\infty}^{\infty} \frac{\phi_{Qn}}{\sqrt{2\pi R}} \sum_{m=-\infty}^{\infty} \frac{\phi_{Um}}{\sqrt{2\pi R}} + \text{h.c.} \\
& + |F_{H_u}|^2 + |F_{H_d}|^2 + \sum_{n=-\infty}^{\infty} |F'_{Qn}|^2 + \sum_{m=-\infty}^{\infty} |F'_{Um}|^2, \quad (2.105)
\end{aligned}$$

and the equations of motion for F -terms,

$$F_{H_u}^* + yU \sum_{n=-\infty}^{\infty} \phi_{Qn} \sum_{m=-\infty}^{\infty} \phi_{Um} + \mu \phi_{H_d} = 0, \quad (2.106)$$

$$F'_{Qn} + yU \phi_{H_u} \sum_{m=-\infty}^{\infty} \phi_{Um} = 0, \quad (2.107)$$

$$F'_{Um} + yU \phi_{H_u} \sum_{n=-\infty}^{\infty} \phi_{Qn} = 0, \quad (2.108)$$

where $y_U \equiv yU5/(2\pi R)$. These conditions are substituted to the Lagrangian,

$$\begin{aligned}
\int_0^{2\pi R} dy \mathcal{L}_{yU5,\phi} = & - \left| yU \sum_{n=-\infty}^{\infty} \phi_{Qn} \sum_{m=-\infty}^{\infty} \phi_{Um} + \mu \phi_{H_d} \right|^2 \\
& - \left| yU \phi_{H_u} \sum_{m=-\infty}^{\infty} \phi_{Um} \right|^2 \times \sum_{n=-\infty}^{\infty} - \left| yU \phi_{H_u} \sum_{m=-\infty}^{\infty} \phi_{Qm} \right|^2 \times \sum_{n=-\infty}^{\infty} \\
& - \sum_{m,n=-\infty}^{\infty} yU \frac{(\alpha + m) + (\alpha + n)}{R} \phi_{H_u} \phi_{Qm} \phi_{Un} + \text{h.c.} \quad (2.109)
\end{aligned}$$

In the second line, there is infinite sum left which is originally from the sum of F'_n -terms. This itself looks to lead infinitely large coupling of $|\phi_{H_u} \phi_{U(Q)m}|^2$ interaction, and one may even worry that the low-energy limit of this theory cannot be the MSSM. However, the amplitude is certainly finite because the other bosonic interaction cancel the infinite sum as in Fig. 2.2. For this cancellation, in the low-energy limit $E \ll 1/R$, vertices which are consistent with the MSSM are actually remained, namely,

$$\begin{aligned}
& - |yU \phi_{Q0} \phi_{U0} + \mu \phi_{H_d}|^2 - |yU \phi_{H_u} \phi_{U0}|^2 - |yU \phi_{H_u} \phi_{Q0}|^2 \\
& - yU \frac{2\alpha}{R} \phi_{H_u} \phi_{Q0} \phi_{U0} + \text{h.c.} \quad (2.110)
\end{aligned}$$

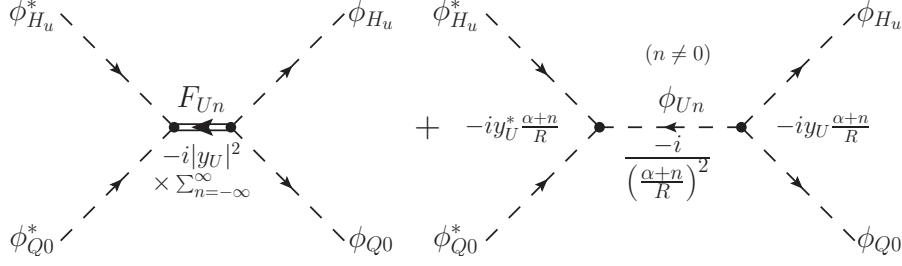


Figure 2.2: Cancellation of infinite sum for $|\phi_{H_u}\phi_{Q_0}|^2$ vertex.

The same cancellation is important when we compute the radiative correction; it look dangerous on first sight, but finally gives a regularized result.

Let us give a comment on the trilinear terms. In the Radion mediation, this dimensionful couplings come from the fifth derivative ∂_5 due to the field redefinition of F as in Eqs. (2.100,2.101) and from the soft supersymmetry breaking of Eq. (2.96), and they are (luckily) combined to an organized form in Eq. (2.109). This result is necessary because in the picture of the Scherk-Schwarz mechanism the soft terms come along with the fifth derivative ∂_5 , and therefore the dimensionful coupling is written in terms of KK mode mass such as $\frac{\alpha+n}{R}$. If we consider a field configuration where H_u is also living in the bulk as well as quark fields, analogous to Eq. (2.109) the trilinear terms are expected to be

$$- \sum_{k,m,n=-\infty}^{\infty} y_U \frac{(\alpha+k) + (\alpha+m) + (\alpha+n)}{R} \phi_{H_u k} \phi_{Q_m} \phi_{U_n}. \quad (2.111)$$

This is certainly true.

Next, we give the fermionic interactions, which are much simpler compared to those of scalars. The fermionic interactions with y_U are

$$\mathcal{L}_{y_U 5, \psi} = \delta(y) y_{U5} \{ -\phi_{H_u} \psi_Q \psi_U - \psi_{H_u} \phi_Q \psi_U - \psi_{H_u} \psi_Q \phi_U \} + \text{h.c.} \quad (2.112)$$

and we perform the KK expansion and y integral,

$$\begin{aligned} \int_0^{2\pi R} dy \mathcal{L}_{y_U 5, \psi} &= -\frac{y_{U5}}{2\pi R} \sum_{m,n=1}^{\infty} 2\eta_m \eta_n \phi_{H_u} \psi_{Q,m} \psi_{U,n} + \text{h.c.} \\ &\quad -\frac{y_{U5}}{2\pi R} \sum_{m=-\infty}^{\infty} \sum_{n=1}^{\infty} \sqrt{2} \eta_m \psi_{H_u} (\phi_{Q_m} \psi_{U,n} + \psi_{Q,n} \phi_{U_m}) + \text{h.c.} \end{aligned} \quad (2.113)$$

where the KK expansion for fermions are

$$\psi_{Q(U)}(y) = \sum_{n=0}^{\infty} \frac{\eta_n}{\sqrt{\pi R}} \psi_{Q(U),n} \cos \frac{ny}{R}. \quad (2.114)$$

where $\eta_n = (1/\sqrt{2})\delta_{n,0}$. The non-zero modes are Dirac fermions, so we write the Lagrangian

in four component spinors,

$$\begin{aligned}
\int_0^{2\pi R} dy \mathcal{L}_{y_U^5, \psi} &= \sum_{m,n=1}^{\infty} (-2\eta_m \eta_n) (y_U \phi_{H_u} \bar{\Psi}_{Qm}^c P_L \Psi_{Un} + y_U^* \bar{\Psi}_{Un} P_R \Psi_{Qm}^c \phi_{H_u}^*) \\
&+ \sum_{m=-\infty}^{\infty} \sum_{n=1}^{\infty} (-\sqrt{2}\eta_n) (y_U \bar{\Psi}_{H_u} \phi_{Qm} P_L \Psi_{Un} + y_U^* \bar{\Psi}_{Un} \phi_{Qm}^* P_R \Psi_{H_u}) \\
&+ \sum_{m=1}^{\infty} \sum_{n=-\infty}^{\infty} (-\sqrt{2}\eta_m) (y_U \bar{\Psi}_{H_u} P_L \Psi_{Qm} \phi_{Un} + y_U^* \phi_{Un}^* \bar{\Psi}_{Qm} P_R \Psi_{H_u}) \quad (2.115)
\end{aligned}$$

where the four component spinors are

$$\Psi_{H_u} \equiv \begin{pmatrix} \psi_{H_u} \\ \bar{\psi}_{H_u} \end{pmatrix}, \quad \Psi_{Q(U)0} \equiv \begin{pmatrix} \psi_{Q(U),0} \\ \bar{\psi}_{Q(U),0} \end{pmatrix}, \quad \Psi_{Q(U)n} \equiv \begin{pmatrix} \psi_{Q(U),n} \\ \bar{\psi}_{Q^c(U^c),n} \end{pmatrix}. \quad (2.116)$$

Note that we can rewrite the above interactions according to the situation using relations below,

$$\begin{aligned}
\bar{\Psi}_{Qm}^c P_L \Psi_{Un} &= \bar{\Psi}_{Un}^c P_L \Psi_{Qm}, & \bar{\Psi}_{Un} P_R \Psi_{Qm}^c &= \bar{\Psi}_{Qm} P_R \Psi_{Un}^c, \\
\bar{\Psi}_{H_u} P_L \Psi_{Un} &= \bar{\Psi}_{Un}^c P_L \Psi_{H_u}, & \bar{\Psi}_{Un} P_L \Psi_{H_u} &= \bar{\Psi}_{H_u} P_R \Psi_{Un}^c, \\
\bar{\Psi}_{H_u} P_L \Psi_{Qn} &= -\bar{\Psi}_{Qn}^c P_L \Psi_{H_u}, & \bar{\Psi}_{Qn} P_L \Psi_{H_u} &= -\bar{\Psi}_{H_u} P_R \Psi_{Qn}^c.
\end{aligned} \quad (2.117)$$

The minus sign in the last line is due to $SU(2)_L$ contraction.

2.5.4 Lagrangian on brane with gauge coupling

Now we investigate gauge interactions on the brane. Here we consider gauge fields of non-abelian group. These gauge interactions are basically as same as those in ordinary $\mathcal{N} = 1, D = 4$, except for $\delta(y)$ factor. The interactions together with bulk D -term are

$$\begin{aligned}
\mathcal{L}_{\text{gauge5}, \phi_H} &= \frac{1}{2} D'^a(y) D'^a(y) - \delta(y) \{ g_5 D^a(y) \phi_{H_u}^* T^a \phi_{H_u} \} \\
&+ \delta(y) (i g_5 A_\mu^a(y)) \{ \phi_{H_u}^* T^a (\partial^\mu \phi_{H_u}) - (\partial^\mu \phi_{H_u}^*) T^a \phi_{H_u} \} \\
&+ \delta(y) \{ g_5^2 A_\mu^a(y) A^{b\mu}(y) \phi_{H_u}^* T^a T^b \phi_{H_u} \} \\
&+ \delta(y) \left\{ -\sqrt{2} g_5 \phi_{H_u}^* T^a \psi_{H_u} \lambda_1^a(y) - \sqrt{2} g_5 \bar{\lambda}_1^a(y) \bar{\psi}_{H_u} T^a \phi_{H_u} \right\} \\
&\quad + (H_u \leftrightarrow H_d) \\
&= \frac{1}{2} D'^a(y) D'^a(y) - \delta(y) \{ g_5 (D'^a(y) - \mathcal{D}_5 \Sigma^a(y)) \phi_{H_u}^* T^a \phi_{H_u} \} \\
&+ \delta(y) (i g_5 A_\mu^a(y)) \{ \phi_{H_u}^* T^a (\partial^\mu \phi_{H_u}) - (\partial^\mu \phi_{H_u}^*) T^a \phi_{H_u} \} \\
&+ \delta(y) \{ g_5^2 A_\mu^a(y) A^{b\mu}(y) \phi_{H_u}^* T^a T^b \phi_{H_u} \} \\
&+ \delta(y) \left\{ -\sqrt{2} g_5 \phi_{H_u}^* T^a \psi_{H_u} \lambda_1^a(y) - \sqrt{2} g_5 \bar{\lambda}_1^a(y) \bar{\psi}_{H_u} T^a \phi_{H_u} \right\} \\
&\quad + (H_u \leftrightarrow H_d) \quad (2.118)
\end{aligned}$$

where $D'^a = D^a + \mathcal{D}_5 \Sigma^a$. As for Yukawa interaction, we perform the KK expansion and y integral,

$$\begin{aligned}
\int_0^{2\pi R} dy \mathcal{L}_{\text{gauge5}, \phi_H} &= \frac{1}{2} \sum_{n=-\infty}^{\infty} (D'_n)^2 - \sum_{n=-\infty}^{\infty} g D'_n{}^a (\phi_{H_u}^* T^a \phi_{H_u}) \\
&+ \sum_{n=1}^{\infty} \sqrt{2} g \frac{n}{R} \Sigma_n^a \{ \phi_{H_u}^* T^a \phi_{H_u} + \phi_{H_d}^* T^a \phi_{H_d} \} \\
&+ \sum_{n=0}^{\infty} (i\sqrt{2}\eta_n) g A_{(n)\mu}^a \{ \phi_{H_u}^* T^a (\partial^\mu \phi_{H_u}) - (\partial^\mu \phi_{H_u}^*) T^a \phi_{H_u} \} \\
&+ \sum_{m,n=0}^{\infty} (2\eta_m \eta_n) g A_{(m)\mu}^a A_{(n)}^{b\mu} \phi_{H_u}^* T^a T^b \phi_{H_u} \\
&- \sum_{n=-\infty}^{\infty} \sqrt{2} g \{ \phi_{H_u}^* T^a \bar{\Psi}_{H_u} P_L \lambda_n^a + \bar{\lambda}_n^a P_R \Psi_{H_u} T^a \phi_{H_u} \} \\
&\quad + (H_u \leftrightarrow H_d)
\end{aligned} \tag{2.119}$$

where the KK expansions of D' , A_μ , Σ , and λ_1 , are,

$$\begin{aligned}
D'(y) &= \sum_{n=-\infty}^{\infty} \frac{D'_n}{\sqrt{2\pi R}} \cos \frac{ny}{R}, \quad A_\mu(y) = \sum_{n=0}^{\infty} \frac{\eta_n A_{(n)\mu}}{\sqrt{\pi R}} \cos \frac{ny}{R}, \\
\Sigma(y) &= \sum_{n=0}^{\infty} \frac{\Sigma_n}{\sqrt{\pi R}} \sin \frac{ny}{R}, \quad \lambda_1(y) = \sum_{n=-\infty}^{\infty} P_L \frac{\lambda_n}{\sqrt{2\pi R}} \cos \frac{ny}{R}.
\end{aligned} \tag{2.120}$$

The equation of motion for D' -terms is given by,

$$D'_n{}^a = g (\phi_{H_u}^* T^a \phi_{H_u}) + g (\phi_{H_d}^* T^a \phi_{H_d}) + \dots \tag{2.121}$$

Here, \dots represents terms from other matters, but they are irrelevant for the later calculation of $\phi_{H_{u,d}}$ vacuum polarizations since the generator is traceless $\text{Tr}(T^a) = 0$.³ The equation of motion for D -term leads to,

$$\begin{aligned}
&\frac{1}{2} \sum_{n=-\infty}^{\infty} (D'_n)^2 - \sum_{n=-\infty}^{\infty} g D'_n{}^a (\phi_{H_u}^* T^a \phi_{H_u} + \phi_{H_d}^* T^a \phi_{H_d} + \dots) \\
&\rightarrow -\frac{g^2}{2} \sum_{n=-\infty}^{\infty} (\phi_{H_u}^* T^a \phi_{H_u} + \phi_{H_d}^* T^a \phi_{H_d} + \dots)^2.
\end{aligned} \tag{2.122}$$

Similar to the case of Yukawa interaction, these quartic couplings have infinite sum, but they are also cancelled by the effective quartic couplings from Σ exchange.

³For the $U(1)_Y$ case, the generator is not traceless, but the terms from matters such as $|\phi_{H_u}|^2 |\phi_Q|^2$ are again irrelevant. This comes from the fact that $U(1)_Y$ gauge symmetry is anomaly free but not from consequence of supersymmetry. This is understood by the renormalization of tadpole term $\int d^4\theta V \supset D$ which is allowed only for abelian gauge field. Since this is in the Kähler potential and has a coefficient of $(\text{mass})^2$, quadratic divergences proportional to $U(1)_Y$ charge actually appear for this D -term. The cancellation condition of this term is $\text{Tr}Y=0$ which corresponds to one of the conditions of anomaly cancellation. See Ref. [40] for derivation.

2.6 Radiative Corrections

2.6.1 Dimensional analysis for radiative corrections

The expressions in Eq. (2.97) receive corrections from physics above and at $1/R$. In the 5D picture, corrections above $1/R$ come from brane-localized kinetic terms for the gauge and matter supermultiplets, and affect $M_{1/2}$, $m_f^2 \equiv m_{\tilde{Q}, \tilde{U}, \tilde{D}, \tilde{L}, \tilde{E}}^2$, and A_0 . These terms have tree-level (threshold) contributions at Λ and radiative ones between $1/R$ and Λ . From dimensional analysis, the size of the radiative contributions is

$$\frac{\delta M_{1/2}}{M_{1/2}}, \frac{\delta m_f^2}{m_f^2}, \frac{\delta A_0}{A_0} \approx \mathcal{O}\left(\frac{g^2, y^2}{16\pi^2} \log(\Lambda R)\right). \quad (2.123)$$

Then we discuss what scale is appropriate for the cutoff, to be more explicit, up to what scale of the cutoff the prediction from the Scherk-Schwarz mechanism is valid. This is estimated by *Naïve Dimensional Analysis* in higher dimension [41]. Higher dimensional theories are not renormalizable and considered as effective theories. The effective theory picture is not valid at certain energy scale where the radiative correction exceeds tree-level term.

The size of radiative corrections is related to the phase-space factors in loop integrals which is dimension-dependent. In D -dimensional theories, the typical loop integral is

$$\int \frac{d^D p}{(2\pi)^D} \sim \frac{\Omega_{D-1}}{(2\pi)^2} \int \frac{dp^2}{2} p^{D-2} f(p^2) = \frac{\pi^{D/2}}{(2\pi)^D \Gamma(D/2)} \int dp^2 p^{D-2} f(p^2) \quad (2.124)$$

Then each loop integral is suppressed by the loop factor L_D ,

$$L_D = (4\pi)^{D/2} \Gamma(D/2). \quad (2.125)$$

The specific values of L_D are $16\pi^2$ ($D = 4$), $24\pi^3$ ($D = 5$), $128\pi^3$ ($D = 6$), \dots . When one computes radiative corrections of gauge and Yukawa couplings, there appear quadratic- and linear-divergence rather than log-divergence,⁴

$$\begin{aligned} \mathcal{L}_5 \sim & \int d^2\theta \delta(y) \left(1 + \frac{\mathcal{O}(g_4^2)}{16\pi^2} \Lambda R + \frac{\mathcal{O}(y_4^2)}{16\pi^2} (\Lambda R)^2\right) H^\dagger H \\ & + \int d^2\theta \frac{1}{g_5^2} \left(1 + \frac{\mathcal{O}(g_5^2)}{24\pi^3} \Lambda\right) W^\alpha W_\alpha. \end{aligned} \quad (2.126)$$

The loop factors are different because the Yukawa interactions are localized on the brane at $y = 0$ while the gauge fields are living in the bulk. Thus our effective higher dimensional field theory is valid for $\Lambda R \lesssim 4\pi$, and according to Eqs. (2.123, 2.163) the corrections to Eq. (2.97) from physics above $1/R$ are always subdominant. (The same can also be seen in the 4D picture. In this picture, $\mathcal{N} = 2$ supersymmetry existing for the $n > 0$ modes leads to nontrivial cancellations of the corrections to $M_{1/2}$, m_f^2 and A_0 from these modes. In order to see the cancellations for the gauge multiplets, the effect of anomalies must be taken into account correctly. The explicit demonstration of these nontrivial cancellations will be given elsewhere.)

⁴Power of divergences can be understood by dimensional analysis. For instance, the gauge coupling in the 5D has mass dimension of $-1/2$, and the radiative corrections along with g_5^2 are linearly divergent.

2.6.2 Finite threshold corrections

The corrections from physics at $1/R$ arise from non-local operators in 5D. They affect all the supersymmetry-breaking masses, and are of order $1/16\pi^2$. Here we calculate only the contributions to the Higgs mass parameters, which could potentially affect the analysis of electroweak symmetry breaking.

It is known that these radiative corrections from all the KK modes are surprisingly finite. The reason is because SUSY breaking of the Scherk-Schwartz mechanism is non-local in 5D while UV divergence is local effect. More discussion is found in Ref. [42] and also even two-loop level calculation is performed in Ref. [43].

In order to *match* and *run*, we need to know the threshold corrections at $E \approx 1/R$ after integrating out the non-zero KK modes. Since the low-energy theory is matched onto the MSSM, we can use MSSM renormalization group running. While the radiative corrections from all the KK modes are finite, they include the MSSM (zero mode) contributions, and then we subtract them in \overline{DR} scheme. Schematically, the procedure is as follows. For some mass parameter M , the corrections in full theory and the MSSM are

$$\delta M|_{\text{KK}} = \text{finite} \quad (2.127)$$

$$\delta M|_{\text{MSSM}(Q)} = \text{log-div} \quad (2.128)$$

where Q is the renormalization scale in the \overline{DR} scheme. Then the threshold correction at $E \approx 1/R$ is given by

$$\delta M(Q) = \delta M|_{\text{KK}} - \delta M|_{\text{MSSM}(Q)}. \quad (2.129)$$

This value can be used as initial condition of RG running at scale Q . For the check of this calculation, we must observe the cancelation of $\log \alpha$ because this term comes from IR-physics and is not the effect of integrating out massive particles.

We first calculate radiative corrections from all the KK modes to $m_{H_u}^2$ with Yukawa interaction for up-type quark in Fig. 2.3 . The contributions of bosonic loops in the limit of zero external momentum are

$$\begin{aligned} -i\Pi_{\text{Bosonic}}^{y_U} &= N_c \int \frac{d^4 k}{(2\pi)^4} \sum_{m,n=-\infty}^{\infty} \left\{ -i|y_U|^2 \frac{i}{k^2 - (\hat{m} + \hat{\alpha})^2} \times 2 \right. \\ &\quad \left. -iy_U (2\hat{\alpha} + \hat{m} + \hat{n}) \frac{i}{k^2 - (\hat{\alpha} + \hat{n})^2} (-iy_U^*) (2\hat{\alpha} + \hat{m} + \hat{n}) \frac{i}{k^2 - (\hat{\alpha} + \hat{m})^2} \right\} \end{aligned} \quad (2.130)$$

$$\begin{aligned} &= N_c \int \frac{d^4 k}{(2\pi)^4} \sum_{m,n=-\infty}^{\infty} \left\{ 2|y_U|^2 k^2 \frac{1}{k^2 - (\hat{m} + \hat{\alpha})^2} \frac{1}{k^2 - (\hat{n} + \hat{\alpha})^2} \right. \\ &\quad \left. + 2|y_U|^2 \frac{\hat{m} + \hat{\alpha}}{k^2 - (\hat{m} + \hat{\alpha})^2} \frac{\hat{n} + \hat{\alpha}}{k^2 - (\hat{n} + \hat{\alpha})^2} \right\}, \end{aligned} \quad (2.131)$$

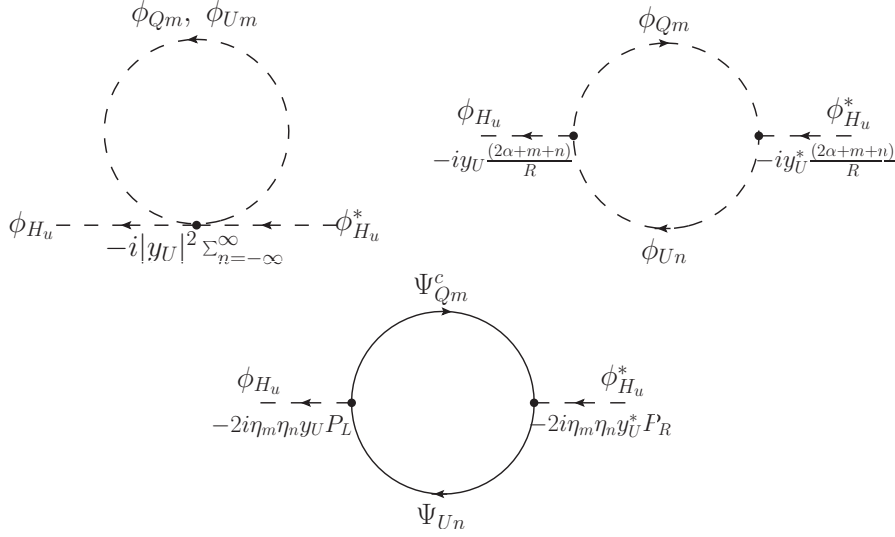


Figure 2.3: Bosonic loops of radiative corrections to $m_{H_u}^2$ with Yukawa coupling are on the top, and fermionic loops are on the bottom.

where $\hat{\alpha} = \frac{\alpha}{R}$, $\hat{m} = \frac{m}{R}$ and $\hat{n} = \frac{n}{R}$. The contributions of fermionic loops are

$$\begin{aligned}
-i\Pi_{\text{Fermionic}}^{y_U} &= -N_c \int \frac{d^4k}{(2\pi)^4} \sum_{m,n=0}^{\infty} \eta_n^2 \eta_m^2 \text{Tr} \left[(-2iy_U) P_L \frac{i}{\not{k} + \hat{m}} (-2iy_U^*) P_R \frac{i}{\not{k} + \hat{n}} \right] \\
&= N_c \int \frac{d^4k}{(2\pi)^4} \sum_{m,n=0}^{\infty} (-4 \times 2) \eta_n^2 \eta_m^2 |y_U|^2 k^2 \frac{1}{k^2 - \hat{m}^2} \frac{1}{k^2 - \hat{n}^2} \\
&= N_c \int \frac{d^4k}{(2\pi)^4} \sum_{m,n=-\infty}^{\infty} (-2) |y_U|^2 k^2 \frac{1}{k^2 - \hat{m}^2} \frac{1}{k^2 - \hat{n}^2}. \tag{2.132}
\end{aligned}$$

We perform summation and integral after combining them,

$$\begin{aligned}
\delta m_{H_u}^2|_{\text{KK}}^{y_U} &= \Pi_{\text{Bosonic+Fermionic}}^{y_U} \\
&= 2iN_c |y_U|^2 \int \frac{d^4k}{(2\pi)^4} \sum_{m,n=-\infty}^{\infty} \left\{ \frac{k^2}{(k^2 - (\hat{\alpha} + \hat{m})^2)(k^2 - (\hat{\alpha} + \hat{n})^2)} \right. \\
&\quad \left. \frac{\hat{m} + \hat{\alpha}}{k^2 - (\hat{m} + \hat{\alpha})^2} \frac{\hat{n} + \hat{\alpha}}{k^2 - (\hat{n} + \hat{\alpha})^2} - \frac{k^2}{(k^2 - \hat{m}^2)(k^2 - \hat{n}^2)} \right\} \tag{2.133}
\end{aligned}$$

$$= \frac{N_c |y_U|^2}{16\pi^2} \frac{3}{\pi^2 R^2} [\text{Li}_3(e^{2\pi i \alpha}) + \text{Li}_3(e^{-2\pi i \alpha}) - 2\zeta(3)] \tag{2.134}$$

$$\approx \frac{N_c |y_U|^2}{16\pi^2} \left(\frac{\alpha}{R} \right)^2 [6 \log(2\pi \alpha)^2 - 18]. \tag{2.135}$$

We leave the detail calculations in the Appendix C. A key for analytic calculations is that sums of m and n are factorized. Divergences appear from bosonic and fermionic diagrams with the same amount and are cancelled exactly leaving the finite results. In the last line, we expand with respect to α .

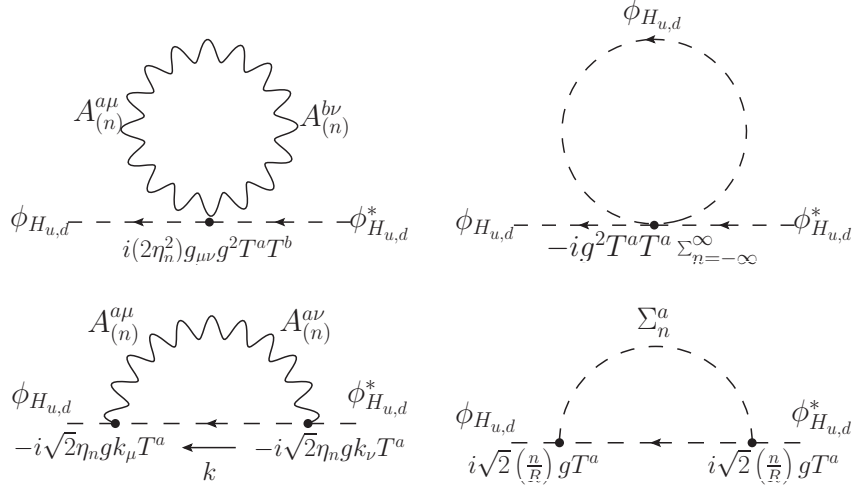


Figure 2.4: Bosonic loops of radiative corrections to $m_{H_{u,d}}^2$ with the gauge coupling.

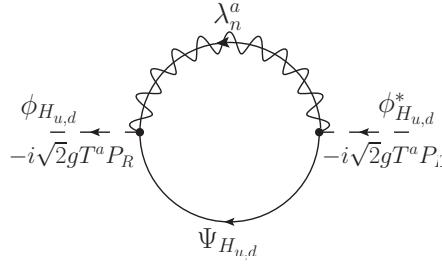


Figure 2.5: Fermionic loops of radiative corrections to $m_{H_{u,d}}^2$ with the gauge coupling.

Radiative corrections from all the KK modes with gauge interaction to $m_{H_{u,d}}^2$ are calculated. The contributions of bosonic loops in Fig. 2.4 are

$$\begin{aligned}
-i\Pi_{\text{Bosonic}}^g &= C_2(r) \int \frac{d^4k}{(2\pi)^4} \left\{ \sum_{n=0}^{\infty} i(2\eta_n^2)g^2 g_{\mu\nu} \frac{-ig^{\mu\nu}}{k^2 - \hat{n}^2} + \sum_{n=-\infty}^{\infty} -ig^2 \frac{i}{k^2} \right. \\
&\quad + \sum_{n=0}^{\infty} (-i\sqrt{2}\eta_n g) k_\mu \frac{-ig_{\mu\nu}}{k^2 - \hat{n}^2} (-i\sqrt{2}\eta_n g) k_\nu \frac{i}{k^2} \\
&\quad \left. + \sum_{n=0}^{\infty} (i\sqrt{2}g\hat{n}) \frac{i}{k^2 - \hat{n}^2} (i\sqrt{2}g\hat{n}) \frac{i}{k^2} \right\} \quad (2.136)
\end{aligned}$$

$$= C_2(r)g^2 \int \frac{d^4k}{(2\pi)^4} \sum_{n=-\infty}^{\infty} \left\{ \frac{4}{k^2 - \hat{n}^2} + \frac{1}{k^2} - \frac{1}{k^2 - \hat{n}^2} + \frac{\hat{n}^2}{k^2 - \hat{n}^2} \frac{1}{k^2} \right\} \quad (2.137)$$

$$= C_2(r)g^2 \int \frac{d^4k}{(2\pi)^4} \sum_{n=-\infty}^{\infty} \frac{4}{k^2 - \hat{n}^2}, \quad (2.138)$$

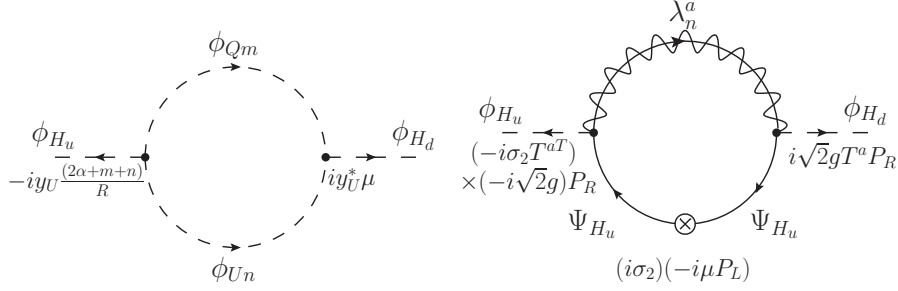


Figure 2.6: Loops of radiative corrections to b through Yukawa coupling (*left*) and through gauge coupling (*right*).

where $C_2(r)$ is Casimir invariant. Contributions of fermionic loops in Fig. 2.5 are

$$\begin{aligned}
-i\Pi_{\text{Fermionic}}^g &= -C_2(r) \int \frac{d^4k}{(2\pi)^4} \sum_{n=-\infty}^{\infty} \text{Tr} \left[-i\sqrt{2}gP_R \frac{i}{\not{k} + \hat{\alpha} + \hat{n}} (-i\sqrt{2}gP_L) \frac{i}{\not{k}} \right] \\
&= -C_2(r)g^2 \int \frac{d^4k}{(2\pi)^4} \sum_{n=-\infty}^{\infty} \frac{4}{k^2 - (\hat{\alpha} + \hat{n})^2}. \tag{2.139}
\end{aligned}$$

We combine them and perform summation and integral,

$$\begin{aligned}
\delta m_H^2|_{\text{KK}}^g &= \Pi_{\text{Bosonic+Fermionic}}^g \\
&= iC_2(r)g^2 \int \frac{d^4k}{(2\pi)^4} \sum_{n=-\infty}^{\infty} \left\{ \frac{4}{k^2 - \hat{n}^2} - \frac{4}{k^2 - (\hat{\alpha} + \hat{n})^2} \right\} \tag{2.140}
\end{aligned}$$

$$= \frac{C_2(r)g^2}{16\pi^2} \frac{-2}{\pi^2 R^2} [\text{Li}_3(e^{2\pi i\alpha}) + \text{Li}_3(e^{-2\pi i\alpha}) - 2\zeta(3)] \tag{2.141}$$

$$\approx \frac{C_2(r)g^2}{16\pi^2} \left(\frac{\alpha}{R}\right)^2 [-4 \log(2\pi\alpha)^2 + 12] \tag{2.142}$$

Also another Higgs soft mass, b , is radiatively generated. The contributions from all the KK modes with Yukawa coupling in left of Fig. 2.6 are

$$\begin{aligned}
-i(\delta b|_{\text{KK}}^{y_U}) &= N_c \int \frac{d^4k}{(2\pi)^4} \sum_{m,n=-\infty}^{\infty} -iy_U(2\hat{\alpha} + \hat{m} + \hat{n}) \frac{i}{k^2 - (\hat{\alpha} + \hat{m})^2} \frac{i}{k^2 - (\hat{\alpha} + \hat{n})^2} iy_U^* \mu \\
&= -2N_c |y_U|^2 \mu \int \frac{d^4k}{(2\pi)^4} \sum_{m,n=-\infty}^{\infty} \frac{(\hat{\alpha} + \hat{m})}{k^2 - (\hat{\alpha} + \hat{m})^2} \frac{1}{k^2 - (\hat{\alpha} + \hat{n})^2} \tag{2.143}
\end{aligned}$$

$$= \frac{N_c |y_U|^2}{16\pi^2} \mu \frac{(-1)}{\pi R} [\text{Li}_2(e^{2\pi i\alpha}) - \text{Li}_2(e^{-2\pi i\alpha})] \tag{2.144}$$

$$\approx -i \frac{N_c |y_U|^2}{16\pi^2} \mu \left(\frac{\alpha}{R}\right) [-2 \log(2\pi\alpha)^2 + 4]. \tag{2.145}$$

The contributions from all the KK modes with gauge coupling in right graph of Fig. 2.6 are

$$\begin{aligned}
-i(\delta b|_{\text{KK}}^g) &= C_2(r) \int \frac{d^4 k}{(2\pi)^4} \sum_{n=-\infty}^{\infty} \text{Tr} \left[(-i\sqrt{2}gP_R) \frac{i}{\not{k}} (-i\mu P_L) \frac{i}{\not{k}} (i\sqrt{2}gP_R) \frac{i}{\not{k} + \hat{\alpha} + \hat{n}} \right] \\
&= 4C_2(r)g^2\mu \int \frac{d^4 k}{(2\pi)^4} \sum_{n=-\infty}^{\infty} \frac{(\hat{\alpha} + \hat{n})}{k^2 - (\hat{\alpha} + \hat{n})^2} \frac{1}{k^2}
\end{aligned} \tag{2.146}$$

$$= \frac{C_2(r)g^2}{16\pi^2} \mu \frac{2}{\pi R} [\text{Li}_2(e^{2\pi i\alpha}) - \text{Li}_2(e^{-2\pi i\alpha})] \tag{2.147}$$

$$\approx -i \frac{C_2(r)g^2}{16\pi^2} \mu \left(\frac{\alpha}{R} \right) [4 \log(2\pi\alpha)^2 - 8] \tag{2.148}$$

where mass insertion is used for μ . The mass insertion of μ and gaugino-Higgs-Higgsino interaction are given by

$$\begin{aligned}
-\mu\psi_{H_u}\psi_{H_d} &= -\mu\psi_{H_u}^\alpha (i\sigma_2)_{\alpha\beta}\psi_{H_d}^\beta \\
&= -\mu\bar{\Psi}_{H_u}^\alpha (i\sigma_2)_{\alpha\beta}P_L\Psi_{H_d}^\beta
\end{aligned} \tag{2.149}$$

$$\begin{aligned}
\bar{\lambda}_n^a P_R \Psi_{H_u} T^a \phi_{H_u} &= \phi_{H_u} T^{aT} \bar{\lambda}_n^a P_R \Psi_{H_u} \\
&= (\phi_{H_u} i\sigma_2) (-i\sigma_2 T^{aT}) \bar{\lambda}_n^a P_R \Psi_{H_u}
\end{aligned} \tag{2.150}$$

Here we explicitly show $(i\sigma_2)$ for contraction of $SU(2)_L$ doublets. And we use a relation,

$$(-i\sigma_2)T^{aT}(i\sigma_2) = -T^a. \tag{2.151}$$

On the other hand, contributions from the MSSM to the same parameters are computed subtracting logarithmic divergences in \overline{DR} scheme. The results are given by

$$\delta m_{H_u}^2|_{\text{MSSM}}^{y_U} = \frac{N_c|y_U|^2}{16\pi^2} \left(\frac{\alpha}{R} \right)^2 \left[-6 \log \left(\frac{Q^2}{\alpha^2/R^2} \right) - 2 \right], \tag{2.152}$$

$$\delta m_{H_{u,d}}^2|_{\text{MSSM}}^g = \frac{C_2(r)}{16\pi^2} \left(\frac{\alpha}{R} \right)^2 \left[4 \log \left(\frac{Q^2}{\alpha^2/R^2} \right) + 4 \right], \tag{2.153}$$

$$\delta b|_{\text{MSSM}}^{y_U} = \frac{N_c|y_U|^2}{16\pi^2} \mu \left(\frac{\alpha}{R} \right) \left[2 \log \left(\frac{Q^2}{\alpha^2/R^2} \right) \right], \tag{2.154}$$

$$\delta b|_{\text{MSSM}}^g = \frac{C_2(r)}{16\pi^2} \mu \left(\frac{\alpha}{R} \right) \left[-4 \log \left(\frac{Q^2}{\alpha^2/R^2} \right) - 4 \right], \tag{2.155}$$

We the corrections of $m_{H_u}^2$, $m_{H_d}^2$ and b from all the KK modes and from only the MSSM, respectively, and apply the results for y_t , g_1 , and g_2 couplings following Eq. (2.129). The Casimir invariants for $SU(2)_L$ and $U(1)_Y$ in $SU(5)$ normalization are $C_{2,SU(2)_L}^h = 3/4$ and $C_{2,U(1)_Y}^h = 3/20$. We combine Eqs. (2.135, 2.142, 2.145, 2.148) with Eqs. (2.152, 2.153, 2.154,

2.155),

$$\begin{aligned} \delta m_{H_u}^2(Q) &= \frac{N_c y_t^2}{16\pi^2} \left(\frac{\alpha}{R}\right)^2 \left\{ 6 \log \left[\frac{Q^2}{(2\pi R)^{-2}} \right] - 16 \right\} \\ &\quad + \frac{\sum_{A=1,2} C_A^h g_A^2}{16\pi^2} \left(\frac{\alpha}{R}\right)^2 \left\{ -4 \log \left[\frac{Q^2}{(2\pi R)^{-2}} \right] + 8 \right\} + \mathcal{O}(\alpha^4) \end{aligned} \quad (2.156)$$

$$\delta m_{H_d}^2(Q) = \frac{\sum_{A=1,2} C_A^h g_A^2}{16\pi^2} \left(\frac{\alpha}{R}\right)^2 \left\{ -4 \log \left[\frac{Q^2}{(2\pi R)^{-2}} \right] + 8 \right\} + \mathcal{O}(\alpha^4) \quad (2.157)$$

$$\begin{aligned} \delta b(Q) &= \frac{N_c y_t^2}{16\pi^2} \mu \left(\frac{\alpha}{R}\right) \left\{ -2 \log \left[\frac{Q^2}{(2\pi R)^{-2}} \right] + 4 \right\} \\ &\quad + \frac{C_2^h g_A^2}{16\pi^2} \mu \left(\frac{\alpha}{R}\right) \left\{ 4 \log \left[\frac{Q^2}{(2\pi R)^{-2}} \right] - 4 \right\} + \mathcal{O}(\alpha^3) \end{aligned} \quad (2.158)$$

We check $\log \alpha$ are certainly cancelled. And we choose the renormalization scale,

$$Q_{\text{RG}} = \frac{1}{2\pi R}. \quad (2.159)$$

and then we find

$$\delta m_{H_u}^2 = \left(-\frac{3y_t^2}{\pi^2} + \frac{3(g_2^2 + g_1^2/5)}{8\pi^2} \right) \left(\frac{\alpha}{R}\right)^2, \quad (2.160)$$

$$\delta m_{H_d}^2 = \frac{3(g_2^2 + g_1^2/5)}{8\pi^2} \left(\frac{\alpha}{R}\right)^2, \quad (2.161)$$

$$\delta b = \left(\frac{3y_t^2}{4\pi^2} - \frac{3(g_2^2 + g_1^2/5)}{16\pi^2} \right) \mu \frac{\alpha}{R}. \quad (2.162)$$

Using the above results, we run MSSM parameters down to low-energy to discuss phenomenology in the next chapter. ⁵

2.7 Brane Kinetic Terms at Tree-Level

In addition to brane-kinetic terms which are radiatively generated, those at tree-level which can be considered as threshold corrections at the cutoff scale are potentially dangerous because they may change the prediction of Eq. (2.97) or may be strongly constrained by low-energy measurements. Therefore, basically we assume the tree-level contributions do not exceed the radiative ones of Eq. (2.123) with $\log(\Lambda R) \rightarrow \mathcal{O}(1)$, that is,

$$\left. \frac{\delta M_{1/2}}{M_{1/2}}, \frac{\delta m_{\tilde{f}}^2}{m_{\tilde{f}}^2}, \frac{\delta A_0}{A_0} \right|_{\text{at } \Lambda} \approx \mathcal{O} \left(\frac{g^2, y^2}{16\pi^2} \right). \quad (2.163)$$

This assumption can be reasonable because effects from brane kinetic terms are reduced by the volume of the extra dimension [44]. Let us focus on \mathcal{P} even chiral superfields which

⁵The factor difference from the original result in Ref. [26] is due to scheme difference. In Ref. [26] cutoff regularization rather than \overline{DR} scheme is used when zero mode contributions are subtracted.

have zero modes and hence are relevant to low-energy physics. Then kinetic terms for them are, for example,

$$\int d^4x dy \int d^4\theta \left[Z_{\text{bulk},Q} \delta^{ij} + Z_{\text{brane},Q}^{ij} \delta(y) \right] Q_i^\dagger Q_j, \quad (2.164)$$

where i, j are flavor indices. Now suppose the bulk and brane kinetic terms have “comparable” sizes at the cutoff scale Λ . It is natural to rescale Z_{brane} by Λ such as $Z_{\text{brane}} = \tilde{Z}_{\text{brane}}/\Lambda$, and the comparable sizes of kinetic terms imply

$$Z_{\text{bulk}} \approx \tilde{Z}_{\text{brane}}. \quad (2.165)$$

We normalize Z_{bulk} to be 1, and Eq. (3.9) is rewritten as

$$\int d^4x dy \int d^4\theta \left[1 + \frac{c_Q^{ij}}{\Lambda} \delta(y) \right] Q_i^\dagger Q_j. \quad (2.166)$$

where $c_Q^{ij} = Z_{\text{bulk},Q}/Z_{\text{bulk},Q} \approx \mathcal{O}(1)$. If we perform y integral and KK-expansion of the chiral superfield, the kinetic term for zero mode is

$$\int d^4x \int d^4\theta \left[1 + \frac{c_Q^{ij}}{(2\pi R)\Lambda} \right] Q_i^{(0)\dagger} Q_j^{(0)}. \quad (2.167)$$

When we take the maximum value of the cutoff which we discussed in Sec. 2.6.1, the effect of brane terms is suppressed,

$$\frac{c_Q}{2\pi\Lambda R} \sim \frac{c_Q}{8\pi^2} \sim \mathcal{O}(0.01). \quad (2.168)$$

Thus we expect the effect of brane kinetic terms is small. Although unlikely, it is possible to have anomalously large coefficients for brane terms. We briefly discuss this impact to the phenomenology in Sec. 3.3.3.

3

Phenomenology of Compact Supersymmetry

The Compact Supersymmetry leads to viable phenomenology despite the fact that it essentially has two less free parameters than the conventional CMSSM. In the low-energy, we can treat the model as the MSSM. Using the common notation in the MSSM, parameters at the scale $\frac{1}{2\pi R}$ are given by

$$\begin{aligned} M_{1/2} &= \frac{\alpha}{R}, \quad m_{\tilde{Q}, \tilde{U}, \tilde{D}, \tilde{L}, \tilde{E}}^2 = \left(\frac{\alpha}{R}\right)^2, \quad A_0 = -\frac{2\alpha}{R}, \\ \mu &\neq 0, \quad b = \left(\frac{3y_t^2}{4\pi^2} - \frac{3(g_2^2 + g_1^2/5)}{16\pi^2}\right) \mu \frac{\alpha}{R}, \\ m_{H_u}^2 &= \left(-\frac{3y_t^2}{\pi^2} + \frac{3(g_2^2 + g_1^2/5)}{8\pi^2}\right) \left(\frac{\alpha}{R}\right)^2, \quad m_{H_d}^2 = \frac{3(g_2^2 + g_1^2/5)}{8\pi^2} \left(\frac{\alpha}{R}\right)^2. \end{aligned} \tag{3.1}$$

We discuss the Higgs sector, the spectrum, experimental limits and dark matter phenomenology.

3.1 Higgs Sector

3.1.1 Electroweak symmetry breaking

This model has essentially three parameters: $\mu, 1/R, \alpha/R$. Since the measured VEV can be as a condition of EWSB, there are only two free parameters. We treat α/R and $1/R$ as free parameters and the other electroweak parameters ($\mu, \tan\beta$) are determined by the EWSB conditions. In Fig. 3.1, we show μ and $\tan\beta$ at the scale of α/R in terms of α/R and $1/R$. For this calculation `SOFTSUSY 3.3.1` [45] is used.

The result is basically understood by tree-level EWSB conditions. The vacuum conditions for H_u and H_d are

$$m_{H_u}^2 + |\mu|^2 - b \cot\beta - (m_Z^2/2) \cos(2\beta) = 0, \tag{3.2}$$

$$m_{H_d}^2 + |\mu|^2 - b \tan\beta + (m_Z^2/2) \cos(2\beta) = 0. \tag{3.3}$$

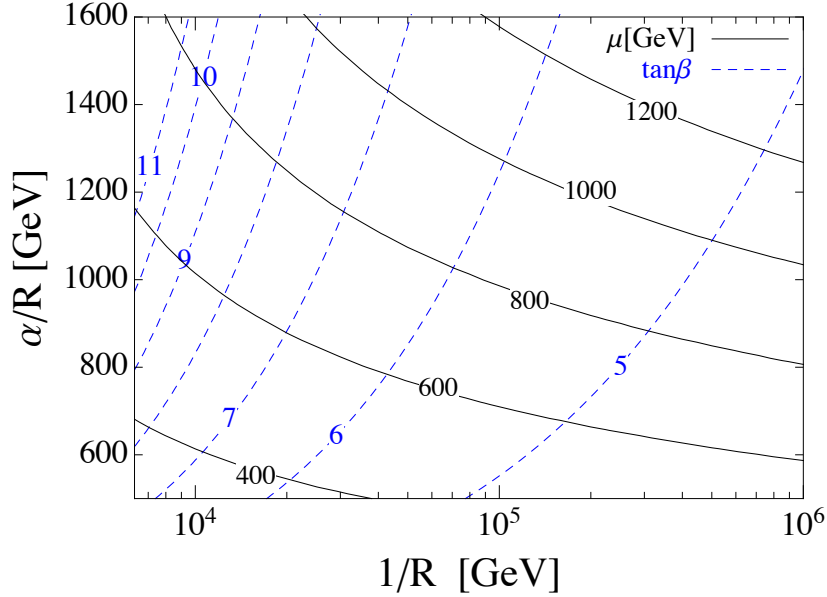


Figure 3.1: μ and $\tan\beta$ at SUSY scale ($Q = \alpha/R$) as a function of α/R and $1/R$.

Let us estimate μ analytically. Eq. (3.2) is approximated to $-|\mu|^2 \approx m_{H_u}^2$ neglecting m_Z and b , and $m_{H_u}^2$ is estimated by the threshold correction and one-loop RGE,

$$\begin{aligned}
 -|\mu|^2 \approx m_{H_u}^2 &\approx \delta m_{H_u}^2 + \frac{dm_{H_u}^2}{d \log Q} L \\
 &\sim -\frac{3y_t^2}{\pi^2} \left(\frac{\alpha}{R}\right)^2 - \frac{9y_t^2}{4\pi^2} \left(\frac{\alpha}{R}\right)^2 L.
 \end{aligned} \tag{3.4}$$

where $L = \log \frac{(2\pi R)^{-1}}{\alpha/R}$ is RGE leading-logarithm. The size of μ scales with α/R , and μ becomes larger for larger $1/R$ as shown in Fig. 3.1. For better estimation, we should consider next-to-leading logs by RGEs of $m_{\tilde{Q}_3}$, $m_{\tilde{u}_3}$, and A_t .

It is rather complicated for $\tan\beta$ behavior. We approximate Eq.(3.3) and consider RGE of b ,

$$\tan\beta \approx \frac{|\mu|^2}{b}, \tag{3.5}$$

$$\frac{db}{d \log Q} L \approx \frac{3y_t^2}{4\pi^2} \mu \frac{\alpha}{R} L. \tag{3.6}$$

From Eqs. (3.4,3.5,3.6), roughly speaking, b grows with $L^{3/2}$ whereas $|\mu|^2$ grows with L , and hence $\tan\beta$ decreases for large $1/R$. The numerical result is shown by dashed line of Fig. 3.1.

3.1.2 Higgs mass and naturalness

We calculate the MSSM mass spectrum using SOFTSUSY 3.3.1 [45] and the lightest Higgs boson mass using FeynHiggs 2.8.6 [46]. In Fig. 3.2, we plot the contours of the mass of the

lightest Higgs boson, M_H , and the fine-tune parameter, defined by Δ^{-1} where

$$\Delta \equiv \max \left| \frac{\partial \log m_Z^2}{\partial \log x} \right|, \quad x = \alpha, \mu, 1/R, g_3, y_t. \quad (3.7)$$

in the $1/R$ - α/R plane. The fine-tuning parameter is determined mostly by $x = \mu$. It is

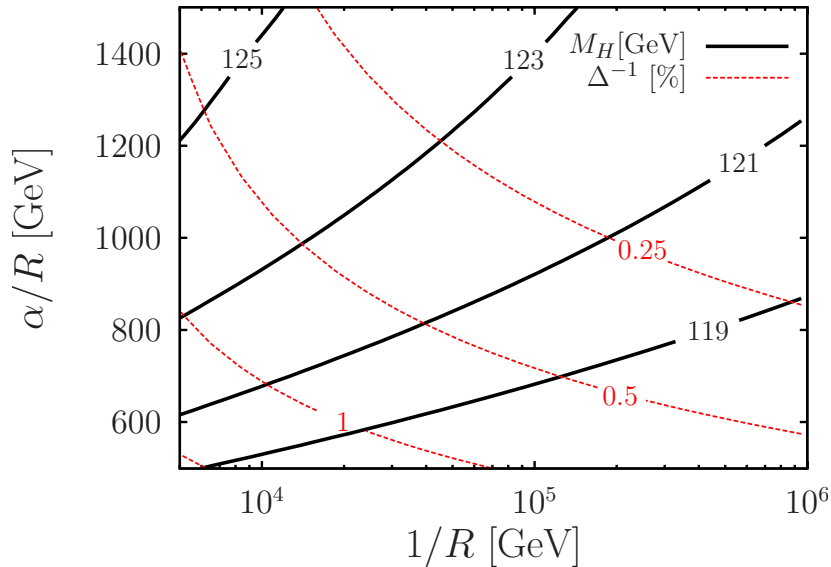


Figure 3.2: The lightest Higgs boson mass M_H (in GeV) and the fine-tune parameter Δ^{-1} . Note that there is an approximately 3 GeV systematic error in theoretical computation of M_H .

understood from Eq.(3.2) some cancellation between $m_{H_u}^2$ and $|\mu|^2$ is needed to give observed m_Z . It turns out that the tuning level is $\mathcal{O}(1)\%$.

The lightest Higgs boson mass is enhanced because the radiative correction from stop left-right mixing A_t is nearly maximized. The overall mass is larger with large $\tan\beta$ (small $1/R$). In the calculation, we have used the top-quark mass of $m_t = 173.2$ GeV [47]. Varying it by 1σ , $\Delta m_t = \pm 0.9$ GeV, affects the Higgs boson mass by $\Delta M_H \approx \pm 1$ GeV. Also, theoretical errors in M_H are large with $|\Delta M_H| \approx 2 - 3$ GeV in `FeynHiggs 2.8.6`, which is also implied by Ref. [48], so the regions with $M_H \gtrsim 121 - 123$ GeV in the plot are not necessarily incompatible with the 125 GeV Higgs boson at the LHC [1, 29]. Indeed, using the recently-released program `H3m` [49], which includes a partial three-loop effect, we find that the corrections to M_H from higher order effects are positive and of order a few GeV in most of the parameter region in the plot.

3.2 Sparticle Spectrum

In Fig. 3.3, the masses of selected sparticles (the lightest neutralino $\tilde{\chi}_1^0$, the lighter top squark \tilde{t}_1 , and the gluino \tilde{g}) are shown. The gluino is generically the heaviest for the RGE effect.

For the stops, the left-right mixing term, $y_t A_0 v \sin \beta \approx -2y_t \frac{\alpha}{R} v \sin \beta$, leads to a mass splitting. Since the stop mass-squared is

$$m_{\tilde{t}_{1,2}}^2 \approx \left(\frac{\alpha}{R}\right)^2 \pm 2y_t \frac{\alpha}{R} v \sin \beta, \quad (3.8)$$

the relative mass splitting becomes small as α/R increases. The lightest neutralino is mostly Higgsino-like and the mass scale is mostly determined by μ . As discussed in Sec. 3.1.1, μ basically scales with α/R . When μ approaches α/R in larger $1/R$, the LSP has a significant composition of EW-inos.

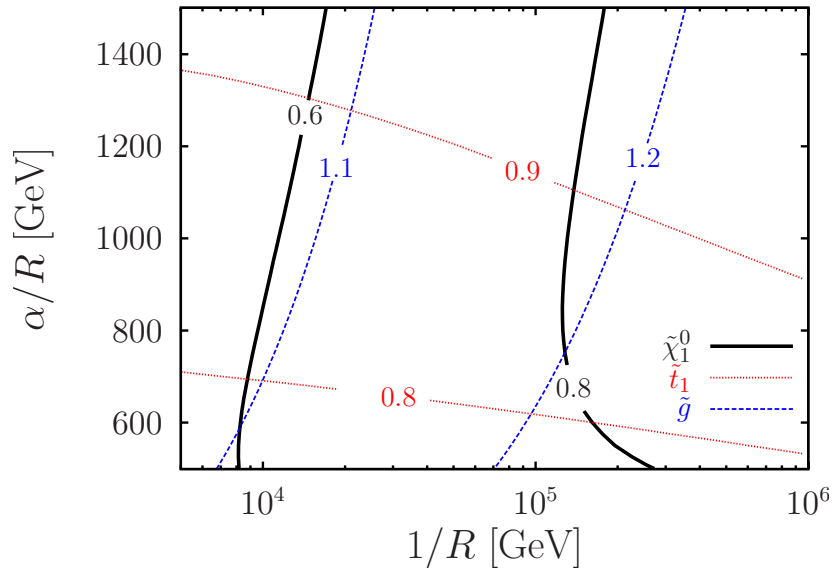


Figure 3.3: Masses of the lightest neutralino $\tilde{\chi}_1^0$, the lighter top squark \tilde{t}_1 , and the gluino \tilde{g} normalized to α/R .

The masses of the first and second generation squarks are almost the same as gluino mass. The masses of the electroweak sparticles are close to α/R , except for the lightest two neutralinos $\tilde{\chi}_{1,2}^0$ and the lighter chargino $\tilde{\chi}_1^\pm$, which are Higgsino-like (and thus close in mass) in most of the parameter space. The spectrum is more compressed for larger $1/R$ where μ approaches α/R . We find that the masses of the sparticles are compressed at a 20% level, except for the Higgsinos which can be significantly lighter (up to a factor of ≈ 2). We give full mass spectra for two points in Table. 3.1.

3.3 Experimental Limits

3.3.1 LHC Run I

As we have seen, the model naturally predicts a compressed mass spectrum for sparticles. This has strong implications on supersymmetry searches at the LHC. Because of the mass degeneracy, production of high p_T jets and large missing energy is suppressed. Therefore, typical searches, based on high p_T jets and large missing energy, are less effective for the

Particle	Point1	Point2	Particle	Point1	Point2
\tilde{g}	1494	1174	–	–	–
\tilde{u}_L	1467	1162	\tilde{u}_R	1459	1144
\tilde{d}_L	1469	1165	\tilde{d}_R	1458	1143
\tilde{b}_2	1460	1142	\tilde{b}_1	1430	1086
\tilde{t}_2	1557	1192	\tilde{t}_1	1267	885
$\tilde{\nu}$	1411	1027	$\tilde{\nu}_\tau$	1410	1027
\tilde{e}_L	1413	1030	\tilde{e}_R	1406	1013
$\tilde{\tau}_2$	1417	1032	$\tilde{\tau}_1$	1402	1011
$\tilde{\chi}_1^0$	767	783	$\tilde{\chi}_2^0$	777	815
$\tilde{\chi}_3^0$	1384	946	$\tilde{\chi}_4^0$	1410	1010
$\tilde{\chi}_1^\pm$	771	793	$\tilde{\chi}_2^\pm$	1409	1008
h^0	125	122	H^0	819	872
A^0	819	872	H^\pm	822	875

Table 3.1: Phenomenologically viable mass spectrum of the benchmark points (in GeV). Point1: $1/R = 10^4$ GeV, $\alpha/R = 1400$ GeV and Point2: $1/R = 10^5$ GeV, $\alpha/R = 1000$ GeV.

present model. We first show limits presented in our work of Ref. [26] based 7 TeV run, and next show an updated limit based on 8 TeV run.

In 7 TeV study, in order to estimate the number of supersymmetric events, we have used ISAJET 7.72 [50] for the decay table of sparticles, Herwig 6.520 [51] for the generation of supersymmetric events, AcerDET 1.0 [52] for the detector simulation, and NLL-fast [53] for estimation of the production cross section including next-to-leading order QCD corrections and the resummation at next-to-leading-logarithmic accuracy. To constrain the parameter space, we compare the obtained event numbers with the results of ATLAS searches for multi-jets plus large missing energy with and without a lepton at $L = 4.7 \text{ fb}^{-1}$ at $\sqrt{s} = 7$ TeV [54, 55]. In Fig. 3.4, we show the resulting LHC constraint on the model.

Other searches such as those for b -jets and/or multi-leptons are less effective. We find that for $1/R \gtrsim 10^5$ GeV, the case that $m_{\tilde{g}} \simeq m_{\tilde{q}} \lesssim 1$ TeV is allowed for this integrated luminosity. This constraint is significantly weaker than that on the CMSSM, which excludes $m_{\tilde{g}} \lesssim 1.5$ TeV for $m_{\tilde{g}} \simeq m_{\tilde{q}}$ [54]. (We have checked that our naive method of estimating the LHC constraints adopted here reproduces this bound for the CMSSM spectra.)

We also study a limit based on the result of $\sqrt{s} = 8$ TeV run. Here, PYTHIA 6.4 [56] is adopted for supersymmetric event generation and showering, and PGS 4 [57] is used for the detector simulation. We again use NLL-fast [53] for estimation of the production cross section. We compare the obtained event numbers with the results of ATLAS searches for multi-jets plus large missing energy without lepton at $L = 20.3 \text{ fb}^{-1}$ at $\sqrt{s} = 8$ TeV [21], and the result is shown in Fig. 3.5. We find the exclusion limit is extended up to $m_{\tilde{q}} \simeq 1$ TeV, and for a region at $1/R \sim 10^4$ GeV the limit is stronger as $m_{\tilde{q}} \gtrsim 1.2$ TeV. In contrast, the CMSSM and simplified model are more constrained as the limit is $m_{\tilde{q}} \gtrsim 1.7$ TeV.

Hence, in the Compact Supersymmetry, the bounds from the current searches at the LHC are certainly ameliorated. We discuss potential improvement of the search in Appendix D

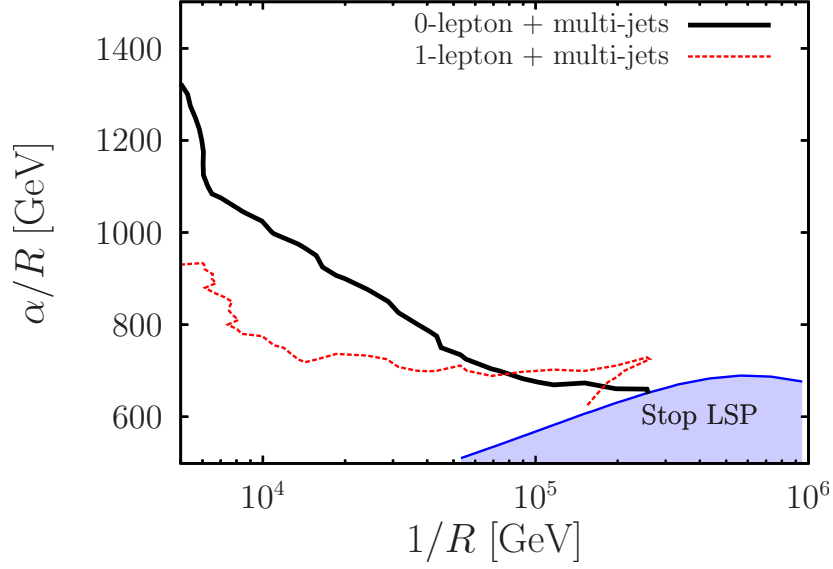


Figure 3.4: The LHC constraint on the model using 7 TeV run data.

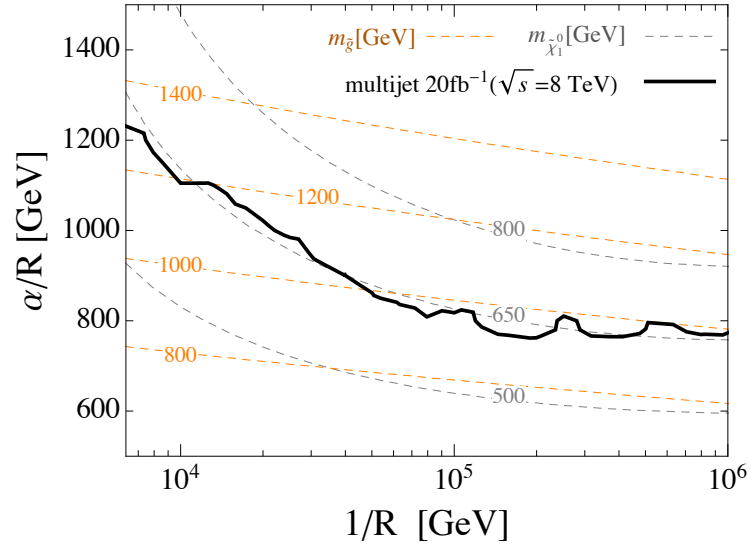


Figure 3.5: The LHC constraint on the model using 8 TeV run data.

based on Ref. [27]. This possibility is that a kinematic variable, M_{T2} , can be useful since the Standard Model background is systematically removed by requiring $M_{T2} > m_{\text{top}}$. On the other hand, the signal along with a compressed spectrum is still extracted because M_{T2} for the signal becomes larger with energetic initial state radiation. We demonstrate this technique for a typical compressed model, the Minimal Universal Extra Dimension (MUED).

3.3.2 Other measurements

First of all, for the geometric nature of supersymmetry breaking there are no extra flavor-violation and CP-violation. We typically find $\tan\beta \sim 4 - 10$, which allows for the model to avoid the constraint from $b \rightarrow s\gamma$, despite the large A terms.

The contribution of the non-zero KK states to the electroweak precision parameters bounds $1/R \gtrsim$ a few TeV [58]. Since we consider the region $1/R \gtrsim 10$ TeV, however, the model is not constrained by the electroweak precision data.

3.3.3 Comment on brane kinetic terms

As we mentioned in Sec. 2.7, if the brane kinetic terms introduce additional wave functions to fields, they affect tree-level prediction of the model. Here, we discuss brane kinetic terms for quarks, parameterized by

$$\int d^4x \int d^4\theta \left[1 + \frac{c_Q^{ij}}{8\pi^2} \right] Q_i^{(0)\dagger} Q_j^{(0)} + \left[1 + \frac{c_U^{ij}}{8\pi^2} \right] U_i^{(0)\dagger} U_j^{(0)} + \left[1 + \frac{c_D^{ij}}{8\pi^2} \right] D_i^{(0)\dagger} D_j^{(0)}. \quad (3.9)$$

When $c_{Q,U,D} \approx \mathcal{O}(1)$, the bulk and brane kinetic terms have comparable sizes. First, let us consider a case of no additional flavor violation through the kinetic terms, that is, $c_{Q,U}^{ij} \propto \delta^{ij}$. Then, the brane kinetic terms still change mass of each squark, and an important effect is from $c_{Q,U}^{33}$ because one stop is light due to the large mixing and can be the LSP with some amount of $c_{Q,U}^{33}$. Fig. 3.3 tells that 30% reduction of the lighter stop mass leads the stop to be the LSP and LHC phenomenology is completely changed. So if we have large brane terms such as

$$c_Q^{33} = c_U^{33} \gtrsim 0.3 \times 8\pi^2 \sim 24, \quad (3.10)$$

the LSP is the lighter stop rather than neutral sparticle.

Next, we consider the flavor violations in brane kinetic terms. There many constraints on additional flavor violations from low-energy measurements, and here let us consider only a stringent constraint from $K^0 - \bar{K}^0$ mixing. Assuming no CP violation, analysis based on mass insertion method [59] together with a constraint from Ref. [60] gives limits for soft mass mixing between first and second generations. If c_D^{12} is an unique source of flavor violation, $K^0 - \bar{K}^0$ mixing excludes

$$c_D^{12} \gtrsim \mathcal{O}(0.1) \times 8\pi^2 \sim \mathcal{O}(10), \quad (3.11)$$

for MSSM particles at 1 TeV. If we introduce an additional source, c_Q^{12} , such that $c_D^{12} = c_Q^{12}$, the exclusion limit gets severer,

$$c_D^{12} = c_Q^{12} \gtrsim \mathcal{O}(0.01) \times 8\pi^2 \sim \mathcal{O}(1). \quad (3.12)$$

If there is additionally CP violation, the limit could be stronger by one order of magnitude. Thus brane kinetic terms have to be adequately small in presence of these flavor violations.

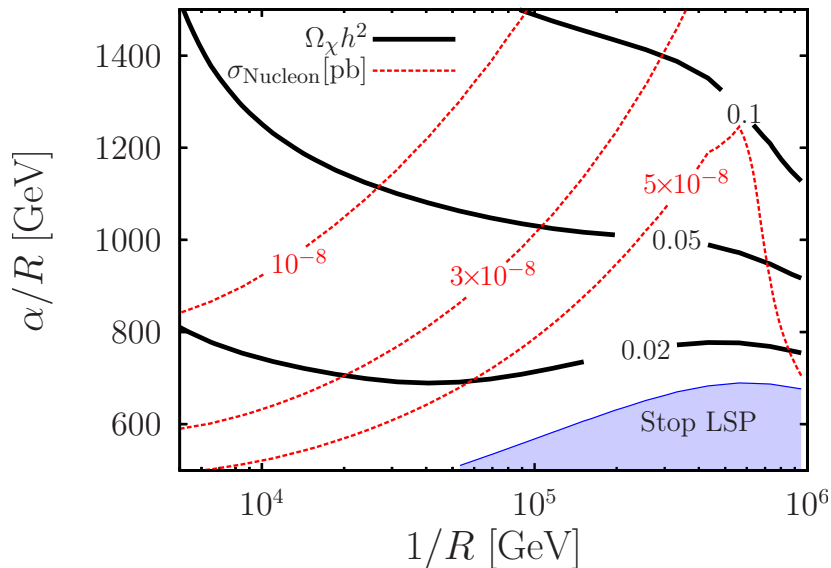


Figure 3.6: The thermal relic abundance, $\Omega_\chi h^2$, and the spin-independent cross section with a nucleon, σ_{Nucleon} , of $\tilde{\chi}_1^0$. The solid (black) lines are the contours of $\Omega_\chi h^2$, while the dotted (red) lines are those of σ_{Nucleon} .

3.4 Dark Matter

In the present model, the dark matter candidate is the lightest neutralino $\tilde{\chi}_1^0$, whose dominant component is the Higgsino. In Fig. 3.6, we show the thermal relic abundance, $\Omega_\chi h^2$, and the spin-independent cross section with a nucleon, σ_{Nucleon} , of $\tilde{\chi}_1^0$, assuming R -parity conservation. To estimate these, we have used `micrOMEGAs 2.4` [61]. For the strange quark form factor we have adopted $f_s = 0.02$, suggested by lattice calculations [62], instead of the default value of `micrOMEGAs` ($f_s = 0.26$).

As seen in Fig. 3.6, the thermal relic abundance of $\tilde{\chi}_1^0$ is much smaller than the observed dark matter density $\Omega_{\text{DM}} h^2 \simeq 0.1$, unless $\tilde{\chi}_1^0$ is rather heavy $\sim \text{TeV}$ (in the upper-right corner of the plot). This is due to the Higgsino-like nature of $\tilde{\chi}_1^0$. Therefore, in most parameter regions, $\tilde{\chi}_1^0$ cannot be the dominant component of dark matter if only the thermal relic abundance is assumed. It must be produced nonthermally to saturate $\Omega_{\text{DM}} h^2$, or some other particle(s), e.g. the axion/axino, must make up the rest.

The spin-independent scattering with nuclear of $\tilde{\chi}_1^0$ is mostly mediated by the lightest Higgs boson exchange between the lightest neutralino and quarks inside the nucleon. The relevant coupling at tree-level originate from gaugino-Higgsino-Higgs interactions, $H\tilde{H}\tilde{B}$ and $H\tilde{H}\tilde{W}$. Hence, the scattering does not occur for pure Higgsino or pure EW-ino. When the lightest neutralino is well-tempered mixture of Higgsinos and pure EW-inos, the scattering is enhanced, and the enhancement in $1/R \sim 10^{5.7}$ GeV and $\alpha/R \lesssim 1.2$ TeV is for this reason. Beyond $1/R \sim 10^{5.7}$ GeV, the scattering cross section is damped for the purity of Bino.

It is natural to expect that at least the thermal abundance of $\tilde{\chi}_1^0$ remains as a (sub-)component of dark matter. In this case, direct and indirect signatures of the relic neutralino

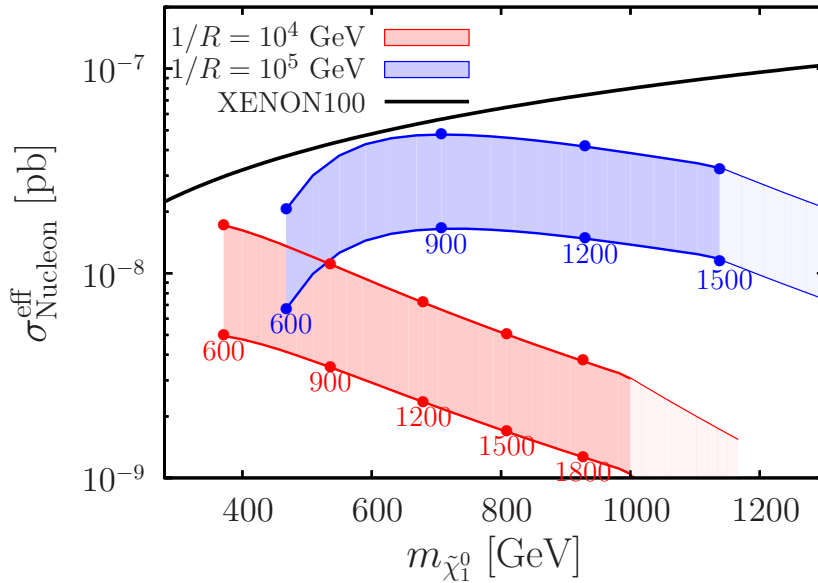


Figure 3.7: Effective dark matter-nucleon cross section for $1/R = 10^4$ GeV (lower, red shaded) and 10^5 GeV (upper, blue shaded). In each region, the upper and lower borders correspond to $f_s = 0.26$ and 0.02 , respectively, and the dots represent the corresponding values of α/R . (The very light shaded regions are those in which the thermal abundance exceeds Ω_{DM} .) The solid (black) line shows the current upper bound from XENON100.

are expected. To discuss the direct-detection signal, it is useful to define

$$\sigma_{\text{Nucleon}}^{\text{eff}} \equiv \sigma_{\text{Nucleon}} \frac{\min\{\Omega_{\tilde{\chi}}, \Omega_{\text{DM}}\}}{\Omega_{\text{DM}}}, \quad (3.13)$$

which is the quantity to be compared with the dark matter-nucleon cross section in the usual direct-detection exclusion plots (which assume $\Omega_{\tilde{\chi}} = \Omega_{\text{DM}}$). In Fig. 3.7, we plot $\sigma_{\text{Nucleon}}^{\text{eff}}$ as a function of $m_{\tilde{\chi}_1^0}$ for $1/R = 10^4$ GeV and 10^5 GeV. To represent the uncertainty from the nucleon matrix element, we show both the $f_s = 0.02$ and 0.26 cases. We also present the current upper bound on $\sigma_{\text{Nucleon}}^{\text{eff}}$ from XENON100 [63]. We find that improving the bound by one or two orders of magnitude will cover a significant portion of the parameter space of the model.¹

3.5 Summary and Discussion

In Ch. 2 and Ch. 3, we pointed out that supersymmetry broken by boundary conditions in extra dimensions, the Scherk-Schwartz mechanism, leads naturally to a compressed sparticle spectrum, ameliorating the limits from experimental searches. We demonstrated the Scherk-Schwartz mechanism is equivalent to the Radion mediation. We presented the simplest model in the S^1/Z_2 orbifold, the Compact Supersymmetry. Despite the fact that it essentially has

¹Recently the LUX experiment reported a new result of spin-independent WIMP-nucleon elastic scattering [64]. The upper limit was improved by a factor compared to XENON100 limit.

two less free parameters than the CMSSM: $1/R$, α/R , and μ , the model can accommodate the Higgs mass and is less fine-tuned than many models. However, the theoretical error of the Higgs mass is still large, $\Delta M_H \approx 2 \sim 3$ GeV.

The LHC limit is weaker by about 500 GeV compared to the CMSSM-like models. We find the LSP is mostly Higgsino-like and can be a component of dark matter. The direct detection experiments for dark matter particle have potential to search for the model. In Table 3.1 we give two representative points in the parameter space, which can serve benchmark points for further phenomenological studies.

The theory presented here can be extended in several different ways. An interesting one is to introduce a singlet field S in the bulk together with superpotential interactions on the $y = 0$ brane: $\lambda S H_u H_d + f(S)$, where $f(S)$ is a polynomial of S with the simplest possibility being $f(S) = -\kappa S^3/3$. This allows for an extra contribution to the Higgs boson mass from λ , and can make the lightest neutralino (which would now contain a singlino component as well) saturate the observed dark matter abundance without resorting to nonthermal production. Furthermore, μ term could be dynamically generated by $\langle S \rangle$ in the same scale of α/R , and therefore the mass degeneracy is theoretically more reasonable. Detailed studies of this possibility will be presented elsewhere.

Part II

Natural Higgs Mass in Supersymmetry with Two Singlets

4

Dirac NMSSM

4.1 Introduction

The discovery of a new resonance at 125 GeV [1], that appears to be the long-sought Higgs boson, marks a great triumph of experimental and theoretical physics. On the other hand, the presence of this light scalar forces us to face the naturalness problem of its mass. Arguably, the best known mechanism to ease the naturalness problem is weak-scale supersymmetry (SUSY), but the lack of experimental signatures is pushing supersymmetry into a tight corner. In addition, the observed mass of the Higgs boson is higher than what was expected in the Minimal Supersymmetric Standard Model (MSSM), requiring fine-tuning of parameters at the 1% level or worse [14]. This comes from a fact that it is necessary for the observed Higgs mass to have the large radiative corrections by large stop mass, $m_{\tilde{t}}^2$, or by large left-right mixing of stops, X_t , where the Higgs mass formula is

$$m_{h,\text{MSSM}}^2 \simeq m_Z^2 \cos 2\beta + \frac{3m_{\tilde{t}}^4}{4\pi^2 v^2} \left(\log \frac{m_{\tilde{t}}^2}{m_t^2} + m_{\tilde{t}}^2 \left(1 - \frac{X_t^2}{12m_{\tilde{t}}^2} \right) \right), \quad (4.1)$$

while these large $m_{\tilde{t}}$ and A_t make the theory unnatural because the Higgs soft mass can be very different from the weak scale by a fast Renormalization Group (RG) evolution,

$$\frac{d}{d \log Q} m_{H_u}^2 \simeq \frac{3y_t^2}{8\pi^2} (2m_{\tilde{t}}^2 + |A_t|^2), \quad (4.2)$$

where A_t is a soft breaking part of X_t .

If supersymmetry is realized in nature, one possibility is to give up on naturalness [65, 30]. Alternatively, theories that retain naturalness must address two problems, (I) the missing superpartners and (II) the Higgs mass. The collider limits on superpartners are highly model-dependent and can be relaxed when superpartners unnecessary for naturalness are taken to be heavy [31], when less missing energy is produced due to a compressed mass spectrum [26, 32]

or due to decays to new states [66], and when R -parity is violated [67]. Even if superpartners have evaded detection for one of these reasons, we must address the surprisingly heavy Higgs mass.

4.1.1 Beyond the MSSM

There have been many attempts to extend the MSSM to accommodate the Higgs mass. In such extensions, new states interact with the Higgs, raising its mass by increasing the strength of the quartic interaction of the scalar potential. If the new states are integrated out supersymmetrically, their effects decouple and the Higgs mass is not increased. On the other hand, SUSY breaking can lead to non-decoupling effects that increase the Higgs mass. One possibility is a non-decoupling F -term, as in the NMSSM (MSSM plus a singlet) [68, 69] or λ SUSY (allowing for a Landau pole) [71]. A second possibility is a non-decoupling D -term that results if the Higgs is charged under a new gauge group [72]. In general, these extensions require new states at the few hundred GeV scale, so that the new sources of SUSY breaking do not spoil naturalness.

For example, consider the NMSSM, where a singlet superfield, S , interacts with the MSSM Higgses, $H_{u,d}$, through the superpotential,¹

$$W \supset \lambda S H_u H_d + \frac{M}{2} S^2 + \mu H_u H_d. \quad (4.3)$$

The F -term of S gives

$$V \supset |F_S|^2 = |\lambda H_u H_d + M S|^2. \quad (4.4)$$

It generates additional Higgs quartic terms which potentially increase the Higgs mass. The potential is

$$\Delta V = \lambda^2 |H_u H_d|^2 - \frac{(\lambda M)^2}{M^2 + m_S^2} |H_u H_d|^2, \quad (4.5)$$

and we can understand it diagrammatically by Fig. 4.1.

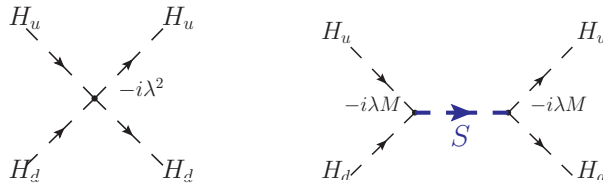


Figure 4.1: Additional Higgs quartic terms

The Higgs mass is increased by,

$$\Delta m_h^2 = \lambda^2 v^2 \sin^2 2\beta \left(\frac{m_S^2}{M^2 + m_S^2} \right), \quad (4.6)$$

¹When $\lambda\langle S \rangle$ is small, explicit μ term is necessary to avoid LEP chargino bounds.

where m_S^2 is the SUSY breaking soft mass $m_S^2|S|^2$, $\tan\beta = v_u/v_d$ is the ratio of the VEVs of the up and down-type Higgses, and $v = \sqrt{v_u^2 + v_d^2} = 174$ GeV. Notice that this term decouples in the supersymmetric limit, $M \gg m_S$, which means m_S should not be too small. On the other hand, m_S feeds into the Higgs soft masses, $m_{H_{u,d}}^2$ at one-loop,

$$\frac{dm_{H_{u,d}}^2}{d\log Q} \supset \frac{\lambda^2 m_S^2}{8\pi^2} \quad (4.7)$$

requiring fine-tuning if $m_S \gg m_h$. This can be easily understood since the singlet directly couples to the Higgs superfields which leads one-loop Supergraph of Fig. 4.2. The soft mass of S , that is $m_S^2\theta^2\bar{\theta}^2 S^\dagger S$, gives $m_{H_u}^2$ along with a logarithmic divergence, and we have Eq.(4.7) as a consequence. Therefore, there is tension between raising the Higgs mass, which requires large m_S , and naturalness, which demands small m_S . Of course, in the limit of $m_S \rightarrow 0$, similar tension which is discussed in the beginning exists with respect to $m_{\tilde{t}}$.

In this chapter, we point out that, contrary to the above example, a *lack of light scalars* can help raise the Higgs mass without a cost to naturalness, if the singlet has a Dirac mass.

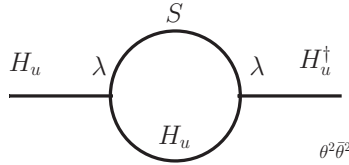


Figure 4.2: Supergraph

4.2 Model Setup

We consider a modification of Eq. 4.3 where S receives a Dirac mass with another singlet, \bar{S} ,

$$W = \lambda S H_u H_d + M S \bar{S} + \mu H_u H_d. \quad (4.8)$$

We call this model the *Dirac NMSSM*.

4.2.1 Spurion analysis

The absence of various dangerous operators (such as large tadpoles $M_{pl}^2 S$ for the singlets) follows from a $U(1)_{PQ} \times U(1)_{\bar{S}}$ Peccei-Quinn-like symmetry,

	Matter	H_u	H_d	S	\bar{S}	μ	M	ε_μ	ε_M
$U(1)_{PQ}$	-1/2	1	1	-2	-2	-2	4	-2	4
$U(1)_{\bar{S}}$	0	0	0	0	1	0	-1	0	-1

Here, $U(1)_{\bar{S}}$ has the effect of differentiating S and \bar{S} and forbidding the operator $\bar{S} H_u H_d$. Because μ and M explicitly break the $U(1)_{PQ} \times U(1)_{\bar{S}}$ symmetry, we regard them to be spurions originating from chiral superfields (“flavons” [73]) so that the superpotential should

not depend on their complex conjugates to avoid certain unwanted terms (“SUSY zeros” [74]). Namely,

$$\varepsilon_\mu(-2, 0) \sim \frac{\mu}{M_{pl}}, \quad \varepsilon_M(4, -1) \sim \frac{M}{M_{pl}} \quad (4.9)$$

are small breaking parameters.

By classifying all possible operators induced by these spurions, we see that a tadpole for \bar{S} is suppressed until the weak scale,

$$W \supset c_{\bar{S}} \mu M \bar{S} \sim \varepsilon_\mu \varepsilon_M M_{pl}^2 \bar{S}, \quad (4.10)$$

where $c_{\bar{S}}$ is a $\mathcal{O}(1)$ coefficient. Some terms involving only singlets

$$S, S^2, S^3, S^2 \bar{S} \quad (4.11)$$

are forbidden by the symmetries. The other terms are suppressed by higher order of $\varepsilon_{\mu, M}$,

$$(\varepsilon_\mu \varepsilon_M)^2 M_{pl} \bar{S}^2, (\varepsilon_\mu \varepsilon_M)^3 \bar{S}^3, \varepsilon_\mu \varepsilon_M^2 M S \bar{S}^2. \quad (4.12)$$

Potentially dangerous tadpoles can appear from Kähler potential with SUSY breaking. Using SUSY breaking spurion \mathcal{Z} ²

$$\mathcal{Z} = m_{SUSY} \theta^2, \quad m_{SUSY} \sim \mathcal{O}(1 \text{ TeV}), \quad (4.13)$$

we can classify such terms and see the size turns out to be safe,

$$\int d^4 \theta \mathcal{Z}^\dagger \mathcal{Z} \mu^\dagger S = m_{SUSY}^2 \mu^\dagger S. \quad (4.14)$$

4.2.2 Dirac NMSSM

From the spurion analysis the superpotential of Higgs sector in the Dirac NMSSM is given by

$$W_{\text{Dirac}} = \lambda S H_u H_d + M S \bar{S} + \mu H_u H_d + c_{\bar{S}} \mu M \bar{S}, \quad (4.15)$$

and the corresponding potential is

$$\begin{aligned} V_{\text{Dirac}} &= |F_{\bar{S}}|^2 + |F_S|^2 + |F_{H_u}|^2 + |F_{H_d}|^2 \\ &= |\lambda H_u H_d + M S|^2 + |M S + c_{\bar{S}} \mu M|^2 \\ &\quad + |(\lambda S + \mu) H_d|^2 + |(\lambda S + \mu) H_u|^2 \end{aligned} \quad (4.16)$$

where terms involving quark and lepton are omitted. The following soft supersymmetry breaking terms are allowed by the symmetries,

$$\begin{aligned} V_{\text{Dirac}}^{\text{soft}} &= m_{H_u}^2 |H_u|^2 + m_{H_d}^2 |H_d|^2 + m_S^2 |S|^2 + m_{\bar{S}}^2 |\bar{S}|^2 \\ &\quad + \lambda A_\lambda S H_u H_d + M B_S S \bar{S} + \mu B H_u H_d + c.c. \\ &\quad + t_{\bar{S}} \bar{S} + t_S S + c.c. \end{aligned} \quad (4.17)$$

The last tadpole arises from a non-holomorphic term $\mu^\dagger S$. Both soft tadpoles naturally have weak-scale sizes due to the symmetry and spurion structure. As described later, the spectrum we consider is one shown in Fig. 4.3

²One may worry that a similar SUSY breaking term, $\bar{\theta}^2 \mu^\dagger S$, in Kähler potential behaves as tadpole of S in superpotential, but it is removed by field redefinition of \bar{S} .

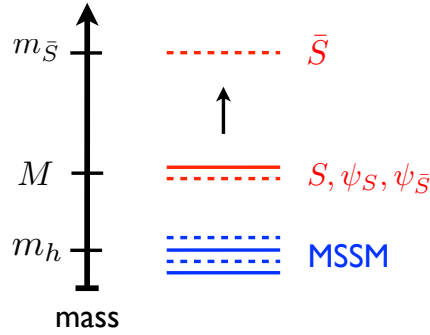


Figure 4.3: Schematic mass spectrum we consider in the Dirac NMSSM.

4.2.3 NMSSM

In the following discussion we consider the NMSSM for comparison. Here $U(1)_{\bar{S}}$ is absent. The non-negligible superpotential classified by spurion analysis of $U(1)_{PQ}$ is

$$W_{\text{NMSSM}} = \lambda S H_u H_d + \frac{M}{2} S^2 + \mu H_u H_d + c_S \mu M S, \quad (4.18)$$

and the corresponding potential is

$$\begin{aligned} V_{\text{NMSSM}} &= |F_S|^2 + |F_{H_u}|^2 + |F_{H_d}|^2 \\ &= |\lambda H_u H_d + M S + c_S \mu M|^2 + |(\lambda S + \mu) H_d|^2 + |(\lambda S + \mu) H_u|^2 \end{aligned} \quad (4.19)$$

where terms involving quark and lepton are omitted. The soft SUSY breaking terms are given by

$$\begin{aligned} V_{\text{NMSSM}}^{\text{soft}} &= m_{H_u}^2 |H_u|^2 + m_{H_d}^2 |H_d|^2 + m_{\bar{S}}^2 |S|^2 \\ &\quad + \lambda A_\lambda S H_u H_d + \frac{M}{2} B_S S^2 + \mu B H_u H_d + t_S S + c.c. \end{aligned} \quad (4.20)$$

4.3 Raising the Higgs Mass without Fine-tuning

Non-decoupling effects to boost the Higgs mass remain when $m_{\bar{S}}$ is extremely large in the Dirac NMSSM. We see the Higgs mass parameters are still stable against the radiative corrections unlike the NMSSM.

4.3.1 Non-decoupling effects

We would like to understand whether the new quartic term, $|\lambda H_u H_d|^2$, can naturally raise the Higgs mass. When we integrate out the S and \bar{S} chiral multiplets, normally we expect that the quartic potential decouples in the limit of heavy singlets. However, we find the S

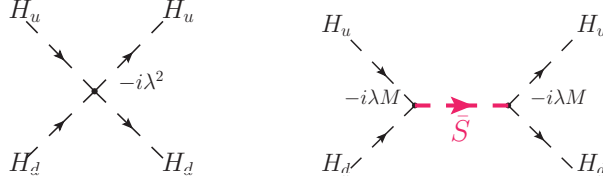


Figure 4.4: Non-decoupling effects in Dirac NMSSM

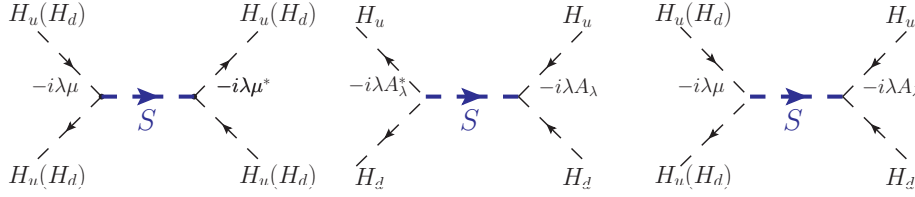


Figure 4.5: Other Higgs quartic terms in Dirac NMSSM

and \bar{S} exchanges do not cancel the quartic term,

$$V_{eff} = |\lambda H_u H_d|^2 \left(1 - \frac{M^2}{M^2 + m_{\bar{S}}^2} \right) - \frac{\lambda^2}{M^2 + m_{\bar{S}}^2} |A_\lambda H_u H_d + \mu^* (|H_u|^2 + |H_d|^2)|^2, \quad (4.21)$$

where we keep leading $(M^2 + m_{\bar{S}}^2)^{-1}$ terms and neglect the tadpole terms for simplicity. The new contribution to the Higgs quartic does not decouple when $m_{\bar{S}}^2$ is large. The SM-like Higgs mass becomes

$$m_h^2 = m_{h,\text{MSSM}}^2(m_{\bar{t}}) + \lambda^2 v^2 \sin^2 2\beta \left(\frac{m_{\bar{S}}^2}{M^2 + m_{\bar{S}}^2} \right) - \frac{\lambda^2 v^2}{M^2 + m_{\bar{S}}^2} |A_\lambda \sin 2\beta - 2\mu^*|^2, \quad (4.22)$$

in the limit where the VEVs and mass-eigenstates are aligned, $H_u \rightarrow v_u + h \sin \beta$ and $H_d \rightarrow v_d + h \cos \beta$. The second term, coming from diagrams of Fig. 4.4, shows so-called non-decoupling effect which is maximized by large $m_{\bar{S}}$. The second line of Eq.(4.22) can be understood by diagrams of Fig. 4.5, and it always reduces the size of quartic coupling.

By the way, in a limit of $M \gg m_{\bar{S}}$, the non-decoupling effect is easily derived by integrating out of S and \bar{S} using equations of motions of superpotential,

$$\int d^4\theta (1 - m_{\bar{S}}^2 \theta^4) \bar{S}^\dagger \bar{S} + S^\dagger S + \left(\int d^2\theta \lambda S H_u H_d + M \bar{S} S + h.c. \right) \quad (4.23)$$

$$\rightarrow \int d^4\theta \frac{\lambda^2 (1 - m_{\bar{S}}^2 \theta^4)}{M^2} (H_u H_d)^\dagger (H_u H_d). \quad (4.24)$$

The SUSY breaking term leads to a new Higgs quartic coupling. Similar analysis for various extensions of MSSM is found in Ref. [75].

4.3.2 Renormalization group equations

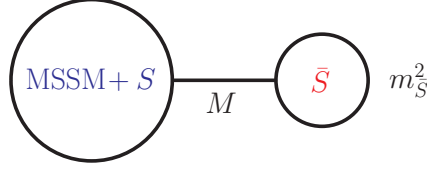


Figure 4.6: Schematic structure of Dirac NMSSM.

The Higgs sector is natural when there are no large radiative corrections to $m_{H_{u,d}}^2$. The renormalization group equations (RGEs) for $m_{H_{u,d}}^2$ are

$$\begin{aligned} \frac{d}{d \log Q} m_{H_u}^2 &= \frac{1}{8\pi^2} \left\{ 3y_t^2 (m_{\tilde{Q}_3}^2 + m_{\tilde{t}_R}^2 + m_{H_u}^2 + |A_t|^2) \right. \\ &\quad \left. + \lambda^2 (m_{\tilde{S}}^2 + m_{H_u}^2 + m_{H_d}^2 + |A_\lambda|^2) \right. \\ &\quad \left. - 3g_2^2 M_2^2 - g_1^2 M_1^2 \right\}, \end{aligned} \quad (4.25)$$

$$\begin{aligned} \frac{d}{d \log Q} m_{H_d}^2 &= \frac{1}{8\pi^2} \left\{ \lambda^2 (m_{\tilde{S}}^2 + m_{H_u}^2 + m_{H_d}^2 + |A_\lambda|^2) \right. \\ &\quad \left. - 3g_2^2 M_2^2 - g_1^2 M_1^2 \right\}. \end{aligned} \quad (4.26)$$

While heavy stops or $m_{\tilde{S}}^2$ lead to fine-tuning, we find that $m_{\tilde{S}}^2$ does not appear. In fact, the RGEs for $m_{H_{u,d}}^2$ are independent of $m_{\tilde{S}}^2$ to all orders in mass-independent schemes such as \overline{MS} and \overline{DR} schemes. This is clarified by dimensional analysis.

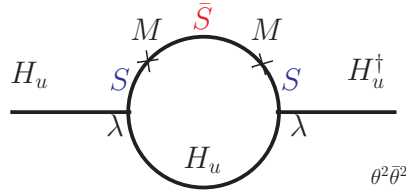
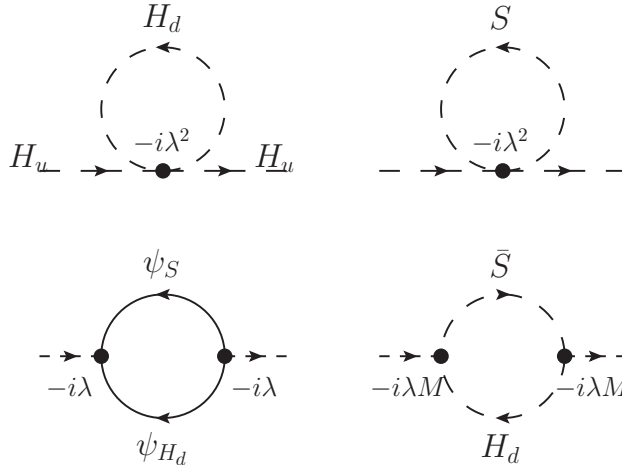
First of all, because \tilde{S} couples to the MSSM+S sector only through the dimensionful coupling M as in Fig. 4.6, their interaction vanishes in $M \rightarrow 0$ limit, and then terms involving $m_{\tilde{S}}^2$ must be proportional to M . Next, for the $U(1)_{\tilde{S}}$ conservation, a combination of lowest mass dimension is $|M|^2 m_{\tilde{S}}^2$, which has too high mass dimension to enter RGEs of the Higgs parameters, $m_{H_u}^2$, $m_{H_d}^2$ and μB , whose mass dimension is only two. Hence, the large $m_{\tilde{S}}$ does not upset naturalness through RGEs.

4.3.3 Threshold corrections

We consider threshold corrections in the effective theory where the scalar component of \tilde{S} is integrated for $m_{\tilde{S}} \gg M, \mu, m_S, m_{H_{u,d}}, A_\lambda, \dots$, and see if important corrections appear for $m_{H_{u,d}}^2$. One can see that the double insertion of M is needed for \tilde{S} to involve $m_{H_{u,d}}^2$ as shown in Fig. 4.27 and consequently there is no quadratic sensitivity to $m_{\tilde{S}}$. In the diagram shown in right-bottom of Fig. 4.8, $m_{\tilde{S}}$ changes only finite piece of log-divergence. Hence there is only logarithmic sensitivity to $m_{\tilde{S}}^2$ from the one-loop finite threshold correction in Fig. 4.8,

$$\delta m_H^2 \equiv \delta m_{H_{u,d}}^2 = \frac{(\lambda M)^2}{(4\pi)^2} \log \frac{M^2 + m_{\tilde{S}}^2}{M^2}, \quad (4.27)$$

which still allows for very heavy $m_{\tilde{S}}^2$ without fine-tuning.

Figure 4.7: Supergraph of $m_{H_u}^2$ correctionFigure 4.8: Threshold corrections to $m_{H_u}^2$

One may wonder if there are dangerous finite threshold corrections to $m_{H_u}^2$ at higher order, after integrating out \bar{S} . In fact, there is no quadratic sensitivity to $m_{\bar{S}}^2$ to all orders again. This follows because any dependence on $m_{\bar{S}}^2$ must be proportional to $|M|^2$ (since \bar{S} decouples when $M \rightarrow 0$ and by conservation of $U(1)_{\bar{S}}$), but $|M|^2 m_{\bar{S}}^2$ has too high mass dimension. The mass dimension cannot be reduced from other mass parameters appearing in the denominator because threshold corrections are always analytic functions of IR mass parameters [76]. This fact is from the matching of IR singularities. The full (UV) theory and the effective theory where the high energy dynamics down to a certain energy scale, e.g., $m_{\bar{S}}$, is integrated out must have same IR structure, namely, IR singularities are same in the both theories. If there are threshold corrections which are not analytic for IR mass parameters, such as,

$$\delta m^2 \sim \frac{|M|^2 m_{\bar{S}}^2}{m_{\text{IR}}^2}, \quad (4.28)$$

they will be new IR singularities when $m_{\text{IR}}^2 \rightarrow 0$, which contradicts the IR matching.

4.3.4 Semi-soft SUSY breaking

It sounds contradictory that naturalness is maintained in the limit of very heavy $m_{\bar{S}}$, since removing the \bar{S} scalar from the spectrum constitutes a hard breaking of supersymmetry. In

the effective theory with $m_{\bar{S}} \rightarrow \infty$, there exist the \bar{S} fermion with a Dirac mass and several terms originating from $F_{\bar{S}}$,

$$\mathcal{L} \supset i\bar{\psi}_{\bar{S}}\bar{\sigma}^{\mu}\partial_{\mu}\psi_{\bar{S}} - M\psi_S\psi_{\bar{S}} - M^2|S + c_{\bar{S}}\mu|^2, \quad (4.29)$$

as well as terms derived by

$$\begin{aligned} \mathcal{K} &\supset H_u^{\dagger}H_u + H_d^{\dagger}H_d + S^{\dagger}S, \\ W &\supset \lambda SH_uH_d + \mu H_uH_d. \end{aligned} \quad (4.30)$$

This theory can be written in superfields and soft breakings if we reintroduce the scalar of $\phi_{\bar{S}'}$ and F -term of $F_{\bar{S}'}$ to form a chiral supermultiplet of

$$\bar{S}' = \phi_{\bar{S}'} + \theta\psi_{\bar{S}} + \theta^2 F_{\bar{S}'} \quad (4.31)$$

Eq.(4.29) is rewritten in superspace as

$$\begin{aligned} \mathcal{K}_{eff} &= \bar{S}'^{\dagger}\bar{S}' - \theta^2\bar{\theta}^2 (M^2|S + c_{\bar{S}}\mu|^2), \\ W_{eff} &= -\theta^2 (M\mathcal{D}^{\alpha}S\mathcal{D}_{\alpha}\bar{S}') \end{aligned} \quad (4.32)$$

where $\phi_{\bar{S}'}$ and $F_{\bar{S}'}$ are completely decoupled from the other states. Therefore, the low energy effective theory even in absence of scalar \bar{S} is equivalent to a theory with only softly broken supersymmetry. We call this mechanism *semi-soft supersymmetry breaking*. It is crucial that \bar{S} couples to the other fields only through dimensionful couplings. Note that Dirac gauginos are a different example where adding new fields can lead to improved naturalness properties [77].

4.4 Higgs Mass at Tree-Level

The most natural region of parameter space, summarized in Fig. 4.3, has m_S and M at the hundreds of GeV scale, to avoid large corrections to m_{H_u} , and large $m_{\bar{S}} \gtrsim 10$ TeV, to maximize the second term of Eq. (4.22). The tree-level contribution to the Higgs mass can be large enough such that $m_{\tilde{t}}$ takes a natural value at the hundreds of GeV scale.

4.4.1 CP-even neutral scalars

For simplicity we assume there are no CP violations in the following studies. The minimization conditions for the Higgs and Singlet scalars are

$$\mu_{eff}^2 + m_{H_d}^2 - b_{eff}\tan\beta + \frac{m_Z^2}{2}\cos 2\beta + \lambda^2 v^2 \sin^2\beta = 0, \quad (4.33)$$

$$\mu_{eff}^2 + m_{H_u}^2 - b_{eff}\cot\beta - \frac{m_Z^2}{2}\cos 2\beta + \lambda^2 v^2 \cos^2\beta = 0, \quad (4.34)$$

$$M^2 + m_{\bar{S}}^2 + \frac{\lambda v^2}{v_S}(\mu + \lambda v_S) + \frac{1}{v_S} \left(MB_S v_{\bar{S}} - \frac{\lambda^2 A_{\lambda} v^2}{2} \sin 2\beta + c_{\bar{S}} M^2 \mu + t_s \right) = 0, \quad (4.35)$$

$$M^2 + m_{\bar{S}}^2 + \frac{1}{v_{\bar{S}}} \left(MB_S v_S - \frac{\lambda M v^2}{2} \sin 2\beta + t_{\bar{S}} \right) = 0. \quad (4.36)$$

where $v_S = \langle S \rangle$ and $v_{\bar{S}} = \langle \bar{S} \rangle$, and it is convenient to use

$$b_{\text{eff}} \equiv \mu B + \lambda(A_\lambda v_S + M v_{\bar{S}}), \quad (4.37)$$

$$\mu_{\text{eff}} \equiv \mu + \lambda v_S, \quad (4.38)$$

$$\bar{m}_A^2 \equiv b_{\text{eff}} / (s_\beta c_\beta). \quad (4.39)$$

The mass matrix of CP-even neutral scalars at tree level is given by $\mathcal{M}_{H^0,ij}^2 (= \mathcal{M}_{H^0,ji}^2)$ in the base of $\text{Re}(H_d^0, H_u^0, S, \bar{S})^T / \sqrt{2}$ where

$$\mathcal{M}_{H^0}^2 = \begin{pmatrix} \mathcal{M}_{H^0,11}^2 & & & & \\ & \mathcal{M}_{H^0,21}^2 & & & \\ & & \mathcal{M}_{H^0,22}^2 & & \\ \lambda v(2\mu_{\text{eff}} c_\beta - A_\lambda s_\beta) & \lambda v(2\mu_{\text{eff}} c_\beta - A_\lambda s_\beta) & M^2 + m_S^2 + \lambda^2 v^2 & & \\ -\lambda v M s_\beta & -\lambda v M c_\beta & M B_S & M^2 + m_{\bar{S}}^2 & \end{pmatrix} \quad (4.40)$$

and where

$$\begin{aligned} \mathcal{M}_{H^0,11}^2 &= \bar{m}_A^2 s_\beta^2 + m_Z^2 c_\beta^2, \\ \mathcal{M}_{H^0,22}^2 &= \bar{m}_A^2 c_\beta^2 + m_Z^2 s_\beta^2, \\ \mathcal{M}_{H^0,21}^2 &= -(\bar{m}_A^2 + m_Z^2 - 2\lambda^2 v^2) s_\beta c_\beta. \end{aligned} \quad (4.41)$$

Here $s_\beta(c_\beta)$ denotes $\sin\beta(\cos\beta)$, and the vacuum conditions of Eqs.(4.33, 4.34) are used for $\mathcal{M}_{H^0,11}^2$ and $\mathcal{M}_{H^0,22}^2$. Note that non-decoupling effect can be seen in $\mathcal{M}_{H^0,12}^2$, which completely remains when $m_{\bar{S}} \rightarrow \infty$.

4.5 Radiative Corrections

We take into account radiative corrections to the mass matrix. It is particularly important to estimate stop mass. The one-loop level calculation of y_t is easy to perform, which raises the SM-like Higgs mass, but it is well-known that the two-loop contributions tend to reduce the Higgs mass. Since only one-loop calculation leads optimistic result about naturalness, we adopt RG-improved one-loop calculation which is consistent enough with two-loop calculation of the MSSM. The similar result is given by Ref.[78].

4.5.1 One-loop corrections

The corrections are included by two parts. One is at $\mathcal{O}(y_t^4)$ calculated by effective potential, and the other is at $\mathcal{O}(y_t^2 g_1^2, y_t^2 g_2^2)$ involving $\mathcal{O}(y_t^2)$ corrections to wave function. The effective

potential at one-loop is given by

$$\Delta V^{(1)}(H, Q) = \frac{3}{32\pi^2} \left\{ m_{\tilde{t}_1}^4(H) \left(\log \frac{m_{\tilde{t}_1}^2(H)}{Q^2} - \frac{3}{2} \right) + m_{\tilde{t}_2}^4(H) \left(\log \frac{m_{\tilde{t}_2}^2(H)}{Q^2} - \frac{3}{2} \right) - 2m_t^4(H) \left(\log \frac{m_t^2(H)}{Q^2} - \frac{3}{2} \right) \right\}, \quad (4.42)$$

where the mass parameters are $H_{u,d}$ fields dependent,

$$m_t^2(H) = |y_t H_u|^2, \quad (4.43)$$

$$m_{\tilde{t}_1}^2(H) = m_t^2 + |y_t H_u^0|^2 - |y_t \mu H_d^0|, \quad (4.44)$$

$$m_{\tilde{t}_2}^2(H) = m_t^2 + |y_t H_u^0|^2 + |y_t \mu H_d^0|. \quad (4.45)$$

Here we assume $A_t = 0$ and $m_{\tilde{t}_R}^2 = m_{Q_3(\tilde{t}_L)}^2 = m_{\tilde{t}}^2$ for simplicity.

In addition, the corrections of $\mathcal{O}(y_t^2 g_1^2, y_t^2 g_2^2)$ require wave function renormalization as well as vertex corrections. Since both corrections are from the same one-loop supergraph that the fermionic part enters wave function renormalization and the bosonic part enters vertex correction as seen Fig. 4.9, their divergences are canceled leaving finite corrections. We match them onto the Higgs potential,

$$\Delta V^{(2)}(H) = -\frac{g_1^2 + g_2^2}{4} \frac{3y_t^2}{8\pi^2} \ln \frac{m_{\tilde{t}}^2 + m_t^2}{m_t^2} \left(|H_u^0|^4 - \frac{1}{2} |H_u^0|^2 |H_d^0|^2 \right), \quad (4.46)$$

where we neglect the mixing between \tilde{t}_R and \tilde{t}_L .

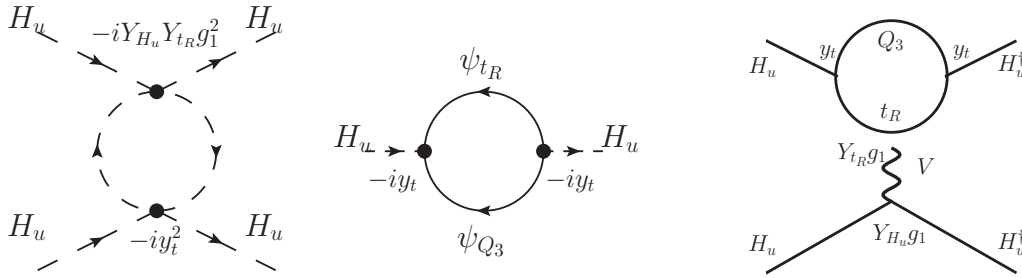


Figure 4.9: *Left*: $\mathcal{O}(y_t^2 g_1^2)$ vertex correction, *center*: wave function renormalization leading corrections of $\mathcal{O}(y_t^2 g_1^2)$. *Right*: One-loop supergraph. The supergraph without attachment of gauge field leads wavefunction renormalization of *center*, and that with gauge field leads vertex corrections of *left*.

For the new potential at one-loop level, the vacuum conditions for $H_{u,d}$ are shifted,

$$\mu_{\text{eff}}^2 + m_{H_d}^2 - b_{\text{eff}} \tan \beta + \frac{m_Z^2}{2} \cos 2\beta + \lambda^2 v^2 \sin^2 \beta + \left\langle \frac{1}{2H_d^0} \frac{\partial \Delta V}{\partial H_d^0} \right\rangle = 0, \quad (4.47)$$

$$\mu_{\text{eff}}^2 + m_{H_u}^2 - b_{\text{eff}} \cot \beta - \frac{m_Z^2}{2} \cos 2\beta + \lambda^2 v^2 \cos^2 \beta + \left\langle \frac{1}{2H_u^0} \frac{\partial \Delta V}{\partial H_u^0} \right\rangle = 0. \quad (4.48)$$

Hence, the mass matrix of Eq.(4.40) is modified by

$$\begin{aligned}\Delta\mathcal{M}_{H^0,11}^2 &= \frac{1}{2}\left\langle\frac{\partial^2\Delta V}{\partial(H_d^0)^2}\right\rangle - \left\langle\frac{1}{2H_d^0}\frac{\partial\Delta V}{\partial H_d^0}\right\rangle \\ &= \frac{3}{32\pi^2}\left((y_t\mu)^2 - \frac{y_t\mu(m_{\tilde{t}}^2 + m_t^2)}{vc_\beta}\log\frac{m_{\tilde{t}_1}^2}{m_{\tilde{t}_2}^2}\right),\end{aligned}\quad (4.49)$$

$$\begin{aligned}\Delta\mathcal{M}_{H^0,22}^2 &= \frac{1}{2}\left\langle\frac{\partial^2\Delta V}{\partial(H_u^0)^2}\right\rangle - \left\langle\frac{1}{2H_u^0}\frac{\partial\Delta V}{\partial H_u^0}\right\rangle \\ &= \frac{3y_t^2m_t^2}{8\pi^2}\ln\frac{m_{\tilde{t}_1}^2m_{\tilde{t}_2}^2}{m_t^4} - m_Z^2s_\beta^2\left(\frac{3y_t^2}{8\pi^2}\ln\frac{m_{\tilde{t}}^2 + m_t^2}{m_t^2}\right),\end{aligned}\quad (4.50)$$

$$\begin{aligned}\Delta\mathcal{M}_{H^0,21}^2 &= \frac{1}{2}\left\langle\frac{\partial^2\Delta V}{\partial H_u^0\partial H_d^0}\right\rangle \\ &= \frac{3y_t^2m_t\mu}{16\pi^2}\log\frac{m_{\tilde{t}_1}^2}{m_{\tilde{t}_2}^2} + m_Z^2s_\beta c_\beta\left(\frac{3y_t^2}{16\pi^2}\ln\frac{m_{\tilde{t}}^2 + m_t^2}{m_t^2}\right).\end{aligned}\quad (4.51)$$

In Eqs.(4.49,4.50), the vacuum shifts must be considered since the vacuum conditions are already used in Eq.(4.40). This result is consistent with Refs.[78].

4.5.2 RG-improved calculation

In the MSSM, it is known that two-loop corrections are not negligible for the Higgs mass estimation. We have taken into account $\mathcal{O}(y_t^4)$ and $\mathcal{O}(y_t^2g_{1,2}^2)$ corrections above. As two-loop contributions the dominant corrections should be at $\mathcal{O}(y_t^4g_s^2)$ and $\mathcal{O}(y_t^6)$.

Although we do not perform explicit two-loop calculation, RG-improved one-loop calculation developed in Ref. [78] deals with some part of corrections of $\mathcal{O}(y_t^4g_s^2)$ and $\mathcal{O}(y_t^6)$. In the one-loop correction with y_t , top quark and squark are always involved and we use y_t value at weak scale. However, the two particles have two different scales, weak scale and m_{SUSY} , and then the scale of y_t we use is not the best one and more appropriately it should be a geometric mean of the two scales,

$$Q \sim \sqrt{m_t(m_{\tilde{t}}^2 + m_t^2)^{1/2}}. \quad (4.52)$$

When we change the scale of y_t , beta functions of y_t^2 and g_s^2 are dominant,

$$y_t \rightarrow y_t \left(1 + (\beta_t + \beta_s)\log\frac{Q}{m_t}\right) \quad (4.53)$$

Thus original correction at $\mathcal{O}(y_t^4)$ leads to $\mathcal{O}(y_t^4g_s^2)$ and $\mathcal{O}(y_t^6)$ through RGE. We expect this scale discrepancy is the main source of two-loop corrections. We adopt beta functions of low energy effective theory that is Type-II two Higgs doublet model,

$$\beta_t = \frac{3y_t^2}{32\pi^2}, \quad \beta_s = -\frac{g_s^2}{2\pi^2}. \quad (4.54)$$

Since the two-loop calculations in the MSSM are available, we can make further improvement. We basically use the renormalization scale,

$$Q = c_{y_t}\sqrt{m_t(m_{\tilde{t}}^2 + m_t^2)^{1/2}}, \quad (4.55)$$

and c_{y_t} should be an $\mathcal{O}(1)$ coefficient but is not strictly determined. We choose c_{y_t} so that our MSSM result ($\lambda \rightarrow 0$) matches with the full two-loop MSSM result given by a software `FeynHiggs` [79]. When we choose the matching point in the MSSM of $\mu = 150$ GeV and $m_{\tilde{t}} = 300$ GeV, the coefficient c_{y_t} turns out to be $\simeq 1.5$ as shown in Fig. 4.10. For other values of μ and $m_{\tilde{t}}$ the difference of the lightest Higgs mass is quite small, $|\Delta m_h| < 1$ GeV. Then we reliably apply this calculation for the upper-left 2×2 mass matrix of CP-even scalars in Eq. (4.40).

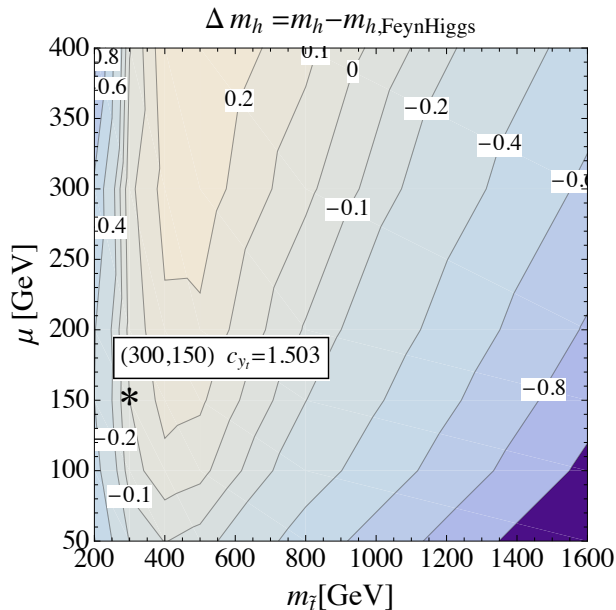


Figure 4.10: The mass difference between the lightest Higgs mass calculated by RG-improved method and that calculated by `FeynHiggs` (in GeV). Our calculation is matched with a result of `FeynHiggs` at $\mu = 150$ GeV and $m_{\tilde{t}} = 300$ GeV. Other parameters in `FeynHiggs` are set to be $\tan \beta = 2$, $A_t = 0$, $m_{A_0} = 1$ TeV, $(M_1, M_1, M_1) = (300, 400, 1000)$ GeV.

4.6 Benchmark Parameters and Stop Mass

When we estimate the stop mass in the Dirac NMSSM, we take M and $m_{\tilde{S}}$ to be free parameters since M is common in both models and $m_{\tilde{S}}$ is essential to discuss the non-decoupling effect. Other parameters are fixed according to the table of benchmark parameters (Table.4.1). We have chosen λ to saturate the upper-limit such that it does not reach a Landau pole below the unification scale [80]. For the NMSSM, we treat m_S as a free parameter instead of $m_{\tilde{S}}$ and correspondingly b_{eff} has a different definition,

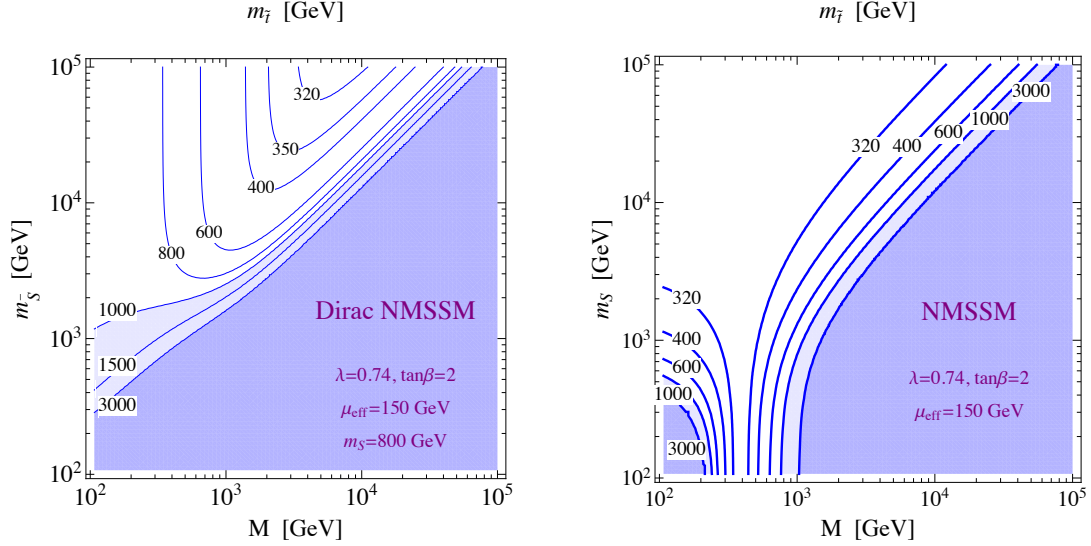
$$b_{eff} \equiv \mu B + \lambda v_S (A_\lambda + M). \quad (4.56)$$

The other parameters are as same as in the Dirac NMSSM.

One may worry about the size of singlet VEVs especially from the tadpoles because we

$\lambda = 0.74$	$\tan \beta = 2$	$\mu_{eff} = 150 \text{ GeV}$
$b_{eff} = (190 \text{ GeV})^2$	$A_\lambda = 0$	$B_s = 100 \text{ GeV}$
$m_S = 800 \text{ GeV}$		

Table 4.1: Benchmark parameters

Figure 4.11: Stop soft mass in the Dirac NMSSM (*left*) and NMSSM (*right*).

fixed μ_{eff} and b_{eff} defined in Eqs.(4.37,4.38). However we can see the VEVs adequately small,

$$v_S \simeq \frac{(c_S^* \mu^* |M|^2 + t_S^*)(|M|^2 + m_S^2)}{(|M|^2 + m_S^2)(|M|^2 + m_S^2)} \sim \mu^* \quad (4.57)$$

$$v_{\bar{S}} \simeq \frac{t_{\bar{S}}^*(|M|^2 + m_S^2)}{(|M|^2 + m_S^2)(|M|^2 + m_S^2)} \sim \frac{(\mu M)^* m_{\bar{S}}}{|M|^2 + m_S^2} \quad (4.58)$$

where the tadpoles scale as $t_S \sim \mu^* m_S^2$ and $t_{\bar{S}} \sim \mu M m_{\bar{S}}$.

We now estimate the stop mass. For each value of $(M, m_{\bar{S}})$, the stop soft masses, $m_{\tilde{t}} = m_{\tilde{t}_R} = m_{\tilde{Q}_3}$, are chosen to maintain the lightest scalar mass at 125 GeV. As results are shown in Fig. 4.11, basically the stop mass becomes small as $m_{\bar{S}}$ increases for the fixed M because more non-decoupling effect remains. Hence, the natural region should spread in large $m_{\bar{S}}$ where naturalness does not suffer from fine-tuning thanks to the semi-soft breaking. However, this argument does not apply for the low M region. This is because the S exchange effect, which is given by the second line of Eq.(4.22), is enhanced and decreases the tree-level Higgs mass when M is small.

4.7 Raising Higgs Mass for Explicit μ in the NMSSM

It is worth mentioning the behavior of stop mass in the NMSSM. Like in the Dirac NMSSM, the larger m_S leads to the more non-decoupling effect, that is the more Higgs mass at tree level. Hence, the stop mass becomes lighter as m_S increases for the fixed M . In this limit, naturalness is worsened by m_S rather than $m_{\tilde{t}}$.

Apart from the non-decoupling effect along with the SUSY breaking, there is a supersymmetric effect to enhance the tree-level Higgs mass in presence of explicit μ term while keeping natural EWSB [69]. After the singlet field is integrated out, new Higgs potential is generated,

$$V_{\text{eff}} = \frac{\mu^2 M^2 - \lambda^2 \mu M (H_u H_d + h.c.) + \lambda^4 |H_u H_d|^2}{M^2 + \lambda^2 (|H_u|^2 + |H_d|^2)} (|H_u|^2 + |H_d|^2) \quad (4.59)$$

where $m_S \rightarrow 0$. It leads to additional Higgs mass at tree level,

$$\Delta m_h^2 = \frac{4\lambda^2 (M\mu \sin 2\beta - \mu^2)}{M^2} \quad (4.60)$$

where the VEVs and mass-eigenstates are aligned, $H_u \rightarrow v_u + h \sin \beta$ and $H_d \rightarrow v_d + h \cos \beta$. This term positively remains only if M and μ have the same sign and the same size. As seen in Fig. 4.11 *right*, the mass correction vanishes when M is a few times larger or smaller than μ .

4.8 Naturalness

In this section, naturalness is evaluated. There are several measures, and we take a bottom-up approach described in Ref. [13] since we do not specify any UV completions and discuss based on low-energy parameters.

The degree of fine-tuning is estimated by

$$\Delta = \frac{2}{m_h^2} \max \left(m_{H_u}^2, m_{H_d}^2, b_{\text{eff}}, \frac{dm_{H_u}^2}{d \ln \mu} L, \frac{dm_{H_d}^2}{d \ln \mu} L, \delta m_H^2 \right), \quad (4.61)$$

where $L \equiv \log(\Lambda_{\text{mess}}/m_{\tilde{t}})$, and Λ_{mess} is a scale at which particle masses are generated. The first three terms of Eq. (4.61) represent magnitude of cancellation between parameters at the electroweak scale, and here $m_{H_u}^2$ and $m_{H_d}^2$ are determined by Eqs. (4.33, 4.34) with benchmark parameters. If any of them is much larger than the electroweak scale, tuning is required to give the right value of VEV. The rest terms of Eq. (4.61) shows fine-tuning from high-scale. Higgs soft masses are radiatively corrected by, for instance, top-stop sector, and if stop mass is extremely large, cancellation among contributions to $m_{H_u}^2$ is needed so that $m_{H_u}^2$ is finally at the electroweak scale. We take two values of Λ_{mess} corresponding to low-scale ($L = 6$) and high-scale ($L = 30$) SUSY breaking. We assume that contributions through gauge couplings to the RGEs for $m_{H_{u,d}}^2$ are subdominant. To be more concrete about Eq. (4.61), the RGE effects to m_{H_u} , for example, are separated by each parameter,

$$\frac{dm_{H_u}^2}{d \ln \mu} L = \left(\frac{3y_t^2 m_{\tilde{Q}_3}^2}{8\pi^2} L, \frac{3y_t^2 m_{\tilde{t}_R}^2}{8\pi^2} L, \frac{\lambda^2 m_S^2}{8\pi^2} L \dots \right). \quad (4.62)$$

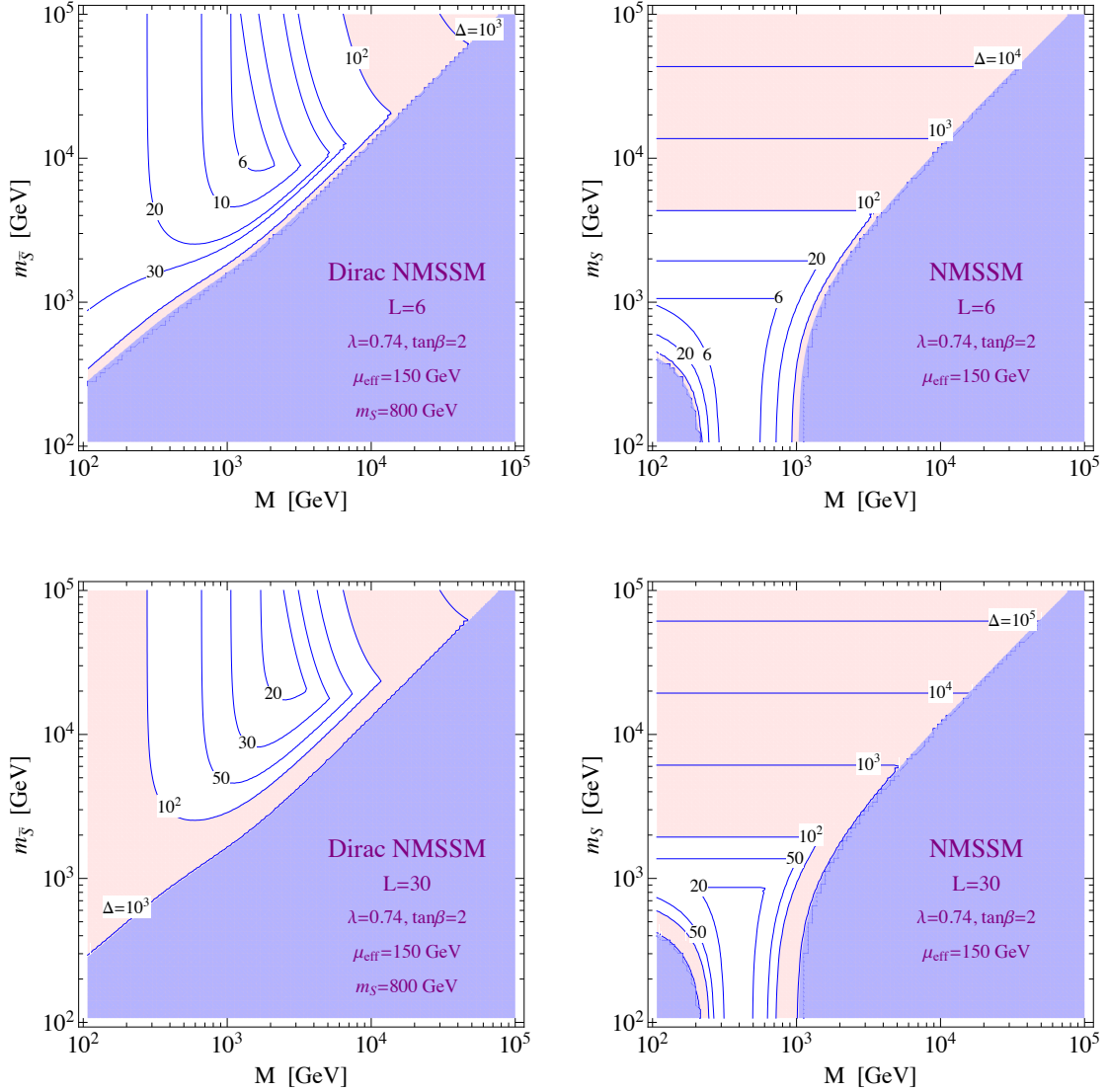


Figure 4.12: The tuning Δ , defined in Eq. eq:tune, for the Dirac NMSSM is shown on the *left* as a function of M and $m_{\bar{S}}$. For comparison, the tuning of the NMSSM is shown on the *right*, as a function of M and m_S . The red region has high fine-tuning, $\Delta > 100$, and the purple region requires $m_{\tilde{t}} > 2$ TeV, signaling severe fine-tuning $\gtrsim \mathcal{O}(10^3)$. The tuning is evaluated with $L = 6$ (30) in the *upper* (*lower*) plots.

The results are shown in Fig. 4.12.

In the Dirac NMSSM, the degree of tuning Δ is mostly determined by the RGE effect from $m_{\tilde{t}}$. When M is quite large, $M > 1$ TeV, Δ is determined by the threshold correction given in Eq. (4.27). Actually as shown in Figs. 4.11 and 4.12, the shape of curves almost corresponds to that of stop mass, and only upper-right region is dominated by the threshold

correction. The difference between low- and high-scale SUSY breaking cases is basically the difference of absolute value by a factor of 5. The tuning level is as low as $\Delta^{-1} \approx 20\%$ (5%) for low-scale (high-scale) SUSY breaking.

We see that the least-tuned region of the Dirac NMSSM corresponds to $M \sim 2$ TeV and $m_{\bar{S}} \gtrsim 10$ TeV, where the tree-level correction to the Higgs mass is maximized. The fact that the large SUSY breaking, $m_{\bar{S}}$, leads to more natural theory is counter-intuitive, but, thanks to the mechanism introduced as semi-soft SUSY breaking, this particular SUSY breaking is irrelevant to naturalness.

On the other-hand, the tuning in the NMSSM is determined by the RGE effects not only through stop mass ($m_{\tilde{t}_R}, m_{\tilde{Q}_3}$) but also m_S . The NMSSM becomes highly tuned when m_S is large, and then $m_S \lesssim 500$ GeV is favored. Note that region of low-tuning in the NMSSM extends to the supersymmetric limit, $m_S \rightarrow 0$. In this region the Higgs mass is increased by a new contribution to the quartic coupling proportional to $\lambda^2(M\mu \sin 2\beta - \mu^2)/M^2$ as described in Sec. 4.7 (see Ref.[69] for more details).

In order to estimate the SM-like Higgs mass at one-loop level, we only need to consider Higgs and singlet sector plus corrections from stop-top sector, and do not specify gaugino masses. However, when the mediation scale is high or gluino mass is large, the main source of tuning can be gluino mass scale because stop masses are corrected by gluino mass with a large coefficient through RGE,

$$m_{\tilde{Q}_3, \tilde{t}_R} = \frac{g_s^2}{4\pi^2} \frac{N_C^2 - 1}{N_C} M_3^2 + \dots \quad (4.63)$$

This point is studied with the latest LHC constraints in Ref.[81], and a recent study discusses it in the context of Dirac NMSSM [82]. The gluino mass contribution to tuning is roughly estimated by

$$\Delta_{\tilde{g}} = \frac{2}{m_h^2} \left[\frac{3y_t^2}{8\pi^2} \frac{8\alpha_s}{3\pi} M_3^2 \right] \frac{L^2}{2} \sim 30 \left(\frac{M_3}{400 \text{ GeV}} \right)^2 \left(\frac{L}{30} \right)^2. \quad (4.64)$$

This is independent of M , m_S , and $m_{\bar{S}}$. For high-scale mediation where $L = 30$, gluino mass more than a few hundreds GeV becomes dominant in tuning and affects the lowest tuned parameter region of Fig. 4.12, regardless of $m_{\tilde{t}}$, m_S , and $m_{\bar{S}}$.

5

Phenomenology of Dirac NMSSM

We now discuss the experimental signatures of the Dirac NMSSM. The phenomenology of the NMSSM is well-studied [14, 83]. In the natural region of the Dirac NMSSM, the singlet states are too heavy to be produced at the LHC. The low-energy Higgs phenomenology is that of a two Higgs doublet model, and we focus here on the nature of the lightest SM-like Higgs, h , and the heavier doublet-like Higgs, H [84]. The properties of the two doublets differ from the MSSM due to the presence of the non-decoupling quartic coupling $|\lambda H_u H_d|^2$ in Eq. (4.40), which raises the Higgs mass by the semi-soft SUSY breaking, described above.

For the fixed λ and $\tan\beta$, the essential parameter is only b_{eff} in upper-left 2×2 mass matrix of Eq. (4.40). Therefore, we treat b_{eff} as a free parameter, and all the results are given in terms of the heavier Higgs mass, m_H , which is roughly proportional to b_{eff} . The other parameters are fixed as follows.

benchmark parameters			
$\lambda = 0.74$	$\tan\beta = 2$	$\mu_{eff} = 150 \text{ GeV}$	$A_\lambda = 0$
$M = 1 \text{ TeV}$	$m_{\tilde{g}} = 10 \text{ TeV}$	$B_s = 100 \text{ GeV}$	

5.1 Current Constraints

5.1.1 SM-like Higgs

We consider the potential with radiative corrections from top-stop sector, and we find that the couplings of the SM-like Higgs to leptons and down-type quarks are lowered due to mixing between two Higgs fields, while couplings to up-type quarks are slightly increased compared to those in the SM for relatively low $\tan\beta$. In Fig. 5.1, we plot deviations of couplings relative

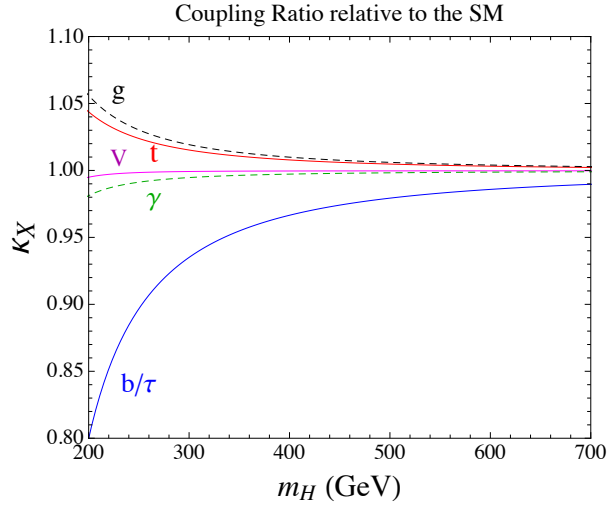


Figure 5.1: Deviations of SM-like Higgs couplings normalized to the SM values on the left as a function of m_H . Here t , b , and τ represent all up-type quarks, down-type quarks, and charged leptons, respectively.

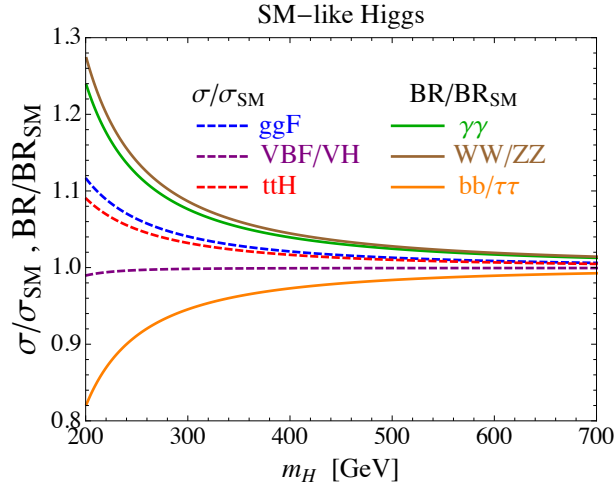


Figure 5.2: The branching ratios and production cross sections of the SM-like Higgs are shown normalized to the SM values on the right as a function of m_H

to values in the SM using

$$\kappa_X \equiv \frac{XXh \text{ coupling}|_{\text{Dirac NMSSM}}}{XXh \text{ coupling}|_{\text{SM}}} . \quad (5.1)$$

The couplings of Higgs to gluons and photons occur at loop levels, and then the deviation of them comes from the other couplings. For example, the $h\gamma\gamma$ effective coupling has mainly two contributions that are from the W boson loop and top quark loop, and we simply multiply κ_V^2 and κ_t^2 in each loop diagram.

The smaller coupling of $hb\bar{b}$ results in the deviations to the cross sections and decay patterns shown in Fig. 5.2. These effects decouple in a limit of $m_H \gg m_h$, which corresponds

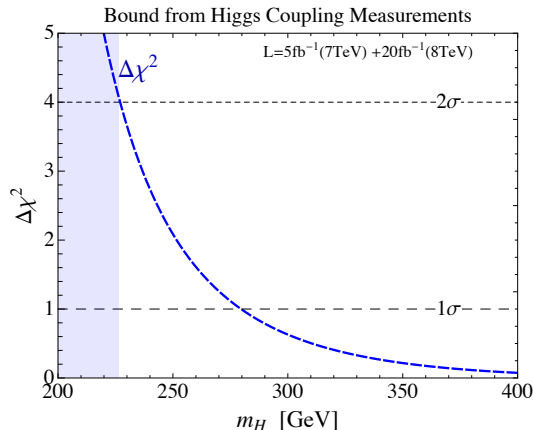


Figure 5.3: $\Delta\chi^2$ for the SM-like Higgs couplings with the 7 and 8 TeV datasets from the ATLAS and CMS [85, 86, 87, 88]. The shaded region is excluded at 95% C.L.

to large b_{eff} .¹ For the branching fraction calculation, we utilize the Higgs decay widths given by the LHC Higgs Cross Section Working Group [15] and multiply each width by appropriate factors of κ to get our width.

The first constraint on the Higgs sector of the Dirac NMSSM comes from measurements of the couplings of the SM-like Higgs from ATLAS [85, 86] and CMS [87, 88] with integrated luminosity of 5 fb^{-1} at 7 TeV and 20 fb^{-1} at 8 TeV. We perform $\Delta\chi^2$ test on the Dirac NMSSM, which excludes $m_H \lesssim 220 \text{ GeV}$ at 95% C.L.

5.1.2 Heavier doublet-like Higgs

We also show, in Fig. 5.4, the decay branching ratios of H . Due to the non-decoupling term, di-Higgs decay, $H \rightarrow 2h$, becomes the dominant decay once its threshold is opened, $m_H \gtrsim 250 \text{ GeV}$. For the calculation of decay widths to SM particles (t, b, Z, W, τ, g), the widths given by the LHC Higgs Cross Section Working Group [15] are utilized again.

Bellow this threshold, direct searchers of the heavier state decaying to dibosons, $H \rightarrow ZZ, WW$ [86, 88], can constraint the model. It extends the limit to $m_H \sim 260 \text{ GeV}$ as in Fig. 5.5 (except for a small gap near $m_H \approx 235 \text{ GeV}$).

5.2 Future Reach

We also estimate the future reach to probe m_H with future Higgs coupling (or width) measurements [89, 90, 91, 92]. Those precisions are summarized in Tables 5.1 and 5.2.

Two different studies of ILC [90, 91] have different estimates of theoretical errors while the same experimental precisions are used in both. And recently (2013 August) Snowmass Higgs working group gave an estimate of coupling measurements with the highest precision based on integration of high-luminosity ILC runs. This is not only experimental challenge

¹Corrections from sparticles to the Higgs decay and production are not included.

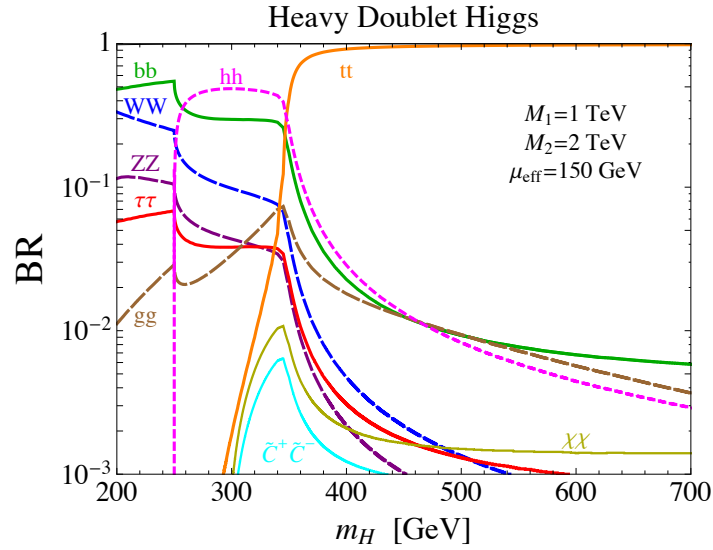


Figure 5.4: Several branching ratios of the heavy doublet-like Higgs as a function of its mass. Note that the location of the chargino/neutralino thresholds depend on the -ino spectrum. Here we take heavy gauginos and $\mu_{eff} = 150$ GeV.

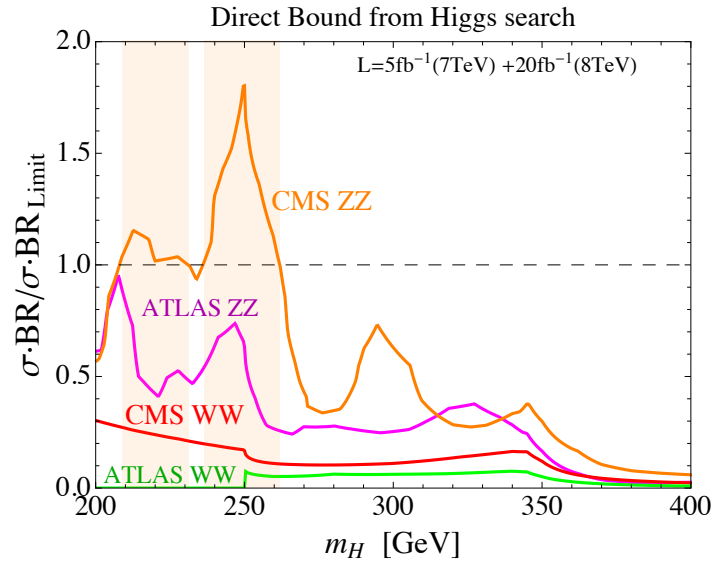


Figure 5.5: σ/σ_{lim} for direct searches, $H \rightarrow ZZ, WW$ [86, 88]. The shaded region is excluded at 95% C.L.

but also theoretical challenge because the theoretical error of b quark mass is expected to decrease up to 0.1% level.

The expected accuracies of coupling measurement give the future reach in Fig. 5.6. The 2σ exclusion reach is $m_H \simeq 280$ GeV at the high-luminosity LHC [89], $m_H \simeq 400$ GeV with theoretical uncertainty at ILC500 [91], and $m_H \simeq 550$ GeV without theoretical uncertainty.

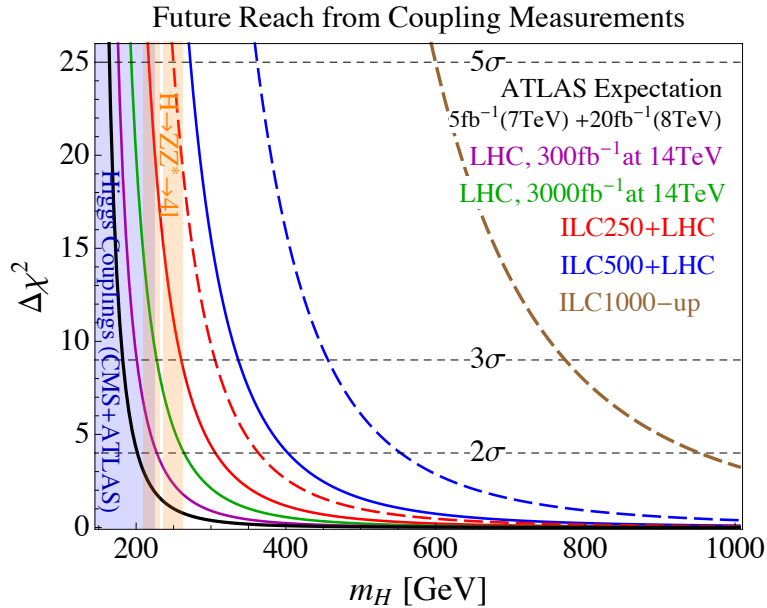


Figure 5.6: The curves show the expected $\Delta\chi^2$ from combined measurements of the Higgs-like couplings at the high-luminosity LHC at $\sqrt{s} = 14$ TeV [89] and the ILC at $\sqrt{s} = 250, 500, 1000$ GeV. The optimistic [90, 92] (conservative [91]) ILC reach curves are solid (dashed) and neglect (include) theoretical uncertainties in the Higgs branching ratios. The ILC analyses include the expected LHC measurements. For comparison we show the present limits and also the expected limit of the current ATLAS measurements (solid, black). The shaded regions show current constraints on our model by the SM-like Higgs coupling measurements and direct searches of H .

	HL-LHC 300 fb ⁻¹	HL-LHC 3000 fb ⁻¹
Γ_Z/Γ_g	0.523	0.284
Γ_t/Γ_g	0.519	0.230
Γ_μ/Γ_Z	0.448	0.142
Γ_τ/Γ_Z	0.417	0.206
Γ_γ/Γ_Z	0.110	0.029
$\Gamma_g \cdot \Gamma_Z/\Gamma_H$	0.159	0.029

Table 5.1: Expected relative uncertainties on the ratios of Higgs boson partial widths with theory systematic errors (Tables 6, 7 in Ref. [89]). Γ_H is the total width, and $\sqrt{s} = 14$ TeV.

The reach extends to $m_H \simeq 950$ GeV at upgraded ILC1000 [92]. The increased sensitivity at the ILC is dominated by the improved measurements projected for the $b\bar{b}$ and $\tau^+\tau^-$ couplings [90, 92] since those have larger deviation compared to SM values as in Fig. 5.1.

in %	(a) ILC250 +LHC	(b)ILC250 +LHC	(a)ILC500 +LHC	(b)ILC500 +LHC	ILC1000-up
$\Delta\kappa_W$	± 1.9	± 4	± 0.24	$^{+1.0}_{-1.1}$	± 0.13
$\Delta\kappa_Z$	± 0.44	$^{+0.9}_{-1.0}$	± 0.30	± 0.8	± 0.22
$\Delta\kappa_b$	± 2.7	$^{+5}_{-4}$	± 0.94	$^{+3}_{-2}$	± 0.31
$\Delta\kappa_\tau$	± 3.3	± 4	± 1.9	± 3	± 0.72
$\Delta\kappa_{t,c}$	± 4.7	± 4	± 2.5	± 3	± 0.76

Table 5.2: Expected precisions on the Higgs couplings. ILC250(ILC500) represents an analysis with ILC data of 250(500) fb^{-1} at $\sqrt{s} = 250(500)$ GeV plus LHC data of 300 fb^{-1} at $\sqrt{s} = 14$ TeV. The values in (a) are given by M. Peskin [90] and used in ILC Technical Design Report(TDR), and the different group includes more theoretical errors giving conservative values of (b) [91]. ILC1000-up assumes upgraded ILC and integrates all the data of 1150($\sqrt{s} = 250$ GeV) + 1600(500 GeV) + 2500(1 TeV) fb^{-1} [92].

5.3 Summary and Discussion

The LHC has discovered a new particle, consistent with the Higgs boson, with a mass near 125 GeV. Weak-scale supersymmetry must be reevaluated in light of this discovery. Naturalness demands new dynamics beyond the minimal theory, such as a non-decoupling F -term, but this implies new sources of SUSY breaking that themselves threaten naturalness. In Ch. 4, we have identified a new model where the Higgs couples to a singlet field with a Dirac mass. The non-decoupling F -term is naturally realized through semi-soft SUSY breaking, because large $m_{\tilde{g}}$ helps raise the Higgs mass but does not threaten naturalness.

The key feature of semi-soft SUSY breaking in the Dirac NMSSM is that \tilde{S} couples to the MSSM only through the dimensionful Dirac mass, M . We noted that interactions between \tilde{S} and other new states are not constrained by naturalness, even if these states experience SUSY breaking. Therefore, the Dirac NMSSM represents a new type of portal, whereby our sector can interact with new sectors, with large SUSY breaking, without spoiling naturalness in our sector.

The first collider signatures of the Dirac NMSSM are expected to be those of the MSSM fields, with the singlet sector naturally heavier than 1 TeV. In Ch. 5, we discussed the phenomenology focusing on the Higgs sector, which is a two Higgs doublet model with low $\tan\beta$. We obtained constraints from direct searches for heavier Higgs boson and coupling measurements for the lightest Higgs boson at the LHC. We also studied the future reach based on prospects of high-luminosity LHC and ILC, and showed large parameter space can be probed.

6

Overall Summary

The main accomplishment of LHC Run I is discovery of a Higgs boson, and it is a momentous step towards understanding electroweak symmetry breaking. However, there are still many experimental evidences that cannot be explained in the Standard Model and require some new physics, as represented by dark matter. Furthermore the SM Higgs sector is not theoretically satisfactory for the naturalness problem. Supersymmetry cures this problem and is regarded as a prime candidate for physics beyond the Standard Model.

However there are tensions between low-energy supersymmetry and the LHC results. We discussed them in Ch. 1. First of all, searches at the LHC for sparticles have not found any signal and give strong bounds on the conventional CMSSM. Next, the observed Higgs mass of 125 GeV is not easily accommodated in the MSSM, where one has to rely on the radiative corrections to boost the Higgs mass beyond the tree-level upper bound of $m_Z \simeq 91$ GeV. This requirement push sparticles scale well beyond the TeV within CMSSM, leading to fine-tuning of $\Delta^{-1} \lesssim 1\%$. In this thesis we particularly have investigated two scenarios of supersymmetry originating the tensions.

A compressed spectrum ameliorates the bounds from the current searches at the LHC whereas the CMSSM typically generates a widely spread spectrum. For the lack of SUSY signal, the scenario with a compressed spectrum recently has more attentions but it has not been theoretically justified based on simple and explicit models of SUSY breaking.

Supersymmetry broken geometrically in extra dimensions, by the Scherk-Schwartz mechanism, naturally leads to a compressed spectrum. In Ch. 2 we have built a minimal such model with a single extra dimension of S^1/\mathbb{Z}_2 , “Compact Supersymmetry.” After reviewing construction of 5D SUSY, we demonstrated the Scherk-Schwartz mechanism is equivalent to the Radion Mediation. In the model, gauge, quark and lepton superfields are living in the full 5D while Higgs fields are localized on a brane. The model has only three parameters, a size of extra dimension, SUSY breaking scale, and supersymmetric Higgs mass, and hence it is

explicitly testable. For the nature of geometrical SUSY breaking, the universality of gaugino masses and fermion masses is present. We presented radiative corrections generating Higgs parameters which are absent at tree-level.

We matched the full theory onto the MSSM and studied phenomenology of the model in Ch. 3. The conditions for the EWSB were studied at first to determine all the parameters. The spectrum certainly tends to be compressed. We found predicted near-maximal mixing in the scalar top sector with $|A_t| \approx 2m_{\tilde{t}}$ boosts the lightest Higgs boson mass. The Higgs mass in large parameter space is about $121 \sim 125$ GeV, but this is not necessarily incompatible with 125 GeV for the large theory uncertainty. Despite the rather constrained structure, the theory is less fine-tuned than many supersymmetric models. The LSP is Higgsino-like and can be a component of dark matter. We found direct detection experiments will cover a large portion of parameter space. The theory does not suffer from the supersymmetric flavor or CP problem because of universality of geometric breaking. The collider constraint on the Compact Supersymmetry is certainly weaker than that on the CMSSM such that gluino and squark mass bound is relaxed from $m_{\tilde{g},\tilde{q}} \lesssim 1.7$ TeV down to $m_{\tilde{g},\tilde{q}} \lesssim 1$ TeV.

Naturalness implies new dynamics beyond the minimal theory. There have been many attempts to extend the MSSM to accommodate the Higgs mass. If the new states are integrated out supersymmetrically, their effects decouple and the Higgs mass is not increased. On the other hand, SUSY breaking can lead to non-decoupling effects that increase the Higgs mass. However, in general, these extensions require new states at the few hundred GeV scale, so that the new sources of SUSY breaking do not spoil naturalness.

In Ch. 4, we have identified a new model where the Higgs couples to two singlet fields with a Dirac mass, which we call Dirac NMSSM,

$$W \supset \lambda SH_u H_d + M \bar{S} \tilde{S}.$$

The non-decoupling F -term increases the Higgs mass while maintaining naturalness even in the presence of large SUSY breaking in the singlet sector, namely, $m_{\tilde{S}} \gtrsim 10$ TeV. The key feature in the Dirac NMSSM is that \tilde{S} couples to the MSSM only through the dimensionful Dirac mass, M . We pointed out that interactions between \tilde{S} and other new states are not constrained by naturalness, even if \tilde{S} states experience SUSY breaking. We call this mechanism semi-soft SUSY breaking. Therefore, the Dirac NMSSM represents a new type of portal, whereby our sector can interact with new sectors, with large SUSY breaking, without spoiling naturalness in our sector.

Collider signatures of the Dirac NMSSM are discussed in Ch. 5. The low-energy phenomenology is that of a two Higgs doublet model. We obtained constraints from direct searches for heavier Higgs boson and coupling measurements for the lightest Higgs boson at the LHC. We also studied the future reach based on prospects of high-luminosity LHC and future international linear collider, and show large parameter space can be probed.

Acknowledgments

First of all, I am deeply grateful to Prof. Hitoshi Murayama. He always encourages me for the research progress, and he leads me to the interesting fields in particle physics with his knowledge, experience, and foresight. I also appreciate that he let me stay at University of California, Berkeley for about a year. During the stay, I had the best lectures ever by him about Quantum Field Theory and particle phenomenology. His international connections enabled me to know various researchers all over the world even when I was at Kavli IPMU. These extraordinary experience brought by him stimulates my research and makes me enjoy the research.

I wish to acknowledge Yuuko Enomoto for her great help. For her support and corporation, I could find discussion time with my advisor and conduct research at Kavli IPMU. I would like to express my gratitude to Mihoko M. Nojiri for patiently teaching me the basics of collider phenomenology. Without her guidance, my first research project would not be possible.

Many results obtained in this dissertation were never obtained without collaborations with Yasunori Nomura and Satoshi Shirai, and Xiaochuan Lu and Joshua T. Ruderman at University of California, Berkeley. I have learned a lot of things about supersymmetry and phenomenology from them. I also thank Brian Henning for a lot of discussion. The collaborations and communication made my stay at Berkeley very fruitful. I thank collaborators of the other projects, Tomohiro Abe, Keisuke Harigaya, Junji Hisano, Teppei Kitahara, Shigeki Matsumoto, Ryosuke Sato and Norimi Yokozaki. I would particularly thank Junji Hisano for taking care of informal reading course of supersymmetry in the beginning of graduate program.

I spent most of my graduate school days at Kavli IPMU. I enjoyed talking with people in various research fields at the tea time of the institute. I would like to thank all researchers, visitors, and administrative staff in the institute for making my daily life enjoyable and supporting my research activities. At Kavli IPMU, I had fruitful discussion with researchers, Won Sang Cho, Masahiro Ibe, Ryoichi Nishio, Seong Chan Park, Ryosuke Sato, Taizan Watari, Tsutomu Yanagida, Kazuya Yonekura and many others. I would like to especially thank students with whom I shared my office, namely, Takeshi Kobayashi, Hironao Miyatake, Ryoichi Nishio, Sourav Mandal, Takashi Moriya, William L. Klemm, Xu-Feng Wang, Kimihiko Nakajima, Tomonori Ugajin, Ayuki Kamada, Tomohiro Fujita, Keisuke Harigaya, Masato Shirasaki, Gen Chiaki, Wen Yin, Hidemasa Oda, Yuuki Nakaguchi, Yusuke Ono, Noriaki Watanabe, Ryo Matsuda and many visitors from all over the world.

I enjoyed a lot of informal discussion with friends in the same grade, Hiraku Fukushima, Manami Hashi, Yuji Hirono, Kenta Hotokezaka, Yohei Kikuta and Natsumi Nagata. Communication with them always raises my motivation of research.

I would like to express my sincere gratitude to my parents, Hisaya Tobioka and Shizuko

Tobioka. My interest in nature was originated from my young days with my parents in Aso, Kumamoto. I appreciate they allowed me to study at Tohoku University, Sendai, and even supported my studying abroad at University of California, San Diego during undergraduate. And without their special supports I would not have accomplished my research. Thank you from the bottom of my heart.

This research is supported by the Japan Society for the Promotion of Science Research Fellowship for Young Scientists, World Premier International Research Center Initiative (WPI Initiative), MEXT, Japan.



Structure of 5D Supersymmetry

A.1 Gauge Invariance of 5D Supersymmetry Action

We check the gauge invariance of 5D gauge field strength. The non-trivial part in Eq. (2.3) is

$$\int d^4\theta \text{Tr} \left[(\sqrt{2}\partial_5 + \chi^\dagger)e^{-V}(-\sqrt{2}\partial_5 + \chi)e^V + (\partial_5 e^{-V})(\partial_5 e^V) + \frac{\chi^\dagger\chi^\dagger + \chi\chi}{2} \right]. \quad (\text{A.1})$$

We redefine gauge fields to absorb gauge coupling as $2gV \rightarrow V, 2g\chi \rightarrow \chi$. Note that the last term vanishes after performing θ integrals, but it is essential for gauge invariance. In addition, in the Radion mediation, we have supersymmetry breaking in front this term, which means it does not vanish by θ integrals.

Under the non-abelian gauge transformation, the vector and adjoint chiral superfields transform as

$$\begin{aligned} e^{-V} &\rightarrow U^\dagger e^{-V} U, & e^V &\rightarrow U^{-1\dagger} e^V U^{-1} \\ \chi &\rightarrow U^{-1}(\chi - \sqrt{2}\partial_5)U, & \chi^\dagger &\rightarrow U^\dagger(\chi^\dagger + \sqrt{2}\partial_5)U^{-1\dagger}. \\ H_1 &\rightarrow U^{-1}H_1, & H_2 &\rightarrow H_2 U^\dagger \end{aligned} \quad (\text{A.2})$$

First let us see the first term,

$$(\sqrt{2}\partial_5 + \chi^\dagger)e^{-V} \rightarrow \sqrt{2}\partial_5(U^\dagger e^{-V}U) + [U^\dagger(\chi^\dagger + \sqrt{2}\partial_5)U^{-1\dagger}]U^\dagger e^{-V}U \quad (\text{A.3})$$

$$\begin{aligned} &= \sqrt{2} \left\{ (\partial_5 U^\dagger) e^{-V} U + U^\dagger (\partial_5 e^{-V}) U + U^\dagger e^{-V} \partial_5 U \right\} \\ &\quad + U^\dagger \chi^\dagger e^{-V} U + \sqrt{2} U^\dagger (\partial_5 U^{-1\dagger}) U^\dagger e^{-V} U \\ &= \sqrt{2} \left\{ (\partial_5 U^\dagger) e^{-V} U + U^\dagger (\partial_5 e^{-V}) U + U^\dagger e^{-V} \partial_5 U \right\} \\ &\quad + U^\dagger \chi^\dagger e^{-V} U - \sqrt{2} U^\dagger U^{-1\dagger} (\partial_5 U^\dagger) e^{-V} U \\ &= \sqrt{2} \left\{ U^\dagger (\partial_5 e^{-V}) U + U^\dagger e^{-V} \partial_5 U \right\} + U^\dagger \chi^\dagger e^{-V} U \\ &= U^\dagger \left\{ \sqrt{2}\partial_5 e^{-V} + \chi^\dagger e^{-V} \right\} U + \sqrt{2} U^\dagger e^{-V} \partial_5 U \end{aligned} \quad (\text{A.4})$$

Here we used an identity

$$\partial_5(U^{-1}U) = (\partial_5 U^{-1})U + U^{-1}(\partial_5 U) = 0. \quad (\text{A.5})$$

Similarly,

$$(-\sqrt{2}\partial_5 + \chi)e^V \rightarrow \sqrt{2}\partial_5(U^{-1}e^V U^{-1\dagger}) + [U^{-1}(\chi - \sqrt{2}\partial_5)U]U^{-1}e^V U^{-1\dagger} \quad (\text{A.6})$$

$$\begin{aligned} &= \sqrt{2} \left\{ (\partial_5 U^{-1}) e^V U^{-1\dagger} + U^{-1} (\partial_5 e^V) U^{-1\dagger} + U^{-1} e^V \partial_5 U^{-1\dagger} \right\} \\ &\quad + U^{-1} \chi e^V U^{-1\dagger} - \sqrt{2} U^{-1} [-U (\partial_5 U^{-1})] e^V U^{-1\dagger} \\ &= U^{-1} \left\{ \sqrt{2}\partial_5 e^V + \chi e^V \right\} U^{-1\dagger} + \sqrt{2} U^{-1} e^V \partial_5 U^{-1\dagger}. \end{aligned} \quad (\text{A.7})$$

We combine Eq.(A.4,A.7) and take trace of it,

$$\text{Tr}[(\text{A.4}) \times (\text{A.7})] \quad (\text{A.8})$$

$$\begin{aligned} &= \text{Tr} \left[(\sqrt{2}\partial_5 e^{-V} + \chi^\dagger e^{-V})(\sqrt{2}\partial_5 e^V + \chi e^V) - 2U^\dagger e^{-V} (\partial_5 U) U^{-1} e^V (\partial_5 U^{-1\dagger}) \right. \\ &\quad \left. - \sqrt{2} U^\dagger (\sqrt{2}\partial_5 e^{-V} + \chi^\dagger e^{-V}) e^V (\partial_5 U^{-1\dagger}) \right. \\ &\quad \left. + \sqrt{2} e^{-V} (\partial_5 U) U^{-1} (\sqrt{2}\partial_5 e^V + \chi e^V) \right] \\ &= \text{Tr} \left[(\sqrt{2}\partial_5 e^{-V} + \chi^\dagger e^{-V})(\sqrt{2}\partial_5 e^V + \chi e^V) - 2^\dagger e^{-V} (\partial_5 U) U^{-1} e^V (\partial_5 U^{-1\dagger}) U \right. \\ &\quad \left. - 2(\partial_5 e^{-V}) e^V (\partial_5 U^{-1\dagger}) U^\dagger - \sqrt{2} \chi^\dagger (\partial_5 U^{-1\dagger}) U^\dagger \right. \\ &\quad \left. - 2(\partial_5 e^V) e^{-V} (\partial_5 U) U^{-1} + \sqrt{2} \chi (\partial_5 U) U^{-1} \right] \end{aligned} \quad (\text{A.9})$$

The second term of Eq.(A.1) transforms as

$$\text{Tr} [(\partial_5 e^{-V})(\partial_5 e^V)] \quad (\text{A.10})$$

$$\begin{aligned} &\rightarrow \text{Tr} \left[\{ (\partial_5 U^\dagger) e^{-V} U + U^\dagger (\partial_5 e^{-V}) U + U^\dagger e^{-V} \partial_5 U \} \right. \\ &\quad \left. \times \{ (\partial_5 U^{-1}) e^V U^{-1\dagger} + U^{-1} (\partial_5 e^V) U^{-1\dagger} + U^{-1} e^V \partial_5 U^{-1\dagger} \} \right] \end{aligned} \quad (\text{A.11})$$

$$\begin{aligned} &= \text{Tr} \left[(\partial_5 e^{-V})(\partial_5 e^V) + 2(\partial_5 e^V) e^{-V} (\partial_5 U) U^{-1} + 2(\partial_5 e^{-V}) e^V (\partial_5 U^{-1\dagger}) U^\dagger \right. \\ &\quad \left. + 2e^{-V} (\partial_5 U) U^{-1} e^V (\partial_5 U^{-1\dagger}) U^\dagger + \partial_5 U^\dagger \partial_5 U^{-1\dagger} + \partial_5 U \partial_5 U^{-1} \right], \end{aligned} \quad (\text{A.12})$$

and the last terms of Eq.(A.1) transform as

$$\text{Tr} \left[\frac{\chi\chi}{2} \right] \rightarrow \frac{1}{2} \text{Tr} \left[U^{-1}(\chi U - \sqrt{2}\partial_5 U)U^{-1}(\chi U - \sqrt{2}\partial_5 U) \right] \quad (\text{A.13})$$

$$\begin{aligned} &= \frac{1}{2} \text{Tr} \left[\chi\chi + 2U^{-1}(\partial_5 U)U^{-1}(\partial_5 U) - 2\sqrt{2}(\partial_5 U)U^{-1}\chi \right] \\ &= \text{Tr} \left[\frac{\chi\chi}{2} - (\partial_5 U^{-1})(\partial_5 U) - \sqrt{2}\chi(\partial_5 U)U^{-1} \right] \end{aligned} \quad (\text{A.14})$$

$$\text{Tr} \left[\frac{\chi^\dagger \chi^\dagger}{2} \right] \rightarrow \text{Tr} \left[\frac{\chi^\dagger \chi^\dagger}{2} - (\partial_5 U^\dagger)(\partial_5 U^{-1\dagger}) - \sqrt{2}\chi^\dagger U^{-1\dagger}(\partial_5 U^\dagger) \right]. \quad (\text{A.15})$$

As a result, we prove the gauge invariance of Eq.(A.1),

$$\begin{aligned} &(\text{A.9}) + (\text{A.12}) + (\text{A.14}) + (\text{A.15}) \\ &= \text{Tr} \left[(\sqrt{2}\partial_5 + \chi^\dagger)e^{-V}(-\sqrt{2}\partial_5 + \chi)e^V + (\partial_5 e^{-V})(\partial_5 e^V) + \frac{\chi^\dagger \chi^\dagger + \chi\chi}{2} \right]. \end{aligned} \quad (\text{A.16})$$

A.2 $SU(2)_R$ invariance

In this section, we prove the $SU(2)_R$ invariance for Eq.(2.27). The terms with auxiliary fields F_χ and D^a in Eq.(2.27) do not seem $SU(2)_R$ invariant. To see the invariance, we must combine them with $|F_\chi^a|^2$ and $(D^a)^2$ from the gauge sector. We obtain following four point interactions for squarks (sleptons) by completing squares:

$$|F_\chi^a|^2 - (\sqrt{2}gF_\chi^a\phi_2 T^a\phi_1 + \text{h.c.}) + \frac{1}{2}(D^a)^2 - gD^a(\phi_1^* T^a\phi_1 - \phi_2 T^a\phi_2^*) \quad (\text{A.17})$$

$$\rightarrow -2g^2(\phi_1^* T^a\phi_2^*)(\phi_2 T^a\phi_1) - \frac{1}{2}g^2(\phi_1^* T^a\phi_1 - \phi_2 T^a\phi_2^*)^2. \quad (\text{A.18})$$

For convenience, we use Φ_i as $(\Phi_1, \Phi_2) = (\phi_1, \phi_2^*)$ and we omit the gauge coupling. Then eq.(A.18) is,

$$-\frac{1}{2}(\Phi_1^* T^a\Phi_1)^2 - \frac{1}{2}(\Phi_2^* T^a\Phi_2)^2 + (\Phi_1^* T^a\Phi_1)(\Phi_2^* T^a\Phi_2) - 2(\Phi_1^* T^a\Phi_2)(\Phi_2^* T^a\Phi_1), \quad (\text{A.19})$$

but the invariance is still not clear.

Now we pick up an explicit $SU(2)_R$ invariant form of the squark four-point interaction.

$$\sum_{m=1,2,3} (\Phi_i^* \sigma_{ij}^m T^a \Phi_j)(\Phi_k^* \sigma_{kl}^m T^a \Phi_l) \quad (\text{A.20})$$

where i, j, k , and l are indices of the $SU(R)$ doublet. For this term, we can use a formula of pauli matrices (Fierz identity):

$$\sum_m \sigma_{ij}^m \sigma_{kl}^m = 2\delta_{il}\delta_{jk} - \delta_{ij}\delta_{kl}, \quad (\text{A.21})$$

and then eq.(A.20) becomes,

$$(\Phi_i^* T^a \Phi_j)(\Phi_k^* T^a \Phi_l)(2\delta_{il}\delta_{jk} - \delta_{ij}\delta_{kl}) \quad (\text{A.22})$$

$$\begin{aligned} &= 2\Phi_1^* T^a(\Phi_1\Phi_1^* + \Phi_2\Phi_2^*)T^a\Phi_1 + 2\Phi_2^* T^a(\Phi_1\Phi_1^* + \Phi_2\Phi_2^*)T^a\Phi_2 \\ &\quad - (\Phi_1^* T^a\Phi_1 + \Phi_2^* T^a\Phi_2)^2 \end{aligned} \quad (\text{A.23})$$

$$\begin{aligned} &= (\Phi_1^* T^a\Phi_1)^2 + (\Phi_2^* T^a\Phi_2)^2 - 2(\Phi_1^* T^a\Phi_1)(\Phi_2^* T^a\Phi_2) \\ &\quad + 4(\Phi_1^* T^a\Phi_2)(\Phi_2^* T^a\Phi_1) \end{aligned} \quad (\text{A.24})$$

As a result, (A.18) = $-\frac{1}{2} \times$ (A.24), and therefore the four-point interactions are $SU(2)_R$ invariant.

B

Kaluza-Klein Expansion

Here is a summary of bulk Lagrangian:

$$\begin{aligned}
\mathcal{L}_5^{\text{YM}} = & -\frac{1}{4}F^{aMN}F_{MN}^a + \frac{1}{2}\left[i\bar{\lambda}_i^a\bar{\sigma}^\mu\mathcal{D}_\mu\lambda_i^a + \lambda_i^a\varepsilon_{ij}\mathcal{D}_5\lambda_j^a + \text{h.c.}\right] \\
& + \frac{1}{2}\mathcal{D}_M\Sigma^a\mathcal{D}^M\Sigma^a + \frac{g}{2}f^{abc}\Sigma^a(i\lambda_i^b\varepsilon_{ij}\lambda_j^c + \text{h.c.}) + \frac{1}{2}(D'^a)^2 + |F_\chi^a|^2 \quad (\text{B.1})
\end{aligned}$$

$$\begin{aligned}
\mathcal{L}_5^{\text{Hyper}} = & |F'_1|^2 + |F'_2|^2 + (\mathcal{D}^M\phi_1)^\dagger\mathcal{D}_M\phi_1 + (\mathcal{D}^M\phi_2^*)^\dagger\mathcal{D}_M\phi_2^* \\
& + i(\psi_2, \bar{\psi})\begin{pmatrix} -i\mathcal{D}_5 & \sigma^\mu\mathcal{D}_\mu \\ \bar{\sigma}^\mu\mathcal{D}_\mu & i\mathcal{D}_5 \end{pmatrix}\begin{pmatrix} \psi_1 \\ \bar{\psi}_2 \end{pmatrix} \\
& -g^2(\Sigma^a T^a\phi_1)^\dagger(\Sigma^a T^a\phi_1) - g^2(\Sigma^a T^a\phi_2^*)^\dagger(\Sigma^a T^a\phi_2^*) \\
& + g\Sigma^a(\psi_2 T^a\psi_1 + \bar{\psi}_1 T^a\bar{\psi}_2) \\
& + \sqrt{2}g(\phi_1^*, \phi_2)T^a\left\{\psi_1\begin{pmatrix} -\lambda_1^a \\ \lambda_2^a \end{pmatrix} + \bar{\psi}_2\begin{pmatrix} \bar{\lambda}_2^a \\ \bar{\lambda}_1^a \end{pmatrix}\right\} + \text{h.c.} \\
& -gD'^a(\phi_1^* T^a\phi_1) + gD'^a(\phi_2 T^a\phi_2^*) \\
& + \phi_2[-\sqrt{2}gF_\chi^a T^a]\phi_1 + \text{h.c.} \quad (\text{B.2})
\end{aligned}$$

$$\begin{aligned}
\mathcal{L}_{5,\text{soft}} = & -\left(\frac{\alpha}{R}\right)^2|\phi_1|^2 - \left(\frac{\alpha}{R}\right)^2|\phi_2^*|^2 \\
& + \frac{\alpha}{R}\left(\phi_1^\dagger\mathcal{D}_5\phi_2^* - (\phi_2^*)^\dagger\mathcal{D}_5\phi_1 - (\mathcal{D}_5\phi_1)^\dagger\phi_2^* + (\mathcal{D}_5\phi_2^*)^\dagger\phi_1\right) \\
& + \frac{1}{2}\frac{\alpha}{R}\lambda_1^a\lambda_1^a + \frac{1}{2}\frac{\alpha}{R}\lambda_2^a\lambda_2^a + \text{h.c.} \quad (\text{B.3})
\end{aligned}$$

B.1 KK Expansion in S^1/\mathbb{Z}_2

In a flat extra dimension without orbifold, the field which has a condition, $\varphi(x, y + 2\pi R) = \varphi(x, y)$, is expanded to discrete Fourier modes, called Kaluza-Klein modes,

$$\varphi(x, y) = \frac{1}{\sqrt{2\pi R}} \sum_{n=-\infty}^{\infty} \varphi_n(x) e^{iny/R}. \quad (\text{B.4})$$

From here we omit 4D position labels such as x for simplicity. Under $\mathcal{P} : y \rightarrow -y$ (orbifold), the field can have two different conditions,

$$\phi_{\text{even}}(y) = +\phi_{\text{even}}(-y), \quad (\text{B.5})$$

$$\phi_{\text{odd}}(y) = -\phi_{\text{odd}}(-y). \quad (\text{B.6})$$

We introduce SUSY breaking by Radion Mediation, which is equivalent to the Scherk-Schwarz mechanism but is simpler in calculation than using the twist. The even and odd fields are expanded as

$$\phi_{\text{even}}(y) = \sum_{n=0}^{\infty} \frac{\eta_n}{\sqrt{\pi R}} \phi_n^{\text{even}} \cos \frac{ny}{R}, \quad (\text{B.7})$$

$$\phi_{\text{odd}}(y) = \sum_{n=1}^{\infty} \frac{1}{\sqrt{\pi R}} \phi_n^{\text{odd}} \sin \frac{ny}{R}, \quad (\text{B.8})$$

where we have a wave function factor,

$$\eta_n \equiv \begin{cases} \frac{1}{\sqrt{2}} & (n = 0) \\ 1 & (n \neq 0) \end{cases}. \quad (\text{B.9})$$

The wave function factor is necessary for the proper normalization of bilinear terms since y integral gives,

$$\int_0^{2\pi R} dy \cos \frac{my}{R} \cos \frac{ny}{R} = \delta_{m,n} \times \begin{cases} 2\pi R & (n = 0) \\ \pi R & (n \neq 0) \end{cases}, \quad (\text{B.10})$$

$$\int_0^{2\pi R} dy \sin \frac{my}{R} \sin \frac{ny}{R} = \delta_{m,n} \pi R. \quad (\text{B.11})$$

B.2 Mass Matrix and Propagator

B.2.1 Squarks and sleptons

This is the easiest example. For the requirement of chiral fermion, one chiral superfield in Hypermultiplet must be odd under $\mathcal{P} : y \rightarrow -y$ while the other chiral superfield is even, and correspondingly one complex scalar, say ϕ_1 , is even and the other one, ϕ_2 , is even. The mass

matrix of them is

$$\begin{aligned} \mathcal{L}_\phi(x) &= \int dy (\phi_1^*(y), \phi_2(y)) \begin{pmatrix} -\partial^2 + \partial_5^2 - \hat{\alpha}^2 & 2\hat{\alpha}\partial_5 \\ -2\hat{\alpha}\partial_5 & -\partial^2 + \partial_5^2 - \hat{\alpha}^2 \end{pmatrix} \begin{pmatrix} \phi_1(y) \\ \phi_2^*(y) \end{pmatrix} \end{aligned} \quad (\text{B.12})$$

$$\begin{aligned} &= \phi_{1,0}^*(-\partial^2 - \hat{\alpha}^2)\phi_{1,0} \\ &+ \sum_{n=1}^{\infty} (\phi_{1,n}^*, \phi_{2,n}) \begin{pmatrix} -\partial^2 - \hat{n}^2 - \hat{\alpha}^2 & 2\hat{\alpha}\hat{n} \\ 2\hat{\alpha}\hat{n} & -\partial^2 - \hat{n}^2 - \hat{\alpha}^2 \end{pmatrix} \begin{pmatrix} \phi_{1,n} \\ \phi_{2,n}^* \end{pmatrix} \end{aligned} \quad (\text{B.13})$$

Here we used

$$\begin{aligned} \int dy 2\hat{\alpha} \phi_2(y) \partial_5 \phi_1(y) &= 2\hat{\alpha} \int dy \sum_{n,m} \left[\frac{\phi_{2,m}}{\sqrt{\pi R}} \sin \frac{my}{R} \right] \left(\frac{n}{R} \right) \left[\frac{\eta_n \phi_{1,n}}{\sqrt{\pi R}} \cos \frac{ny}{R} \right] \\ &= 2\hat{\alpha} \sum_{n,m} \phi_{2,m} \phi_{1,n} (-\delta_{m,n}) \left(\frac{n}{R} \right) \\ &= -2\hat{\alpha}\hat{n} \sum_{n=1}^{\infty} \phi_{2,n} \phi_{1,n} \end{aligned} \quad (\text{B.14})$$

for off-diagonal elements. Mass eigenstates are given by

$$\phi_{\pm,n} \equiv \frac{\phi_{1,n} \mp \phi_{2,n}^*}{\sqrt{2}} \quad (n > 0), \quad (\text{B.15})$$

with mass $(\hat{\alpha} \pm \hat{n})^2$. It is convenient that they are combined with zero mode,

$$\phi_n \equiv \begin{cases} \phi_{+,n} & (n > 0) \\ \phi_{1,0} & (n = 0) \\ \phi_{-,|n|} & (n < 0) \end{cases}, \quad (\text{B.16})$$

Using these mass eigenstates the KK expansion is rewritten by,

$$\begin{aligned} \phi_1(y) &= \frac{1}{\sqrt{2\pi R}} \phi_{1,0} + \sum_{n=1}^{\infty} \frac{\phi_{+,n} + \phi_{-,n}}{\sqrt{2\pi R}} \cos \frac{ny}{R} \\ &= \sum_{n=-\infty}^{\infty} \frac{\phi_n}{\sqrt{2\pi R}} \cos \frac{ny}{R}, \end{aligned} \quad (\text{B.17})$$

$$\begin{aligned} \phi_2^*(y) &= \sum_{n=1}^{\infty} \frac{-\phi_{+,n} + \phi_{-,n}}{\sqrt{2\pi R}} \sin \frac{ny}{R} \\ &= - \sum_{n=-\infty}^{\infty} \frac{\phi_n}{\sqrt{2\pi R}} \sin \frac{ny}{R}. \end{aligned} \quad (\text{B.18})$$

Then the mass matrix is simplified,

$$\mathcal{L}_\phi = \sum_{n=-\infty}^{\infty} \phi_n^* \{ \partial^2 - (\hat{\alpha} + \hat{n})^2 \} \phi_n, \quad (\text{B.19})$$

and the propagator is

$$\langle \phi_n(p) \phi_n^*(p) \rangle \sim \frac{i}{p^2 - (\hat{\alpha} + \hat{n}^2)}. \quad (\text{B.20})$$

Here we denote,

$$\langle \phi_n(p) \phi_n^*(q) \rangle \equiv \int d^4x \int d^4y e^{ipx} e^{-iqy} \langle |\mathbf{T} \phi_n(x) \phi_n^*(y)| \rangle \quad (\text{B.21})$$

$$\begin{aligned} &= \int d^4x \int d^4y e^{ipx} e^{-iqy} \int \frac{d^4k}{(2\pi)^4} \frac{i e^{-ik(x-y)}}{k^2 - (\hat{\alpha} + \hat{n})^2 + i\varepsilon} \\ &= (2\pi)^4 \delta^4(p - q) \left(\frac{i}{p^2 - (\hat{\alpha} + \hat{n})^2 + i\varepsilon} \right). \end{aligned} \quad (\text{B.22})$$

The prefactor of $(2\pi)^4 \delta^4(p - q)$ is common, so we omit this. For the case of real field propagator, the delta function becomes $\delta^4(p + q)$.

B.2.2 Quarks and leptons

To obtain a chiral fermion, one fermion ψ_1 is even under $\mathcal{P} : y \rightarrow -y$, while the other fermion ψ_2 is odd. The kinetic term of quark is

$$\begin{aligned} \mathcal{L}_\psi &= \int dy i (\psi_2(y), \bar{\psi}_1(y)) \begin{pmatrix} i\partial_5 & \sigma^\mu \partial_\mu \\ \bar{\sigma}^\mu \partial_\mu & -i\partial_5 \end{pmatrix} \begin{pmatrix} \psi_1(y) \\ \bar{\psi}_2(y) \end{pmatrix} \\ &= i\bar{\psi}_{1,0} \bar{\sigma}^\mu \partial_\mu \psi_{1,0} + \sum_{n=1}^{\infty} (\psi_{2,n}, \bar{\psi}_{1,n}) \begin{pmatrix} n/R & i\sigma^\mu \partial_\mu \\ i\bar{\sigma}^\mu \partial_\mu & n/R \end{pmatrix} \begin{pmatrix} \psi_{1,n} \\ \bar{\psi}_{2,n} \end{pmatrix} \\ &= \frac{i}{2} \bar{\Psi}_0 \not{\partial} \Psi_0 + \sum_{n=1}^{\infty} \bar{\Psi}_n (i\not{\partial} + \hat{n}) \Psi_n = \sum_{n=0}^{\infty} (\eta_n^2) \bar{\Psi}_n (i\not{\partial} + \hat{n}) \Psi_n \end{aligned} \quad (\text{B.23})$$

where

$$\Psi_0 \equiv \begin{pmatrix} \psi_{1,0} \\ \bar{\psi}_{1,0} \end{pmatrix}, \quad \Psi_n \equiv \begin{pmatrix} \psi_{1,n} \\ \bar{\psi}_{2,n} \end{pmatrix}. \quad (\text{B.24})$$

Since we work on calculations in four components notation, it is convenient to mention charge conjugate of the fermions, that is,

$$\Psi_n^c = C \bar{\Psi}_n^T \equiv \begin{pmatrix} \psi_{2,n} \\ \bar{\psi}_{1,n} \end{pmatrix}, \quad (\text{B.25})$$

where $C = i\gamma_0\gamma_2$. The propagator is given by

$$\langle \Psi_n(p) \bar{\Psi}_n(p) \rangle \sim \langle \Psi_n^c(p) \bar{\Psi}_n^c(p) \rangle \sim \frac{i}{\not{p} + \hat{n} + i\varepsilon}. \quad (\text{B.26})$$

B.2.3 Gauginos

Gaugino λ_1 is even under $\mathcal{P} : y \rightarrow -y$ because $V \supset A_\mu$ must be even for the gauge invariance while λ_2 which comes along with A_5 is odd. Their kinetic term with soft breaking is given by,

$$\begin{aligned} \mathcal{L}_\lambda &= \int dy i (\lambda_2(y), \bar{\lambda}(y)_1) \begin{pmatrix} i\partial_5 & \sigma^\mu \partial_\mu \\ \bar{\sigma}^\mu \partial_\mu & -i\partial_5 \end{pmatrix} \begin{pmatrix} \lambda_1(y) \\ \bar{\lambda}_2(y) \end{pmatrix} \\ &\quad + \frac{1}{2} \hat{\alpha} (\lambda_1(y)\lambda_1(y) + \lambda_2(y)\lambda_2(y) + \text{h.c.}) \\ &= \sum_{n=0}^{\infty} \left\{ (\lambda_{2,n}, \bar{\lambda}_{1,n}) \begin{pmatrix} \hat{n} & i\sigma^\mu \partial_\mu \\ i\bar{\sigma}^\mu \partial_\mu & \hat{n} \end{pmatrix} \begin{pmatrix} \lambda_{1,n} \\ \bar{\lambda}_{2,n} \end{pmatrix} \right. \\ &\quad \left. + \hat{\alpha} (\lambda_{1,n}\lambda_{1,n} + \lambda_{2,n}\lambda_{2,n}) + \text{h.c.} \right\} \end{aligned} \quad (\text{B.27})$$

For mass eigenstates, we use two majorana fermions,

$$\lambda_0 \equiv \begin{pmatrix} \lambda_{1,0} \\ \bar{\lambda}_{1,0} \end{pmatrix}, \quad \lambda_{\pm,n} \equiv \frac{1}{\sqrt{2}} \begin{pmatrix} \lambda_{1,n} \pm \lambda_{2,n} \\ \bar{\lambda}_{1,n} \pm \bar{\lambda}_{2,n} \end{pmatrix} \quad (n > 0), \quad (\text{B.28})$$

where the mass of λ_0 is $\hat{\alpha}$, and the masses of $\lambda_{\pm,n}$ are $(\hat{\alpha} + \hat{n})$. Similar to the squark and slepton, we combine these gauginos of mass eigenstate,

$$\lambda_n \equiv \begin{cases} \lambda_{+,n} & (n > 0) \\ \lambda_0 & (n = 0) \\ \lambda_{-,|n|} & (n < 0) \end{cases}, \quad (\text{B.29})$$

and the KK expansion of gauginos are also given in the mass eigenstates,

$$\begin{aligned} \lambda_1(y) &= \frac{1}{\sqrt{2\pi R}} P_L \lambda_0 + \sum_{n=1}^{\infty} P_L \frac{\lambda_{+,n} + \lambda_{-,n}}{\sqrt{2\pi R}} \cos \frac{ny}{R} \\ &= \sum_{n=-\infty}^{\infty} P_L \frac{\lambda_n}{\sqrt{2\pi R}} \cos \frac{ny}{R}, \end{aligned} \quad (\text{B.30})$$

$$\begin{aligned} \lambda_2(y) &= \sum_{n=1}^{\infty} P_L \frac{\lambda_{+,n} - \lambda_{-,n}}{\sqrt{2\pi R}} \sin \frac{ny}{R} \\ &= \sum_{n=-\infty}^{\infty} P_L \frac{\lambda_n}{\sqrt{2\pi R}} \sin \frac{ny}{R}. \end{aligned} \quad (\text{B.31})$$

The kinetic terms are written by

$$\begin{aligned} \mathcal{L}_\lambda &= \frac{1}{2} \bar{\lambda}_0 (i\not{\partial} + \hat{\alpha}) \lambda_0 \\ &\quad + \sum_{n=1}^{\infty} \frac{1}{2} \bar{\lambda}_{-,n} (i\not{\partial} + (\hat{\alpha} - \hat{n})) \lambda_{-,n} + \sum_{n=1}^{\infty} \frac{1}{2} \bar{\lambda}_{+,n} (i\not{\partial} + (\hat{\alpha} + \hat{n})) \lambda_{+,n} \\ &= \sum_{n=-\infty}^{\infty} \bar{\lambda}_n (i\not{\partial} + (\hat{\alpha} + \hat{n})) \lambda_n, \end{aligned} \quad (\text{B.32})$$

and then the propagator is

$$\langle \lambda_n(p) \bar{\lambda}_n(p) \rangle \sim \frac{i}{\not{p} + (\hat{\alpha} + \hat{n}) + i\varepsilon}. \quad (\text{B.33})$$

B.2.4 Gauge fields

We calculate the propagator of $U(1)$ gauge fields, and the extension to non-abelian cases is straightforward. In the 4D picture, non-zero KK modes of A_μ are massive and their longitudinal degrees of freedom comes from non-zero KK modes of A_5 , and therefore A_5 behaves as Nambu-Goldstone boson. So we take R_ξ gauge,

$$\mathcal{L}_{5,R_\xi} = -\frac{1}{2\xi} (\partial^\mu A_\mu + \xi \partial^5 A_5)^2, \quad (\text{B.34})$$

and the field strength is,

$$\mathcal{L}_{5,\text{gauge}} = -\frac{1}{4} F^{MN} F_{MN} = -\frac{1}{4} F^{\mu\nu} F_{\mu\nu} - \frac{1}{2} F^{\mu 5} F_{\mu 5}. \quad (\text{B.35})$$

Under $y \rightarrow -y$, clearly A_μ is even and A_5 is odd. Then KK expansion of A_μ and A_5 are given by Eq. (B.8) and Eq. (B.7), respectively. The mixing term of them vanishes,

$$\begin{aligned} -\frac{1}{2} F^{\mu 5} F_{\mu 5} + \mathcal{L}_{5,R_\xi} &= -\frac{1}{2} (\partial^\mu A^5 \partial_\mu A_5 + \partial^5 A^\mu \partial_5 A_\mu - 2\partial^\mu A^5 \partial_5 A_\mu) \\ &\quad - \frac{1}{2\xi} \{ (\partial^\mu A_\mu)^2 + \xi^2 (\partial^5 A_5)^2 \} - \partial^\mu A^5 \partial_5 A_\mu \end{aligned} \quad (\text{B.36})$$

$$\begin{aligned} &= \frac{1}{2} \{ \partial^\mu A_5 \partial_\mu A_5 - \xi (\partial_5 A_5)^2 \} \\ &\quad + \frac{1}{2} \left\{ \partial_5 A^\mu \partial_5 A_\mu - \frac{1}{\xi} (\partial^\mu A_\mu)^2 \right\} \end{aligned} \quad (\text{B.37})$$

For A_5 KK modes,

$$\int dy \frac{1}{2} \{ \partial^\mu A_5(y) \partial_\mu A_5(y) - \xi (\partial_5 A_5(y))^2 \} = \sum_{n=1}^{\infty} \frac{1}{2} A_{5n} \left(-\partial^2 - \frac{\xi n^2}{R^2} \right) A_{5n} \quad (\text{B.38})$$

the propagator is,

$$\langle A_{5,n}(p) A_{5,n}(-p) \rangle \sim \frac{i}{p^2 - \xi \frac{n^2}{R^2} + i\varepsilon} \quad (\text{B.39})$$

For A_μ KK modes,

$$\begin{aligned} &\int dy -\frac{1}{4} F^{\mu\nu} F_{\mu\nu} + \frac{1}{2} \partial_5 A^\mu(y) \partial_5 A_\mu(y) - \frac{1}{2\xi} (\partial^\mu A_\mu(y))^2 \\ &= \int dy \frac{1}{2} A_\mu(y) \{ g^{\mu\nu} (\partial^2 - \partial_5^2) - \partial^\mu \partial^\nu (1 - \xi^{-1}) \} A_\nu(y) \\ &= \sum_{n=0}^{\infty} \frac{1}{2} A_{(n)\mu} \left\{ g^{\mu\nu} \left(\partial^2 + \frac{n^2}{R^2} \right) - \partial^\mu \partial^\nu (1 - \xi^{-1}) \right\} A_{(n)\nu} \end{aligned} \quad (\text{B.40})$$

the propagator is,

$$\langle A_{(n)\mu}(p) A_{(n)\nu}(-p) \rangle \sim \frac{-i}{p^2 - \frac{n^2}{R^2} + i\varepsilon} \left(g_{\mu\nu} - (1 - \xi) \frac{p_\mu p_\nu}{p^2 - \xi \frac{n^2}{R^2}} \right) \quad (\text{B.41})$$

B.2.5 Adjoint real scalars

The mass and propagator of adjoint real scalar Σ is simple,

$$\mathcal{L}_\Sigma = \int_0^{2\pi R} dy \frac{1}{2} \Sigma^a(y) (-\partial^2 + \partial_5^2) \Sigma^a(y) \quad (\text{B.42})$$

$$= \sum_{n=1}^{\infty} \frac{1}{2} \Sigma_n^a (-\partial^2 + \partial_5^2) \Sigma_n^a \quad (\text{B.43})$$

and the propagator is

$$\langle \Sigma_n^a(p) \Sigma_n^a(-p) \rangle \sim \frac{i}{p^2 - \frac{n^2}{R^2} + i\varepsilon}. \quad (\text{B.44})$$

B.3 Formulae

B.3.1 Formulae for KK Expansion

In order to obtain interactions of KK modes, there appear many integrals of sin and cos. The interactions are either four-point or three-point, the integrals are summarized in the following formulae. For integers, k, l, m, n , four point interactions have integrals of

$$\begin{aligned} M_1^{klmn} &\equiv \frac{2}{\pi} \int_0^{2\pi} dx \cos(kx) \cos(lx) \cos(mx) \cos(nx) \\ &= \delta_{k+l+m+n,0} + \delta_{k+l-m-n,0} + \delta_{k+l-m+n,0} + \delta_{k+l+m-n,0} \\ &\quad + \delta_{k-l+m+n,0} + \delta_{k-l-m-n,0} + \delta_{k-l-m+n,0} + \delta_{k-l+m-n,0}, \end{aligned} \quad (\text{B.45})$$

$$\begin{aligned} M_2^{kl,mn} &\equiv \frac{2}{\pi} \int_0^{2\pi} dx \cos(kx) \cos(lx) \sin(mx) \sin(nx) \\ &= -\delta_{k+l+m+n,0} - \delta_{k+l-m-n,0} + \delta_{k+l-m+n,0} + \delta_{k+l+m-n,0} \\ &\quad - \delta_{k-l+m+n,0} - \delta_{k-l-m-n,0} + \delta_{k-l-m+n,0} + \delta_{k-l+m-n,0}, \end{aligned} \quad (\text{B.46})$$

$$\begin{aligned} M_3^{klmn} &\equiv \frac{2}{\pi} \int_0^{2\pi} dx \sin(kx) \sin(lx) \sin(mx) \sin(nx) \\ &= \delta_{k+l+m+n,0} + \delta_{k+l-m-n,0} - \delta_{k+l-m+n,0} - \delta_{k+l+m-n,0} \\ &\quad - \delta_{k-l+m+n,0} - \delta_{k-l-m-n,0} + \delta_{k-l-m+n,0} + \delta_{k-l+m-n,0}. \end{aligned} \quad (\text{B.47})$$

Relative signs are easily understood by changing a sign of argument in sin functions, for instance, $M_2^{kl,(-m)n} = -M_2^{kl,mn}$. This results in that the integral of odd number of sin

functions vanishes. The useful combinations are

$$M_4^{kl,mn} \equiv \frac{1}{2}(M_1^{klmn} + M_2^{kl,mn}) \quad (\text{B.48})$$

$$= \delta_{k+l+m-n,0} + \delta_{k+l-m+n,0} + \delta_{k-l+m-n,0} + \delta_{k-l-m+n,0}$$

$$M_5^{kl,mn} \equiv \frac{1}{2}(M_1^{klmn} - M_2^{kl,mn}) \quad (\text{B.49})$$

$$= \delta_{k+l+m+n,0} + \delta_{k+l-m-n,0} + \delta_{k-l+m+n,0} + \delta_{k-l-m-n,0}$$

$$M_6^{kl,mn} \equiv \frac{1}{2}(M_2^{kl,mn} + M_3^{kl,mn}) \quad (\text{B.50})$$

$$= -\delta_{k-l+m+n,0} - \delta_{k-l-m-n,0} + \delta_{k-l+m-n,0} + \delta_{k-l-m+n,0}$$

$$M_7^{kl,mn} \equiv \frac{1}{2}(M_2^{kl,mn} - M_3^{kl,mn}) \quad (\text{B.51})$$

$$= -\delta_{k+l+m+n,0} - \delta_{k+l-m-n,0} + \delta_{k+l+m-n,0} + \delta_{k+l-m+n,0}$$

Formulae for three-point interactions are

$$N_1^{kmn} \equiv \frac{2}{\pi} \int_0^{2\pi} dx \cos(kx) \cos(mx) \cos(nx) \quad (\text{B.52})$$

$$= \delta_{k+m+n,0} + \delta_{k-m-n,0} + \delta_{k-m+n,0} + \delta_{k+m-n,0}$$

$$N_2^{k,mn} \equiv \frac{2}{\pi} \int_0^{2\pi} dx \cos(kx) \sin(mx) \sin(nx) \quad (\text{B.53})$$

$$= -\delta_{k+m+n,0} - \delta_{k-m-n,0} + \delta_{k-m+n,0} + \delta_{k+m-n,0}$$

$$N_3^{k,mn} \equiv \frac{1}{2}(N_1^{kmn} + N_2^{k,mn}) = \delta_{k+m-n,0} + \delta_{k-m+n,0} \quad (\text{B.54})$$

$$N_4^{k,mn} \equiv \frac{1}{2}(N_1^{kmn} - N_2^{k,mn}) = \delta_{k+m+n,0} + \delta_{k-m-n,0} \quad (\text{B.55})$$

B.4 Interactions

Using the above formulae, we can derive some Feynman rules. Note that some interactions with 5D derivative must be combined with soft terms since they are essentially from the same term in the 5D. Here is an example, squark-squark- $A_{\mu(5)}$ Interaction.

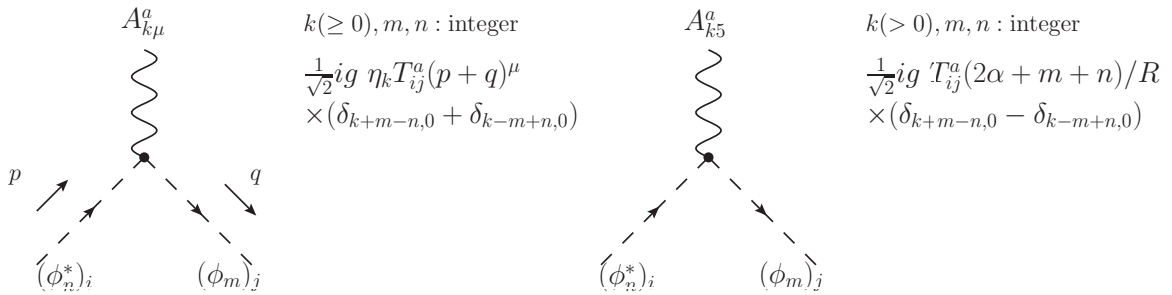
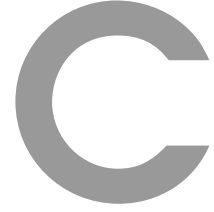


Figure B.1: Squark-Squark- A_μ interaction and Squark-Squark- A_5 interaction.



Formulae for Summation and Integral

C.1 Infinite Sum to Analytic Function

For a function that has no singularities on the real z axis, the useful relation is

$$\sum_{n=-\infty}^{\infty} f(k, n + \alpha) = \sum_{n=-\infty}^{\infty} \oint_{C_n^\alpha} dz f(k, z) \frac{\coth[i\pi(z - \alpha)]}{2}. \quad (\text{C.1})$$

Where the contour C_n^α is a path which rounds about $z = n + \alpha$ with a small radius. When $z \rightarrow \alpha$,

$$\frac{\coth[i\pi(z - \alpha)]}{2} = \frac{1}{2i\pi(z - \alpha)} + \mathcal{O}(z - \alpha), \quad (\text{C.2})$$

and the function above is periodic under a transformation of $z \rightarrow z + n\pi$, so each $\oint_{C_n^\alpha} dz$ generates discrete point of $f(k, z)$. We change the path as in C.1,

$$\begin{aligned} & \sum_{n=-\infty}^{\infty} \oint_{C_n^\alpha} dz f(k, z) \frac{\coth[i\pi(z - \alpha)]}{2} \\ &= \left(\int_{\infty+i\varepsilon}^{-\infty+i\varepsilon} dz + \int_{-\infty-i\varepsilon}^{\infty-i\varepsilon} dz \right) f(k, z) \frac{\coth[i\pi(z - \alpha)]}{2} \end{aligned} \quad (\text{C.3})$$

$$\begin{aligned} &= \int_{-\infty-i\varepsilon}^{\infty-i\varepsilon} dz \left\{ f(k, z) \frac{\coth[i\pi(z - \alpha)]}{2} - f(k, -z) \frac{\coth[i\pi(-z - \alpha)]}{2} \right\} \\ &= \int_{-\infty}^{\infty} dz \left\{ \frac{f(k, z) + f(k, -z)}{2} \right\} \\ &+ \int_{-\infty-i\varepsilon}^{\infty-i\varepsilon} dz \left\{ \frac{f(k, z)}{e^{2i\pi(z-\alpha)} - 1} + \frac{f(k, -z)}{e^{2i\pi(z+\alpha)} - 1} \right\}. \end{aligned} \quad (\text{C.4})$$

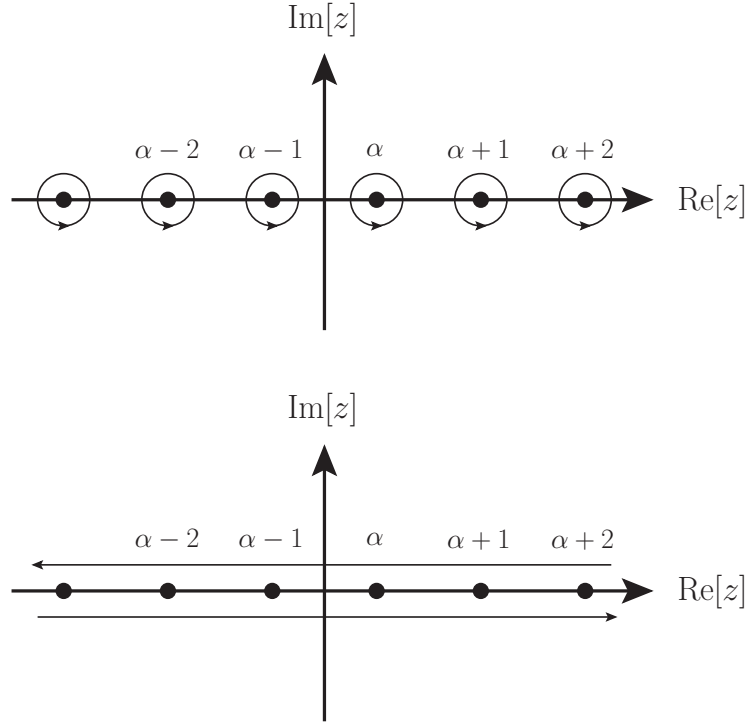


Figure C.1: Integral path of C_n^α . They are combined as shown in the lower plot.

Here, we used

$$\coth(x) = 1 + \frac{2}{e^{2x} - 1} = - \left(1 + \frac{2}{e^{-2x} - 1} \right) \quad (\text{C.5})$$

We are interested in $f(k, z) = 1/(k^2 + z^2)$, $z/(k^2 + z^2)$, and hence, for such functions that damps for $z \rightarrow \pm\infty - i\varepsilon$ and can be suppressed by $e^{2\pi|z|}$ for $z \rightarrow -i\infty$, the second expression of Eq.(C.4) can enclose the path, referred as to C_∇ , in the negative imaginary z plane,

$$\begin{aligned} \sum_{n=-\infty}^{\infty} f(k, n + \alpha) &= \int_{-\infty}^{\infty} dz \left\{ \frac{f(k, z) + f(k, -z)}{2} \right\} \\ &+ \oint_{C_\nabla} dz \left\{ \frac{f(k, z)}{e^{2i\pi(z-\alpha)} - 1} + \frac{f(k, -z)}{e^{2i\pi(z+\alpha)} - 1} \right\}. \end{aligned} \quad (\text{C.6})$$

If $f(k, z)$ has poles inside the closed path C_∇ , the second term on the right-hand side becomes a function of k , otherwise it vanishes. In the following section, we will see the cases of,

$$f(k, z) = \frac{1}{k^2 + z^2}, \quad \frac{z}{k^2 + z^2}. \quad (\text{C.7})$$

C.1.1 Formulae

Using Eq. (C.6) formulae for infinite sum:

$$\begin{aligned} \bullet F_1^\alpha(k) &\equiv \sum_{n=-\infty}^{\infty} \frac{1}{k^2 + (n + \alpha)^2} \\ &= \int_{-\infty}^{\infty} \frac{dz}{k^2 + z^2} + \frac{\pi}{k} \left\{ \frac{1}{e^{2\pi(k-i\alpha)} - 1} + \frac{1}{e^{2\pi(k+i\alpha)} - 1} \right\} \end{aligned} \quad (\text{C.8})$$

$$= \frac{\pi}{k} + \frac{\pi}{k} \left\{ \frac{1}{e^{2\pi(k-i\alpha)} - 1} + \frac{1}{e^{2\pi(k+i\alpha)} - 1} \right\} \quad (\text{if } k \neq 0) \quad (\text{C.9})$$

$$\begin{aligned} \bullet F_2^\alpha(k) &\equiv \sum_{n=-\infty}^{\infty} \frac{(n + \alpha)}{k^2 + (n + \alpha)^2} \\ &= (-i\pi) \left\{ \frac{1}{e^{2\pi(k-i\alpha)} - 1} - \frac{1}{e^{2\pi(k+i\alpha)} - 1} \right\} \end{aligned} \quad (\text{C.10})$$

Formulae for momentum integral:

$$\bullet G_1^n(\pm\alpha) \equiv \int_0^\infty dx \frac{x^n}{e^{x \pm 2\pi i \alpha} - 1} = n! \text{Li}_{n+1}[e^{\mp 2\pi i \alpha}] \quad (\text{C.11})$$

$$\bullet G_2^n(\pm\alpha) \equiv \int_0^\infty dx \frac{x^n}{(e^{x \pm 2\pi i \alpha} - 1)^2} = n! (\text{Li}_n[e^{\mp 2\pi i \alpha}] - \text{Li}_{n+1}[e^{\mp 2\pi i \alpha}]) \quad (\text{C.12})$$

$$\begin{aligned} \bullet G_3^n(\pm\alpha) &\equiv \int_0^\infty dx \frac{x^n}{(e^{x+2\pi i \alpha} - 1)(e^{x-2\pi i \alpha} - 1)} \\ &= \frac{i}{2 \sin(2\pi \alpha)} n! (\text{Li}_{n+1}[e^{\mp 2\pi i \alpha}] - \text{Li}_{n+1}[e^{\pm 2\pi i \alpha}]) \end{aligned} \quad (\text{C.13})$$

$$\rightarrow n! [\zeta(n) - \zeta(n+1)] \quad (\text{if } \alpha \rightarrow 0) \quad (\text{C.14})$$

$$\bullet G_1^n(\pm\alpha) + G_2^n(\pm\alpha) = n! \text{Li}_n[e^{\mp 2\pi i \alpha}] \quad (\text{C.15})$$

C.1.2 Loop integral of infinite sum

We combine formulae for infinite sum (F) and those for momentum integral (G) for radiative corrections of KK tower.

$$\begin{aligned} \bullet &\int_0^\infty \frac{dk}{8\pi^2} k^n (F_1^\alpha(k)) \\ &= \frac{1}{(2\pi)^{n+1}} \int_0^\infty \frac{dx}{8\pi^2} x^n (F_1^\alpha\left(\frac{x}{2\pi}\right)) \end{aligned} \quad (\text{C.16})$$

$$= \frac{2\pi^2}{(2\pi)^{n+1} 8\pi^2} \left[\left(\int_0^\infty dx x^{n-1} \right) + G_1^{n-1}(+\alpha) + G_1^{n-1}(-\alpha) \right] \quad (\text{C.17})$$

$$= \frac{1}{4(2\pi)^{n+1}} \left[\left(\int_0^\infty dx x^{n-1} \right) + (n-1)! (\text{Li}_n[e^{2\pi i \alpha}] + \text{Li}_n[e^{-2\pi i \alpha}]) \right] \quad (\text{C.18})$$

- $$\int_0^\infty \frac{dk}{8\pi^2} k^n \left(F_1^\alpha(k) \right)^2$$

$$= \frac{1}{(2\pi)^{n+1}} \int_0^\infty \frac{dx}{8\pi^2} x^n \left(F_1^\alpha \left(\frac{x}{2\pi} \right) \right)^2 \quad (\text{C.19})$$

$$= \frac{(2\pi)^2 \pi^2}{(2\pi)^{n+1} 8\pi^2} \left[\left(\int_0^\infty dx x^{n-2} \right) + 2 \left(G_1^{n-2}(\alpha) + G_1^{n-2}(-\alpha) \right) \right. \\ \left. + \left(G_2^{n-2}(\alpha) + G_2^{n-2}(-\alpha) + 2G_3^{n-2}(\alpha) \right) \right] \quad (\text{C.20})$$

$$= \frac{1}{8(2\pi)^{n-1}} \left[\left(\int_0^\infty dx x^{n-2} \right) + 2(n-2)! \left(\text{Li}_{n-1}[e^{2\pi i \alpha}] + \text{Li}_{n-1}[e^{-2\pi i \alpha}] \right) \right. \\ \left. + (n-2)! \left(\text{Li}_{n-2}[e^{2\pi i \alpha}] - \text{Li}_{n-1}[e^{2\pi i \alpha}] + \text{Li}_{n-2}[e^{-2\pi i \alpha}] - \text{Li}_{n-1}[e^{-2\pi i \alpha}] \right) \right. \\ \left. + 2(n-2)! \frac{i}{2 \sin(2\pi \alpha)} \left(e^{2\pi i \alpha} \text{Li}_{n-1}[e^{-2\pi i \alpha}] - e^{-2\pi i \alpha} \text{Li}_{n-1}[e^{2\pi i \alpha}] \right) \right] \\ = \frac{1}{8(2\pi)^{n-1}} \left[\left(\int_0^\infty dx x^{n-2} \right) \right. \\ \left. + (n-2)! \left(\text{Li}_{n-2}[e^{2\pi i \alpha}] + \text{Li}_{n-1}[e^{2\pi i \alpha}] + \text{Li}_{n-2}[e^{-2\pi i \alpha}] + \text{Li}_{n-1}[e^{-2\pi i \alpha}] \right) \right. \\ \left. + 2(n-2)! \frac{i}{2 \sin(2\pi \alpha)} \left(e^{2\pi i \alpha} \text{Li}_{n-1}[e^{-2\pi i \alpha}] - e^{-2\pi i \alpha} \text{Li}_{n-1}[e^{2\pi i \alpha}] \right) \right] \quad (\text{C.21})$$

- $$\int_0^\infty \frac{dk}{8\pi^2} k^n \left(F_2^\alpha(k) \right)^2$$

$$= \frac{1}{(2\pi)^{n+1}} \int_0^\infty \frac{dx}{8\pi^2} x^n \left(F_2^\alpha \left(\frac{x}{2\pi} \right) \right)^2 \quad (\text{C.22})$$

$$= \frac{-\pi^2}{(2\pi)^{n+1} 8\pi^2} \left[G_2^n(\alpha) + G_2^n(-\alpha) - 2G_3^n(\alpha) \right] \quad (\text{C.23})$$

$$= \frac{-1}{8(2\pi)^{n+1}} \left[n! \left(\text{Li}_n[e^{2\pi i \alpha}] - \text{Li}_{n+1}[e^{2\pi i \alpha}] + \text{Li}_n[e^{-2\pi i \alpha}] - \text{Li}_{n+1}[e^{-2\pi i \alpha}] \right) \right. \\ \left. - 2n! \frac{i}{2 \sin(2\pi \alpha)} \left(e^{2\pi i \alpha} \text{Li}_{n-1}[e^{-2\pi i \alpha}] - e^{-2\pi i \alpha} \text{Li}_{n-1}[e^{2\pi i \alpha}] \right) \right] \quad (\text{C.24})$$

Useful combinations:

- $$\int_0^\infty \frac{dk}{8\pi^2} k^n \left[F_1^\alpha(k) - F_1^0(k) \right]$$

$$= \frac{(n-1)!}{4(2\pi)^{n+1}} \left(\text{Li}_n[e^{2\pi i \alpha}] + \text{Li}_n[e^{-2\pi i \alpha}] - 2\zeta(n) \right) \quad (\text{C.25})$$

$$\begin{aligned}
& \bullet \int_0^\infty \frac{dk}{8\pi^2} k^n \left[k^2 \left(F_1^\alpha(k) \right)^2 - k^2 \left(F_1^0(k) \right)^2 - \left(F_2^\alpha(k) \right)^2 \right] \\
&= \frac{1}{8(2\pi)^{n+1}} \left[\left(\int_0^\infty dx x^n \right) \right. \\
&\quad + \left(2G_1^n(\alpha) + 2G_1^n(-\alpha) + G_2^n(\alpha) + G_2^n(-\alpha) + 2G_3^n(\alpha) \right) \\
&\quad - \left(\int_0^\infty dx x^n \right) - \left(4G_1^n(0) + 4G_2^n(0) \right) \\
&\quad \left. + \left(G_2^n(\alpha) + G_2^n(-\alpha) - 2G_3^n(\alpha) \right) \right] \\
&= \frac{1}{4(2\pi)^{n+1}} \left[G_1^n(\alpha) + G_1^n(-\alpha) + G_2^n(\alpha) + G_2^n(-\alpha) - 2G_1^n(0) - 2G_2^n(0) \right] \\
&= \frac{n!}{4(2\pi)^{n+1}} \left[\text{Li}_n[e^{2\pi i\alpha}] + \text{Li}_n[e^{-2\pi i\alpha}] - 2\zeta(3) \right] \tag{C.26}
\end{aligned}$$

C.2 Example: $m_{H_u}^2$ from all KK particles with top-Yukawa coupling

We use Eq. (C.26) for threshold correction to $m_{H_u}^2$. All the infinite sums are factorized in the following way,

$$\begin{aligned}
-im_{H_u}^2|_{\text{Yukawa}} &= \frac{iN_c y_t^2}{R^2} \int_0^\infty \frac{dk}{8\pi^2} k^3 \left[2k^2 \left(\sum_{n=-\infty}^\infty \frac{1}{k^2 + n^2} \right) \left(\sum_{m=-\infty}^\infty \frac{1}{k^2 + m^2} \right) \right. \\
&\quad - 2k^2 \left(\sum_{n=-\infty}^\infty \frac{1}{k^2 + (n+\alpha)^2} \right) \left(\sum_{m=-\infty}^\infty \frac{1}{k^2 + (m+\alpha)^2} \right) \\
&\quad \left. + 2 \left(\sum_{n=-\infty}^\infty \frac{n+\alpha}{k^2 + (n+\alpha)^2} \right) \left(\sum_{m=-\infty}^\infty \frac{m+\alpha}{k^2 + (m+\alpha)^2} \right) \right] \tag{C.27}
\end{aligned}$$

$$\begin{aligned}
&= \frac{iN_c y_t^2}{R^2} (-2) \int_0^\infty \frac{dk}{8\pi^2} k^3 \left[k^2 \left(F_1^\alpha(k) \right)^2 - k^2 \left(F_1^0(k) \right)^2 - \left(F_2^\alpha(k) \right)^2 \right] \\
&= \frac{iN_c y_t^2}{R^2} \frac{-2 \cdot 3!}{4(2\pi)^4} \left[\text{Li}_3[e^{2\pi i\alpha}] + \text{Li}_3[e^{-2\pi i\alpha}] - 2\zeta(3) \right] . \tag{C.28}
\end{aligned}$$

If we expand Polylog functions with respect to α ,

$$\text{Li}_3[e^{2\pi i\alpha}] = \zeta(3) + \frac{i\pi^3}{3}\alpha + \pi^2 \left(-3 + 2\ln(2\pi\alpha) - \frac{i\pi}{2} \right) \alpha^2 + \mathcal{O}(\alpha^3) \tag{C.29}$$

$$\text{Li}_3[e^{2\pi i\alpha}] + \text{Li}_3[e^{-2\pi i\alpha}] = 2\zeta(3) + 2\pi^2 (-3 + 2\ln(2\pi\alpha)) \alpha^2 + \mathcal{O}(\alpha^3), \tag{C.30}$$

Hence,

$$-im_{H_u}^2|_{\text{Yukawa}} = \frac{-iN_c y_t^2}{16\pi^2} \left(\frac{\alpha^2}{R^2} \right) \left(12\ln(2\pi\alpha) - 18 \right) + \mathcal{O}(\alpha^3) . \tag{C.31}$$



Search for New Physics with Compressed Spectrum by M_{T2}

D.1 Introduction

When the MSSM has a compressed (nearly degenerate) spectrum like the Compact Supersymmetry, their limits from the LHC are much weaker than those on the CMSSM which has a widely spread spectrum. Ameliorating limits is generally true for various new physics models with a compressed spectrum and a invisible stable particle like dark matter particle. We refer these (BSM) models to as compressed models. In this chapter we point out a kinematic variable, M_{T2} , is effective for a compressed model search. The effectiveness of M_{T2} [93, 94] to search for conventional MSSM was discussed in [95, 96], and M_{T2} was already applied in several searches for supersymmetry [97, 98].

New physics models, as represented by the MSSM, are basically searched based on the missing energy, \cancel{E}_T , because created colored particles like gluino and squark decay into invisible particles with large momentum thanks to expected large mass gap between them. Large \cancel{E}_T is a distinct signature from the SM processes. The difficulty of the search for compressed models is that \cancel{E}_T is significantly smaller in each event due to mass degeneracy even if their mass scale of the process is very high. In the SM processes missing energy is actually generated for the neutrino emission, and in particular $t\bar{t}$ pair production, with a subsequent decay of $t \rightarrow bW \rightarrow bl\nu$, leads to \cancel{E}_T . This SM process is quite similar to the new physics process. The current searches by multijet, *e.g.* in Ref. [54], are optimized to search for the CMSSM, and therefore the event elections imposed here is too strong to keep enough signal events of compressed models. On the other hand, if selection criterion are weakened, there could be a lot of contamination of background.

Note that initial state radiation (ISR) is important in searches for compressed models. While energy emitted from the decay relies on the mass gap, energy scale of QCD radiation,

particularly ISR, roughly increases with mass scale of colored particle, and therefore the QCD radiation scale of new physics is larger than that of the SM. In the search for compressed model, this is an important feature.

Throughout this appendix we adopt the MUED as a benchmark model [99] (see [100] for review). In the MUED all the SM fields propagate in a compactified flat extra dimension, S^1/\mathbb{Z}_2 , and the model provides a good candidate of dark matter particle [101, 102]. The collider phenomenology is basically same as the MSSM: first excited KK states of SM field behave as superpartners of the SUSY, and KK parity instead of R -parity stabilize the lightest particle, called LKP. The spectrum is highly compressed at masses of $1/R$ where R is radius of the extra dimension. Experimental sensitivity to the MUED needs to be improved since the favored scale is pretty high as $1/R \sim 1.5$ TeV [102] while current LHC limit is still $1/R \lesssim 800$ GeV [54].

After briefly describing the MUED, we review the definition of M_{T2} and next effectiveness of this variable as a event selection as discussed in [95, 96]. Then we discuss M_{T2} cut is useful for compressed model search. Event selections with M_{T2} cut is applied for a typical compressed model, the MUED [27].

D.2 MUED

In the case of the 5D UED, there is a compactified flat extra dimension in which all the SM fields universally propagate in addition to the 4D Minkowski space-time. Fields are expanded in the KK modes (KK particles) in the 4D effective theory, and each zero mode corresponds to the SM particle. The mass of n th mode is given by $m_n^2 = m_{SM}^2 + (n/R)^2$. R denotes the radius of the extra dimension, and m_{SM} denotes a SM particle mass. The fifth dimensional momentum is the mass in the 4D effective theory, and this is much greater than m_{SM} , because $1/R \sim \mathcal{O}(\text{TeV})$. Therefore, we can neglect m_{SM} : $m_n \simeq n/R$, which means the mass spectrum of each KK level is highly degenerate.

Since the simple compactified extra dimension S^1 gives vector-like fermions, an orbifold compactified extra dimension S^1/\mathbb{Z}_2 with an identification of $y \leftrightarrow -y$ is considered in order to obtain chiral fermions in the zero mode. The orbifold compactification results in another significant characteristic, the KK parity. KK number is conserved by virtue of the fifth dimensional momentum conservation on S^1 compactification, but this is broken down to the KK parity by the orbifold compactification. The KK parity reflects "evenness" and "oddness" of the KK number. All the SM particles have the even KK parity. The lightest particle with the odd KK parity, called the lightest Kaluza-Klein particle (LKP), is stable since it cannot decay into lighter SM particles due to its oddness. The stable LKP, typically the first KK photon $\gamma^{(1)}$, can be a weakly interacting massive particle (WIMP) and therefore a good Dark Matter candidate.

To discuss collider phenomenology, we have to determine the mass spectrum. In this paper, we discuss the Minimal Universal Extra Dimension model (MUED). The MUED is a minimal extension of the 4D SM Lagrangian to the 5D UED. At the cutoff scale Λ it contains only SM fields and no other terms, especially no localized terms at two fixed points $y = 0, \pi R$ led by orbifold compactification. The model parameters of MUED are only three: 5D radius R , cutoff scale of MUED Λ , and the SM Higgs mass m_h .

D.2.1 Mass spectrum

Radiative corrections to masses of the KK modes at the one-loop level were studied in Refs. [119, 120]. This correction enlarges mass splitting for each KK level away from the highly degenerate mass spectrum. The corrected masses are:

$$m_{X^{(n)}}^2 = \frac{n^2}{R^2} + m_{X^{(0)}}^2 + \delta m_{X^{(n)}}^2 \quad (\text{D.1})$$

where $m_{X^{(0)}}$ is a SM particle (zero mode) mass. The neutral gauge bosons of $U(1)_Y$ and $SU(2)_L$ are mixed up in the SM, but mass eigenstates of the KK neutral gauge bosons, $\gamma^{(n)}$ and $Z^{(n)}$, are nearly $U(1)_Y$ and $SU(2)_L$ gauge eigenstates, $B^{(n)}$ and $W^{3(n)}$, respectively because the diagonal components of mass matrix dominates as

$$\begin{pmatrix} B^{(n)} & W^{3(n)} \end{pmatrix} \begin{pmatrix} \frac{n^2}{R^2} + \delta m_{B^{(n)}}^2 + \frac{1}{4}g_1^2 v^2 & \frac{1}{4}g_1 g_2 v^2 \\ \frac{1}{4}g_1 g_2 v^2 & \frac{n^2}{R^2} + \delta m_{W^{3(n)}}^2 + \frac{1}{4}g_2^2 v^2 \end{pmatrix} \begin{pmatrix} B^{(n)} \\ W^{3(n)} \end{pmatrix} \quad (\text{D.2})$$

where g_1 is the gauge coupling of $U(1)_Y$, g_2 is that of $SU(2)_L$, and $v = 246$ GeV is the vacuum expectation value of the Higgs field. The radiative corrections to gauge boson masses are given by

$$\begin{aligned} \delta m_{B^{(n)}}^2 &= -\frac{39}{2} \frac{g_1^2 \zeta(3)}{16\pi^2} \frac{1}{R^2} + \frac{n^2}{R^2} \left(-\frac{1}{6} \frac{g_1^2}{16\pi^2} \right) \log(\Lambda R)^2 \\ \delta m_{W^{(n)}}^2 &= -\frac{5}{2} \frac{g_2^2 \zeta(3)}{16\pi^2} \frac{1}{R^2} + \frac{n^2}{R^2} \left(\frac{15}{2} \frac{g_2^2}{16\pi^2} \right) \log(\Lambda R)^2 \\ \delta m_{g^{(n)}}^2 &= -\frac{3}{2} \frac{g_s^3 \zeta(3)}{16\pi^2} \frac{1}{R^2} + \frac{n^2}{R^2} \left(\frac{23}{2} \frac{g_s^2}{16\pi^2} \right) \log(\Lambda R)^2 \end{aligned} \quad (\text{D.3})$$

where $\zeta(3) = 1.20205\dots$ and g_s is the gauge coupling of $SU(3)_C$. The second terms in the corrections are dominant, so $m_{W^{(n)}}$ is lifted, and $m_{B^{(n)}}$ is slightly lowered.

The mixings of the KK quarks (KK leptons) are also negligible, and they become $U(1)_Y$ and $SU(2)_L$ gauge eigenstates. Neglecting m_{SM} , radiative corrections to the KK quarks and KK leptons are given by

$$\begin{aligned} \delta m_{Q^{(n)}} &= \frac{n}{R} \left(3 \frac{g_s^2}{16\pi^2} + \frac{27}{16} \frac{g_2^2}{16\pi^2} + \frac{1}{16} \frac{g_1^2}{16\pi^2} \right) \log(\Lambda R)^2 \\ \delta m_{u^{(n)}} &= \frac{n}{R} \left(3 \frac{g_s^2}{16\pi^2} + \frac{g_1^2}{16\pi^2} \right) \log(\Lambda R)^2 \\ \delta m_{d^{(n)}} &= \frac{n}{R} \left(3 \frac{g_s^2}{16\pi^2} + \frac{1}{4} \frac{g_1^2}{16\pi^2} \right) \log(\Lambda R)^2 \\ \delta m_{L^{(n)}} &= \frac{n}{R} \left(\frac{27}{16} \frac{g_2^2}{16\pi^2} + \frac{9}{16} \frac{g_1^2}{16\pi^2} \right) \log(\Lambda R)^2 \\ \delta m_{e^{(n)}} &= \frac{n}{R} \left(\frac{9}{4} \frac{g_1^2}{16\pi^2} \right) \log(\Lambda R)^2 \end{aligned} \quad (\text{D.4})$$

where $Q^{(n)}$ and $L^{(n)}$ denote the $SU(2)_L$ doublet, and $u^{(n)}$, $d^{(n)}$, and $e^{(n)}$ denote the $SU(2)_L$ singlet. For the KK top quark we should consider the correction from its Yukawa coupling, but the production cross section is small. We do not consider the processes of KK top quark.

Most KK particles receive positive mass corrections. The heaviest particle in each level is $g^{(n)}$ for the largest correction, and the lightest particle in each level is typically $\gamma^{(n)}$. Then the LKP is $\gamma^{(1)}$ with the mass $m_{\gamma^{(1)}} \cong 1/R$. In the analysis, we fix the Higgs mass at $m_h = 120$ GeV for simplicity.

The corrections are basically proportional to $\log \Lambda R$, so the degeneracy is crucial for the smaller ΛR . The cutoff scale of the UED was discussed in [123], and the appropriate cutoff scale should be several dozen $1/R$ for a given R . As the energy scale grows, more KK particles appear, and the logarithmic running of the gauge coupling changes into power law running above the MUED scale $1/R$. The $U(1)_Y$ gauge coupling blows up (Landau pole) at the energy scale $\sim 40/R$, so we should set the cutoff scale below the Landau pole. The very small ΛR is also not appropriate because we should consider the higher dimensional operators, and the MUED framework is not a good effective theory any more. In our analysis, we considered $10 \leq \Lambda R \leq 40$.

D.2.2 Production and decay at the LHC

At the LHC, the first KK particles of the odd KK parity are pair-produced, and they eventually decay into the LKP. The dominant production processes are KK gluon+KK quark ($g^{(1)} + Q^{(1)}/q^{(1)}$) and KK quark+KK quark ($Q^{(1)}/q^{(1)} + Q^{(1)}/q^{(1)}$). The cross sections of the colored particles are shown in Ref. [121]. For our benchmark point, $\sigma(g^{(1)} + Q^{(1)}/q^{(1)}) = 12.2$ pb and $\sigma(Q^{(1)}/q^{(1)} + Q^{(1)}/q^{(1)}) = 7.4$ pb at $\sqrt{s} = 14$ TeV.

The $g^{(1)}$ decays into $Q^{(1)}Q$ and $q^{(1)}q$ with branching ratios, $\text{BR}(g \rightarrow Q^{(1)}Q) \sim 40\%$ and $\text{BR}(g \rightarrow q^{(1)}q) \sim 60\%$, respectively. The ratio of inclusive KK quark productions is roughly $Q^{(1)}Q^{(1)} : q^{(1)}q^{(1)} : Q^{(1)}q^{(1)} = 1 : 1 : 2$. Because $q^{(1)}$ only has the $U(1)_Y$ gauge interaction, it directly decays into $\gamma^{(1)}q$. The hard jets mainly come from this decay. The branching ratios of $Q^{(1)}$ are typically $\text{BR}(Q^{(1)} \rightarrow QW^{\pm(1)}) \sim 65\%$, $\text{BR}(Q^{(1)} \rightarrow QZ^{(1)}) \sim 32\%$, and $\text{BR}(Q^{(1)} \rightarrow Q\gamma^{(1)}) \sim 3\%$. Once $W^{(1)}$ and $Z^{(1)}$ appear from $Q^{(1)}$, they cannot decay hadronically for kinematical reasons. They democratically decay into all lepton flavors: $W^{\pm(1)} \rightarrow \gamma^{(1)}l\nu$ and $Z^{(1)} \rightarrow \gamma^{(1)}\nu\bar{\nu}$ or $\gamma^{(1)}l^+l^-$ through $l^{(1)}$ or $\nu^{(1)}$.

This collider signature has been studied in clean channels of multilepton such as $4l + E_T^{\text{miss}}$ [107, 108, 109], dilepton, and trilepton [109, 122]. The leptons arise only from the KK gauge boson $W^{(1)}$ or $Z^{(1)}$ production. The $4l + E_T^{\text{miss}}$ channel has been the most promising one because the background is extremely small, but the fraction of the MUED events going to this channel is about 1%: from the $Q^{(1)}Q^{(1)}$ production, each $Q^{(1)}$ should decay as $Q^{(1)} \rightarrow QZ^{(1)} \rightarrow Ql^+l^-\gamma^{(1)}$ with the branching ratio of 16%.

Multijet channels without requiring multileptons are statistically advantageous, so we use the multijet + lepton channel. This is accessible to about 65% of the MUED total production. The requirement of one lepton is only to avoid the QCD background.

D.3 Definition of M_{T2}

In this section, we briefly review the definition of M_{T2} . M_{T2} , an extension of transverse mass M_T , was originally proposed as a mass measurement variable in the situation with two invisible particles with $\mathbf{p}_T^{\text{inv}(1)}$ and $\mathbf{p}_T^{\text{inv}(2)}$ [93, 94]. In each event, we only know the total

missing transverse momentum, $\not{\mathbf{p}}_T$, but each transverse momentum of the invisible particle cannot be measured. The definition of M_{T2} is :

$$M_{T2} \equiv \min_{\mathbf{p}_T^{\text{inv}(1)} + \mathbf{p}_T^{\text{inv}(2)} = \not{\mathbf{p}}_T} \left[\max \left\{ M_T^{(1)}, M_T^{(2)} \right\} \right] \quad (\text{D.5})$$

where M_T is defined by

$$\begin{aligned} M_T^{(i)} &= M_T(m_{\text{vis}(i)}, m_{\text{inv}(i)}, \mathbf{p}_T^{\text{vis}(i)}, \mathbf{p}_T^{\text{inv}(i)}) \\ &\equiv \sqrt{m_{\text{vis}(i)}^2 + m_{\text{inv}(i)}^2 + 2 \left(E_T^{\text{vis}(i)} E_T^{\text{inv}(i)} - \mathbf{p}_T^{\text{vis}(i)} \cdot \mathbf{p}_T^{\text{inv}(i)} \right)}, \end{aligned} \quad (\text{D.6})$$

and where $m_{\text{vis}(i)}$ and $m_{\text{inv}(i)}$ are visible (observed) particle mass and invisible particle mass in system i , respectively. The transverse energy E_T is given by

$$E_T \equiv \sqrt{m^2 + |\mathbf{p}_T|^2}. \quad (\text{D.7})$$

In calculating M_{T2} , we first construct transverse mass $M_T^{(i=1,2)}$ and take the maximum of them for one partition of $\mathbf{p}_T^{\text{inv}(1)}$ and $\mathbf{p}_T^{\text{inv}(2)}$ satisfying $\mathbf{p}_T^{\text{inv}(1)} + \mathbf{p}_T^{\text{inv}(2)} = \not{\mathbf{p}}_T$. Then, all the possible partitions are considered, and the minimum value among them is taken.

Let us consider the simple case where the same parent particles are produced and each of them directly decay to a visible particle and an invisible particle. In the MUED, such a example is $q^{(1)}q^{(1)} \rightarrow \gamma^{(1)}\gamma^{(1)}qq$ process: first KK (right-handed) quarks, $q^{(1)}$, are produced and each one directly decays into a quark and the LKP, KK photon, $\gamma^{(1)}$. If the invisible particle mass m_{inv} is known, M_T is bounded by the parent particle mass, $M_T \leq m_{\text{parent}}$ in the correct partition. Then, as seen from the definition, M_{T2} is also bounded by the parent particle mass, $M_{T2} \leq M_{T2}^{\text{max}} = m_{\text{parent}}$. We can also interpret M_{T2}^{max} as the invariant mass. Transverse mass M_T , essential component of M_{T2} , actually acted as *invariant* mass to successfully measure W boson mass in leptonic decay in UA1 [103]. This method worked because invisible particle of the decay is known to be massless neutrino.

Boost dependence

In practice, m_{inv} is not known. In calculating M_{T2} , we need to set a test mass for the invisible particle. Many attempts were made to simultaneously determine the masses of the parent and invisible particles [104, 105, 106]. One of them [106] utilizes the effect of Upstream Radiations (USR). USR is defined as visible particles which are emitted before parent particles of our interest are produced. The transverse momentum of USR, \mathbf{P}_T , is given by

$$\mathbf{p}_T^{\text{vis}(1)} + \mathbf{p}_T^{\text{vis}(2)} + \not{\mathbf{p}}_T = -\mathbf{P}_T \quad (\text{USR}). \quad (\text{D.8})$$

\mathbf{P}_T is a measure of the recoil of the parent particles. The source of USR is mainly initial state radiations (ISR). The decay products can be USR if the decay is before the production

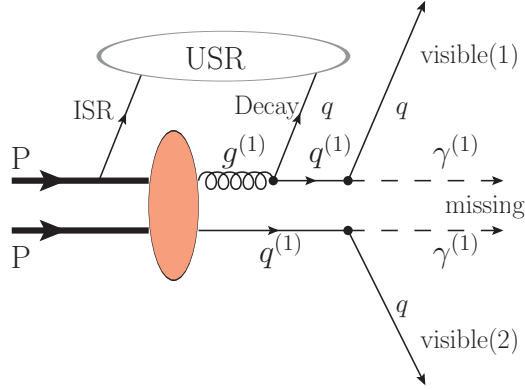


Figure D.1: Schematic picture of typical MUED process, $g^{(1)}q^{(1)}$ production. When two jets from $q^{(1)} \rightarrow \gamma^{(1)}q$ and used as visible particles to construct M_{T2} , a jet from the decay of $g^{(1)} \rightarrow q^{(1)}q$ and ISR become USR.

of the parent particles of our interest. Fig. D.3 illustrates USR in a case of $g^{(1)}q^{(1)}$ production where $g^{(1)}$ is first KK gluon. When we are interested in $q^{(1)}$, a quark emitted from the decay of $g^{(1)}$ and ISR are considered as USR.

Of course, M_{T2}^{\max} has different behaviors depending on whether the test mass is correct. When we set a correct test mass, M_{T2}^{\max} corresponds to the parent particle mass independent of USR. But, when we set a wrong test mass, M_{T2}^{\max} varies with USR, *i.e.* it is not Lorentz boost invariant quantity. This is because M_T varies with USR and is no longer bounded by the parent particle mass. This property can be used in the search for compressed models.

D.4 Use of M_{T2} as event selection

D.4.1 Properties

For SM background

The features of M_{T2} for the purpose of event selection were studied in [95, 96]. We use the M_{T2} cut as an event selection setting the *test mass* to zero. The set test mass is a correct value for SM because the only invisible particles of the SM are neutrinos. In this case, M_{T2} of the most background events, especially $t\bar{t}$ events, is lower than the top quark mass m_t ,

$$\max_{\text{SM events}} [M_{T2}] \simeq m_t. \quad (\text{D.9})$$

This is because we can measure the parent particle mass with the correct test mass, and the top quark is the heaviest parent particle in the SM. If a significant excess of M_{T2} above m_t is observed, it is likely to be new physics signal. An advantage of M_{T2} cut is that the value has physical meaning because this is originally a mass measurement variable unlike most of cut variables.

There are other good features. It is found that events without missing momentum or with fake missing momentum which is parallel to a mismeasured jet have very small values of

M_{T2} [95]. The proof is as follows. Suppose one of two energetic jets is mismeasured leading to missing momentum of $\mathbf{p}_T \parallel \mathbf{p}_T^{\text{vis}(1)}$, and all the jet masses are set to be zero for simplicity. We can take a partition of $\mathbf{p}_T^{\text{inv}(1)} = \mathbf{p}_T$ and $\mathbf{p}_T^{\text{inv}(2)} = 0$, and then $M_T^{(1)} = 0$ and $M_{T2} = 0$ by definition. This result is extended for a case with two mismeasured visible objects, and this proof and other properties are discussed in Ref. [95].

For new physics signal

M_{T2} of new physics is not bounded by the parent particle mass because the test mass is wrong for massive invisible particles. The upper bound of M_{T2} is a mass combination of the parent particle and the invisible particle in the absence of USR,

$$M_{T2}^{\text{max}} = \frac{m_{\text{parent}}^2 - m_{\text{inv}}^2}{m_{\text{parent}}} \equiv \mu_0. \quad (\text{D.10})$$

In this case, the signal is extracted from the background for models with a large mass splitting but not for models with a degenerate mass spectrum particularly for $\mu_0 \leq m_t$ because the signal is buried in the background.

However, considering the recoil momentum of parent particles by USR, M_{T2} is still a useful variable for the event selection in searching for compressed models. M_{T2}^{max} varies with USR and can exceed μ_0 due to the wrong test mass. For example, when parent particles of same mass are produced and directly decay to invisible particles emitting visible particles ($q^{(1)}q^{(1)} \rightarrow qq\gamma^{(1)}\gamma^{(1)}$), M_{T2}^{max} [105, 106] is given by

$$M_{T2}^{\text{max}} = \sqrt{\mu_0^2 F^2(P_T) + P_T \mu_0 F(P_T)} \geq \mu_0, \quad (\text{D.11})$$

where

$$\begin{aligned} F(P_T) &\equiv \left(\sqrt{1 + \left(\frac{P_T}{2m_{\text{parent}}} \right)^2} - \frac{P_T}{2m_{\text{parent}}} \right) \\ &\rightarrow \left(\frac{m_{\text{parent}}}{P_T} \right) \quad \text{for } P_T \gg m_{\text{parent}}. \end{aligned} \quad (\text{D.12})$$

Here P_T is the magnitude of the momentum of USR. There is a rich source of USR because processes of heavy particles tend to come along with hard QCD radiations including ISR. Hard ISR gives large recoil of produced particles, and M_{T2}^{max} can have a large value depending on USR. Note that the background events do not have M_{T2} dependence on USR because the test mass is correct, so most events are kept lower than m_t .

D.4.2 Comparison in realistic situation

When analyzing events, we cannot tell the origins of visible particles: whether the particles come from decays of heavier particles or are QCD radiations. Practically, leading two jets in p_T are used as visible particles to construct M_{T2} . If they correspond to two ‘‘correct’’ particles, namely if each particle is a decay product of each pair-produced particle, M_{T2} behaves as discussed above. However, the leading particles can be decay products of one

parent particle, and also hard ISR can be one or both of the leading particles. These cases are called “combinatorics.”

In many events, M_{T2} of the leading particles corresponds to M_{T2} of the correct particles. For instance, the rate of correspondence is about half for $q^{(1)}q^{(1)}$ or $t\bar{t}$ as shown later. Combinatorics smears the M_{T2} distribution. The smearing effect is significant for high M_{T2} , and it is different in each process.

In order to see the effects of USR and combinatorics, we generated the $q^{(1)}q^{(1)}$ production of the MUED benchmark point and the $t\bar{t}$ production adding up to one jet in the parton level¹, and constructed M_{T2} with the correct partons and with the leading partons/jets. These M_{T2} distributions are shown in Fig. D.2.

The green (red) shaded area shows M_{T2} with (without) an additional jet in the parton level using correct two partons: quarks from the direct decay $q^{(1)} \rightarrow q\gamma^{(1)}$ for $q^{(1)}q^{(1)}$ and b quarks from $t \rightarrow bW$ for $t\bar{t}$. LKPs and neutrinos produce \cancel{p}_T . For the signal, M_{T2} without USR (red shaded area) is bounded by the mass combination $\mu_0 = 210$ GeV given by (D.10). Including USR (green shaded area) M_{T2} varies with P_T and exceeds μ_0 as (D.11), and theoretically it reaches about 440 GeV with extremely large P_T . For the $t\bar{t}$ background, M_{T2} of correct two partons with USR (green shaded area) does not exceed m_t as expected.

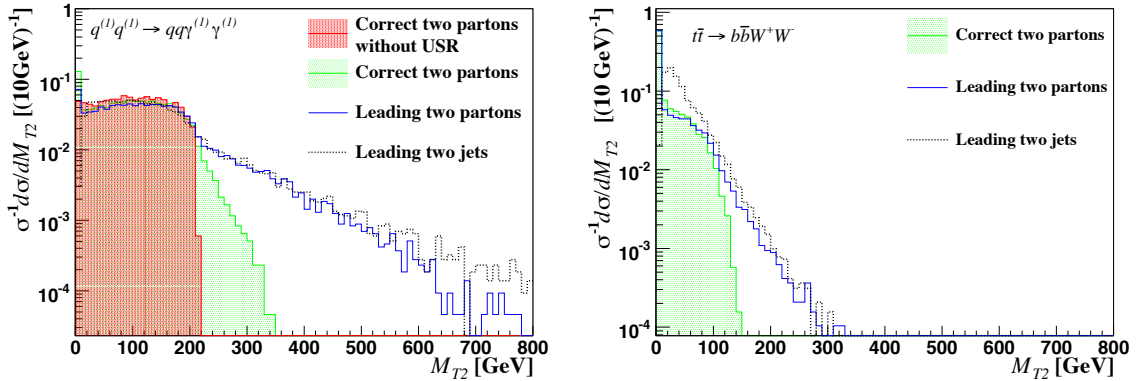


Figure D.2: Distributions of M_{T2} for $q^{(1)}q^{(1)} \rightarrow qq\gamma^{(1)}\gamma^{(1)}$ in the left and $t\bar{t} \rightarrow b\bar{b}W^+W^-$ in the right generated by MadGraph/MadEvent 4.4 [110] where $m_{q^{(1)}} = 912.5$ GeV, $m_{\gamma^{(1)}} = 800.1$ GeV, and $\mu_0 = 211.0$ GeV. M_{T2} is constructed with the correct two partons (green shaded area), the leading two partons (blue solid line), and leading two jets (dotted line). Also, events were generated without additional jets, that is, without USR in the parton level, and M_{T2} was calculated with the correct two partons (red shaded area). The distributions are normalized to 1.

Parton level	$q^{(1)}q^{(1)} \rightarrow qq\gamma^{(1)}\gamma^{(1)} + 0, 1 \text{ jet}$	$t\bar{t} \rightarrow b\bar{b}W^+W^- + 0, 1 \text{ jet}$
$M_{T2}^{\text{leading}} = M_{T2}^{\text{correct}}$	61.6%	49.1%
$M_{T2}^{\text{leading}} > M_{T2}^{\text{correct}}$	30.3% (78.9%)	22.4% (44%)
$M_{T2}^{\text{leading}} < M_{T2}^{\text{correct}}$	8.10% (21.1%)	28.5% (56%)

Table D.1: The evaluation of combinatorics for $q^{(1)}q^{(1)}$ of the benchmark point and $t\bar{t}$. M_{T2} is constructed in the parton level. We compare M_{T2} of leading partons and correct partons in each event.

Combinatorics

When the leading partons are used for M_{T2} (blue solid line), combinatorics smears the M_{T2} distribution. M_{T2} of the leading partons spreads over the endpoint of M_{T2} of correct partons to roughly double the value at the endpoint as in Fig. D.2. Table D.1 shows the evaluation of combinatorics. The leading partons correspond to the correct partons for 60% of the time for $q^{(1)}q^{(1)}$ and for 50% for $t\bar{t}$. The smearing effect due to combinatorics is different in each process: $M_{T2}^{\text{leading}} > M_{T2}^{\text{correct}}$ for three quarters of the combinatorics events of $q^{(1)}q^{(1)}$, while $M_{T2}^{\text{leading}} < M_{T2}^{\text{correct}}$ for more than half of the combinatorics events of $t\bar{t}$. Therefore, combinatorics assists to enhance the signal to background ratio for high M_{T2} .

Also, the detector effects are simulated after the fragmentation and hadronization, and M_{T2} is constructed with the leading two jets (dotted line). The distribution is similar with the M_{T2} distribution with the leading two partons.

The dependence on USR makes the signal excess in the high M_{T2} region even for compressed models, and the smearing effect of combinatorics enhances the excess in this particular example. It can be seen that events with high M_{T2} , say above 200 GeV, are dominated by the $q^{(1)}q^{(1)}$ signal over the $t\bar{t}$ background. Since for the other SM background processes the parent particle is lighter than the top quark, those background events are expected to have M_{T2} lower than m_t . Hence, M_{T2} is an effective event selection to search for the nearly degenerate model.

D.5 Application for the MUED

We explicitly perform M_{T2} event selection for MUED discovery potential. The MUED has two essential parameters relevant to collider phenomenology: R and the cutoff of the theory, Λ . It is known the radiative corrections spreads spectrum and the corrections are proportional to $\ln \Lambda R$. The degeneracy is crucial for the smaller ΛR and $\Lambda R = 10 \sim 40$ is adequate.

For the difficulty of compressed spectrum, promising previous study is $4l + \cancel{E}_T$ channel where the background level is quite low [107, 108, 109]. Relatively many leptons are emitted in the MUED processes. In order to see the use of M_{T2} cut, we also study the discovery potential in $4l + \cancel{E}_T$ channel.

¹The events were generated by MadGraph/MadEvent 4.4 [110] at $\sqrt{s} = 14$ TeV. The fragmentation and hadronization were simulated by PYTHIA 6.4, and the detector effects were simulated by PGS 4 [57]. The simulation setup is the same as the simulation described in Sec. D.5.1 except that here only one jet was added as the Matrix Element correction. The MLM matching [111] was prescribed.

D.5.1 Simulation

Monte Carlo (MC) samples of MUED signal were generated both by a private implementation in `MadGraph/MadEvent 4.4` (MG/ME) [110] and an implementation [112] in `PYTHIA 6.4` [56]. CTEQ5.1L was used as the leading-order (LO) parton distribution function (PDF). In the case of MG/ME, the Matrix Element was calculated by `HELAS` [113], and the fragmentation and hadronization were simulated with `PYTHIA 6.4`. The effects of jet reconstruction and detector smearing were simulated through `PGS 4` [57].

We consider $1/R$ from 400 GeV to 1.6 TeV in steps of 100 GeV with $\Lambda R = 10, 20, 30$, and 40. The remaining parameter, m_h , is set to 120 GeV. The MUED spectrum is simplified by neglecting m_{SM} for the first KK level. The processes we consider are pair productions of the colored first KK particles, $g^{(1)}$, $q^{(1)}$, and $Q^{(1)}$. The signal events corresponding to luminosities of more than 10 fb^{-1} at $\sqrt{s} = 14 \text{ TeV}$ were generated by `PYTHIA 6.4`.

Since we use the M_{T2} dependence on USR , the ISR has an important role. In order to reliably evaluate the hard ISR, we considered the Matrix Element correction in MG/ME adding up to one jet to the pair productions. The MLM matching [111] was applied to remove the overlap between jets from the Matrix Element and ones from the Parton Shower. This prescription was demonstrated for the benchmark point of $\Lambda R = 20$ and $1/R = 800 \text{ GeV}$. The spectrum of this point is listed in table D.2. However it is very time consuming to generate all of the signal MC samples with the Matrix Element correction, so we used `PYTHIA 6.4` rather than MG/ME to generate them for the discovery study. We will show in Sec. D.5.2. that MC samples generated by ME/ME with the Matrix Element correction have larger excess over background than ones generated by `PYTHIA 6.4` for the benchmark point. Hence, the event generation by `PYTHIA 6.4` is conservative.

$m_{\gamma^{(1)}}$	$m_{W^{(1)}}$	$m_{Z^{(1)}}$	$m_{e^{(1)}}$	$m_{L^{(1)}}$	$m_{d^{(1)}}$	$m_{u^{(1)}}$	$m_{Q^{(1)}}$	$m_{g^{(1)}}$	GeV
800.1	847.3	847.4	808.2	822.3	909.8	912.5	929.3	986.4	

Table D.2: Mass spectrum of first KK level for a benchmark point $(1/R, \Lambda R) = (800, 20)$

MC samples of the SM backgrounds: $t\bar{t}(+1j, 2j)$, $W/Z + \text{jets}(1j, 2j)$, Diboson $(+1j, 2j)$,² $Z/W + b\bar{b}$, $t\bar{t} + Z/\gamma^*(\rightarrow ll, \nu\nu)$ and $t\bar{t} + W(\rightarrow l\nu)$, were produced with MG/ME using the PDF set CTEQ6.1L, and fragmentation and hadronization were simulated with `PYTHIA 6.4` in the same way of the signal. For $t\bar{t}$, $W/Z + \text{jets}$, and Diboson, up to two partons were added in the Matrix Element and the MLM matching was prescribed. The MC samples were detector-simulated through `PGS 4`. The dominant background processes, $t\bar{t}$ and $W/Z + \text{jets}$, were normalized to the next-leading-order (NLO) cross section consistent with the inclusive dijet analysis of the ATLAS MC study [114].

For the sake of comparison with the $4l + \cancel{E}_T$ analysis, we generated some multilepton background processes, such as four leptons through off-shell Z^* or γ^* . The luminosities of generated SM background are more than 10 fb^{-1} at $\sqrt{s} = 14 \text{ TeV}$, respectively.

²Diboson denotes WW, WZ and ZZ .

D.5.2 Event selection

The object selection is that an electron and a muon are required to have $p_T > 10$ GeV and $|\eta| < 2.5$ and a jet is required to have $p_T > 20$ GeV and $|\eta| < 2.5$. In order to avoid recognizing a shower from an electron as a jet, a jet within $\Delta R < 0.2$ ($\Delta R = \sqrt{\Delta\eta^2 + \Delta\phi^2}$) from any electron is removed. Charged leptons from hadronic activity also should be removed. If an electron and a jet are found within $0.2 < \Delta R < 0.4$, the jet is kept and the electron is rejected. Similarly, if a muon and a jet are found within $\Delta R < 0.4$, the muon is rejected.

We impose event selections as follows,

- CUT1: $p_T^{\text{jet}} > \{100, 20 \text{ GeV}\}$
- CUT2: $\cancel{E}_T (= \cancel{p}_T) > 100 \text{ GeV}$
- CUT3: At least one lepton with $p_T^{\text{lep}} > 20 \text{ GeV}$
- CUT4: If the number of lepton is one, $M_T^{\text{lep,miss}} > 100 \text{ GeV}$ ³
- CUT5: $M_{T2} > 200 \text{ GeV}$.

In order to demonstrate the effectiveness of M_{T2} for the MUED, we only use the basic cuts 1-4 except one on M_{T2} . The cuts 1-4 are comparable with ones imposed in the ATLAS and CMS new physics searches in one lepton + jets + \cancel{E}_T with low luminosity at $\sqrt{s} = 7$ TeV [115, 116]. We do not use the M_{eff} ⁴ cut and the $\cancel{E}_T/M_{\text{eff}}$ cut which are used to extract the signal especially by the ATLAS collaboration in the search for SUSY [114]. It is common that the $\Delta\phi_{\text{jet,miss}}$ cut is applied to reduce events with fake missing due to the mismeasurement of jets, but this is not necessary because the later M_{T2} cut has a similar role [95].

The cut flow in table D.3 shows that the M_{T2} cut (CUT5) significantly reduces the SM background to a level comparable to the MUED. Since the Matrix Element correction increases event rates in the high M_{T2} region, there remain more signal events generated by MG/ME after CUT5 than ones generated by PYTHIA 6.4. Therefore, the signal rate in the fast event generation by PYTHIA 6.4 is a little underestimated and hence is conservative.

Fig. D.3 shows that the dominant background processes are $t\bar{t}$, W + jets, and Diboson. Background events that remain even after CUT5 mainly come from combinatorics. The peak of MUED events is $M_{T2} < 200$ GeV, but the signal events have a long tail which can be understood as a result of the variant endpoint due to the wrong test mass discussed in section D.4. There is combinatorics for both the signal and the background, and especially it tends to increase M_{T2} of the signal events. Combinatorics help to enhance the signal excess. As a result, we can successfully extract the signal from the background even based on jets.

D.5.3 Discovery potential

For the study of the discovery potential it is necessary to take systematic uncertainties into account in addition to statistical uncertainties. We use the significance Z_B [117], which is provided by the ROOT library [118], using the same approach as in ATLAS discovery

³ $M_T^{\text{lep,miss}} \equiv \sqrt{2(p_T^{\text{lep}} \cancel{p}_T - \mathbf{p}_T^{\text{lep}} \cdot \cancel{\mathbf{p}}_T)}$

⁴ $M_{\text{eff}} \equiv \sum_{\text{jet}}^4 p_T + \sum_{\text{lepton}} p_T + \cancel{E}_T$.

Process		CUT1	CUT2	CUT3	CUT4	CUT5 (Optimal)
$g^{(1)} + g^{(1)}$	MG/ME	1,028	832	119	62	25
	PYTHIA	937	757	108	63	22
$g^{(1)} + q^{(1)}/Q^{(1)}$	MG/ME	9,196	7,218	1,234	675	241
	PYTHIA	8,569	6,694	1,344	731	223
$q^{(1)}/Q^{(1)}$ $+q^{(1)}/Q^{(1)}$	MG/ME	5,315	4,035	863	508	148
	PYTHIA	4,497	3,276	690	436	84
$q^{(1)}/Q^{(1)}$ $+q^{(1)}/\bar{Q}^{(1)}$	MG/ME	1,444	1,075	206	115	27
	PYTHIA	1,301	955	163	112	20
Total MUED	MG/ME	16,983	13,160	2,422	1,360	441
	PYTHIA	15,304	11,682	2,305	1,342	349
$t\bar{t}$		426,074	57,533	23,239	5,620	243
W		400,527	97,907	35,386	1,031	85
Z		142,368	53,801	916	107	12
$W/Z + t\bar{t}/b\bar{b}$		1,121	304	103	49	10
Diboson		29,141	4,482	1,335	252	40
Total Standard Model		999,231	214,027	60,979	7,059	390
Total MUED	MG/ME	0.05	0.17	0.06	0.78	4.10
Z_B	PYTHIA	0.05	0.14	0.05	0.77	3.37 (7.57)

Table D.3: Cut flow for 1 fb^{-1} at $\sqrt{s} = 14 \text{ TeV}$. The MUED benchmark point is $\{1/R, \Lambda R\} = \{800 \text{ GeV}, 20\}$. The MUED signal generated by MadGraph/MadEvent 4.4 (MG/ME) with the MLM matching is normalized to one generated by PYTHIA 6.4. $M_{T2} > 350 \text{ GeV}$ is an optimal cut that maximizes the significance $Z_B = 7.57$.

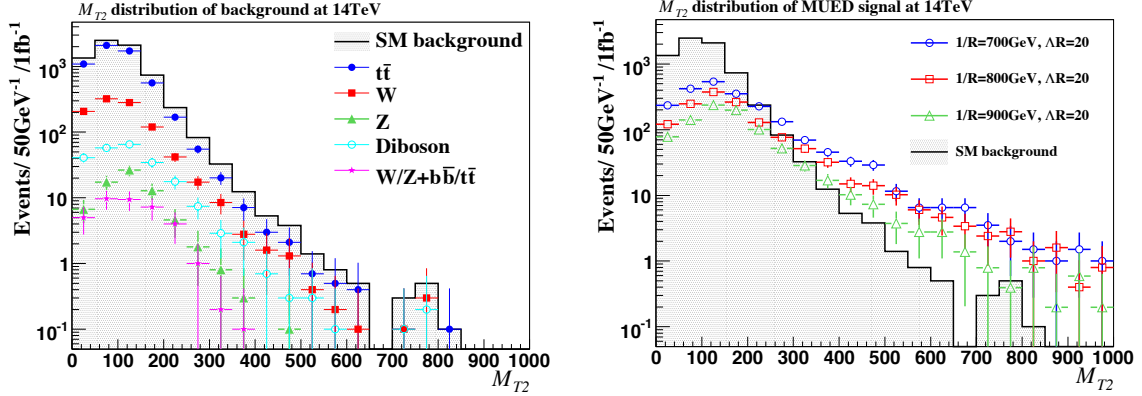


Figure D.3: Distributions of M_{T2} of the leading two jets after CUT4 for each SM background in the left, and total SM background and MUED signal points of $1/R = 700, 800, 900$ GeV and $\Lambda R = 20$ generated by PYTHIA 6.4 in the right.

study for supersymmetry [114]. Z_B is calculated using a convolution of a Poisson and a Gaussian term to account for systematic errors. For the backgrounds except those from QCD, a reasonable estimate of the systematic uncertainty is $\pm 20\%$. The discovery potential is studied by finding the optimal M_{T2} cut (in step of 50 GeV) to maximize the significance Z_B . We define “discovery” when $Z_B > 5$ and more than 10 signal events remain after the cuts.

In order to compare the M_{T2} analysis in the multijet + lepton mode with the previously studied $4l + \cancel{E}_T$ analysis, we also check the discovery potential in $4l + \cancel{E}_T$ using the same MC samples and using the same definition of discovery. In the $4l + \cancel{E}_T$ analysis, the following cuts are imposed [107]: (1) four isolated leptons with $p_T^{\text{lep}} > \{35, 20, 15, 10 \text{ GeV}\}$ are required, (2) $\cancel{E}_T > 50$ GeV, and (3) an invariant mass M_{ll} for all possible pairs of opposite sign same flavor leptons and remove events if $|M_{ll} - m_Z| < 10$ GeV to reduce background from the Z boson. The estimated background from our MC samples is 10 events/100 fb $^{-1}$. The fake leptons should be considered to evaluate the background level of $4l + \cancel{E}_T$ more appropriately, but the fake leptons are not considered since they are not important for our analysis based on jets.

The spectrum is more degenerate for smaller ΛR , which is more difficult for discovery in general. Note that for fixed $1/R$, the MUED with smaller ΛR has a larger cross section simply because the KK gluon and the KK quark become lighter as in Eqs. (D.3) and (D.4). Fig. 4 shows that the discovery potential does not vary with changing ΛR in the M_{T2} analysis. The second run at 14 TeV will discover up to $1/R \sim 1$ TeV with 1 fb $^{-1}$ and $1/R \sim 1.2$ TeV with 10 fb $^{-1}$. In the $4l + \cancel{E}_T$ analysis, the discovery reach at 14 TeV is $1/R \sim 700$ GeV with 1 fb $^{-1}$ and $1/R \sim 1.2$ TeV with 10 fb $^{-1}$ for $20 \leq \Lambda R \leq 40$, but the sensitivity is very low for $\Lambda R = 10$: the discovery reach is only $1/R = 400$ GeV with 1 fb $^{-1}$ and $1/R = 800$ GeV with 10 fb $^{-1}$.

The result shows that our M_{T2} analysis improves the discovery potential. In particular, the improvement is so significant for the most degenerate parameter $\Lambda R = 10$ that the

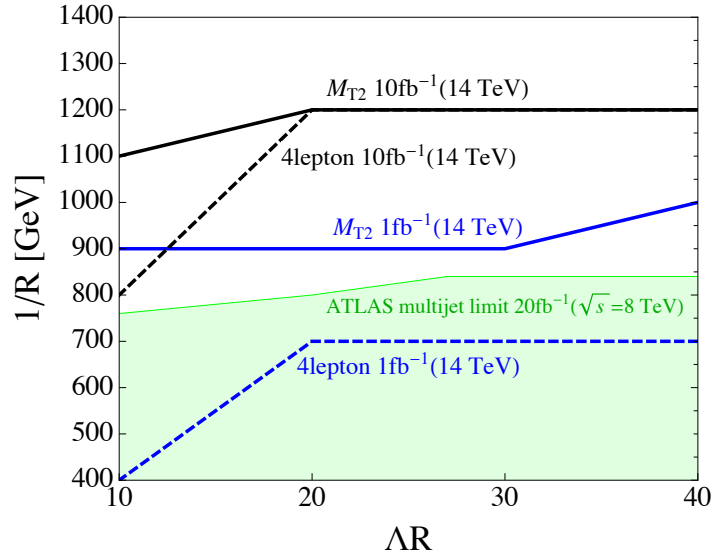


Figure D.4: Discovery potential of the MUED with 1 fb^{-1} and 10 fb^{-1} at $\sqrt{s} = 14 \text{ TeV}$ in the $4l + \cancel{E}_T$ analysis and the M_{T2} analysis. For a given luminosity, the parameter region below the line will be discovered.

discovery potential improves from $1/R = 400 \text{ GeV}$ to 900 GeV .

D.6 Summary and Discussion

The problem of the ordinary multijet + E_T^{miss} analysis is that the signal of compressed models like the Compact Supersymmetry and the MUED are removed too much because the cuts are optimized for the CMSSM-like models. If the event selections are taken to be weaker, the signal is buried in the SM background. This is because the top quark pair production $t\bar{t}$ generates missing particles, neutrinos, and hard jets with a large enough cross section.

Here, we tackled the search in the multijet channel by using a kinematic variable M_{T2} [93, 94]. M_{T2} is bounded by the mass of the produced particles when the true mass of invisible particle is given. We pointed out that M_{T2} is effective in the search for compressed models utilizing USR dependence of M_{T2} .

We set a test mass for the invisible particle to zero for M_{T2} calculation. The set test mass is wrong for the signal events because it is much smaller than the mass of invisible particle. This leads to the M_{T2} dependence on USR which is mainly from ISR. M_{T2} of the signal can be large depending on USR, although, without USR, M_{T2} is small in the compressed spectrum. On the other hand, the test mass is correct for the mass of the SM invisible particle, neutrino. Then, M_{T2} of the SM background does not depend on USR. As shown in Refs. [93, 94], it is mainly below the mass of the heaviest particle in the SM, the top quark, $M_{T2}^{\text{SM}} \lesssim m_t$. Therefore, an excess in the high M_{T2} region beyond m_t can be seen as the signal of new physics, and then, M_{T2} is effective to search for compressed models.

In the analysis of this paper, leading two jets in p_T are used to calculate M_{T2} . They do

not always correspond to jets we want, that is, we have combinatoric issues when choosing jets for defining M_{T2} . Combinatorics smears the M_{T2} distribution, and the smearing effect is different in each process. We found combinatorics makes M_{T2} of the signal larger while M_{T2} of the background does not increase as much as that of the signal. Therefore, the smearing effect of combinatorics enhances the signal excess in the high M_{T2} region.

We apply M_{T2} to the discovery study of the MUED, and we require at least one lepton in addition to multijet to avoid the QCD background. Since the ISR takes an important role in this method, we perform the event generation with the Matrix Element correction which evaluates the hard ISR appropriately. This way, we show that the M_{T2} analysis improves the discovery potential compared to the $4l + E_T^{miss}$ analysis.

This technique is useful to apply for a wide class of models with a compressed spectrum. Since we have now data, the background can be reliably estimated and the multi-jet discovery analysis becomes easier whereas requiring one lepton in our simulation was not essential. Thus the next thing to do is to study discovery potential of the MSSM with a compressed spectrum in multi-jet channel with M_{T2} .

Bibliography

- [1] G. Aad *et al.* [ATLAS Collaboration], Phys. Lett. B **716**, 1 (2012), 1207.7214; S. Chatrchyan *et al.* (CMS Collaboration), Phys. Lett. B **716**, 30 (2012), 1207.7235.
- [2] F. Englert and R. Brout, Phys. Rev. Lett. **13**, 321 (1964). P. W. Higgs, Phys. Lett. **12**, 132 (1964). P. W. Higgs, Phys. Rev. Lett. **13**, 508 (1964). G. S. Guralnik, C. R. Hagen and T. W. B. Kibble, Phys. Rev. Lett. **13**, 585 (1964). P. W. Higgs, Phys. Rev. **145**, 1156 (1966). T. W. B. Kibble, Phys. Rev. **155**, 1554 (1967).
- [3] The LEP Electroweak Working Group <http://lepewwg.web.cern.ch/LEPEWWG/>
- [4] For a review, see, e.g., S. P. Martin, in *Perspectives on Supersymmetry II*, ed. G. L. Kane (World Scientific, Singapore, 2010), p. 1 [hep-ph/9709356].
- [5] http://www.esa.int/Our_Activities/Space_Science/Planck/Planck_reveals_an_almost_perfect_Univ
- [6] H. Murayama, In *Tokyo 1994, Proceedings, Physics with high energy colliders* 357-379, and Lawrence Berkeley Lab. - LBL-36175 (94/06,rec.Oct.) 26 p [hep-ph/9410285].
- [7] J. J. Sakurai, "Advanced quantum physics," Boston, USA: Addison-Wesley
- [8] V. F. Weisskopf, Phys. Rev. **56**, 72 (1939).
- [9] J. Wess and J. Bagger, Princeton, USA: Univ. Pr. (1992) 259 p
- [10] J. R. Ellis, G. Ridolfi and F. Zwirner, Phys. Lett. B **257**, 83 (1991); Y. Okada, M. Yamaguchi and T. Yanagida, Phys. Lett. B **262**, 54 (1991); H. E. Haber and R. Hempfling, Phys. Rev. Lett. **66**, 1815 (1991); Y. Okada, M. Yamaguchi and T. Yanagida, Prog. Theor. Phys. **85**, 1 (1991).
- [11] R. Barbieri and G. F. Giudice, Nucl. Phys. B **306**, 63 (1988).
- [12] For a partial list (and references therein): B. de Carlos and J. A. Casas, Phys. Lett. B **309**, 320 (1993) [arXiv:hep-ph/9303291]. P. H. Chankowski, J. R. Ellis and S. Pokorski, Phys. Lett. B **423**, 327 (1998) [hep-ph/9712234]. R. Barbieri and A. Strumia, Phys. Lett. B **433**, 63 (1998) [hep-ph/9801353]. G. L. Kane and S. F. King, Phys. Lett. B **451**, 113 (1999) [hep-ph/9810374]. L. Giusti, A. Romanino and A. Strumia, Nucl. Phys. B **550**, 3 (1999) [hep-ph/9811386]. Z. Chacko, Y. Nomura and D. Tucker-Smith, Nucl. Phys. B **725**, 207 (2005) [hep-ph/0504095]. K. Choi, K. S. Jeong, T. Kobayashi and K. -i. Okumura, Phys. Lett. B **633**, 355 (2006) [hep-ph/0508029]. R. Kitano and Y. Nomura, Phys. Lett. B **631**, 58 (2005) [hep-ph/0509039]. P. Athron and D. J. Miller, 2, Phys.

- Rev. D **76**, 075010 (2007) [arXiv:0705.2241 [hep-ph]]. S. Cassel, D. M. Ghilencea and G. G. Ross, Nucl. Phys. B **825**, 203 (2010) [arXiv:0903.1115 [hep-ph]]. R. Barbieri and D. Pappadopulo, JHEP **0910**, 061 (2009) [arXiv:0906.4546 [hep-ph]]. M. Asano, H. D. Kim, R. Kitano and Y. Shimizu, JHEP **1012**, 019 (2010) [arXiv:1010.0692 [hep-ph]].
- [13] R. Kitano and Y. Nomura, Phys. Rev. D **73**, 095004 (2006) [hep-ph/0602096].
- [14] L. J. Hall, D. Pinner and J. T. Ruderman, JHEP **1204**, 131 (2012), 1112.2703.
- [15] S. Dittmaier *et al.* [LHC Higgs Cross Section Working Group Collaboration], arXiv:1101.0593 [hep-ph].
- [16] S. Dittmaier, S. Dittmaier, C. Mariotti, G. Passarino, R. Tanaka, S. Alekhin, J. Alwall and E. A. Bagnaschi *et al.*, arXiv:1201.3084 [hep-ph].
- [17] ATLAS Collaboration, ATLAS-CONF-2013-014
- [18] CMS Collaboration, CMS-PAS-HIG-13-005
- [19] G. Aad *et al.* [ATLAS Collaboration], Phys. Lett. B **726**, 120 (2013) [arXiv:1307.1432 [hep-ex]]; CMS Collaboration, CMS-HIG-13-002, CMS-PAS-HIG-13-016; and references therein.
- [20] ATLAS Collaboration, ATLAS-CONF-2013-014
- [21] ATLAS Collaboration, ATLAS-CONF-2013-047.
- [22] Talk at SUSY 2013 international conference “Overview of SUSY results from the ATLAS experiment” by Jamie Boyd, http://susy2013.ictp.it/lecturenotes/03_Wednesday/Boyd.pdf and references therein.
- [23] A. H. Chamseddine, R. Arnowitt and P. Nath, Phys. Rev. Lett. **49**, 970 (1982); R. Barbieri, S. Ferrara and C. A. Savoy, Phys. Lett. B **119**, 343 (1982); L. Hall, J. Lykken and S. Weinberg, Phys. Rev. D **27**, 2359 (1983).
- [24] ATLAS Collaboration, ATLAS-CONF-2013-091.
- [25] H. Baer, V. Barger, P. Huang, D. Mickelson, A. Mustafayev and X. Tata, Phys. Rev. D **87**, no. 3, 035017 (2013) [arXiv:1210.3019 [hep-ph]] and reference therein.
- [26] H. Murayama, Y. Nomura, S. Shirai and K. Tobioka, Phys. Rev. D **86**, 115014 (2012) [arXiv:1206.4993 [hep-ph]].
- [27] H. Murayama, M. M. Nojiri and K. Tobioka, Phys. Rev. D **84**, 094015 (2011) [arXiv:1107.3369 [hep-ph]].
- [28] X. Lu, H. Murayama, J. T. Ruderman and K. Tobioka, arXiv:1308.0792 [hep-ph].
- [29] G. Aad *et al.* [ATLAS Collaboration], Phys. Lett. B **710**, 49 (2012) [arXiv:1202.1408 [hep-ex]]; S. Chatrchyan *et al.* [CMS Collaboration], Phys. Lett. B **710**, 26 (2012) [arXiv:1202.1488 [hep-ex]].

- [30] N. Arkani-Hamed and S. Dimopoulos, JHEP **06**, 073 (2005) [hep-th/0405159]; L. J. Hall and Y. Nomura, JHEP **01**, 082 (2012) [arXiv:1111.4519 [hep-ph]].
- [31] S. Dimopoulos and G. F. Giudice, Phys. Lett. B **357**, 573 (1995) [hep-ph/9507282]; A. Pomarol and D. Tommasini, Nucl. Phys. B **466**, 3 (1996) [hep-ph/9507462]; A. G. Cohen, D. B. Kaplan and A. E. Nelson, Phys. Lett. B **388**, 588 (1996) [hep-ph/9607394]; M. Papucci, J. T. Ruderman and A. Weiler, JHEP **1209**, 035 (2012) [arXiv:1110.6926 [hep-ph]]; C. Brust, A. Katz, S. Lawrence and R. Sundrum, JHEP **1203**, 103 (2012) [arXiv:1110.6670 [hep-ph]].
- [32] See, e.g., T. J. LeCompte and S. P. Martin, Phys. Rev. D **85**, 035023 (2012) [arXiv:1111.6897 [hep-ph]]; ATLAS-CONF-2011-155, and references therein.
- [33] J. Scherk and J. H. Schwarz, Phys. Lett. B **82**, 60 (1979); Nucl. Phys. B **153**, 61 (1979).
- [34] A. Pomarol and M. Quirós, Phys. Lett. B **438**, 255 (1998) [hep-ph/9806263]; I. Antoniadis, S. Dimopoulos, A. Pomarol and M. Quirós, Nucl. Phys. B **544**, 503 (1999) [hep-ph/9810410]; R. Barbieri, L. J. Hall and Y. Nomura, Phys. Rev. D **63**, 105007 (2001) [hep-ph/0011311].
- [35] R. Barbieri, L. J. Hall and Y. Nomura, Phys. Rev. D **66**, 045025 (2002) [hep-ph/0106190]; Nucl. Phys. B **624**, 63 (2002) [hep-th/0107004].
- [36] N. Arkani-Hamed, T. Gregoire and J. G. Wacker, JHEP **0203**, 055 (2002) [hep-th/0101233].
- [37] D. Marti and A. Pomarol, Phys. Rev. D **64**, 105025 (2001) [hep-th/0106256]; D. E. Kaplan and N. Weiner, hep-ph/0108001.
- [38] N. Arkani-Hamed, L. J. Hall, Y. Nomura, D. Tucker-Smith and N. Weiner, Nucl. Phys. B **605**, 81 (2001) [hep-ph/0102090].
- [39] R. Barbieri, L. J. Hall, G. Marandella, Y. Nomura, T. Okui, S. J. Oliver and M. Papucci, Nucl. Phys. B **663**, 141 (2003) [hep-ph/0208153].
- [40] W. Fischler, H. P. Nilles, J. Polchinski, S. Raby and L. Susskind, Phys. Rev. Lett. **47**, 757 (1981).
- [41] Z. Chacko, M. A. Luty and E. Ponton, JHEP **0007**, 036 (2000) [hep-ph/9909248].
- [42] N. Arkani-Hamed, L. J. Hall, Y. Nomura, D. Tucker-Smith and N. Weiner, Nucl. Phys. B **605**, 81 (2001) [hep-ph/0102090]; A. Delgado, G. von Gersdorff, P. John and M. Quiros, Phys. Lett. B **517**, 445 (2001) [hep-ph/0104112].
- [43] A. Delgado, G. von Gersdorff and M. Quiros, Nucl. Phys. B **613**, 49 (2001) [hep-ph/0107233].
- [44] L. J. Hall and Y. Nomura, Phys. Lett. B **532**, 111 (2002) [hep-ph/0202107].
- [45] B. C. Allanach, Comput. Phys. Commun. **143**, 305 (2002) [hep-ph/0104145].

- [46] S. Heinemeyer, W. Hollik and G. Weiglein, *Comput. Phys. Commun.* **124**, 76 (2000) [hep-ph/9812320].
- [47] The Tevatron Electroweak Working Group, arXiv:1107.5255 [hep-ex].
- [48] B. C. Allanach, A. Djouadi, J. L. Kneur, W. Porod and P. Slavich, *JHEP* **09**, 044 (2004) [hep-ph/0406166].
- [49] P. Kant, R. V. Harlander, L. Mihaila and M. Steinhauser, *JHEP* **08**, 104 (2010) [arXiv:1005.5709 [hep-ph]].
- [50] F. E. Paige, S. D. Protopopescu, H. Baer and X. Tata, hep-ph/0312045.
- [51] G. Corcella, I. G. Knowles, G. Marchesini, S. Moretti, K. Odagiri, P. Richardson, M. H. Seymour and B. R. Webber, *JHEP* **01**, 010 (2001) [hep-ph/0011363]; hep-ph/0210213.
- [52] E. Richter-Was, hep-ph/0207355.
- [53] <http://web.physik.rwth-aachen.de/service/wiki/bin/view/Kraemer/SquarksandGluinos>
- [54] ATLAS Collaboration, ATLAS-CONF-2012-033.
- [55] ATLAS Collaboration, ATLAS-CONF-2012-041.
- [56] T. Sjostrand, S. Mrenna, and P. Z. Skands, *JHEP* **05** (2006) 026, [hep-ph/0603175].
- [57] J. Conway, <http://www.physics.ucdavis.edu/conway/research/software/pgs/pgs4-general.htm>.
- [58] See, e.g., A. Delgado and M. Quirós, *Nucl. Phys. B* **607**, 99 (2001) [hep-ph/0103058]; A. Delgado, A. Pomarol and M. Quiros, *JHEP* **0001**, 030 (2000) [hep-ph/9911252].
- [59] W. Altmannshofer, A. J. Buras, S. Gori, P. Paradisi and D. M. Straub, *Nucl. Phys. B* **830**, 17 (2010) [arXiv:0909.1333 [hep-ph]].
- [60] M. Bona *et al.* [UTfit Collaboration], *JHEP* **0803**, 049 (2008) [arXiv:0707.0636 [hep-ph]].
- [61] G. Bélanger, F. Boudjema, P. Brun, A. Pukhov, S. Rosier-Lees, P. Salati and A. Semenov, *Comput. Phys. Commun.* **182**, 842 (2011) [arXiv:1004.1092 [hep-ph]]; G. Bélanger, F. Boudjema, A. Pukhov and A. Semenov, *Comput. Phys. Commun.* **149**, 103 (2002) [hep-ph/0112278]; *Comput. Phys. Commun.* **174**, 577 (2006) [hep-ph/0405253].
- [62] H. Ohki *et al.* [JLQCD Collaboration], *Phys. Rev. D* **78**, 054502 (2008) [arXiv:0806.4744 [hep-lat]]; D. Toussaint and W. Freeman [MILC Collaboration], *Phys. Rev. Lett.* **103**, 122002 (2009) [arXiv:0905.2432 [hep-lat]].

- [63] E. Aprile *et al.* [XENON100 Collaboration], Phys. Rev. Lett. **107**, 131302 (2011) [arXiv:1104.2549 [astro-ph.CO]].
- [64] D. S. Akerib *et al.* [LUX Collaboration], arXiv:1310.8214 [astro-ph.CO].
- [65] J. D. Wells, hep-ph/0306127;
- [66] J. Fan, M. Reece and J. T. Ruderman, JHEP **1111**, 012 (2011) [arXiv:1105.5135 [hep-ph]]; J. Fan, M. Reece and J. T. Ruderman, JHEP **1207**, 196 (2012) [arXiv:1201.4875 [hep-ph]]; M. Baryakhtar, N. Craig and K. Van Tilburg, JHEP **1207**, 164 (2012) [arXiv:1206.0751 [hep-ph]].
- [67] For a review, R. Barbier, C. Berat, M. Besancon, M. Chemtob, A. Deandrea, E. Dudas, P. Fayet and S. Lavignac *et al.*, Phys. Rept. **420**, 1 (2005) [hep-ph/0406039]. For recent studies, see for example, C. Csaki, Y. Grossman and B. Heidenreich, Phys. Rev. D **85**, 095009 (2012) [arXiv:1111.1239 [hep-ph]]. P. W. Graham, D. E. Kaplan, S. Rajendran and P. Saraswat, JHEP **1207**, 149 (2012) [arXiv:1204.6038 [hep-ph]]. J. T. Ruderman, T. R. Slatyer and N. Weiner, arXiv:1207.5787 [hep-ph].
- [68] J. R. Espinosa and M. Quiros, Phys. Lett. B **279**, 92 (1992); U. Ellwanger, C. Hugonie and A. M. Teixeira, Phys. Rept. **496**, 1 (2010) [arXiv:0910.1785 [hep-ph]];
- [69] Y. Nomura, D. Poland and B. Tweedie, Phys. Lett. B **633**, 573 (2006) [hep-ph/0509244]; A. Delgado, C. Kolda, J. P. Olson and A. de la Puente, Phys. Rev. Lett. **105**, 091802 (2010) [arXiv:1005.1282 [hep-ph]];
- [70] G. G. Ross and K. Schmidt-Hoberg, Nucl. Phys. B **862**, 710 (2012) [arXiv:1108.1284 [hep-ph]]. G. G. Ross, K. Schmidt-Hoberg and F. Staub, JHEP **1208**, 074 (2012) [arXiv:1205.1509 [hep-ph]].
- [71] R. Harnik, G. D. Kribs, D. T. Larson and H. Murayama, Phys. Rev. D **70**, 015002 (2004) [hep-ph/0311349]; R. Barbieri, L. J. Hall, Y. Nomura and V. S. Rychkov, Phys. Rev. D **75**, 035007 (2007) [hep-ph/0607332];
- [72] P. Batra, A. Delgado, D. E. Kaplan and T. M. P. Tait, JHEP **0402**, 043 (2004) [hep-ph/0309149]; A. Maloney, A. Pierce and J. G. Wacker, JHEP **0606**, 034 (2006) [hep-ph/0409127]; C. Cheung and H. L. Roberts, arXiv:1207.0234 [hep-ph].
- [73] N. Arkani-Hamed, C. D. Carone, L. J. Hall and H. Murayama, Phys. Rev. D **54**, 7032 (1996) [hep-ph/9607298].
- [74] M. Leurer, Y. Nir and N. Seiberg, Nucl. Phys. B **420**, 468 (1994) [hep-ph/9310320].
- [75] M. Dine, N. Seiberg and S. Thomas, Phys. Rev. D **76**, 095004 (2007) [arXiv:0707.0005 [hep-ph]].
- [76] H. Georgi, Ann. Rev. Nucl. Part. Sci. **43**, 209 (1993).
- [77] P. J. Fox, A. E. Nelson and N. Weiner, JHEP **0208**, 035 (2002) [hep-ph/0206096].

- [78] H. E. Haber and R. Hempfling, Phys. Rev. D **48**, 4280 (1993) [hep-ph/9307201]. M. S. Carena, J. R. Espinosa, M. Quiros and C. E. M. Wagner, Phys. Lett. B **355**, 209 (1995) [hep-ph/9504316], H. E. Haber, R. Hempfling and A. H. Hoang, Z. Phys. C **75**, 539 (1997) [hep-ph/9609331]. M. S. Carena, J. R. Ellis, A. Pilaftsis and C. E. M. Wagner, Nucl. Phys. B **586**, 92 (2000) [hep-ph/0003180].
- [79] M. Frank, T. Hahn, S. Heinemeyer, W. Hollik, H. Rzehak and G. Weiglein, JHEP **0702**, 047 (2007) [hep-ph/0611326].
- [80] R. Barbieri, L. J. Hall, A. Y. Papaioannou, D. Pappadopulo and V. S. Rychkov, JHEP **0803**, 005 (2008) [arXiv:0712.2903 [hep-ph]].
- [81] A. Arvanitaki, M. Baryakhtar, X. Huang, K. Van Tilburg and G. Villadoro, arXiv:1309.3568 [hep-ph].
- [82] A. Kaminska, G. G. Ross, K. Schmidt-Hoberg and F. Staub, arXiv:1401.1816 [hep-ph].
- [83] For recent studies, see for example, U. Ellwanger, JHEP **1203**, 044 (2012) [arXiv:1112.3548 [hep-ph]]; K. Agashe, Y. Cui and R. Franceschini, JHEP **1302**, 031 (2013) [arXiv:1209.2115 [hep-ph]]; R. T. D'Agnolo, E. Kuflik and M. Zanetti, JHEP **1303**, 043 (2013) [arXiv:1212.1165 [hep-ph]]; T. Gherghetta, B. von Harling, A. D. Medina and M. A. Schmidt, JHEP **1302**, 032 (2013) [JHEP **1302**, 032 (2013)] [arXiv:1212.5243 [hep-ph]]; C. Cheung, S. D. McDermott and K. M. Zurek, JHEP **1304**, 074 (2013) [arXiv:1302.0314 [hep-ph]]; R. Barbieri, D. Buttazzo, K. Kannike, F. Sala and A. Tesi, arXiv:1304.3670 [hep-ph].
- [84] For recent studies, see for example, N. Craig, J. A. Evans, R. Gray, C. Kilic, M. Park, S. Somalwar and S. Thomas, JHEP **1302**, 033 (2013) [arXiv:1210.0559 [hep-ph]]; N. Craig, J. Galloway and S. Thomas, arXiv:1305.2424 [hep-ph].
- [85] [ATLAS Collaboration], ATLAS-CONF-2013-034, ATLAS-CONF-2013-012, ATLAS-CONF-2013-030, ATLAS-CONF-2012-160.
- [86] [ATLAS Collaboration], ATLAS-CONF-2013-013, ATLAS-CONF-2013-067.
- [87] [CMS Collaboration], CMS-PAS-HIG-13-001, CMS-PAS-HIG-13-004, CMS-PAS-HIG-12-044.
- [88] [CMS Collaboration], CMS-PAS-HIG-13-002, CMS-PAS-HIG-13-003.
- [89] ATLAS-collaboration, ATL-PHYS-PUB-2012-004.
- [90] M. E. Peskin, arXiv:1207.2516 [hep-ph].
- [91] M. Klute, R. Lafaye, T. Plehn, M. Rauch and D. Zerwas, Europhys. Lett. **101**, 51001 (2013) [arXiv:1301.1322 [hep-ph]].

- [92] <http://www.snowmass2013.org/tiki-index.php?page=The+Higgs+Boson> HiggsSnowmassReport_Sep3.pdf
- [93] C. Lester and D. Summers, Phys.Lett. **B463** (1999) 99–103, [hep-ph/9906349].
- [94] A. Barr, C. Lester, and P. Stephens, J.Phys.G **G29** (2003) 2343–2363, [hep-ph/0304226].
- [95] A. J. Barr and C. Gwenlan, Phys. Rev. **D80** (2009) 074007, [hep-ph/0907.2713].
- [96] C. Lester and A. Barr, JHEP **0712** (2007) 102, [hep-ph/0708.1028].
- [97] **ATLAS** Collaboration, J. B. G. da Costa *et al.*, [hep-ex/1102.5290].
- [98] **CMS** Collaboration, CMS-PAS-SUS-11-005; CMS Collaboration [CMS Collaboration], CMS-PAS-SUS-12-002.
- [99] T. Appelquist, H.-C. Cheng, and B. A. Dobrescu, Phys. Rev. **D64** (2001) 035002, [hep-ph/0012100].
- [100] D. Hooper and S. Profumo, Phys.Rept. **453** (2007) 29–115, [hep-ph/0701197].
- [101] G. Servant and T. M. P. Tait, Nucl. Phys. **B650** (2003) 391–419, [hep-ph/0206071]. K. Kong and K. T. Matchev, JHEP **0601** (2006) 038, [hep-ph/0509119]. F. Burnell and G. D. Kribs, Phys.Rev. **D73** (2006) 015001, [hep-ph/0509118]. M. Kakizaki, S. Matsumoto, Y. Sato, and M. Senami, Nucl. Phys. **B735** (2006) 84–95, [hep-ph/0508283]. M. Kakizaki, S. Matsumoto, Y. Sato, and M. Senami, Phys. Rev. **D71** (2005) 123522, [hep-ph/0502059].
- [102] G. Belanger, M. Kakizaki, and A. Pukhov, JCAP **02** (2011) 009, [hep-ph/1012.2577].
- [103] G. Arnison *et al.* [UA1 Collaboration], Phys. Lett. B **129**, 273 (1983).
- [104] W. S. Cho, K. Choi, Y. G. Kim, and C. B. Park, Phys. Rev. Lett. **100** (2008) 171801, [hep-ph/0709.0288]. A. J. Barr, B. Gripaios, and C. G. Lester, JHEP **02** (2008) 014, [hep-ph/0711.4008]. W. S. Cho, K. Choi, Y. G. Kim, and C. B. Park, JHEP **02** (2008) 035, [hep-ph/0711.4526]. M. M. Nojiri, Y. Shimizu, S. Okada, and K. Kawagoe, JHEP **06** (2008) 035, [hep-ph/0802.2412].
- [105] M. Burns, K. Kong, K. T. Matchev, and M. Park, JHEP **03** (2009) 143, [hep-ph/0810.5576].
- [106] T. Cohen, E. Kuflik, and K. M. Zurek, JHEP **11** (2010) 008, [hep-ph/1003.2204].
- [107] H.-C. Cheng, K. T. Matchev, and M. Schmaltz, Phys. Rev. **D66** (2002) 056006, [hep-ph/0205314].
- [108] M. Kazana, Acta Phys. Polon. **B38** (2007) 449–458, [CERN-CMS-CR-2006-062].
- [109] G. Bhattacharyya, A. Datta, S. K. Majee, and A. Raychaudhuri, Nucl.Phys. **B821** (2009) 48–64, [hep-ph/0904.0937].

-
- [110] J. Alwall *et al.*, JHEP **09** (2007) 028, [hep-ph/0706.2334].
- [111] J. Alwall *et al.*, Eur. Phys. J. **C53** (2008) 473–500, [hep-ph/0706.2569].
- [112] M. ElKacimi, D. Goujdami, H. Przysiezniak, and P. Z. Skands, Comput. Phys. Commun. **181** (2010) 122–127, [hep-ph/0901.4087].
- [113] H. Murayama, I. Watanabe, and K. Hagiwara.
- [114] ATLAS Collaboration, G. Aad *et al.*, [hep-ex/0901.0512].
- [115] CMS Collaboration, C. Bernet, [hep-ex/1105.5911].
- [116] ATLAS Collaboration, G. Aad *et al.*, Phys.Rev.Lett. **106** (2011) 131802, [hep-ex/1102.2357].
- [117] J. T. Linnemann, [physics/0312059].
- [118] R. Brun and F. Rademakers, Nucl.Instrum.Meth. **A389** (1997) 81–86.
- [119] H.-C. Cheng, K. T. Matchev, and M. Schmaltz, Phys. Rev. **D66** (2002) 036005, [hep-ph/0204342].
- [120] H. Georgi, A. K. Grant, and G. Hailu, Phys. Lett. **B506** (2001) 207–214, [hep-ph/0012379].
- [121] C. Macesanu, C. D. McMullen, and S. Nandi, Phys.Rev. **D66** (2002) 015009, [hep-ph/0201300].
- [122] B. Bhattacharjee and K. Ghosh, Phys. Rev. **D83** (2011) 034003, [hep-ph/1006.3043].
- [123] G. Bhattacharyya, A. Datta, S. K. Majee, and A. Raychaudhuri, Nucl. Phys. **B760** (2007) 117–127, [hep-ph/0608208].